

Macroscopic Networks in the Human Brain

Mapping connectivity in healthy and damaged brains

Emil H.J. Nijhuis



DONDERS
series

MACROSCOPIC NETWORKS IN THE HUMAN BRAIN
MAPPING CONNECTIVITY IN HEALTHY AND DAMAGED BRAINS

Emil H.J. Nijhuis

Composition of the graduation committee

Chairman & secretary	prof.dr. G. van der Steenhoven
Promotor	prof.dr. D.G. Norris
Assistent-promotor	dr. A.-M. van Cappellen van Walsum
Members	prof.dr.ir. C.H. Slump prof.dr. C.F. Beckmann prof.dr.rer.nat. M. Koch prof.dr.ir. M.J.A.M. Van Putten dr. R.M. Dijkhuizen

This research presented in this thesis was carried out at the Donders Institute for Brain, Cognition and Behaviour, Centre of Cognitive Neuroimaging, Radboud Universiteit Nijmegen, The Netherlands. The research was financially supported by the MIRA institute for Biomedical Technology and Technical Medicine, Faculty of Science and Technology, University of Twente, Enschede, The Netherlands.

Cover shows a brain and fibre streamlines of a participant used in this dissertation. The background shows a digital potrait of Leo Choi Nijhuis using an UTF-8 stream. Graphics were designed by Emil H.J. Nijhuis and edited by Judith van Stegeren. Thesis layout was accomplished with the KOMA-scripts book-class from \LaTeX 2 ϵ .

Printed by Ipskamp Drukkers, Enschede

ISBN: 978-94-91027-64-2

©Emil H.J. Nijhuis, 2013

No part of this thesis may be reproduced or transmitted in any form or by any means, electronic or mechanical, including photocopy, recording or otherwise without permission of the author.

MACROSCOPIC NETWORKS IN THE HUMAN BRAIN
MAPPING CONNECTIVITY IN HEALTHY AND DAMAGED BRAINS

DISSERTATION

to obtain
the degree of doctor at the University of Twente,
on the authority of the rector magnificus,
prof.dr. H. Brinksma,
on account of the decision of the graduation committee,
to be publicly defended
on Wednesday 10 July, 2013 at 16:45

by

Emil Harald Jeroen Nijhuis

born on 22 May, 1980
in Kiel, Germany

This dissertation has been approved by

the promotor: prof. dr. D.G. Norris

and the assistant-promotor: dr. A.-M. van Cappellen van Walsum

To my family

Preface

It is almost self-evident that we are all connected with one another. Humans often have more in common than we let ourselves recognize. How we influence each other is however entirely unclear and bewildering to those who seek to understand it. It has been said that as little as the flaps of a butterfly's wings can cause large storms to arise. This simile from chaos theory, named butterfly effect, illustrates how, in a complex system, small events can be instrumental to the occurrence of larger events. It is probably my favorite simile, because it reminds me of how subtle life can be sometimes, how life can surprise us, and how something beautiful can unexpectedly become something ugly and vice versa.

Looking back on the emergence of this thesis I cannot help but wonder how little it would have taken for this thesis to have been very different or even for it to have never been written at all. Through numerous of interactions, brief, lengthy, positive and even seemingly negative ones, this thesis has been shaped into what it is today. After my masters in computer science, I was eager to research new interactive learning methods for creating better *Go* programs. Instead, years later, through a series of unforeseen events I arrived in a research position to study brain networks. I still remember my first day at the Donders: how much I was flooded with a torrent of information and how excited I felt about my new work but also felt strangely out of place. Before this I knew very little about the brain and three months prior I never could have imagined that I would do research in neuroscience. Feelings of discomfort however quickly dissipated at work, because the Donders Institute is such a great place for a researcher in neuroscience. It is not only a place for work but it comes together with a diverse group but like-minded individuals, also known as the Donders family, who support one another. I am very grateful that I have been part of it and I would like to express my gratitude to all of them.

I would especially like to thank my supervisors David and Anne-Marie, who created my research position together with Kees and Christian. During my time at the Donders they gave me enough space and freedom to do my research. With their guidance and patience they taught me how to become a better neuroscientist. I am confident that I will continue to benefit from their mentoring for the next stages of my career. Likewise I am grateful to have met and learnt from my co-authors Eelke, Marcel, David, Jasha, Douwe, Anil, Gleb, Bert, Huadong and Janneke and all past and present members of the MR Techniques in Brain Function group. In particular, I would like to thank Rasim and Michiel for being my paranimfs and Erik who acquired a large part of the used data in this thesis. This PhD project consumed an incredible amount of computational power (over 100.000 CPU core hours) and other resources, so it goes without saying that this thesis would have not been possible without the work of our technical and administrative groups to whom I am also very grateful.

Outside the Donders Institute I would like to thank Sang-Hun Lee and his group mem-

bers at the Seoul National University for their hospitality to let me join their lab to work on my thesis. I also would like to thank Lori, Sharon, Robbert and my father for their improvements to the final manuscript.

Finally I want to express my gratitude to all my family as they are the dearest I have in my life. Foremost of them all my muse and loving wife Yowon who inspires my world like no other from moment to moment. “Hun, why don’t you look at this? They want to do something with brain networks. Maybe you should apply!” were probably some of the earliest and most critical butterfly flaps which helped to produce this thesis. Together we were fortunate to welcome our son Leo amongst us. Watching him grow up the past 3 years was a real privilege, although sometimes I felt guilty that I was unable to reciprocate his undying curiosity because I was pondering about my work. But I have to believe that this thesis will produce some positive ripples in time and that the sacrifices we made were worthwhile and hopefully good things will come from it. Maybe you, the reader, could think the same after reading parts of this thesis. In that case flap your wings and tell a friend of yours what you liked about it! Maybe it is you who will unleash a storm.

Contents

Preface	vi
1 General introduction	4
2 Segmenting the brain for macroscopic network models using different MRI techniques	14
3 Topographic hub maps of the human structural neocortical network	34
4 Exploring the connectivity patterns of human neocortical visual areas	58
5 Neocortical network damage assessment by homotopic lesion mapping on healthy subjects	82
6 Summary and discussion	100
Appendix	108
References	109
Nederlandse samenvatting	120
List of publications	123
Curriculum vitae	125
Donders graduate school for cognitive neuroscience series	126
Supplementary material (available in digital version)	132

1

General Introduction

*"If our brains were simple enough for us to understand them,
we'd be so simple that we couldn't."*

-Ian Stewart-

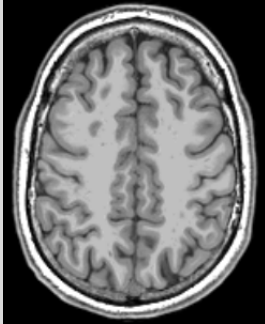
How human cognitive function emerges from neuronal structure and its dynamics is still largely unknown (Sporns et al., 2005). Mapping the neuronal architecture of the brain and its relation to function are therefore key to understand ourselves better. The neurons of the brain form an interconnected network distributed over two main brain components: the grey matter and the white matter. The neurons of the brain are located in the grey matter of the brain, which is made up of the neocortex, cerebellar cortex and subcortical nuclei. Over short distances neurons are interconnected with one another within the grey matter but they are also interconnected over longer distances with myelinated axons that pass through the white matter. If one were to make an analogy between the neuronal network of the brain and the road infrastructure of a country, then grey matter connections can be considered as slow urban roads and white matter connections are the fast highways of the human brain. The distinctive colours of grey and white matter are due to the predominant presence of neurons (grey) and myelin (white). It is estimated that the healthy adult human brain forms a network of more than 130,000,000,000 interconnected neurons (Pakkenberg and Gundersen, 1997; Andersen et al., 2003; Larsen et al., 2006; Pelvig et al., 2008), which is roughly half the estimated number of stars in our Milky Way. Therefore, understanding the architecture and functioning of this complex organ can be as challenging as mapping a small part of our universe. To overcome the complexity of the brain, studies are typically performed on different scopes. These range from molecular to larger-scale levels that consider brain anatomy and physiology under developmental, psychological, social or environmental conditions.

In this thesis magnetic resonance imaging techniques (see box 1) are used to study the neuronal networks of the human brain at the macroscopic level, with a special focus on its white matter highways in relation to brain function. The following sections of this chapter will give a short historical perspective on brain mapping, followed by a description of how this thesis aims to contribute to neuroscience. It will conclude with an outline of the studies presented in this thesis.

BOX 1 |Magnetic Resonance Imaging (MRI)

Magnetic resonance imaging or **MRI** is a technique which has been invented by the Noble prize winners Paul Lauterbur and Peter Mansfield who were able to produce images by introducing the concept of pulsed magnetic field gradients that made spatial localisation of the MR-signal possible. Their work has revolutionised the medical field as MRI scanners are now able to image body parts on a submillimeter level. Today MRI techniques are the most popular methods in neuroscience to investigate the human brain non-invasively. The quality of an image is depending on many factors among which the strength of the main magnetic field plays an important role.

MRI scanners for in-vivo human research exist up to field strengths of up to 11.7 T, however the most common scanners for research applications operate currently at 3T, while 7T scanners are becoming more popular. The studies in this thesis use exclusively MRI techniques at 3T. Since the inception of MRI, different forms of measuring brain structure and function have been developed. A short list of the techniques used in this thesis is given below:



Anatomical MRI is the most basic MRI application and a typical anatomical scan with a resolution of 1mm^3 takes about 5 minutes (see picture at the left). The basic unit of a 3D MRI image is called a voxel. The different contrasts in an anatomical scan are used to demarcate the boundaries between different types of tissue, such as bone structures, skin, neocortical grey matter and cerebral white matter. Anatomical scans are also used as a reference image for other scanning methods like functional MRI and diffusion weighted MRI which are usually acquired at a lower resolution to gain temporal resolution with higher acquisition speeds.

Functional MRI (fMRI) techniques measure time-dependent changes in living tissue. In neuroscience, the most popular way of identifying neuronal activity is by measuring the changes of the haemodynamic response in brain tissue with the blood oxygen level dependent (BOLD) contrast (Ogawa et al., 1990). This is usually accomplished by imaging the brain at intervals between 100-2000ms. For behavioural experiments inside an MRI, the BOLD signal changes can be correlated with the behaviour of a subject, which enables a researcher to associate brain regions with certain cognitive behaviour. Spatially distinct brain areas which respond insync to certain cognitive behaviour are then considered to be functionally connected. A more recent form of applying fMRI techniques is by investigating the brain activity at rest, also called resting-state fMRI. In resting-state fMRI experiments, it is not directly possible to relate brain activity to specific cognitive behaviour, however by comparing the activity patterns between brain regions, functionally connected brain areas can be identified.

Diffusion Weighted MRI (DWI) is inspired by experiments of Hahn (1950), who observed that measurement of the magnetisation of water molecules is affected by the diffusive properties of water molecules. Further research showed that the amount of displacement of water molecules through diffusion can be measured along a certain direction (Basser et al., 1994a, 1994b; Le Bihan, 2003). As a result, imaging diffusion has found an application in brain sciences, because it can be used to model the microstructure of cerebral white matter. The models make use of the fact that diffusion of water molecules can be free (isotropic diffusion) or restricted (anisotropic diffusion) in the absence or presence of obstacles. As axons within the human brain are restricting diffusion in certain directions, the strength of the measured diffusion varies with the measured direction. The simplest model is the diffusion tensor which only requires diffusion measurements in six different directions. More complex diffusion models require a larger amount of measurement which is referred to as high angular resolution diffusion imaging (HARDI) data (Tuch et al., 1999). Using these models with tractography methods (see box 2) it is then possible to estimate fibre streamlines.

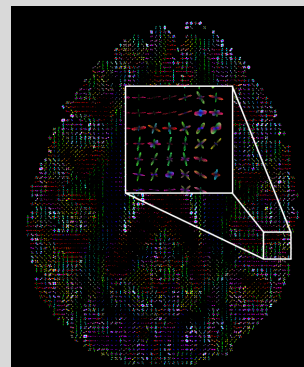
A short historical background on brain mapping

Over the past two centuries enormous strides have been made in mapping brain architecture and function. On the functional side one of the most notable discoveries was the localisation of Broca's area, named after Pierre Paul Broca who first reported in 1861 its association with speech production. After his notable finding, the idea of functionally specialised brain areas took hold, which considers that specific cognitive functions are localised in specific brain areas that correspond in their anatomical location across subjects. Since then many more functionally specialised brain regions have been identified such as Wernicke's area which is involved in language processing, motor cortices which are involved in body movements (Ferrier, 1876), visual cortices which process signals coming from the eyes (Talbot and Marshall, 1941; Wandell and Winawer, 2011), the hippocampus which plays an important role in the consolidation of short-term memory to long-term memory (Scoville and Milner, 1957), and the prefrontal cortex where complex forms of cognition are executed (Miller, 1999). The functioning of the visual system has been extensively investigated, because it could be studied in different species which enabled researchers to record electrocardiographs from neurons invasively during visual stimulation of the eyes. In the past decades, the efforts to localise cognitive function in the brain were aided by experimentation with functional magnetic resonance imaging (fMRI) and positron emission topography (PET) methods. These techniques catalysed the discoveries of specific functional areas in the human brain. The most notable discovery was that certain brain areas demonstrate a higher activity during rest; these areas are now called: "the default mode network" (Gusnard and Raichle, 2001). To this day not all brain areas can be attributed to a specific function, however research has expanded to studying the dynamics of distinct brain areas and their interactions.

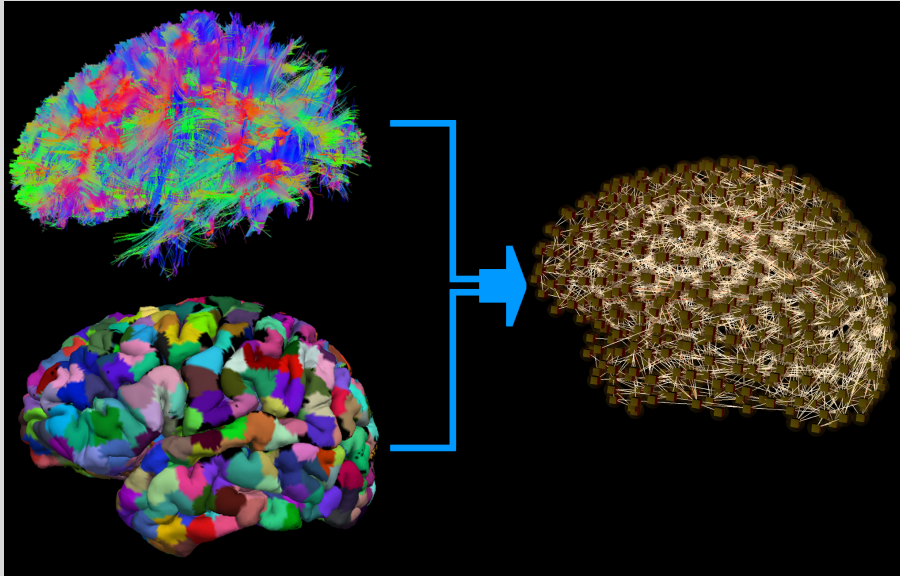
BOX 2 | Fibre tractography & macroscopic brain networks

Fibre tractography concerns itself with the identification of axons which are long distance nerve fibres which transverse through the cerebral white matter to connect distant neuronal populations in neocortical and subcortical areas. The basis for tractography methods is the modelling of the diffusivity in tissue, which is typically done in the unit cubes of a 3D Cartesian grid overlaying the tissue (Mori et al., 1999; Xue et al., 1999). The simplest used model is the diffusion tensor model (Basser et al., 1994a, 1994b). which is however only able to indicate one main diffusion direction and therefore inadequately characterises crossing or kissing fiber situations.

In this thesis, multi-directional diffusion models (Alexander, 2005) derived from HARDI data are used (e.g. see figure at the right displaying an axial slice of the brain and the reconstructed orientation distribution functions for each voxel) to perform either **deterministic** (Xue et al., 1999) or **probabilistic** (Behrens, Woolrich, et al., 2003) tractography.



For the deterministic approach, fibres are determined by seeding a fibre tract in every voxel which is then tracked through the brain by following main diffusion directions (see figure below for an example result). Probabilistic tractography methods start by modelling diffusion with a probabilistic density function in every voxel which can then be used to randomly draw a likely main fibre direction when tracking through it. The connectedness of a voxel of interest to other areas can then be estimated by seeding and tracking multiple (5000) times from that voxel.



A macroscopic network model of the brain can then be constructed by dividing a brain into multiple areas and then using the estimated fibres between the areas as connections (see illustration above). Alternatively it is also possible to consider the functional connectedness between brain areas as measured for instance with fMRI during rest. Once a network of the brain is constructed, graph theoretical methods and network measures can be applied to analyse its characteristics (see box 3).

In parallel to understanding brain function, early histological research starting with Theodor H. Meynert (1872) has described the cellular structure of the brain. This led to the formation of the neuron doctrine by Santiago Ramón y Cajal (y Cajal and Azoulay, 1894) which identified the neuron as the basic building block of our central nervous system. Some of the most widely used cellular descriptions of the brain are the contributions by Korbinian Brodmann who mapped the human neocortex of post-mortem brains by subdividing them into areas with similar cytoarchitecture (Brodmann, 1909). The underlying argument for separating brain areas on the basis of cytoarchitecture is that differences in cell arrangement may mark differences in biological function. In his investigation Brodmann also related his findings to cognitive brain function. However these relationships are to this day enigmatic and cannot be translated into meaningful

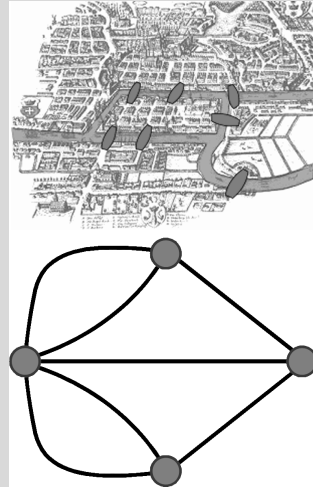
theories of how brain cytoarchitecture elicits brain function. Brodmann areas are still used for describing the anatomical location of brain regions. Like neocortical anatomy, cytoarchitecture has also considerable inter-subject variability and Brodmann areas cannot be determined on the basis of anatomical landmarks (Amunts et al., 1999). Until recently, cytoarchitecture only could be mapped effectively with invasive histological methods (Eickhoff et al., 2005). Newer non invasive cytoarchitectural methods potentially play an important role in future research to localize brain function once the arrangement of neurons is better understood.

A more promising avenue of research to relate structure to function beyond anatomical locations is the study of long distance white matter fibre tracts, as it lays bare the macroscopic organisation of the brain. White matter tracts have been studied in early neuroanatomical research and were first recognized to play an important functional role by Meynert (Catani and Ffytche, 2005). His student Karl Wernicke then devised a disconnection theory. This theory recognized that language processing is distributed across Wernicke's and Broca's area and correctly predicted that a lesion to the connection of the two brain areas would lead to a form of language dysfunction (Catani and Ffytche, 2005). Synthesising clinical observations to white matter anatomy, Norman Geschwind listed a group of disorders under the umbrella term disconnection syndromes (Geschwind, 1965).

Over time, it has thus become evident that to fully understand brain function it is not only important to associate specific grey matter areas with function but also to consider the white matter connections between them. Consequently, research started to approach brain function and its structural substrates as distributed networks (Mesulam, 1981). This precept can best be illustrated by invasive research with chemical tracers in macaque monkeys aiming to map the visual system, the network of brain areas involved in visual processing (Felleman and Van Essen, 1991). To combine the findings across different researches in macaques, a database was created with the description of distinctive functional areas and their connections (Reid et al., 2009). As techniques used in macaques are too invasive, research in humans was not able to reproduce such detailed descriptions of interconnected functional brain areas until recent developments in MRI. Experiments with functional MRI have become standard techniques to localise brain activity related to specific cognitive behaviour, while diffusion weighted imaging with tractography (see box 2) is the sole technique which can non-invasively map white matter tracts within an entire brain. These developments led Sporns et al. (2005) to call for a systematic effort to assemble a connectivity matrix, named the human connectome, which would describe the brain's networks on the microscopic, mesoscopic and the macroscopic scales. Networks are now ubiquitously used in neuroscience to describe various forms of connectedness between entities, measured with magnetoencephalography (MEG), electroencephalography (EEG), invasive electrocorticography (ECoG), PET and MRI. Graph theoretical approaches (see box 3) to analyse these networks are frequently used to investigate the human brain for group, developmental and clinical differences.

BOX 3 | Graphs & networks

The concept of using graphs to analytically solve problems dates back to the Königsberg bridge problem solved by Leonhard Euler in 1736. The problem considers whether it is possible to find a walk through the city by crossing every bridge of the city only once. Euler came to a negative solution by reducing the problem to an abstraction in the form of a graph with nodes (land masses) and edges (bridges). Today graphs and networks are constructed in many scientific disciplines to describe and render observations of connected entities. Consequently many measures and techniques have been developed to study the properties of networks. A classic use of network measures is to determine and localise important structures within a network. **Node degree**, which is the number of nodes a node is connected with and **betweenness centrality**, which is number of shortest paths which pass through a specific node are frequently used to determine the importance of a particular node within a network (Barthelemy, 2004). Nodes



with high node degree or high betweenness centrality are often described as **hubs**. Studying the architecture of different complex networks appearing in nature has lead to the identification and characterisation of unifying topological principles, of which some are identified by the appearance of their node degree distribution $P(k)$: the probability of a node with degree k . **Random**, **scale-free** and **small-world** networks depict concepts which are often used to describe topological features. Random networks are generated by a random process and have a characteristic Gaussian node degree distribution (Bullmore and Sporns, 2009). Scale-free networks have a node degree distribution which follows a power law. A typical example of a scale-free network is the world wide web. The small-world property refers to nodes within the network being connected with one another with an average shortest path length which is comparable to a matched random network (Humphries and Gurney, 2008). As the node degree distribution of small-world networks have different shapes, small-world networks are further differentiated into scale-free, **broad-scale** and **single scale** (Amaral et al., 2000). The macroscopic network of the human brain has small-world properties, while there are different reports of its scale (Bullmore and Sporns, 2009).

Aim and outline of the thesis

This thesis will present four studies investigating the brain's functional and structural macroscopic networks and their relationships to brain function and cognition in both the healthy and diseased brains. Probing the neuronal network structure of the brain is limited by technical constraints. However recent advances in diffusion weighted and functional magnetic resonance imaging techniques (DWI and fMRI) have provided access to the organisational principles between large scale neuronal populations at the macroscopic scale. The macroscopic scale of the brain is not well defined; however it

could be argued that contemporary in-vivo MRI techniques operate at this scale, as they are not able to image below a resolution of 50 μm which is considered as the starting point of the brain's mesoscopic scale by Sporns and his colleagues (Sporns et al., 2005).

The following chapters investigate the macroscopic network organisation of the human brain. The methods and analysis used in the chapters 2-5 are guided by four main research questions:

Chapter 2: Is it possible to automatically parcel individual human neocortices into functional specific brain areas? The genesis of this question lies in the requirement to have appropriate nodal configurations when the brain is modelled as a network as in chapter 3-5. The problem of automatically parcelling the neocortex into functional specific brain areas is explored with three types of MRI data: anatomical scans, diffusion weighted imaging scans and functional resting-state scans.

Chapter 3: Where are the neocortical hubs in the human brain? The third chapter addresses this question with a structurally informed parcelling technique developed from chapter 2 in combination with deterministic tractography to create macroscopic neocortical network models for a sample population of young adults. The networks were then analysed with graph theoretical methods to create topographic maps displaying the hubs of the neocortex.

Chapter 4: What are the structural connectivity patterns between visual areas? In chapter 4 the structural connectivity patterns between functionally defined areas of the visual system are analysed. This study aims to better understand the relationships between the structural connectivity and the functional organisation of the visual system.

Chapter 5: What is the effect of a brain lesion to the neocortical network? The last research question in chapter 5 extends on the approach used in chapter 3 by homotopically mapping stroke lesions from subjects, with visual field defect symptoms in a healthy control population. The effect of a lesion is then simulated by comparing network measures in the neocortical network with and without the presence of a lesion.

The dissertation is concluded in chapter 6 with a summary of the main findings, a general discussion on the research of this thesis and concludes with an outlook on future work.

2

**Segmenting the brain
for macroscopic network models
using different MRI techniques**

Abstract

The segmentation of the neocortex into modules has an important potential role in the generation of macroscopic network models of the brain. In this article we show how the neocortex can be segmented using three methods each based on different MRI techniques: high angular resolution diffusion imaging (HARDI), structural MRI and resting state fMRI. The first method uses a connectivity measure based on probabilistic tractography at the voxel-level in combination with a flow simulation (or random walk) paradigm for graphs. The method provides, to the best of our knowledge, the first whole brain segmentation based on fibre information extracted from diffusion weighted imaging data. The second method uses the geometric information of grey matter voxels in T1 images by applying a k-means clustering algorithm. The third method segments the brain on the basis of networks derived from independent component analysis of resting-state fMRI data.

"All truths are easy to understand once they are discovered; the point is to discover them."

-Galileo Galilei-

Introduction

The development of network models which capture essential characteristics of the human brain are vital to advance understanding of this organ (Sporns et al., 2005). Accurate whole brain segmentation is considered key to the development of representative macroscopic brain models (Zalesky et al., 2010).

Network models can be used for different types of analyses and simulations, such as network structure comparison across patients and healthy control subjects (Bassett et al., 2008; Rubinov et al., 2009) and network flow and drop-out simulations (Alstott et al., 2009), and provide a framework for strengthening cognitive neuroscientific hypotheses. The possible future applications of network models include assisting surgeons in the identification of eloquent brain tissue, prediction of aphasia in neurodegenerative and cerebral vascular diseases and informing neurologists on possible underlying neuronal damage based on the patients' symptoms.

Due to the absence of standardized cortical segmentation methods that can delineate cortical modules, contemporary research into brain networks relies on the use of anatomical brain templates with less than 100 defined cortical regions such as the AAL (Gong, He, et al., 2009) or similar templates (Achard et al., 2006; Achard and Bullmore, 2007; Iturria-Medina et al., 2008). The use of these templates limits the analysis to showing basic brain network properties such as network efficiency and small-world organization where hubs have a critical functional role. Ideally, the number of regions and their location should be automatically determined by an objective segmentation criteria, such as the changes of the connectivity profiles along the cortical surface derived from diffusion weighted images (Scholz et al., 2009) or cytoarchitectural profile transitions in the cortex that can be found in high resolution T1 images (Eickhoff et al., 2005); both approaches are as yet unexplored for whole brain cortical segmentation.

The brain is known to show incredible resilience in adversity, such as being able to cope with large tumours or haemorrhages. In contrast modern computer systems are prone to collapse by inflicting only minor damage. Recent work by (Hagmann et al., 2008; Alstott et al., 2009; Honey et al., 2009) has shown that by using a thousand regions of interest (ROIs) in a macroscopic brain model more advanced network analysis such as the modelling the impact of lesions in the human brain is feasible. The consensus is that the human brain network is organized in such a way that randomly situated damage within the network will not significantly perturb other parts of the network as it continues to function (Honey et al., 2010). In these papers the authors relied on a manual, anatomically informed segmentation of the brain into equally sized ROIs, and

a better segmentation would presumably have improved their model.

In this paper we describe three methods we initially developed for the cortical segmentation challenge in the Pittsburgh Connectivity Competition 2009 (Schneider, 2009), which attempted to identify the best segmentation methods then available by evaluating them in comparison with maps obtained from fMRI localizer experiments. The underlying argument for this type of approach is that areas from any kind of brain segmentation should show a considerable overlap with known cortical modules such as V1, V2 in order to be meaningful. For the methods presented in this paper we were awarded a joint first prize.

The first method segments the brain using a high angular resolution diffusion imaging (HARDI) based connectivity measure in combination with a flow simulation or random walk paradigm. Diffusion weighted imaging (DWI) techniques are popular due to their ability to estimate the orientation of fibre axons at the voxel level (Le Bihan, 2003). By using deterministic or probabilistic tractography methods it is possible to quantify cortical voxels as being connected with one another via a fibre tract. However as fibre tracking methods are still being developed, a standard metric for measuring cortical fibre connectivity has yet to emerge. Hagmann et al., 2008; Alstott et al., 2009; Honey et al., 2009 rely on DWI based connectivity measures to determine the strength of connectivity between their template based ROIs. In contrast, we use the DWI information to delineate ROIs in a quite similar fashion to Johansen-Berg and Rushworth, 2009 and Klein et al., 2010 by mainly looking at the organization of cortical connections. The advantage of our approach compared to previous DWI based segmentation approaches is that it is able to automatically segment the entire neocortex using a single theoretical paradigm without being influenced by manual ROI selection criteria.

The second presented method segments the brain on the basis of geometrical organization of grey matter voxels by clustering the neocortex using a k-means algorithm (MacKay, 2002). The method takes into account the folding patterns of individual brains and therefore produces a good approximation of functional units on the neocortex.

For the third method we investigated how networks found through Independent Component Analysis (ICA) can segment the brain. ICA based network analysis has recently gained popularity due to its ability to identify spatio-temporal networks in the resting-state fMRI (Beckmann et al., 2005) such as the default mode network (Raichle and Snyder, 2007). As some of these networks are known to be reproducible across subjects we were interested as to whether the networks would also delineate cortical modules as derived through fMRI localizer experiments.

Materials and methods

In this section we describe the dataset provided by the spring 2009 Pittsburgh Connectivity Competition as well as the scoring metrics used (Schneider, 2009). We then present three cortical segmentation methods, which we believe represent compelling approaches. Each method is based on the three different types of MR imaging modalities made available by the competition: anatomical, resting-state fMRI and HARDI

data.

The first method exploits the Probabilistic Index of Connectivity (PICO) (Parker et al., 2003) a measure for cortical connectivity extracted from HARDI data by combining it with a random walk paradigm and the Markov Clustering Algorithm (MCL) for graphs (Van Dongen, 2000; Enright et al., 2002). The second method uses structural scans of the brain by applying a k-means clustering algorithm to the geometric arrangement of grey matter voxels. And finally the third method segments the brain by clustering the grey matter using networks derived from independent component analysis (ICA) on resting state fMRI time series (Beckmann et al., 2005).

Data acquisition and preprocessing

The dataset consisted of MRI measurements of 3 different healthy human brains acquired on a Siemens 3T TIM Trio system with a 32 channel head coil. For each brain a high resolution MPAGE structural scan, a diffusion weighted scan and a resting-state fMRI scan were provided. One brain, subsequently called brain0, was additionally provided with functional maps of the visual, motor and cognitive control networks, which were obtained using localiser tasks.

Structural data

High resolution anatomical scans were acquired using a 3D MPAGE sequence for brain0 with TE=2.13ms, TR=1620ms, TI=800ms, a flip angle of 8° and 0.9 mm slices resulting in a $256 \times 256 \times 224$ matrix with $1.0 \times 1.0 \times 0.9 \text{ mm}^3$ voxel size. Brain1 was recorded with TE=2.98ms, TR=2300ms, TI=900ms, a flip angle of 9° and 160 1.2mm slices with 1mm in plane resolution. Brain2 was recorded with: TE=2.63ms, TR=2110ms, TI=1100ms, a flip angle of 8° and 176 1mm slices with 1mm in plane resolution.

Diffusion imaging data

Diffusion weighted imaging volumes were acquired using a single-shot echo-planar imaging (EPI) sequence, with TE=108ms and TR=11.6s. The voxel size was $2 \times 2 \times 2 \text{ mm}^3$ with a matrix size of 128×128 using a 3/4 partial Fourier acquisition in the phase encoding direction. Each volume consisted of 68 slices. DWI were acquired in 256 non-collinear directions at a b-value of 1500 s/mm^2 . In addition, 28 volumes were acquired with no diffusion weighting ($b=0 \text{ s/mm}^2$).

Resting-state fMRI

An eyes closed resting-state fMRI experiment for brain0 was recorded with the following parameters: TR = 2000ms, TE = 29ms, a flip angle of 90° , 300 volumes, voxel size $3 \times 3 \times 3 \text{ mm}^3$ and for brain1 and brain2 with parameters: TR = 2000ms, TE = 30ms, a flip angle of 90° , 210 volumes, voxel size $3.75 \times 3.75 \times 3.8 \text{ mm}^3$.

Functional maps

Functional maps were acquired using an assortment of localizer experiments for brain0: 6 retinal fields maps (V1, V2 dorsal and V2 ventral, each for the right and left hemisphere) (Wandell et al., 2007), 4 motor system field maps (hand and tongue, each for both hemispheres) (Vincent et al., 2006), 2 language maps (Broca's and Wernicke's areas) (Berntsen et al., 2006) and 7 cognitive control maps (medial frontal cortex, right anterior insula/frontal operculum, right dorsal lateral prefrontal cortex, left/right inferior frontal junction, left/right dorsal pre-motor cortex) (Cole and Schneider, 2007).

Preprocessing

The diffusion-weighted volumes were checked for motion, cardiac and table vibration-induced artefacts using the PATCH algorithm (Zwiers, 2010). With the default threshold, no artefacts were detected. The volumes were then realigned and corrected for eddy current-induced distortions using the integrated approach described in Andersson and Skare, 2002. In order to visualize clusters and their corresponding fibres with TrackVis (Wang et al., 2007) deterministic tractography was performed using the Diffusion Toolkit from (Wang et al., 2007) with a Q-Ball reconstruction model, and the FACT propagation algorithm with an angle threshold of 70° (Mori et al., 1999) yielding approximately 300.000 fibres per brain.

For the resting-state datasets we used several standard preprocessing steps. The first five images were discarded because of the possible spin saturation effects. After motion correction, the data were linearly coregistered with the DWI images using a affine transformation and resampled to a 2mm isotropic voxel size using FLIRT (Smith et al., 2004). The images were then temporally filtered with a low frequency cut-off of 0.01Hz and a high frequency cut-off of 0.1Hz using a fifth order Butterworth filter to reduce the effects of low and high frequency non-neural activity. Following this, the images were spatially smoothed using a Gaussian kernel of 5mm full width at half maximum.

Freesurfer (Dale et al., 1999; Fischl et al., 2004) was used on the anatomical scans to produce a white/grey matter segmentation as well as to determine surface representations of the cortex. The white/grey matter segmentation was then coregistered with the DWI data using a rigid-body linear transformation.

Scoring metric

According to (Schneider, 2009) the quality of a segmentation can be estimated by calculating the overlap of the clusters found with functional maps determined with localizer experiments. These functional maps are subdivided using three identifiers: a green ('hit'), a yellow ('unknown') and a red ('false positive') area. The voxels belonging to the green area of a map are considered to be definitely attributed to a specific brain function, while voxels belonging to the red area can definitely not be attributed to the respective function. Voxels inside a yellow area have high uncertainty of belonging to

the map's function and are neutral in the scoring process. For each map a score is then determined with Equation 2.1.

$$clusterscore_{map} = \frac{\#c_{voxels \in map_{green}} - \#c_{voxels \in map_{red}}}{\#voxels \in map_{green}} \quad (2.1)$$

For example if a cluster of 150 voxels in a segmentation would have an overlap of 50 voxels with a functional map of 200 green voxels, while 60 voxels would definitely not overlap with the functional map (leaving 40 voxels with unknown affiliation), then the score of the cluster in relation to that map would be 0% as $(50-60)/200 < 0$. The three best scoring clusters for a single map are added to the map score.

Using this metric obtaining a score of more than 0% for a functional map by chance is unlikely. The score for a whole brain is then the average of maximum scoring clusters for each functional map. The scoring standard required the participants to provide a segmentation with at most 600 clusters for each brain. Since the scores of the 19 functional areas are statistically independent and since scoring single functional maps by chance with more than 0% is unlikely, it is reasonable to assume that the scoring method provides a proper metric to evaluate the quality of a clustering. To give more statistical significance to this measure it is desirable to quantify probabilities for achieving specific scores by chance using random segmentations.

Method 1: Flow simulation based segmentation of high dimensional brain connectivity matrices

The method presented relies on graph theoretical principles and consists of two main steps. In step 1 we produce a voxel-based connectivity matrix using probabilistic tractography, which effectively creates the most detailed cortical network representation possible given the dataset. This network or graph can then be segmented using clustering methods specifically designed to identify groups within a graph. In step 2, we used the Markov Clustering Algorithm (MCL) by Van Dongen, 2000; Enright et al., 2002, which is designed to cluster large graphs into natural groups. As the algorithm only takes into account the adjacency matrix, it is bound to find cliques within the small-world network organization of the brain, unbiased by spatial or anatomical information.

Step 1: Probabilistic tractography

We used the probabilistic Q-Ball PICO approach, which is part of the Camino package (Cook et al., 2006), to build a grey matter (GM-to-GM) connectivity matrix. The Q-Ball reconstruction method was chosen because it is relatively fast and yet allows for the resolution of multiple-fibre structures, which are not handled satisfactorily by the diffusion tensor model. Probabilistic tractography was performed with 1000 iterations per principal diffusion direction per seed voxel. The connectivity matrix was built by tracking from one voxel in the GM mask at a time and storing the corresponding hit counts for all other voxels in the mask in a row. The rows of the matrix were then normalized by

dividing them by the number of iterations for the corresponding seed voxel. Note that as the tractography method employed is not symmetrical under exchange of seed and target, neither is the connectivity matrix.

Step 2: Clustering of the connectivity matrix using flow simulation

We applied graph clustering by flow simulation (van Dongen, 2000) to the connectivity matrix, a method suitable for finding natural clusters in a graph structure, which is also used to detect protein families (Enright et al., 2002). Clusters in a graph are characterised by the presence of many edges between the members of the cluster. Following this observation it can also be noted that flow or random walks on the graph will infrequently go from one cluster to another. The algorithm exploits this by iteratively pruning graph edges if they have a low probability of being traversed during flow simulation. At the same time edges which are crossed relatively often during flow simulation will be iteratively reinforced and receive a higher current. See Figure 2.1 for an illustration of this process.

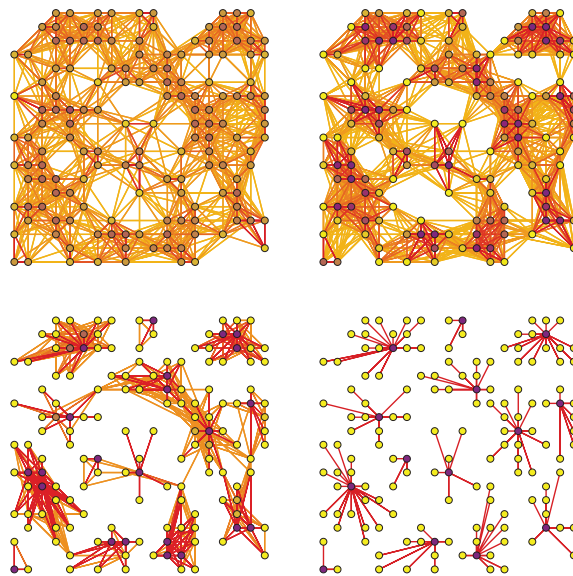


Figure 2.1

Figure adapted from van Dongen (2000). An illustration of how the MCL algorithm clusters a complex graph within 4 tuples of inflation/expansion steps. The color coding of edges and vertices indicates the probability of being traversed after the expansion step (purple indicates a higher probability than yellow). The inflation step prunes those edges with low probability of being traversed until an equilibrium state is reached, which in the case of this example consists of 14 clusters.

The MCL algorithm mainly simulates flow using two alternating algebraic operations on a stochastic matrix. The first operation, also called the expansion step, is a simple multiplication of the matrix with itself which is analogous to the spreading out of flow or

making flow in the graph more homogeneous. Another way of looking at the expansion is to consider it as a single step of a random walk. The second operation, conventionally called the inflation step (or pruning step), is modelling the contraction of flow, which makes regions of higher current thicker and regions of lower current thinner, while pruning edges where current hardly flows. The mathematical operation for the inflation step is a Hadamard power followed by a diagonal scaling which is expressed with the function Γ in Algorithm 1. The expansion and inflation operations are alternated until an equilibrium state is reached in the form of a doubly idempotent matrix, a matrix that does not change under the two operations.

Algorithm 1: Pseudocode of the MCL algorithm.

```

G is a graph;
set  $\Gamma$  with inflation parameter  $I$  ;           /* affects granularity */
set  $M_1$  to be the matrix of random walks of G;
while (change) do
     $M_2 = M_1 * M_1$  ;                           /* expansion */
     $M_1 = \Gamma(M_2)$  ;                         /* inflation */
    change = difference( $M_1, M_2$ );
end
set CLUSTERING as the components of  $M_1$ ;

```

The matrix operation steps of the MCL algorithm have been parallelized, which allows for a reasonable computational execution time given modern computer architecture. The method was applied using three inflation factors $I=1.5$, $I=2.0$, $I=2.5$, producing clusterings with different granularities. The higher the inflation factor chosen, the faster the pruning of the graph structure will be performed and the more clusters will result by applying MCL.

Method 2: Structural k-means

In the second method we investigated clusters found among grey matter voxels using k-means clustering with the Euclidean distance measure of the spatial location of the voxels. K-means clustering (MacKay, 2002) is an unsupervised clustering method that is able to find the centres of natural clusters in data. It is similar to the expectation-maximization algorithm for Gaussian mixtures, with the advantage that it is computationally faster. We have used the method under the assumption that functional regions that are generated based on fMRI measurements are closely related to basic anatomical structures such as sulci and gyri on the cerebral cortex. This is in accordance with the evolutionary theory as proposed by (Essen, 1997).

Method 3: Clustering of ICA networks

For the third method, we first used independent component analysis (ICA) to capture the spatial-temporal dynamics of the resting state networks. As resulting networks can

overlap spatially, we then clustered the grey matter using the resting state networks with their z-scores in a second step.

Step 1: Independent Component Analysis on resting-state data

To minimize the computational burden, only the voxels within the grey matter mask were used for further analysis. Independent component analysis (ICA) was performed on the masked data using FSL version 4.1 MELODIC (Smith et al., 2004). ICA is able to separate the time series of the whole brain into different spatio-temporal components (Beckmann et al., 2005). When applied to resting state data, ICA can identify artefactual components such as head movements during scanning and low-frequency (0.01 - 0.1Hz) neural networks such as those associated with working memory, motor function, language and the default mode network (Damoiseaux et al., 2006; Seeley et al., 2009). The output number of components was set to 40 (approximately 1/8 the data points of the time course). The non-neural noise components were identified by visual inspection and were excluded from further analysis.

Step 2: Clustering based on z-scores of independent components

Each of the grey matter voxels was subsequently assigned to the component with a maximal z-score value, which resulted in slightly less than 40 network clusters. A network cluster would mostly then consist of several larger clouds of contiguous voxels, which would then be separated such that non-neighbouring voxels were assigned to their final clusters.

Results

In the following subsections we present the outcomes for each method.

Method 1: Flow simulation based segmentation of high dimensional brain connectivity matrices

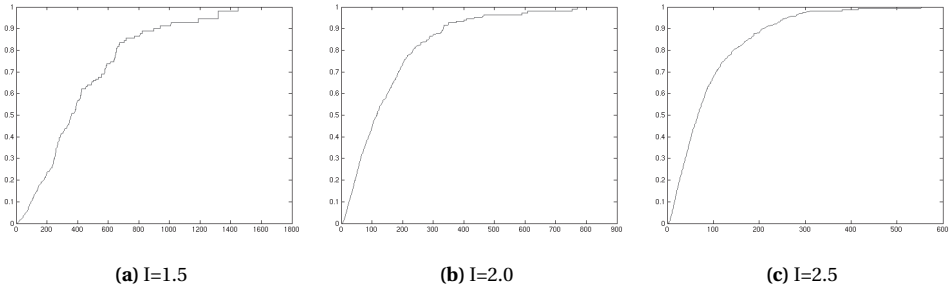
The dimensionality of the initial connectivity matrices ranged from approximately 60,000 to 75,000 nodes. The sparsity of a matrix describes how densely or sparse a matrix is populated and is given by the percentage of non-zero elements of a matrix. The first step of the method produced matrices with sparsity between 0.7% and 1.1% (or between 1.2% and 1.8% if we consider the symmetry of the found connections). The tractography process is computationally intensive and typically was possible within 110 CPU-core hours per brain.

For the graph clustering step, we used the MCL algorithm with three different inflation factors: $I=1.5$, 2.0 and 2.5, this resulted in brain segmentations of approximately 400, 1300 and 2200 clusters for all brains see Table 2.1. These findings are indicative that the approach is consistent across brains, despite the varying dimensions and sparsities of the initial connectivity matrices. This result is also indicative that the brains have similar topological organization. We found that with an inflation factor of $I=2.0$, only

id	I=1.5	I=2.0	I=2.5
Brain 0	413	1367	2194
Brain 1	437	1383	2167
Brain 2	392	1330	2189

Table 2.1

The table shows the number of clusters for all three brains using different MCL inflation factors.

**Figure 2.2**

Cumulative distributions for the three investigated inflation factors are displayed. The charts show the percentage of voxels on the y-axis assigned against the maximum cluster size on the x-axis.

20% of all grey matter is segmented into clusters with less than 50 voxels, as can be seen in the cumulative distribution in Figure 2.2, leaving most clusters with a higher voxel count.

As can be seen from Figure 2.3, clusters are mostly contiguous on the cortical sheet, which is a typical perceived brain organization in fMRI experiments. Using Freesurfer we mapped the grey matter segmentations of brain0 to the cortical surface in Figure 2.4, which illustrates this finding more convincingly. Using $I=1.5$ the method also produces clusters which are not contiguous and located in separate brain regions such as the sample cluster in Figure 2.5. When putting the cluster in contrast with fibres estimated using deterministic tractography it can be seen that a large portion of the fibres passing through the cluster are inherently related to the long segment of the arcuate fasciculus, a well described fibre bundle belonging to the language network (Catani et al., 2005). This provides evidence that the clustered cortical regions are related to fibre bundle organization within the brain.

We also investigated the correspondence between the clusters and the maps found in the fMRI localizer experiments. By applying the Pittsburgh scoring metric on brain0, we found that the clustering showed an overall overlap of approximately 65% on all maps using an inflation factor of $I=2.0$, which corresponds to a score of 30%. Most notably, V1 of the right hemisphere showed the highest correspondence with the segmentation as an overlap of 70% was found, illustrated in Figure 2.6. Using MCL with inflation

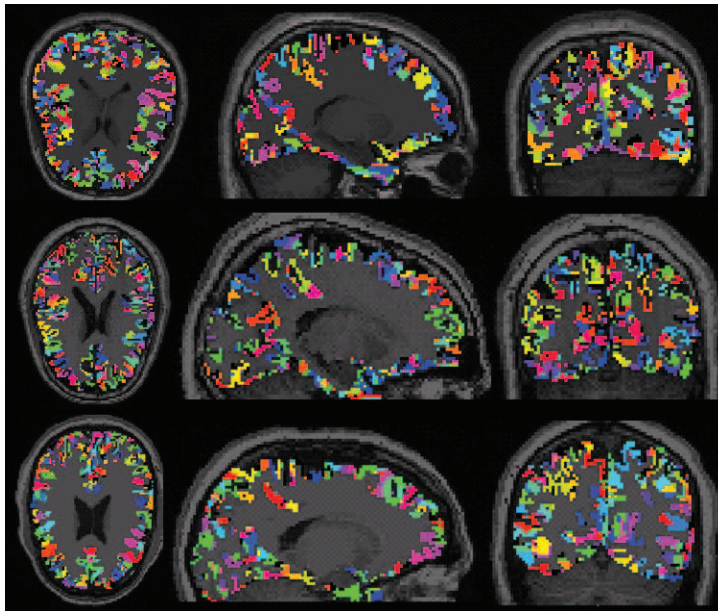


Figure 2.3

Shows a MCL segmentation using $I=2.0$ for all 3 brains displayed with an axial, a sagittal and a coronal slice using a voxel representation.

factor $I=1.5$ results in a much lower score of 16% as the clusters found tend to be too large, which increases the false positive rate. By looking at the language related areas Broca and Wernicke for instance, we find that using $I=2.0$ the scores are 35% and 13% respectively, while they are both 0% using $I=1.5$. If we look at the best matching clusters for the $I=1.5$ segmentation with Broca's and Wernicke's area in Figure 2.7, the discerning viewer will see that although the scores are 0% for both areas, there is still a visible overlap for Broca's area. And while the exact location of Broca's area using in-vivo scanning methods is dependent upon the experimental setup, it is generally understood that Broca's and Wernicke's area should be connected through the long segment of the arcuate fasciculus, a property demonstrated in Figure 2.8. It should be noted that some of the motor tasks used in the experimental setup did not separate sensory- and motor-related cortical activation distinctively and therefore lower overlap in these areas was to be expected. However, overall, the results indicate that there is a relationship between cortical DWI profiles and neuronal activity as measured with fMRI (Koch et al., 2002).

Method 2: Structural k-means clustering

A segmentation of brain0 with $k=570$ clusters can be seen in Figure 2.9, displayed in different ways. We found that structural k-means clustering visibly distinguishes between cortical structures such as gyri and sulci as shown in Figure 2.10 in the sagittal and coronal view. However different banks of a single sulcus are often not differentiated on the given resolution. Using between $k=150$ and $k=2050$ clusters per hemisphere, we found that the resulting segmentation shows a good correspondence with the maps

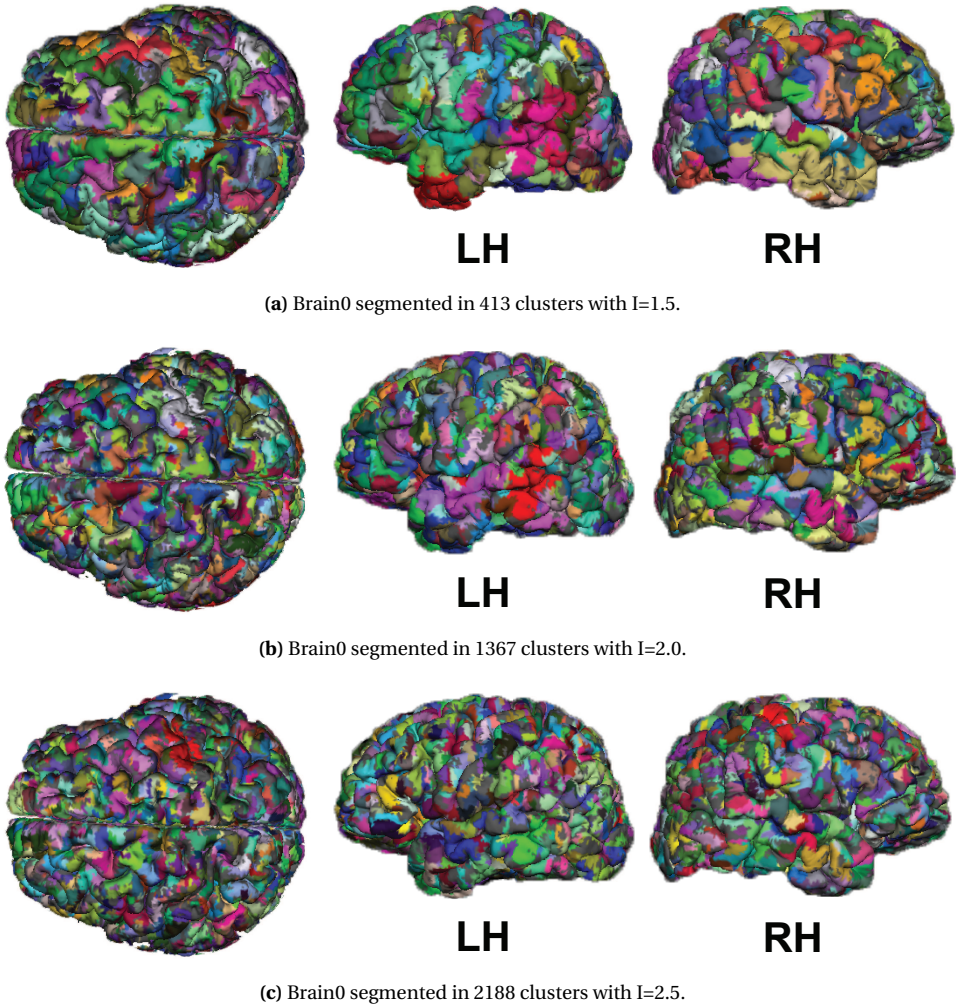


Figure 2.4 Shows clusters mapped onto the pial surface using different inflation factors I .

determined with fMRI experiments, with scores ranging from 30 to 35% (corresponding to 65 to 67.5% overlap) as displayed in Figure 2.10. The optimum number of clusters with respect to the scoring standards and method is approximately 1000 clusters. The variability of the scores is explained by the sensitivity of the scoring method as well as the dependence of a segmentation on the semi-random initialization of the means. However the location of the clusters will always align with cortical structures giving it a high probability of success.

Method 3: Clustering of ICA networks

The segmentation method generated approximately 400 contiguous clusters capturing temporal dynamics on the global scale, resulting from the ICA based approach. By

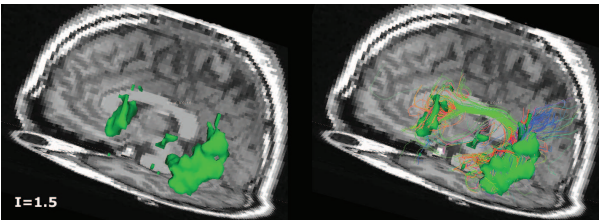


Figure 2.5
Shows a single cluster of a MCL segmentation using $I=1.5$ on brain0 and related fibres with endpoints in the cluster.

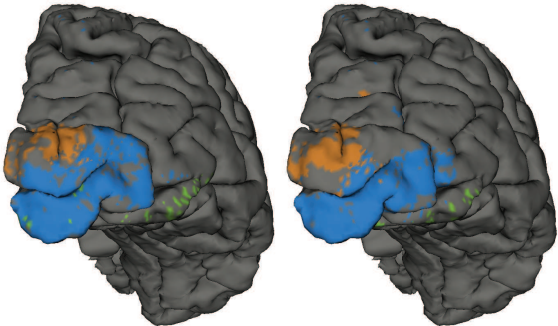


Figure 2.6
Displayed are the visual areas V1 (in blue) and V2 dorsal (in brown) at the left as determined with fMRI (included are the 'hit' and 'unknown' areas), while at the right the corresponding counterparts using MCL with $I=2.0$ are shown.

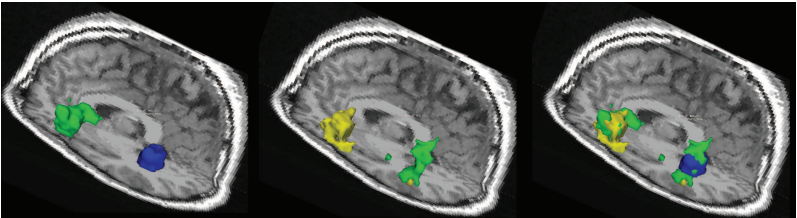


Figure 2.7
In the left section, Broca's area(left) and Wernicke's area (right) are displayed as determined with fMRI for brain0 (included are the 'hit' and 'unknown' areas). In the middle the corresponding clusters using MCL ($I=1.5$) are displayed, while the right displays their overlap with the presumed areas.

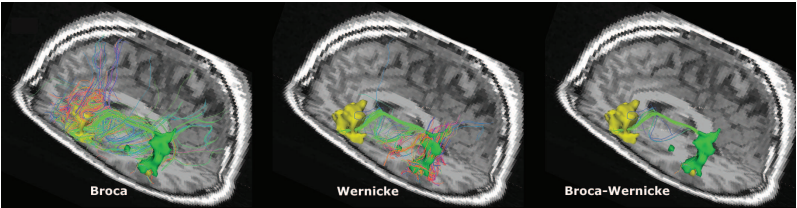


Figure 2.8
Displays the fibres with endpoints in Broca's area (left brain) and Wernicke's area (right brain) as determined with the MCL method ($I=1.5$) for brain0, while the right brain shows all fibres with endpoints in both areas.

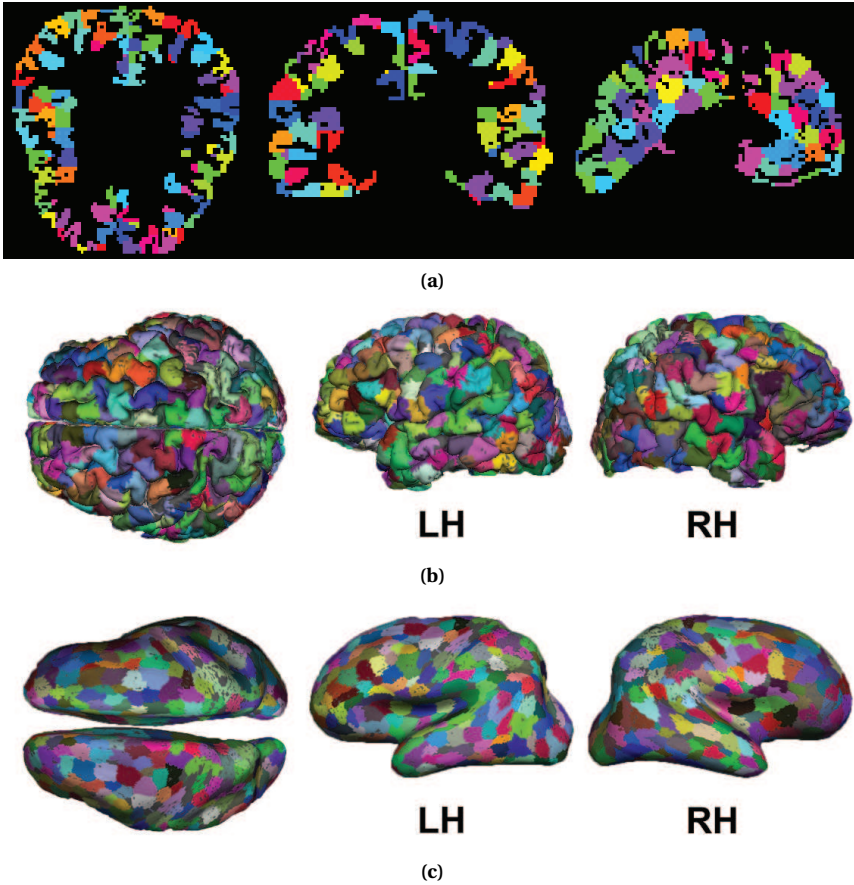


Figure 2.9

Shows a sample k-means segmentation using $k=570$ displayed with an axial, a coronal and an sagittal slice using a voxel representation (a), and a cortical representation using Freesurfer on the pial (b) and inflated (c) surface.

looking at a sample segmentation such as in Figure 2.11, we find that most clusters are rather large compared to the other two approaches. With a 5.7% overall score of these clusters, the match with the task related fMRI is relatively low. For the generation of macroscopic network models of the human brain the approach presented here is therefore not yet suitable. This result is in line with previous results (Beckmann et al., 2005; Damoiseaux et al., 2006) showing that ICA mainly detects large scale networks such as the default mode network.

The clusters however showed to have correspondences with fiber tracts, which can be indicative for the methods potential. For example in Figure 2.12, an inter hemispherical cluster located at the superior part of the postcentral gyrus is contrasted with intersecting fibers using a seed regional approach. We find that the cluster is related to two major fiber bundles, namely a part of the corpus callosum and the ascending fibres leading to the somatosensory cortex, as can be seen in Figure 2.12(c).

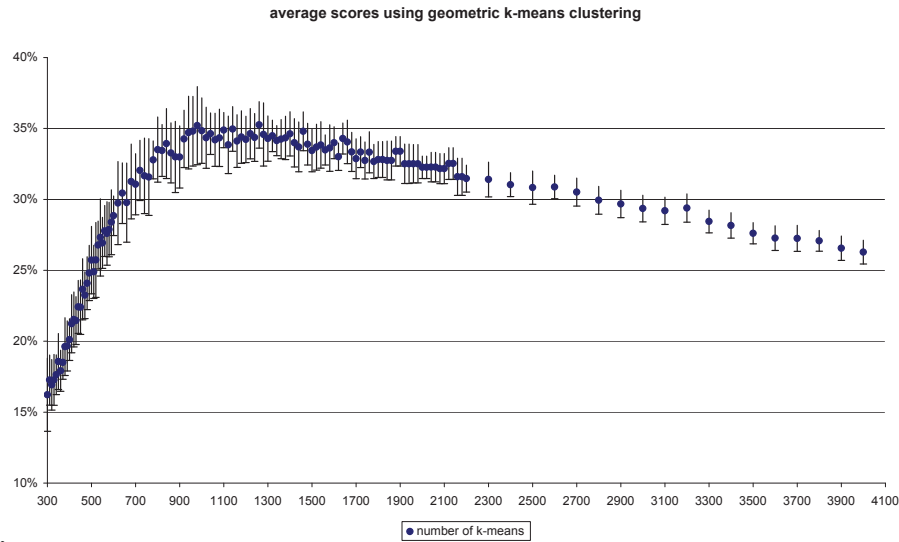


Figure 2.10
The chart shows the average scores on 19 maps determined with fMRI for $k > 300$. Each dot represents the average score over 20 trials for a given k . The error bars show the standard deviation of the scores.

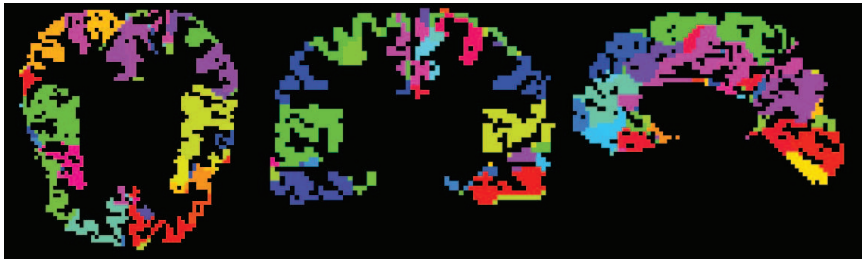


Figure 2.11
Shows a segmentation based on z-scores of resting-state fMRI ICA components visualized using a voxel representation of an axial, a coronal and a sagittal slice.

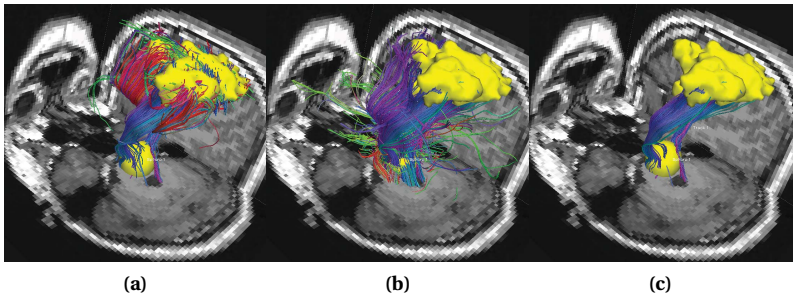


Figure 2.12
All sub-figures show in yellow a single cluster from the segmentation using method 3 as well as a manually positioned ROI at the brain stem. Sub-figure (a) shows all fibres with endpoints in the cluster from method 3; (b) shows all fibres going through the ROI; (c) shows all fibres with endpoints in the found cluster while passing through the brainstem.

Discussion

In this article we have presented three methods to segment the brain, each using different types of information. All the clusters obtained from the methods show significant overlap with the functional regions determined by the PBC2009. In our opinion the geometry based clustering method is a good starting point to compare clustering methods that seek to identify functional regions. A better geometric baseline clustering can probably be created by fitting Gaussian mixture models with the EM-algorithm. The scores from the k-means methods are however indicative that the anatomical structure is closely linked with functional areas. The fairly high correspondence with the fMRI maps is in accordance with the evolutionary theory on the cortical organization of the brain described in Essen, (1997). The k-means method can also be employed for generating a finer anatomically sound segmentation of larger clusters, for example those found by method three.

We have successfully generated whole brain segmentations for individual brains using a singular graph theoretical random walk paradigm. The underlying assumption of the flow simulation based approach is that brain connections and their endpoints are organized in such a way that random flow simulation within the pathways would identify regions that work together as single units. The assumption can be warranted with the Hebbian theory, which postulated that cells which fire together wire together.

Although the initial results of applying the MCL method to segment the brain appear to be promising, we believe that there still is room for significant improvement. The quality of the segmentation is bound by the connectivity measures used between grey matter voxels. The more accurate the connectivity measure is, the better will be the final outcome. In this regard it could be argued that tractography should be seeded on the interface between grey and white matter, as tractography in grey matter may be problematic. However, because of the rather coarse resolution of the DWI data compared to the actual thickness of the surface, this is likely to be difficult in practice. Moreover, the probabilistic tracking algorithms employed here do not suffer nearly as much as deterministic methods from starting in low-anisotropy GM voxels. The main obstacle in any tractography based method remains the limitation of the DWI resolution and that the found fibre tracts cannot be validated.

In our research we have focused solely on the segmentation of the neocortex, but (Behrens, Johansen-Berg, et al., 2003; Klein et al., 2010; Solano-Castiella et al., 2010) have showed that tractography based methods also can be used to segment sub-cortical nuclei such as the thalamus or amygdala, which can be a good argument to include these nuclei in future versions of this method. Considering graph theoretical principles, the results represented should be improved by adding sub-cortical cortices such as the grey matter from amygdala or the hippocampus. A problem of integrating a sub-cortical nucleus like the thalamus could be that axons are starting, terminating and passing through the nucleus cannot be distinguished with current DWI techniques. In the neocortex however, axons either start or terminate.

In conclusion on the MCL method, it is our belief that the application of flow sim-

ulation or random walks is a promising technique to segment the brain into clusters useful for macroscopic models. We also favour the delineation of functional regions using connectivity profiles, as any effective connection between brain regions in two different loci and their information exchange can only be facilitated with the existence of an axonal connection.

We found that the resting-state fMRI based approach without any additional geometrical constraints or fibre structure information has trouble to identify the regions specified by the competition. This is particularly interesting because these regions are determined through task-related fMRI experiments. But using more ICA components, we believe that a methodologically similar approach might produce better results with respect to the scoring method. However by considering network principles it is more difficult to determine effective connectivity on the basis of functional activity as it would be if we would consider actual fibre connections. A similar conclusion has been drawn by Honey et al., 2009, who have shown that it is possible to predict functional connectivity from structural connectivity but not vice-versa.

The main disadvantage all methods have in common is that the clusters are difficult to align between subjects, which leads to the question as to whether the present methods are usable for group network comparison analysis. On the other hand, these segmentations allow us to perform detailed individual based network analysis, free of the imposed cortical landmark biases of the AAL or similar templates. The consequence is that for using these methods optimally we need to develop inter-subject network alignment methods, based on topological connectivity patterns. And while at this point there are no specific solutions available for resolving topological alignment of complex networks, we consider it a challenge to overcome this issue using graph theoretic means rather than choosing to continue using templates. In our opinion, this holds a brighter future, as the comparison between brains over a standardized brain may lead to a mismatch of functional identical regions across subjects. Another reason for developing better brain networks is the prospect that they could give us better insight on the relationship between loss of brain function with respect to a lesion and the resulting brain reorganization. In a way the connectomes developed by Hagmann et al., 2008 and the papers that resulted from using these matrices (Bassett et al., 2009; Honey et al., 2009) indicate a trend towards developing better analysis techniques on individual networks. At some point it is desirable to compare the essential properties of these networks between subjects and in order to do that, it is important to depart from the conventional idea of using templates or arbitrary segmentations.

Finally it should be mentioned that all methods have been evaluated using fMRI localizer experiments, typically using 3mm voxels. The accuracy of the presented scoring results is therefore subject to yet undefined error margins and the emphasis of the article should be on how the presented methods actually segment the brain rather than how well they do it. We believe that the scoring methods used can be improved using high-resolution fMRI experimental setups. As there are currently no gold standards for most parts of the brain as to what constitutes a cortical unit in the

brain, we also believe it would be helpful to further develop accurate maps for the scoring metric. The fairly well-defined visual areas are considered suitable for the use of a scoring gold standard, but the inclusion of other well-defined areas would improve the quality estimation of segmentation methods.

3

**Topographic hub maps of the human
structural neocortical network**

Abstract

Hubs within the neocortical structural network determined by graph theoretical analysis play a crucial role in brain function. We mapped neocortical hubs topographically, using a sample population of 63 young adults. Subjects were imaged with high resolution structural and diffusion weighted magnetic resonance imaging techniques. Multiple network configurations were then constructed per subject, using random parcellations to define the nodes and using fibre tractography to determine the connectivity between the nodes. The networks were analysed with graph theoretical measures. Our results give reference maps of hub distribution measured with betweenness centrality and node degree. The loci of the hubs correspond with key areas from known overlapping cognitive networks. Several hubs were asymmetrically organized across hemispheres. Furthermore, females have hubs with higher betweenness centrality and males have hubs with higher node degree. Female networks have higher small-world indices.

Adapted from: Nijhuis, EHJ, Van Cappellen van Walsum, A-M, Norris, DG, 2013. Topographic Hub Maps of the Human Structural Neocortical Network. *PLoS ONE* 8, e65511.

“The whole is more than the sum of its parts.”

-Aristotle-

Introduction

Recent studies have investigated the human connectome with graph theory by dividing the neocortex into 100-1000 parcels and examining the anatomical connections derived from diffusion weighted magnetic resonance imaging (DW-MRI or DWI) techniques (Hagmann et al., 2007, 2008; Iturria-Medina et al., 2008; Gong, He, et al., 2009; Kaiser, 2011; van den Heuvel and Sporns, 2011). Hubs, highly connected regions, have been of particular interest. They were extensively investigated because of their presumed criticality for the function of the brain (Alstott et al., 2009; van den Heuvel and Sporns, 2011). To date it has been shown that neocortical hubs can be found in regions associated with the default mode network (Gusnard and Raichle, 2001; Hagmann et al., 2008; van den Heuvel and Sporns, 2011). At the same time lesion studies have identified critical brain regions related to important neurocognitive networks (Mesulam, 1998; Nieuwenhuys et al., 2007; Turken and Dronkers, 2011). These critical regions should be considered as candidate hubs, as they are located in highly connected association cortices.

We therefore hypothesized that, besides the default network, other important neurocognitive networks should contain hubs that would be detectable by means of graph theoretical analysis. To test this hypothesis we extend previous work with a detailed map of the neocortex which displays the distribution of its hubs. This is in accordance with previous suggestions to investigate the human connectome in more detail with a larger dataset (Van den Heuvel and Sporns, 2011). Here we present hub maps based on high resolution data, which can be used as a reference for the location of neocortical hubs.

The hubs of a network can be broadly separated into two types: provincial and connector hubs (Guimerà and Amaral, 2005; Guimerà et al., 2005; Bullmore and Sporns, 2009). Hubs are usually determined with measures which capture the structural importance of a node with respect to the rest of the network (Sporns et al., 2007; Bullmore and Sporns, 2009). The simplest measure is the degree of a node, which is the number of connections to other nodes and reflects the local importance of a node (Barthelemy, 2004). Betweenness centrality, which describes the fraction of shortest paths through a specific node, is a good additional measure as it also incorporates global information (Barthelemy, 2004). We consider it axiomatic that provincial hubs must show high node degree, whereas connector hubs must show a high betweenness centrality. In this paper we used node degree and the betweenness centrality measures to identify hub regions.

To create topographic maps which show how the hubs are distributed, four key aspects were considered in the mapping procedure. First, we used a homogeneous group of 63 young adults with similar age, education and same handedness scanned with a

high resolution MRI protocol, which allowed us to make high resolution connectivity matrices. Secondly, we excluded subcortical nuclei from the analysis. The resulting connectivity maps consider exclusively the neocortex and thus avoid mixing polysynaptic with monosynaptic cortico-cortical connections. Thirdly we analysed multiple randomly generated parcellations for each subject in order to have a topographic display of hubs and to minimize node selection biases. And fourthly, to consider the anatomical variability across subjects, we used a surface-based analysis to average the individual maps on a standard brain.

Using our mapping procedure eighteen hub regions on the neocortex were identified which are related to known neurocognitive networks. Furthermore statistically significant differences in the hubs' distribution across hemispheres and between genders were found.

As differences in hub organization should be related to differences in network topology we complemented our analysis with a small-worldness analysis of the entire brain and for each hemisphere. This approach was chosen, because the small-worldness measure describes global network properties and because the human brain has a small-world topology (Honey and Sporns, 2008; Alstott et al., 2009).

Materials and methods

Ethics statement

The study was conducted at the Donders Institute for Brain, Cognition and Behaviour, Radboud University Nijmegen the Netherlands with the general institutional ethics approval from the local ethics committee (Commissie Mensgebonden Onderzoek region Arnhem-Nijmegen, The Netherlands). All participants provided written informed consent in accordance with the declaration of Helsinki.

Participants

Sixty-three healthy subjects [37 females, 26 males, mean age, 22.75 ± 2.94 (SD) yr] from the Donders Institute Connectivity Data Set 1 (DICOD1) with 81 subjects under the age of 35 were included for this study. Exclusion criteria for the used dataset were: left-handedness, incomplete DWI data and neurological or psychiatric disorders.

MRI acquisition

All subjects were scanned on a Siemens 3T TIM Trio system with a 32 channel head coil at the Donders Institute for Brain, Cognition and Behaviour, Radboud University Nijmegen.

Anatomical scan

High resolution anatomical scans were acquired using a T1-weighted 3D MPRAGE sequence with TE=3.03ms, TR=2300ms, TI=1100ms, a flip angle of 8° with 1mm isotropic voxels.

Diffusion weighted imaging

Diffusion weighted imaging volumes were acquired using a single-shot echo-planar imaging (EPI) sequence with phase encoding in the anterior to posterior direction, with TE=101 ms, TR=13.0s, 2mm isotropic voxels and taken in 256 non-collinear directions at a b-value of 1500 s/mm². In addition, 28 volumes with b=0 s/mm² were acquired between the diffusion weighted volumes.

Data analysis

For each of the 63 subjects twenty different connectomes were generated and estimated for each connectome several network measures.

Before calculating network measures to the neocortical network the nodes and edges need to be defined. While edges are considered to be represented by axonal connections in the subcortical white matter and can be estimated using different DWI techniques, the question of what constitutes a neocortical node is undetermined. Previous work has used fixed anatomical based templates across a population of subjects (Hagmann et al., 2007; Gong, He, et al., 2009). Their approach benefits from being able to compare anatomically identical nodes across subjects. Previous work has shown that defining the nodal configuration with anatomical templates may lead to inappropriate node representations which then can lead to incorrect functional network estimates (Smith et al., 2010) or may poorly characterize U-fibres (Zalesky et al., 2010). We therefore resolved this dilemma using a template free approach and individually parcellated each of our 63 subjects twenty times, in order to reduce the effects of node selection biases and potential fragmentation of hubs. A detailed description of the processing steps is given in the following sections.

Step 1: creation of neocortical network nodes

The anatomical scans were analysed using Freesurfer (Dale et al., 1999) to segment the brains into cortical and subcortical structures. We used the recommended processing pipeline which included manually correcting for Talairach alignment, skull removal, white matter surface and grey matter surface errors. One subject was excluded from the DICOD1 dataset as grey matter hyperintensities could not be corrected.

Each neocortical hemisphere was then parceled twenty times into 500 ROIs using the k-means algorithm (Seber, 2008) informed with the Euclidean distances between grey matter voxels. The procedure is not deterministic as the final parcellation depends on the random initialization of the k-means. The process therefore produced twenty different neocortical parcellation schemes for each brain. The contiguous ROIs of a parcellation had an average size of $0.1\% \pm 0.016\%$ (SD) of the total neocortical volume. Each ROI then defined a node in the structural connectivity mapping step.

Step 2: diffusion preprocessing and tractography

The diffusion-weighted images were checked for motion, cardiac and table vibration-induced artefacts using the PATCH algorithm (Zwiers, 2010). The volumes were then

realigned and corrected for eddy current-induced distortions with the integrated approach described in (Andersson and Skare, 2002). Finally the volumes were unwarped in the phase encoding direction onto the anatomical scan to reduce the effects of phase evolution in the EPI read out direction (Visser et al., 2010). We used the multi-fibre reconstruction PASMRI with 16 basis functions (Cook et al., 2006) and performed interpolated deterministic tractography using Euler's algorithm with a 0.2mm step size seeding on the 1mm isotropic voxels of the coregistered Freesurfer white matter mask with a maximum of three main principal diffusion directions. The choice of the reconstruction and tractography methods was driven by results presented in Guevara et al., 2010, who showed that using a spherical deconvolution transform reconstruction in combination with deterministic tractography results in the highest fraction of valid fibre tracts found in a phantom.

Step 3: structural connectivity mapping

For each brain a network was then reconstructed by defining the ROIs as nodes and the number of tracked fibres between ROIs as the edge strengths. The network matrices were then binarized without thresholding the strength of a connection. The appearance of the hub maps did not substantially change when thresholding, therefore we opted against it as any threshold would have been arbitrarily chosen. The connectivity matrices, with an average of $9.77 \pm 1.03\%$ (SD) of all possible connections, were then used for graph theoretical analysis.

Step 4: connectome analysis

A network analysis was performed with the Brain Connectivity Toolbox (Rubinov and Sporns, 2010) to determine the node degree and betweenness centrality for all twenty parcellations of each brain. A correlation analysis (see Figure 3.1) on the node degree and cluster size of all nodes across all brains concluded that the node degree could not be predicted from the cluster size as $r^2_{1259998} = .023$. Therefore it can be assumed that the network measures calculated for each node do not reflect a cluster size dependent artefact induced by the parcellation heuristic.

To compute subject specific hub maps each voxel's degree and betweenness centrality was taken as an average of the twenty clusters which it fell within. The results were then projected from voxelspace onto the cortical surfaces using Freesurfer.

Step 5: mapping network parameters to average surface

In the last steps we registered all subject specific maps to the Freesurfer average surface, to overlay anatomically identical areas. They were then smoothed with a 10 mm full width at half maximum kernel, to decrease spatial variability between subjects of putative hub areas. Finally the individual hub maps were averaged leading to topographic hub maps, displayed in Figures 3.2 and 3.3.

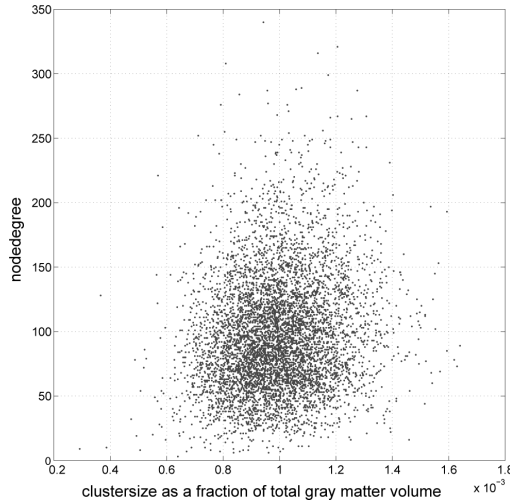


Figure 3.1

Scatter plot describing the relationship between node degree [mean $97.59 \pm 43.73(\text{SD})$] and cluster volume size as a fraction of the entire grey matter volume [median 0.099%, 0.016% (SD)] of a subset of 6,300 brain network nodes from all subjects. The correlation of the measures between all nodes is $r_{1259998} = .15$.

Step 6: identifying hub regions and hub score asymmetry/gender analysis

Regions on the topographic betweenness centrality map with values in the 80th percentile were defined as hub regions (see Figure 3.4). This definition led to large contiguous hub regions in the medial cortices which encompassed several independent peaks. Using Freesurfer ROI drawing tools we then defined regions of interest by separating areas along the inflection points between distinct peaks. For the left anterior superior temporal gyrus and the right inferior parietal lobe / posterior temporal lobe / anterior occipital lobe region two distinct peaks were combined to match the corresponding contra-lateral areas. We then defined the maximum value in node degree or betweenness centrality within a region as its hub score. The regions were also used to determine hub scores for individual subjects. Using a two-sample t-test we then tested for statistically significant differences between the hub scores from individuals of anatomically corresponding regions across hemispheres. We also used the same procedure to test for gender differences in the hub scores.

Step 7: calculating and analysing small-world indices

For each brain small-world indices σ were calculated for the entire connectivity matrix, the subgraph representing the left hemisphere σ_{lh} , the right hemisphere σ_{rh} as well as the difference $\delta_{lh-rh} = \sigma_{lh} - \sigma_{rh}$ of both hemispheres, which we defined as the small-world asymmetry index. Small-world indices were estimated by calculating the fraction σ in Equation 3.1 which is determined by the average cluster coefficients C and C_{rand} of all nodes and the characteristic paths γ and γ_{rand} in a network and an equivalent

random constructed network (Sporns et al., 2005).

$$\sigma = \frac{C * \gamma_{rand}}{\gamma * C_{rand}} \quad (3.2)$$

As each brain was parcelled twenty times the average of each index across the parcellations was used. We analysed the interaction of the small-world indices with each other, with gender and brain volume, as computed by Freesurfer, using SPSS.

Results

We analysed the neocortical connectomes of 63 young adults extracted from a multi-modal MRI dataset and mapped the outcomes on the Freesurfer (Dale et al., 1999) group average brain. In Figures 3.2 and 3.3 the topographic hub maps are displayed on the Freesurfer standard brain surface, resulting from averaging betweenness centrality and the node degree values across subjects.

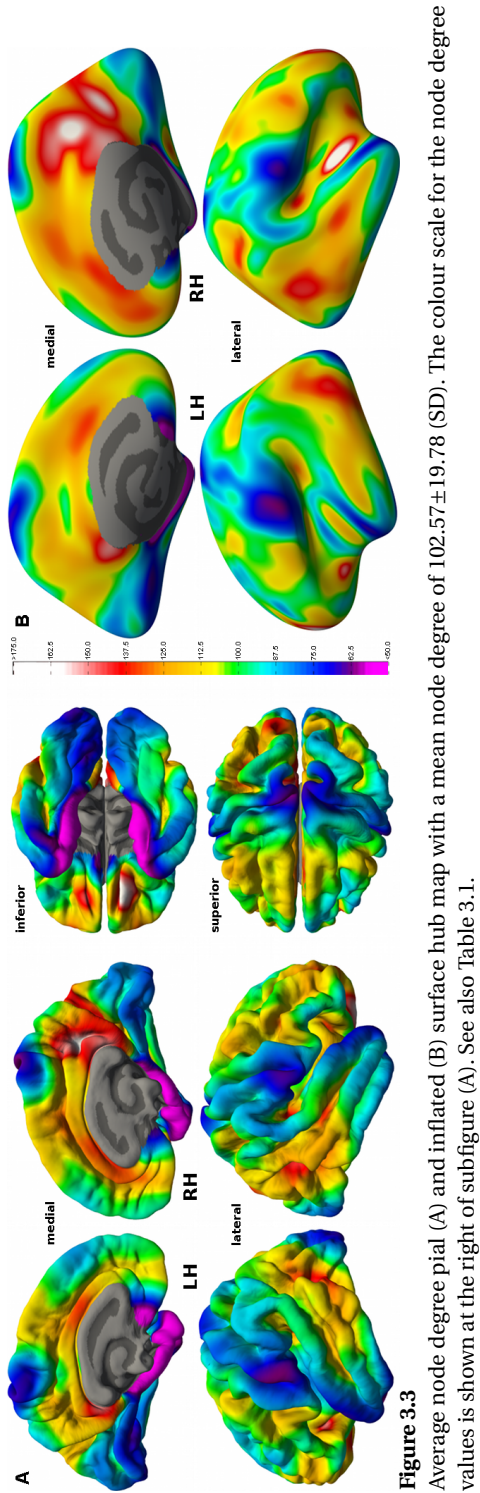
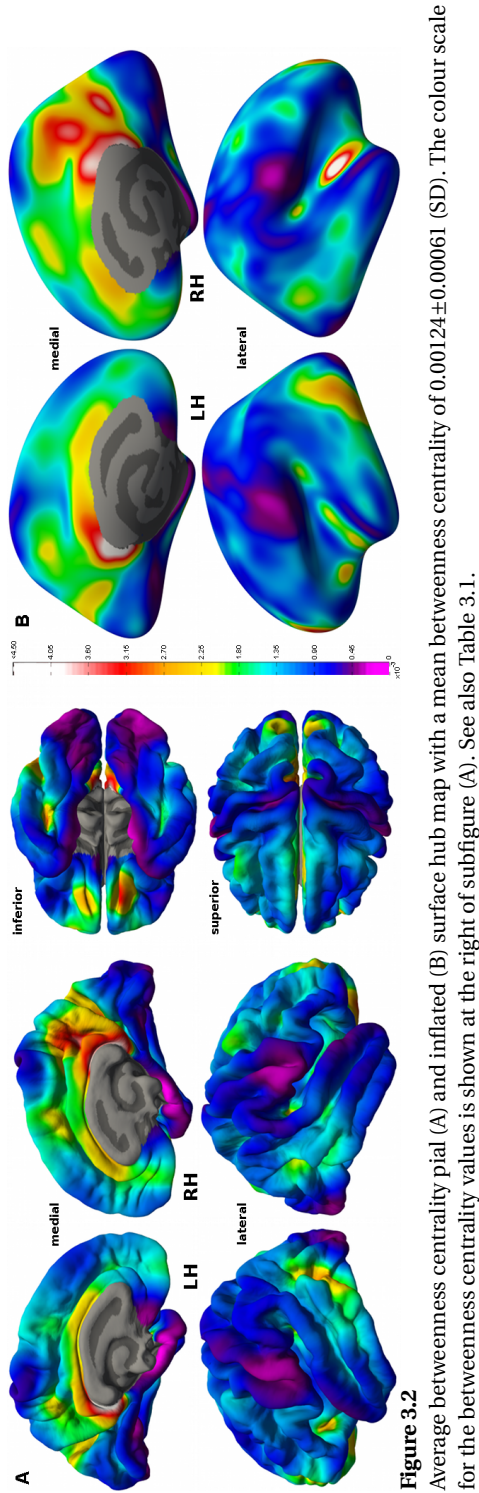
How hub regions were defined

By comparing the node degree and the betweenness centrality maps we observed that in the human brain hub regions are more pronounced in the betweenness centrality map. This can best be explained with regard to the distributions of the hub values. The distribution of betweenness centrality values for individuals appear to follow a power law with a long tail whereas node degree values appear normally distributed skewed to the right with a longer tail. The appearance of the node degree distribution classifies the produced networks as single-scale small-world networks (Amaral et al., 2000). To define hub regions we used the betweenness centrality map, because the distribution of betweenness centrality values had a longer tail than the distribution of node degree values. Following the Pareto principle (Pareto, 1971), we used the 80th percentile of the betweenness centrality map (vertices with values above 0.00164) to define hub regions of interest (see materials and methods step 6).

Anatomical locations of hub regions

We identified eighteen hub regions based on the topographic betweenness centrality hub map (see Figure 3.4). A description of the anatomical locations can be found in the table of Figure 3.4. Neighbouring hub regions were manually separated at their inflection line. For readability we will sometimes refer to hubs with their numbers from the table in Figure 3.4 written in brackets.

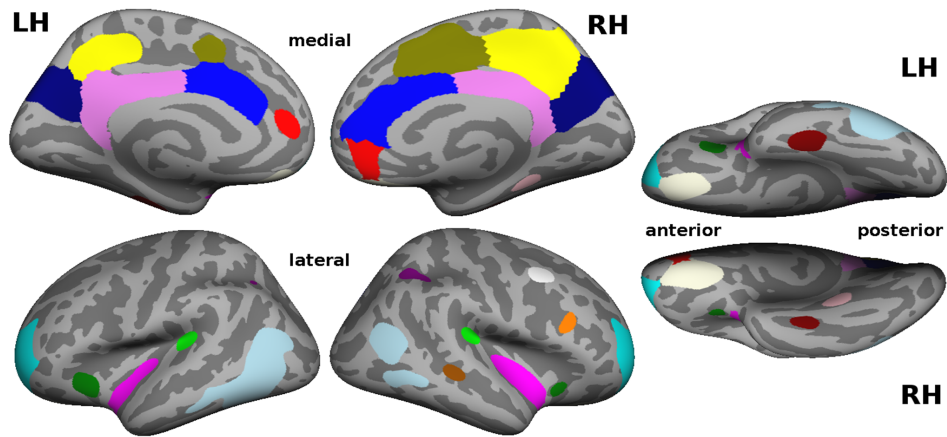
In all but four cases we found bilateral hub representations. For hub (1) the anterior lateral sulcus in the left hemisphere and hub (8) in the angular gyrus and occipito-temporal area, we combined two distinct peaks to a single hub region in order to match the contra-lateral hub region.



id	name of hub region	betweenness centrality		node degree	
		left hemisphere	right hemisphere	left hemisphere	right hemisphere
1	anterior superior temporal gyrus	0.00233	0.00458	120.9	178.7
2	posterior/retrosplenial cingulate gyrus	0.00436	0.00396	152.2	155.0
3	parieto-occipital sulcus	0.00234	0.00368	119.6	158.7
4	precuneus	0.00218	0.00360	122.3	164.6
5	dorsal prefrontal cortex	0.00350	0.00298	163.3	149.1
6	medial orbitofrontal cortex	0.00276	0.00333	146.8	167.9
7	inferior temporal area	0.00292	0.00187	<118.4	121.4
8	angular gyrus and occipito-temporal area	0.00280	0.00205	141.3	142.9
9	Broca's area	0.00265	0.00172	149.6	135.2
10	anterior cingulate gyrus	0.00236	0.00259	134.6	136.3
11	Wernicke's area	0.00205	0.00219	128.2	139.5
12	supplementary motor area	0.00178	0.00213	no seperate peak	131.7
13	middle collateral sulcus †	<0.00164	0.00207	<118.4	132.2
14	ventromedial prefrontal cortex	0.00186	0.00198	<118.4	134.1
15	middle frontal gyrus †	<0.00164	0.00198	<118.4	123.3
16	middle superior temporal sulcus †	<0.00164	0.00180	121.0	136.1
17	inferior frontal sulcus †	<0.00164	0.00178	120.1	130.5
18	intraparietal sulcus	0.00176	0.00178	123.1	136.1

† marks that peak values where below the 80th percentile

Table 3.1 Peak values of hub regions on the topographic hub maps.



no	name of hub region	colour	anatomical description of hub region	lateralization
1	anterior superior temporal gyrus	pink	The hub is located at the anterior superior gyrus (anterior part of BA22) and extends to the anterior part of the insula. The hub has a two distinct peaks on the left hemisphere and only one peak on the right hemisphere.	higher node degree ($p < .001$) in right hemisphere
2	posterior/retrosplenial cingulate gyrus	light pink	The hub extends from the posterior cingulate gyrus (BA23, BA31) to the retrosplenial cingulate gyrus (BA29, BA30).	
3	parieto-occipital sulcus	dark blue	The hub is in the parieto-occipital sulcus which is superior to the calcarine sulcus.	higher node degree ($p < .001$) in right hemisphere
4	precuneus	yellow	The hub region extends from the precuneus (BA7) to the marginal sulcus (BA5) and to parts of the posterior cingulate region (BA31).	higher node degree ($p < .001$) and betweenness centrality ($p < .01$) in right hemisphere
5	dorsal prefrontal cortex	cyan	Dorsal prefrontal cortex within BA9 and BA46.	
6	medial orbitofrontal cortex	light yellow	Medial orbitofrontal cortex within BA11.	higher node degree ($p < .01$) in right hemisphere
7	inferior temporal area	dark red	The hub is located in the inferior temporal area (BA20) within occipito-temporal sulcus.	higher betweenness centrality ($p < .05$) in left hemisphere
8	angular gyrus and occipito-temporal area	light blue	The hub on left hemisphere extends from the angular gyrus (BA39) to the occipito-temporal area (BA37). On the right hemisphere the equivalent area has two distinct peaks.	higher betweenness centrality ($p < .01$) in left hemisphere
9	Broca's area	green	Broca's area between BA44, BA45, BA47.	higher betweenness centrality ($p < .001$) and node degree ($p < .001$) in left hemisphere
10	anterior cingulate gyrus	blue	Anterior cingulate gyrus within BA24 and BA32.	
11	Wernicke's area	light green	Part of Wernicke's area at the posterior end of BA22.	
12	supplementary motor area	olive	The hub is located in the supplementary motor area within the medial part of the premotor cortex (BA6).	higher betweenness centrality ($p < .05$) and node degree ($p < .001$) in right hemisphere
13	middle collateral sulcus	orange	The hub is located in the middle part of the collateral sulcus between the parahippocampal gyrus and fusiform gyrus. On the left hemisphere the middle collateral sulcus is not in the 80th percentile.	
14	ventromedial prefrontal cortex	red	The hub on the right hemisphere extends from the anterior cingulate sulcus to the ventromedial prefrontal cortex (BA11, BA12, BA32). On the left hemisphere the corresponding peak is located in the anterior cingulate sulcus.	higher node degree ($p < .05$) in right hemisphere
15	middle frontal gyrus	light grey	The hub region is on the middle frontal gyrus extending from the lateral premotor cortex (BA6) to lateral BA8. On the left hemisphere the middle frontal gyrus is not in the 80th percentile.	
16	middle superior temporal sulcus	brown	The hub on the right hemisphere is on the middle part of superior temporal sulcus between BA21 and BA22. On the left hemisphere the middle superior temporal sulcus is not in the 80th percentile.	
17	inferior frontal sulcus	orange-red	Inferior frontal sulcus between BA9, BA44, BA45, BA46. On the left hemisphere the inferior frontal cortex is not in the 80th percentile.	
18	intraparietal sulcus	purple	The hubs is located in the intraparietal sulcus between superior BA19 and the angular gyrus (BA39).	higher betweenness centrality ($p < .01$) and node degree ($p < .001$) in right hemisphere

* two-tailed p-values from the two-sample t-test with $df=124$ are Bonferoni corrected for familywise error rate ($n=14$).

Figure 3.4

Hub regions with betweenness centrality scores in the 80th percentile displayed on inflated brain surfaces. The anatomical descriptions and lateralization patterns of the coloured hub regions are given in the table. See also Table 3.2.

id	name of hub region	betweenness centrality		node degree	
		left hemisphere	right hemisphere	left hemisphere	right hemisphere
1	anterior superior temporal gyrus	0.00438	0.00541	145.2	192.8***
2	posterior/retrosplenial cingulate gyrus	0.00664	0.00673	178.8	186.8
3	parieto-occipital sulcus	0.00483	0.00588	158.7	191.2***
4	precuneus	0.00402	0.00645**	162.3	202.0***
5	dorsal prefrontal cortex	0.00538	0.00484	190.4	183.5
6	medial orbitofrontal cortex	0.00376	0.00457	165.5	188.8*
7	inferior temporal area	0.00389*	0.00263	137.7	130.1
8	angular gyrus and occipito-temporal area	0.00584**	0.00410	186.3	180.0
9	Broca's area	0.00333***	0.00216	162.6*	145.5
10	anterior cingulate gyrus	0.00376	0.00477	164.1	179.7
11	Wernicke's area	0.00282	0.00250	143.5	148.1
12	supplementary motor area	0.00275	0.00445*	144.2	173.3***
14	ventromedial prefrontal cortex	0.00264	0.00360	138.9	164.0*
18	intraparietal sulcus	0.00196	0.00289**	135.4	166.4***

*, ** and *** mark that the regions' hub scores across hemispheres differed statistically significantly after Bonferroni correction for familywise error rate (n=14) with $p_{2-tailed,FWER} < .05$; $p_{2-tailed,FWER} < .01$ and $p_{2-tailed,FWER} < .001$ respectively. The degree of freedom for the used two-sample t-tests were $df=124$.

Table 3.2 Results of the hub asymmetry analysis.

id	name of hub region	betweenness centrality		node degree	
		left hemisphere	right hemisphere	left hemisphere	right hemisphere
1	anterior superior temporal gyrus	F>M*	F>M	F>M	M>F
2	posterior/retrosplenial cingulate gyrus	F>M	F>M	F>M	M>F
3	parieto-occipital sulcus	M>F	F>M	M>F**†	M>F**†
4	precuneus	F>M*	F>M	M>F	M>F*
5	dorsal prefrontal cortex	M>F	M>F	M>F**†	M>F**†
6	medial orbitofrontal cortex	F>M	M>F	M>F	M>F*
7	inferior temporal area	F>M	F>M	M>F	M>F*
8	angular gyrus and occipito-temporal area	F>M	F>M	M>F	M>F
9	Broca's area	F>M	F>M	M>F**†	M>F
10	anterior cingulate gyrus	F>M	F>M	M>F	M>F
11	Wernicke's area	F>M	F>M	M>F	M>F
12	supplementary motor area	F>M	F>M	M>F	M>F
13	middle collateral sulcus	n.a.	F>M	n.a.	M>F
14	ventromedial prefrontal cortex	M>F	F>M	M>F*	M>F**†
15	middle frontal gyrus	n.a.	F>M	n.a.	M>F
16	middle superior temporal sulcus	n.a.	M>F	n.a.	M>F**†
17	inferior frontal sulcus	n.a.	M>F	n.a.	M>F
18	intraparietal sulcus	F>M	M>F	M>F**†	M>F***†

F>M marks that the average female hub score was larger than the male average hub score, while M>F marks the opposite. *, ** and *** mark that the regions' hub scores differed statistically significantly without corrections for multiple comparisons between genders with $t_{61}>|2.00|$, $p_{2-tailed}<0.05$; $t_{61}>|2.66|$, $p_{2-tailed}<0.01$ and $t_{61}>|3.46|$, $p_{2-tailed}<0.001$ respectively. † mark that the regions' hub scores differed statistically significantly between genders with false-discovery rate adjusted ($q=0.05$, $n=32$) p-values of $p_{2-tailed,FDR}<0.05$.

Table 3.3 Gender differences of hub scores.

The hub scores, their asymmetry and their gender differences

For all but one hub region we could identify a distinctive peak in the node degree and betweenness centrality hub map. The left supplementary motor area (12) in the node degree map did not have a distinct peak and was merged into hub (10). The peak values for all hub regions on the average brain are listed in Table 3.1.

Every pair of bilateral hub regions was tested for asymmetry by comparing across hemispheres the maximum individual values for each hub region (see materials and methods step 6). With the asymmetry analysis we found statistically significant differences between corresponding hub regions across hemispheres (see table in Figure 3.4 for the outcomes and Table 3.2 for full results). The results were Bonferroni corrected ($n=14$) to account for familywise error rates. Wernicke's area (11) was the only region with a reverse lateralization pattern for the node degree and betweenness centrality hub scores. However neither lateralization was statistically significant. All other regions showed a consistent lateralization for both node degree and betweenness centrality. In total six hub regions showed statistically significant hemispheric differences in their betweenness centrality scores and eight hub regions had statistically significant hemispheric differences in their node degree scores. For four regions both node degree and betweenness centrality scores were statistically significant lateralized.

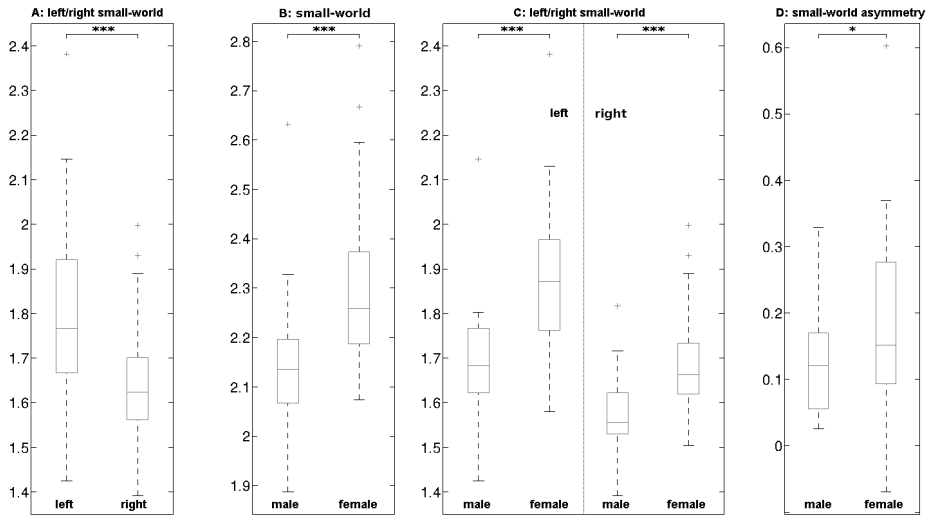
Comparing the hub scores between genders (see Table 3.3) shows that the node degree scores for the male are higher for all but two hubs ($p_{FWER}(X \leq 2) < 10^{-6}$). The betweenness centrality hub scores on the other hand were higher for females in 24 out of a possible 32 regions ($p_{FWER}(X \leq 8) < .01$). The p-values are derived by considering that the inequalities in Table 3.3 should have been binomially distributed in absence of gender differences, including Bonferroni correction ($n=2$) for familywise error rates.

At the single hub level we also performed independent two sample t-tests to determine which hubs differed most between genders. Thirteen out of 32 bilateral hubs were statistically significantly different between genders, without correction for familywise error rates. Nine hubs differed statistically significantly between genders when adjusting the p-values for false discovery rates ($q=0.05$, $n=32$) (Benjamini and Hochberg, 1995). This gives a strong indication that hub scores in general differ between genders, although a larger sample size is needed to more specifically identify the hubs concerned.

Small-world network analysis

For the hub areas most node degree and betweenness centrality scores in the right hemisphere are higher than in the left hemisphere. This result, together with the observed gender differences, indicates that gender differences in the network topologies may exist. To have a more complete understanding of the asymmetry and gender differences in the neocortical network we performed a small-world network analysis (see materials and methods step 7).

The results of the whole brain small-world index analysis are displayed in the boxplots of Figure 3.5 (for mean values and standard deviations see Table 3.4 and 3.5). A correlation analysis between the left and right small-world indices found that these are related



*** and * indicate statistical significant differences with $p_{2-tailed} < .001$ and with $p_{2-tailed} < .05$. The degrees of freedom for the tests are A: $df=124$, B-D: $df=61$. Each boxplot shows the median (middle line), the upper and lower quartile (rectangle), the smallest and largest observations (endpoints of the dashed line) and observations which should be considered as outliers (pluses).

Figure 3.5

The differences between left and right hemispheric small-world indices are shown in boxplot (A). Boxplots grouped by gender are: (B) whole brain small world indices, (C) left and right hemispheric small world indices and (D) small world asymmetry indices. See also Table 3.4 and 3.5.

with $r_{61} = .76$, while a paired t-test revealed that the left hemisphere has a statistically significant higher ($t_{124}=6.09$, $p_{2-tailed} < .001$) small-world index. Using an independent two sample t-test we found statistically significant gender differences ($p_{2-tailed} < .001$) for the whole brain ($t_{61}=3.61$), left ($t_{61}=4.46$), and right ($t_{61}=4.47$) small-world indices. The difference between the small-world indices of each hemisphere was statistically significantly different between genders with ($t_{61}=2.01$, $p_{2-tailed} < .05$). Since the female brain tends to have a smaller volume than the male brain it was plausible that the gender differences in the small-world indices are related to difference in brain volume. Correcting for brain volume with an analysis of covariance showed that brain volume is not a confounding factor for the gender differences. Small-world indices were in fact uncorrelated with grey matter volume ($r_{61} = -.31$), with white matter volume ($r_{61} = -.31$) and with the combined grey and white matter volume ($r_{61} = -.33$).

	σ	σ_{lh}	σ_{rh}	δ_{lh-rh}
male	2.14±0.14 (SD)	1.70±0.13 (SD)	1.57±0.09 (SD)	0.19±0.13 (SD)
female	2.30±0.16 (SD)	1.87±0.17 (SD)	1.69±0.11 (SD)	0.13±0.09 (SD)

Table 3.4
Results of the network topology analysis. The values in the table are small-worldness and small-worldness asymmetry averages with their standard deviations for the female and male group.

	whole brain		left hemisphere		right hemisphere	
	C/C_{rand}	γ/γ_{rand}	C/C_{rand}	γ/γ_{rand}	C/C_{rand}	γ/γ_{rand}
male	2.39±0.18	1.14±0.04	1.70±0.13	1.03±0.02	1.61±0.12	1.02±0.02
fema	2.56±0.18	1.16±0.03	1.87±0.16	1.05±0.03	1.75±0.15	1.04±0.02

Table 3.5
Results of the network topology analysis. The values in the table are averages of clustercoefficients and characteristic path length ratios with their standard deviations for the female and male group.

Discussion

This study shows the distribution of provincial and connector hubs in the healthy human brain. In connection with a network analysis, general conclusions may be drawn regarding the lateralization of the major networks, and gender differences in network structure. These results and their implications will be discussed below after we have addressed some of the methodological considerations associated with the study.

Methodological considerations

A common error source in brain network modelling is the selection of nodes (Zalesky et al., 2010). It has been shown that contemporary structural atlases provide inappropriate node definitions (Smith et al., 2010). By using twenty random parcellations over a single subject we were able to obtain a topographic display of hub regions independent of predefined anatomical boundaries. This template free network reconstruction approach proved to be beneficial, as hub regions were found at the boundaries of classical anatomical areas.

The discovery of false white matter connections is a well established problem in studies using fibre tractography. With no existing gold standard techniques or histological based fibre atlases of the whole human brain, fibre tracts cannot be validated for individual brains. We minimized this potential source for errors by using a sophisticated multi-fibre reconstruction method from the Camino package (Cook et al., 2006) on high angular resolution diffusion imaging (HARDI) data (Tuch et al., 1999) and informed our tractography using the Freesurfer grey and white matter segmentation routines.

Some computed callosal fibre tracts appeared to terminate in the cingulate cortex and while other studies have similar findings (Locke and Yakovlev, 1965; Jarbo et al., 2012) it is possible that their existence is rooted in the limitations of current available

data and processing software, as they are a likely artefact of partial volume voxels (Vos et al., 2011). Reducing errors in the tractography will lead to improved accuracy of hub scores due to reduction of partial volume effects, specifically in regions connected with callosal and uncinate fascicle fibre pathways (Kim, Ronen, et al., 2006; Vos et al., 2011).

The location and ranking of the hubs

Hubs were located on both maps in comparable regions, however the betweenness centrality had more pronounced hub regions than the node degree map. This observation was consistent with our assumption that betweenness centrality is a marker for connector hubs. The betweenness centrality map was therefore used to determine important hub loci on the neocortex.

We identified eighteen peaks reflecting distinctive hub regions. The ranking and location of the hubs shows correspondences with previous literature using structural connectivity analysis (Hagmann et al., 2008; Gong, He, et al., 2009) and partially overlap with hubs determined by network analysis of resting-state functional MRI data (Bassett and Bullmore, 2009; Cole et al., 2010; Tomasi and Volkow, 2011). Because of the topographic approach we discovered new spatial detail in the distribution of the hubs. For instance we found three distinct hubs in the posterior cingulate cortex and medial parietal lobe, while previous findings (Hagmann et al., 2008; Gong, He, et al., 2009) suggested a single hub region in the same area. With the topographic maps some new hub areas become recognizable, such as the inferior temporal area (7), Broca's area (9), the supplementary motor area (12), middle frontal gyrus (15). The new hubs are also known to be key areas in neurocognitive networks (Roland et al., 1980; Chelazzi et al., 1993; Corbetta et al., 1998; Xiang et al., 2010).

The superior temporal gyrus was the hub with the highest peak value for betweenness centrality. This result may be surprising as previous literature considers the medial parietal lobe at the core of the neocortical structural network (Hagmann et al., 2008; Gong, He, et al., 2009). However a higher peak hub value on an average topographic map does not necessarily imply a higher importance, but could be caused by anatomical variability between subjects. For example we observed that the hub in the left superior temporal gyrus (1) had for each subject either an anterior peak or a slightly more posterior peak. Hence the average betweenness centrality hub map showed two peaks, which we assume to belong to the same hub region. The length of the left lateral sulcus is known to be longer than its contralateral homologue, which in turn explains the asymmetric appearance of hub (1). Furthermore as will be discussed below, the medial parietal hub of previous papers is here differentiated into three separate hubs.

Instead of focusing on the precise ranking of the hubs, we will focus in the following paragraphs on the functional roles and the asymmetry patterns of the hubs matching the results to known neurocognitive networks from previous literature. The hubs cover a broad range of functions, but for simplicity we chose to discuss them in the context of four specific networks. All but one hub can be associated with the default mode network, visual processing networks or networks related to language processing. Many of the

hubs can be associated to more than one of those networks. The hubs will therefore be discussed in the context of all three of these networks. The only exception is hub (17) in the right inferior frontal cortex, which is an area associated with the cognitive control network and has been indicated to be an important area for making risk-taking and go/no-go decisions (Konishi et al., 1998; Aron et al., 2004; Steinberg, 2008; Christopoulos et al., 2009).

The hubs related to the default mode network

The largest fraction of hubs can be anatomically linked to the default mode network, a set of neocortical regions which is active during rest (Gusnard and Raichle, 2001). The regions related to the default mode network can be identified using different types of fMRI analysis (Biswal et al., 2010). In total we found thirteen hub regions (2-10, 13, 14, 16, 18) overlapping with the default mode network defined in previous literature (Gusnard and Raichle, 2001; Buckner et al., 2008; Smith et al., 2009; Biswal et al., 2010; Laird et al., 2011).

While studies using functional MRI (fMRI) show differences in what encompasses the default mode network, all consider the posterior medial parietal lobe to be integral to its functioning. Previous studies focusing on the topology of the structural neocortical network found that the precuneus and the posterior cingulate cortex form a hub region (Hagmann et al., 2008; Gong, He, et al., 2009).

The topographic map separated the medial parietal lobe and the posterior cingulate cortex into three hub regions: the posterior/retrosplenial cingulate gyrus (2), the parieto-occipital sulcus (3) and the precuneus (4). This suggests that the posterior part of the default mode network can be further subdivided in three subnetworks. Some recent fMRI studies have subdivided the medial parietal lobe on the basis of functional connectivity patterns and found corresponding results (Margulies et al., 2009; Zhang and Li, 2012). As the default mode network involves a large area around the medial parietal lobe, there is a considerable anatomical overlap with other neurocognitive networks, such as the spatial awareness, working memory and executive function networks (Mesulam, 1998; Gusnard and Raichle, 2001). The precuneus part of the default mode network has been found to overlap with executive activity (Gerlach et al., 2011), whereas the parietal-occipital sulcus can be related to working memory tasks involving visual input (Tuladhar et al., 2007). The three distinctive hub regions could therefore reflect distinctive functional roles of each of the regions.

Considering the lateralization of the hubs in the medial parietal lobe we found that the precuneus (4) and the parietal occipital sulcus (3) had statistically significantly higher node degree scores in the right hemisphere than their contra-lateral homologues. This finding is also consistent with (Gong, He, et al., 2009; van den Heuvel and Sporns, 2011) who identified similar characteristics when using large scale neocortical nodes. However we did not find statistically significant differences between hemispheres for the posterior and retrosplenial cingulate gyrus (2).

The hubs in relation to the visual processing networks

Six hubs (1, 3, 8, 12, 15, 18) can be linked to different networks involving visual processing, such as the network of spatial awareness (Mesulam, 1998; Karnath et al., 2001), visual attention network (Schall, 2004) and networks related to visuo-motor coordination and execution (Laird et al., 2011).

Hubs (3, 12, 15, 18) are anatomically associated with the spatial awareness network, which is lateralized to the right hemisphere (Mesulam, 1998; Gitelman et al., 1999). At the same time the related hubs to the spatial awareness network are lateralized to the right hemisphere, consistent with literature which considers that damage to the right hemisphere causes more severe neglect (Husain and Nachev, 2007).

The hub in the parieto-occipital sulcus (3) links areas in the occipital lobe and in the parietal lobe and is hypothesized to play an important blocking role in the dorsal information flow from visual areas (Tuladhar et al., 2007). Furthermore hub (3) is considered to be part of the network for working memory and executive function (Mesulam, 1998).

Hub (8) can also be associated with both the default mode and language networks. However posterior areas of hub (8) also coincide with associative visual cortex, specifically the subregion TO2 which is part of the MT+ complex (motion-selective cortex) (Amano et al., 2009; Henriksson et al., 2012). Considering the partial overlap with various known neurocognitive networks it is possible that hub (8) is a composite of multiple spatially distinct hubs which are combined because of individual anatomical variability, spatial resolution and the smoothing kernel used. This assumption is strengthened by two distinct peaks on the right hemisphere in the equivalent region.

The hubs related to the language network

Nine hubs (1, 2, 5, 7-9, 13, 14, 16) can be anatomically associated with the language network (Patterson et al., 2007; Binder et al., 2009; Turken and Dronkers, 2011). Six of these hubs in the left hemisphere (1, 5, 8, 9, 11, 16) are critical for auditory sentence comprehension (Turken and Dronkers, 2011).

The hub in anterior superior temporal gyrus (1) encompasses an area important for voice recognition (Belin et al., 2000). Besides the aforementioned anatomical asymmetry of the lateral sulcus, there are also functional hemispheric differences of the anterior superior temporal gyrus related to the emotional processing of voices (Schirmer and Kotz, 2006), which may be related to the statistically significant higher node degree in the right hemisphere.

Areas which had higher betweenness centrality hub scores were: the temporal pole (7), the posterior middle temporal gyrus (8) and Broca's area (9), which is consistent with previous literature which considers that the production of language dominates in the left hemisphere rather than the right (Patterson et al., 2007; Xiang et al., 2010; Turken and Dronkers, 2011). However, unexpectedly Wernicke's (11) area did not show a leftward asymmetry pattern. This may be explained by the importance of the right posterior lateral sulcus for other cognitive processes, such as activities related to music (Alluri et

al., 2012). This view is further supported by lesion studies which find a region around hub (11) to be critical in the right hemisphere (Karnath et al., 2004). The aforementioned asymmetry in the scope of hub (8) may also be related to hemispheric differences in language production. In the left hemisphere the inferior part of hub (8) stretches towards the fusiform gyrus, a region which is related with the visual word form area (Cohen et al., 2002; Dehaene and Cohen, 2011).

Asymmetry of the hubs and the topology of the neocortical network

There is known lateralization of brain function for language and visuo-motor processes, as well as anatomical brain asymmetries (Toga and Thompson, 2003). Recent studies focusing on white matter connectivity have also shown that there are measurable structural hemispheric differences in the superior longitudinal fasciculus and the cingulum, two major fibre pathways in the human brain (Gong et al., 2005; Catani et al., 2007; Thiebaut de Schotten et al., 2011). We therefore expected to measure hemispheric asymmetries in the neocortical network.

Seven hubs had significantly higher node degree scores on the right hemisphere compared to only one hub on the left hemisphere. For the betweenness centrality scores each hemisphere had three hubs which were statistically significantly higher than in the other hemisphere. This indicates that the hubs on the left hemisphere are connected with less brain regions than those on the right hemisphere, while each hemisphere has a set of distinctive hubs with high betweenness centrality. The left hemisphere however has higher small-world indices compared to the right hemisphere. Higher small-world indices imply a more efficient network structure for message passing (Latora and Marchiori, 2001; Humphries and Gurney, 2008).

Gender network differences

With the high resolution connectome analysis we observed several gender differences, which all indicate that the female brain has a higher network efficiency. The results are therefore consistent with previous findings, achieved at a coarser resolution (Gong, Rosa-Neto, et al., 2009).

For the female brain we found that most hubs have higher betweenness centrality compared with hubs in the male brain. On the other hand male brains tend to have hubs with higher node degree compared to the female brain. This shows that female hubs are more economical in the use of connections, while at the same time being more important in their role as connectors. While there is a pattern of gender differences in hub scores, a larger sample size is still needed to more specifically identify the hubs which differ most between genders.

The results of the small-world network analysis between genders were consistent with the observed hub differences. Female brains had higher small-world indices for the whole brain and both hemispheres. This indicates that the female brain, while being smaller in volume and having overall fewer connections in hub regions, has a more effective network structure for message passing (Latora and Marchiori, 2001;

Humphries and Gurney, 2008). The small-world asymmetry index was found to be statistically significantly higher for females than for the males.

Lesion simulation studies have concluded that the targeted removal of connector hubs or regions with highest betweenness centrality causes the most severe and widespread disruption within the neocortical network (Honey and Sporns, 2008; Alstott et al., 2009). This suggests that most female hubs are more critical to their neocortical network than their male counterparts, since their betweenness centrality scores are overall higher. Therefore it is plausible that a network disruption in a female brain is more severe than in males, because the female brain has a more economical network structure than males while at the same time their hub areas have a more critical role. The gender differences identified in this study therefore may have important implications for studies considering brain injury and disease. For instance clinical studies have found that female are more at risk to have post-stroke disability and have a higher mortality rate after most types of strokes (Thorvaldsen et al., 1995; Wyller et al., 1997; Ayala et al., 2002; Reeves et al., 2008; Petrea et al., 2009; Persky et al., 2010). So far, it is undetermined what causes gender differences in stroke impact. Pre-stroke disability, sociodemographic factors and hormone exposure are currently among the possible candidates to explain the sex differences (Petrea et al., 2009; Persky et al., 2010). Evidence has suggested that lesion volume is not the cause of gender disparities in stroke outcomes (Silva et al., 2010).

Future work

With the topographic display of hubs, the scope and lateralization of important brain areas became discernible. Our hypothesis was confirmed that with graph theoretical analysis hubs can be found in important neurocognitive networks, besides the default network.

Future studies may benefit from the maps, because they can be used as a reference and new hypotheses regarding the neocortical hubs can be formulated. To extend this work, several other avenues of research can be considered which cover a broad spectrum of topics.

The presented results may be important to studies concerned with brain disease and injury. This is especially true for diseases with focal pathology such as stroke and tumours, but is also relevant for diseases with more global pathology such as Alzheimer's or Parkinson disease. For instance damage to the hubs after stroke may play an important role in outcome and rehabilitation (Alstott et al., 2009). Our results show profound gender differences in the organization of the neocortical network which are consistent with observations in stroke literature. Therefore this study provides grounds to examine the role of complex structural brain characteristics in stroke outcomes. In patients with glioma, it is hypothesised that a widespread change in the strength and spatial organization of brain networks is responsible for cognitive dysfunction (Bosma et al., 2009). To validate the hypothesis one could examine how changes in functional brain networks relate to changes in structural brain network topology.

Previous work has already shown that the brain measurably changes its functional and structural organization with age (Dosenbach et al., 2010; Hagmann et al., 2010). Brain developmental and brain ageing aspects are therefore other promising areas which may further benefit from this study. This could be done by investigating whether and how the distribution of hubs alters with age progression.

It will be interesting to examine hub differences in healthy populations and relate them to behavioral indices or biological markers. Studies have related structural brain properties such as cortical thickness to candidate genes (Kochunov et al., 2011). Since there are gender differences in the neocortical network topology, there is also potential to link genetic information with network topology descriptors such as hub scores or small-world indices.

4

Exploring the Connectivity Patterns of Human Neocortical Visual Areas

Abstract

In this work we determine and explore the structural connectivity patterns between human neocortical visual areas: V1, V2, V3, V3A, V3B, anterior IPS, posterior IPS, VIP, FEF, hV4, VO1 VO2, MT, MST, LO1 and LO2. The visual areas were determined with functional MRI localiser experiments and their inter-areal connectivity patterns were computed with probabilistic tractography on high angular resolution diffusion imaging (HARDI) data. The results give a description of the visual system's connectivity pattern. With it we explored whether known properties of the visual system are reflected in their connectivity patterns. Using graph theoretical analysis we show that the structural network of the visual system can be grouped into a dorsal and ventral module. Connectivity maps between subregions of visual areas show that inter-areal connectivity patterns have correspondences with activation patterns to visual ring stimuli as seen in eccentricity maps. The cortical projection patterns for the central and peripheral visual field were examined by looking at the posterior and anterior connections from earlier visual areas. The examination of connectivity patterns of higher level visual areas showed that V3A, left V3B, V6, anterior IPS, VO1 and VO2 have more connections to anterior portions than posterior portions of earlier visual areas V1, V2 and V3. Visual areas right V3B and hV4 on the other have more connections to posterior portions than anterior portions of visual areas V1, V2 and V3. A spectral clustering approach on individual visual areas did not produce meaningful segmentations of the cortex. This work provides a plausible description of the complex white matter connectivity patterns between visual areas, as the results are consistent with current literature on visual processing.

Adapted from: Nijhuis EHJ, Swisher JD, Arnoldussen DM, Jehee JFM, van den Berg AV, van Cappellen van Walsum A-M, Norris DG (*in review*).

*“Men who wish to know about the world
must learn about it in its particular details.”*
-Heraclitus-

Introduction

Diffusion based MRI methods are popular techniques to estimate the structural connectivity between brain structures and to probe their microstructures (Stejskal and Tanner, 1965; Le Bihan, 2003; Johansen-Berg et al., 2004; Hagmann et al., 2008). For human studies they are the only techniques to date which provide access to non-invasive in-vivo white matter microstructure. Since their inception there has been continuous advancement in their ability to image the brain at greater detail. The past decade in particular has brought about the rise of parallel imaging with multi-channel head coils (Pruessmann et al., 1999; Griswold et al., 2002), improvements in data post-processing to correct for acquisition related artefacts (Andersson and Skare, 2002; Zwiers, 2010), multi-fibre diffusion models which capture underlying physical processes more realistically (Parker et al., 2003; Parker and Alexander, 2005; Wedeen et al., 2008) and tractography algorithms which are better at locating fibre streamlines (Behrens, Woolrich, et al., 2003; Guevara et al., 2010).

In the human neocortex several areas are associated with the visual system which can be localised with functional MRI (fMRI) in individual subjects (Wandell et al., 2007; Wandell and Winawer, 2011). Many neocortical visual areas are retinotopically organised, that is: the information of the visual field are processed in the neocortex with a corresponding topography (Wandell and Winawer, 2011). For instance within visual areas V1, V2, V3 the central visual field information is processed in posterior sub regions and the peripheral visual field is processed in anterior sub regions of V1, V2 and V3 (Wandell and Winawer, 2011). The current opinion is that the visual areas are broadly grouped into two information streams: a dorsal stream also known as the “where”-stream and the ventral stream which is also known as the “what”-stream (Goodale and Milner, 1992; Ungerleider and Haxby, 1994). Evidence in macaques has suggested that areas associated with the dorsal stream receive preferential input from the peripheral visual field while areas associated with the visual stream receive preferential input from the central visual field (Baizer et al., 1991; Gattas et al., 1997).

With diffusion-based MRI methods one can examine the network of connections between visual areas as defined by retinotopic fMRI (Kim and Kim, 2005; Kim, Ducros, et al., 2006), which we will refer to as the visual system’s projectome (Wandell and Winawer, 2011). In translational research using invasive tracer techniques there have been comprehensive descriptions of the visual system’s projectome of macaques, which have demonstrated a hierarchical organisation (Felleman and Van Essen, 1991; Reid et al., 2009). It has been speculated that for humans with improved imaging techniques a

more detailed projectome can be mapped which characterises the projections between visual maps (Wandell and Winawer, 2011).

In this study we revisit the visual system's projectome of the human using retinotopic functional MRI, diffusion-based MRI and graph theoretical methods. Our main goal for this investigation is to provide an update graphical description of the fibre-streamlines between visual areas, as well as their projection patterns. We then explore the projectome to test several known theories about the visual system with the following hypotheses: (1) Can we separate visual areas into a dorsal and ventral stream with graph theoretical analysis of the visual system's projectome? (2) Is there a correspondence between the retinotopic topography of visual areas and their inter-areal projection patterns? (3) Is there evidence in the visual projectome which suggests that dorsal stream and ventral stream areas receive preferential input from peripheral or central visual field areas (Baizer et al., 1991; Gattas et al., 1997) (4) Is it possible to automatically group (Johansen-Berg et al., 2004; Solano-Castiella et al., 2010) visual areas into their central and peripheral parts based on their connectivity patterns to the rest of the brain?

The richness of the data acquired makes it possible to test a range of hypotheses. Here we restrict ourselves to the examination of widely accepted hypotheses, to demonstrate the plausibility of the projectome presented here. The subsequent analyses show that the patterns of fibre-streamlines between visual areas are consistent with observations from past literature on visual processing and add to them by providing a perspective of inter-areal connectivity patterns.

Material and methods

Ethics statement

The study was conducted at the Donders Institute for Brain, Cognition and Behaviour, Radboud University Nijmegen the Netherlands with the general institutional ethics approval from the local ethics committee (Commissie Mensgebonden Onderzoek region Arnhem-Nijmegen, The Netherlands). All participants provided written informed consent in accordance with the declaration of Helsinki.

Participants & MRI scanner

Six subjects [1 female, 5 male, mean age $34.1\text{yr} \pm 8$ (SD)] were scanned on a Siemens 3T TIM Trio system with a 32 channel head coil at the Donders Institute for Brain, Cognition and Behaviour, Radboud University Nijmegen. The number of participants was similar to that used in previous related studies (Kim and Kim, 2005; Kim, Ducros, et al., 2006). One participant (subject 2) was not used for the average connectivity pattern analysis because the central part of the visual areas V1, V2 and V3 could not be mapped.

Visual experiments & MRI acquisition

Anatomical scan

High resolution anatomical scans were acquired using a T1-weighted 3D MPRAGE sequence TE=3.03ms, TR=2300ms, TI=1100ms, a flip angle of 8°, FOV=256mm, 192 slices with 1mm thickness and a 256x256 imaging matrix resulting in 1mm isotropic voxels.

Visual stimulation fMRI experiments

For this experiment a custom-built visual projection system was used to provide visual stimuli with a field of view of approximately $120 \times 90^\circ$ to the left eye (Arnoldussen et al., 2011). Only the lower coil part (with 20 channels) of the 32-channel head coil was used so that posterior brain regions could be measured with fMRI. The upper part of the coil could not be used, because the equipment to stimulate the full visual field was attached to the lower part of the coil and in close proximity of the participants eyes. Functional scans were obtained using a single-shot echo-planar imaging (EPI) sequence with TE=28ms, TR=2000ms, FOV=256mm, 32 slices with 2mm thickness and a 128x128 imaging matrix resulting in 2mm isotropic voxels.

We aimed to identify the medial temporal area (MT+) and its sub-division into the medial temporal area (MT) and medial superior temporal area (MST) (Dukelow et al., 2001; Huk et al., 2002). We did so, by presenting full field visual flow, left hemifield visual flow, and right hemifield visual flow stimuli (Arnoldussen et al., 2011). Left- and right hemifield visual flow were presented at 15 degrees eccentricity from fixation up to the field border. In the hemifield conditions the remainder of the visual field was filled with a static random dot pattern. These three conditions were presented in a blocked design in which 3 repetitions of each condition were presented in random order, interleaved by a static random dot pattern. All conditions were presented for 18 seconds and each subject completed 2 runs. In the flow conditions, the flow simulated a forward motion of 2 m/s through a cloud of dots with an extent of 10m in depth of the vantage point. At any time about 4000 dots were visible.

To demarcate other visual areas, we used standard retinotopic mapping techniques (Serenio et al., 1995; Engel et al., 1997). For the polar angle mapping, the subject was asked to fixate at the central fixation cross while a black/white chequerboard “wedge” stimulus expanding from the fixation point (wedge width, 60°) moved anticlockwise over the visual field at one revolution in 64 s. For the eccentricity mapping, subjects maintained straight ahead fixation while a radial black/white chequerboard ring moved from inner to outer visual field (maximum eccentricity, 60°) at a speed of 2 °/s. Both ring and wedge consisted of a black/white alternating chequerboard (2 Hz) and were scaled by eccentricity in accordance with the cortical magnification factor (Virsu and Rovamo, 1979).

Structural connectivity scan

High angular resolution diffusion imaging (HARDI) volumes were acquired using a single-shot echo-planar imaging (EPI) sequence with phase encoding in the anterior to

posterior direction, with TE=101 ms, TR=13.0s, FOV=220mm, 70 slices with 2mm thickness and an 110×110 imaging matrix resulting in 2mm isotropic voxels. Measurements were taken in 256 non-collinear directions at a b-value of 1500 s/mm^2 . In addition, 28 volumes were acquired with $b=0 \text{ s/mm}^2$.

Data analysis

Data post-processing

The anatomical scans were processed using Freesurfer (Dale et al., 1999) to segment the brains into cortical and subcortical structures. We used the software's recommended workflow which consists of an automatic processing pipeline interleaved with manual inspection and correction of Talairach alignment, skull removal, white matter surface and grey matter surface errors.

MT/MST localiser runs were processed and analysed using Brainvoyager QX (version 2.6, Maastricht) (Goebel et al., 2006). All runs were corrected for 3D head motion (trilinear/sinc interpolation) and slice acquisition timing (cubic spline interpolation). Subsequently, the resulting time courses of the experimental scans were high-pass filtered by fitting a General Linear Model (GLM) with Fourier basis set of two cycles per run cut-off, including a linear trend. No further spatial smoothing was applied to the functional data.

Retinotopic mapping scans were processed using FSL's mcflirt (Jenkinson et al., 2002) motion correction software with 6 degrees of freedom and trilinear interpolation. No additional post-processing were used. The functional images were aligned to the reconstructed cortical surface using the Freesurfer program bbregister (Greve and Fischl, 2009).

The diffusion-weighted images were checked for motion, cardiac and table vibration-induced artefacts using the PATCH algorithm (Zwiers, 2010). The volumes were then realigned and corrected for eddy current-induced distortions with the integrated approach described in (Andersson and Skare, 2002). Finally the volumes were unwarped in the phase encoding direction onto the anatomical scan to reduce the effects of phase evolution in the EPI read out direction (Studholme et al., 2000; Visser et al., 2010). We used the multi-fibre reconstruction PASMRI with 16 basis functions (Cook et al., 2006) and performed interpolated probabilistic tractography with a 0.2mm step size (Behrens, Woolrich, et al., 2003; Parker et al., 2003; Seunarine et al., 2006). For each brain we generated a voxel based connectivity matrix M . The Freesurfer segmentations were used to inform the tractography. All grey matter voxels adjacent to white matter voxels were used as a seed for probabilistic tractography with 5000 iterations for a maximum of 3 principle diffusion directions. On average the brains had 265,387 seed voxels. In a streamline post-processing step only streamlines which would connect two distinct grey matter voxels were used for further analysis. Streamlines which passed through ventricles or subcortical nuclei were discarded. The number of streamlines from voxel i to j would then be entered at M_{ij} of the connectivity matrix. Each connectivity matrix

was then symmetrised by setting the value of any pair of entries M_{ij} and M_{ji} to their maximum.

Analysis for determining motion-sensitive visual areas

For the MT/MST localiser, a GLM model was applied with three experimental predictors for the three flow conditions (full field flow, left hemifield flow, and right hemifield flow). Subsequent GLM results were projected on an inflated representation of each subjects' left and right hemisphere. The contrast between the full-field flow and the rest condition defined the MT+ complex. MT and MST were defined as sub-regions of MT+. Area MST was demarcated as the anterior part of MT+, including all of the voxels that responded to ipsilateral flow presentation (i.e. ipsilateral with reference to the respective hemisphere analysed) (Dukelow et al., 2001; Huk et al., 2002). Area MT was defined as a region containing contiguous voxels that responded to contralateral, but not ipsilateral, flow (with a significance of at least $p < 0.05$).

Retinotopic analysis

Analysis of the retinotopic mapping data used standard techniques (Serenio et al., 1995; Engel et al., 1997; Swisher et al., 2012). Briefly, the rotating wedge or expanding ring stimuli are assumed to induce a periodic modulation in retinotopically organised cortex, the phase of which can be taken to indicate the relative radial or eccentric position in the visual field to which a given voxel is most responsive. The statistical significance of the periodic modulation is assessed by comparing the amplitude of the response at the stimulation frequency to that at other frequencies. Under the assumption of temporally white noise, this contrast yields an F-ratio, corresponding to the null hypothesis that stimulus-period modulation is no greater than that at other frequencies. Voxels that surpass a lenient statistical threshold of $p < 0.01$ (uncorrected) are rendered in color according to the phase lag of their response, and this color map is projected onto the reconstructed cortical surface for display. Putative retinotopic areas were manually labelled by a skilled operator, following (Wandell et al., 2007). For one subject the central part of the visual areas V1, V2 and V3 could not be identified and were not mapped.

Combining motion-selective and retinotopically defined areas

To combine all visual areas in a common brain space we projected the motion-sensitive visual areas from the Brainvoyager analysis onto the Freesurfer brain. This was accomplished by mapping the motion-selective areas determined in Brainvoyager onto the Freesurfer brain with a rigid-body transformation using FLIRT, after which they were projected onto the Freesurfer surfaces. After projection the motion-selected areas showed holes on the surface, due to software differences in brain surface reconstruction resulting in projection inaccuracies. Minor holes were filled using the Freesurfer automatic label fill function to create contiguous areas. Two larger holes in subject 2 could not be filled using the automatic approach and were uncorrected. In all but one right hemisphere we found that the motion selective areas MT and MST substantially

overlapped with the retinotopically defined areas LO1 and LO2. Previous work (Larsson and Heeger, 2006) has found strong responses to motion and kinetic boundary stimuli within retinotopically defined LO1 and LO2. This led us to exclude LO1 and LO2 in the right hemisphere from further connectivity analysis, to avoid having brain areas assigned to multiple visual areas. On the left hemisphere MT overlapped with LO2 in subject 6 and had minor overlap in subject 1. The visual stimuli were presented only to the left eye, which may explain the observed asymmetric overlapping pattern, as motion boundaries of the right visual field are stimulated less due to nasal interference. In the cases where MT intersected with LO2 in the left hemisphere the overlapping area was assigned to the anatomically smaller area LO2 to prevent their occlusion. After combining the motion-selective areas with the retinotopically defined areas on the Freesurfer surface we projected all areas to regions of interest in the volumetric space which was used for tractography.

Creating the structural network between visual areas

To create the structural network between visual areas we aggregated the connectivity values from the voxel-based connectivity matrix. Combined visual areas LO12 and V3AB, which a skilled operator could not further subdivide were discarded to simplify the projectome. Across all subjects 37 distinct visual areas (27-35 distinct visual areas per subject) remained for further analysis. Table 4.1 lists all measured and used visual areas per subject. The strength of a connection between two visual areas would be determined by the sum of values M_{xy} , where x are all voxels from a particular visual area and y are all voxels from another visual area. This process would result in 6 connectivity matrices, one for each subject, with sizes from 27×27 to 35×35 . The connectivity matrices were then combined into a 37×37 matrix V by averaging the number of available measurements for every entry V_{ij} for the connection strength between visual areas i and j . For each entry V_{ij} an average of four subjects had a possible connections measured. The connectivity matrix V was then displayed and analysed using the Gephi software package (Bastian et al., 2009) to test whether the network between visual areas can be grouped into a dorsal and ventral stream (hypothesis 1). Connections with less than 1000 streamlines were considered to be supported with insufficient evidence and were discarded. Hence the frontal eye field (FEF) and the ventral intra-parietal (VIP) visual areas with no connections to other areas were left out in the final network schema.

Connectivity pattern analysis between visual areas

To obtain a more detailed characterisation of how visual areas are connected with one another each visual area was subdivided into 16 equally sized regions and the connectivity patterns between these regions were investigated. In the following text we refer to V1d, V2d, etcetera as visual areas whereas subregions of those areas will be referred to as visual regions. The visual areas from each subject were subdivided using an automatic clustering process. For the clustering process the visual areas on the inflated Freesurfer surfaces were used, rotated by 20 degrees in the yz-plane to ensure

Visual area		S1	S2	S3	S4	S5	S6	LH	RH
V1d	dorsal primary visual cortex	x x	x x	x x	x x	x x	x x	6	6
V2d	dorsal visual area 2	x x	x x	x x	x x	x x	x x	6	6
V3d	dorsal visual area 3	x x	x x	x x	x x	x x	x x	6	6
V3A	visual complex V3 part A	c x	x x	x x	x x	x x	x c	5	5
V3B	visual complex V3 part B	c x	x x	x x	x x	x x	x c	5	5
V6	visual area 6	- -	x x	x x	x x	x x	x x	5	5
posIPS	posterior intraparietal sulcus	x x	x x	x x	x x	x x	x x	6	6
antIPS	anterior intraparietal sulcus	x x	- x	x x	x x	x x	x x	5	6
VIP	ventral intraparietal area	- -	x -	- x	x x	- -	- x	2	3
FEF	frontal eye field	- -	- -	- x	x x	- -	- -	1	2
V1v	ventral primary visual cortex	x x	x x	x x	x x	x x	x x	6	6
V2v	ventral visual area 2	x x	x x	x x	x x	x x	x x	6	6
V3v	ventral visual area 3	x x	x x	x x	x x	x x	x x	6	6
hV4	human visual area 4	x x	x x	x x	x x	- x	x x	5	6
VO1	ventral occipital cortex area 1	- -	x -	x -	x x	- x	- x	3	3
VO2	ventral occipital cortex area 2	- -	- -	- -	- -	- -	- x	0	1
MT	medial temporal area	x x	x x	x x	x x	x x	x x	6	6
MST	medial superior temporal area	x x	x x	x x	x x	x x	x x	6	6
LO1	lateral occipital cortex area 1	x -	- -	x -	x c	- -	x -	4	0
LO2	lateral occipital cortex area 2	x -	- -	x -	- c	- -	x -	3	0

Table 4.1

List of mapped visual areas per subject. The table shows what visual areas have been mapped per subject (S1-S6). An 'x' marks that the visual area was mapped whereas a dash marks that the visual area was not mapped. Areas V3A, V3B, LO1 and LO2 which were found as composite areas V3AB or LO12 have been marked with 'c'. Within an entry the left side of the horizontal line refers to the left hemisphere and the right side to the right hemisphere. The right side of the table contains summary statistics for the left ('LH') and right hemisphere ('RH').

that the occipital pole had the smallest y-axis values of all surface vertices. The surface vertices of a visual area were then recursively clustered into 16 regions by using the k-means algorithm (Seber, 2008) with 2 clusters on the Euclidean distance between vertices. This means that an area was first clustered into two regions, after which each of those regions were clustered into another two regions, and so on. The k-means algorithm was iterated four times such that each area was parcellated into 16 regions. The clustering process was chosen to ensure that the dorsal and ventral parts of the visual areas V1, V2 and V3 were approximately subdivided into an 8×2 grid. The 16 regions were then indexed from 1 to 16, such that within visual areas more posterior (central) regions had smaller indices compared to anterior (peripheral) regions. This was accomplished by selecting the most anterior vertex x (the vertex with largest value in the y-direction) of a visual area and ranking the 16 regions in descending order by their average path length to x on the inflated surface grid. After parcelling the visual areas on the inflated surface all regions were projected to the same volumetric space which was used for tractography.

With the more finely parcellated visual areas colour coded connectivity surface maps were constructed per subject and per visual area, to test whether there is a correspondence between the retinotopic topography of visual areas and their inter-areal projection patterns (hypothesis 2). The surface maps show which individual regions within a specific visual area have maximum projections onto the remaining brain.

A 592×592 average connectivity matrix was constructed in a similar way as in the previous section only this time the connectivity matrix consists of a 37×37 grid of 16×16 matrices which each describe the connectivity patterns between pairs of visual regions across all subjects. Subject 2 was discarded from the connectivity pattern analysis across different subjects. We then tested whether the connectivity patterns of dorsal and ventral visual areas V3A, V3B, V6, posIPS, hV4, VO1 and VO2 showed differences in their projections to posterior and anterior regions of V1, V2 and V3 (hypothesis 3). In order to test for these difference we applied matrix summation of the relevant 16×16 connectivity matrices (e.g. the inter- and intra-hemispheric connectivity patterns for: V3A to V1d, V1v, V2d, V2v, V3v, V3d). We then compared the distribution of matrix values in the left quadrants (8×16 values) to the values in the right quadrants with a Mann-Whitney U-test.

Voxel based spectral clustering of visual areas

Every visual area for each subject was clustered based on their connectivity pattern to the rest of the brain using a spectral clustering algorithm, to test whether visual areas can be automatically grouped into their central and peripheral parts (hypothesis 4). To cluster a visual area into two groups the voxel based connectivity $m \times m$ matrices were used to extract the n rows relevant to the visual area, resulting in a $n \times m$ matrix. A row can then be considered as the connectivity pattern of a particular voxel to the rest of the brain. From the $n \times m$ matrix a $n \times n$ distance matrix was then constructed by taking the Euclidean distance between any row pair. The $n \times n$ distance matrix was then normalised and transformed to a Gaussian similarity matrix. A spectral clustering algorithm was then applied on the similarity matrix to cluster the n voxels into 2 groups (Shi and Malik, 2000; Luxburg, 2007).

Results

The number of visual areas determined with the functional MRI experiments per subject varied between 27 and 35 as per subject different visual areas were identifiable. A total of 37 distinct visual areas, listed in Table 4.1, were used for connectivity analysis in the following paragraphs. In Figure 4.1 the visual areas of all subjects are shown. In contrast to previous related work (Kim and Kim, 2005; Kim, Ducros, et al., 2006), we identified those areas that can be localised using retinotopic or motion stimuli. Across all subjects it was observed that identical visual areas had anatomical variations (Stensaas et al., 1974; Dougherty et al., 2003; Wilms et al., 2005).

The structural network between visual areas

The average structural network between visual areas was processed and displayed using the Gephi software package (Bastian et al., 2009). The node layout of the network has been accomplished by first applying the force-based algorithm ForceAtlas2 (Fruchterman and Reingold, 1991; Bastian et al., 2009; Jacomy et al., 2011) on the graph after which nodes have been manually repositioned for better visibility and to ensure interhemispheric node symmetry. A graphical representation of the network is given in Figure 4.2 (an interactive web-version of the figure can be found at <http://www.emilnijhuis.com/visualnetwork/>). Several descriptive network analyses have been performed using Gephi which are reported in the following paragraphs (Bastian et al., 2009).

With a network modularity analysis (Blondel et al., 2008; Lambiotte et al., 2008) four distinct modules were discovered with a modularity of $Q=0.569$, indicating a strong community structure (Newman and Girvan, 2004). The largest module was found on the left hemisphere consisting of the visual areas V2d, V3d, V3A, V3B, MT, MST, LO1, LO2, V6, posterior IPS and anterior IPS. An identical module was also found on the right hemisphere (excluding the areas LO1 and LO2). The other remaining modules were the visual areas: V1d, V1v, V2v, V3v, hV4, VO1, VO2 on the right hemisphere and an identical module in the left hemisphere (excluding the area VO2, which was not mapped in the left hemisphere). The results of the modularity analysis show that the network can be separated with the exception of V1 into dorsal and ventral visual areas.

To determine the importance of individual nodes within the visual system's network and its modules we employed several connectivity measures. The node connectivity analysis revealed that the visual V1d, V1v on both hemispheres had the most streamlines (weighted node degree) within the visual network, whereas V3d was connected with the highest number of distinct visual areas (unweighted node degree). V1d, V1v and V3d visual areas were also found to have highest PageRank (Brin and Page, 1998) within the network. The highest weighted betweenness centrality values (Brandes, 2001) were found in the visual areas V3d and V3A.

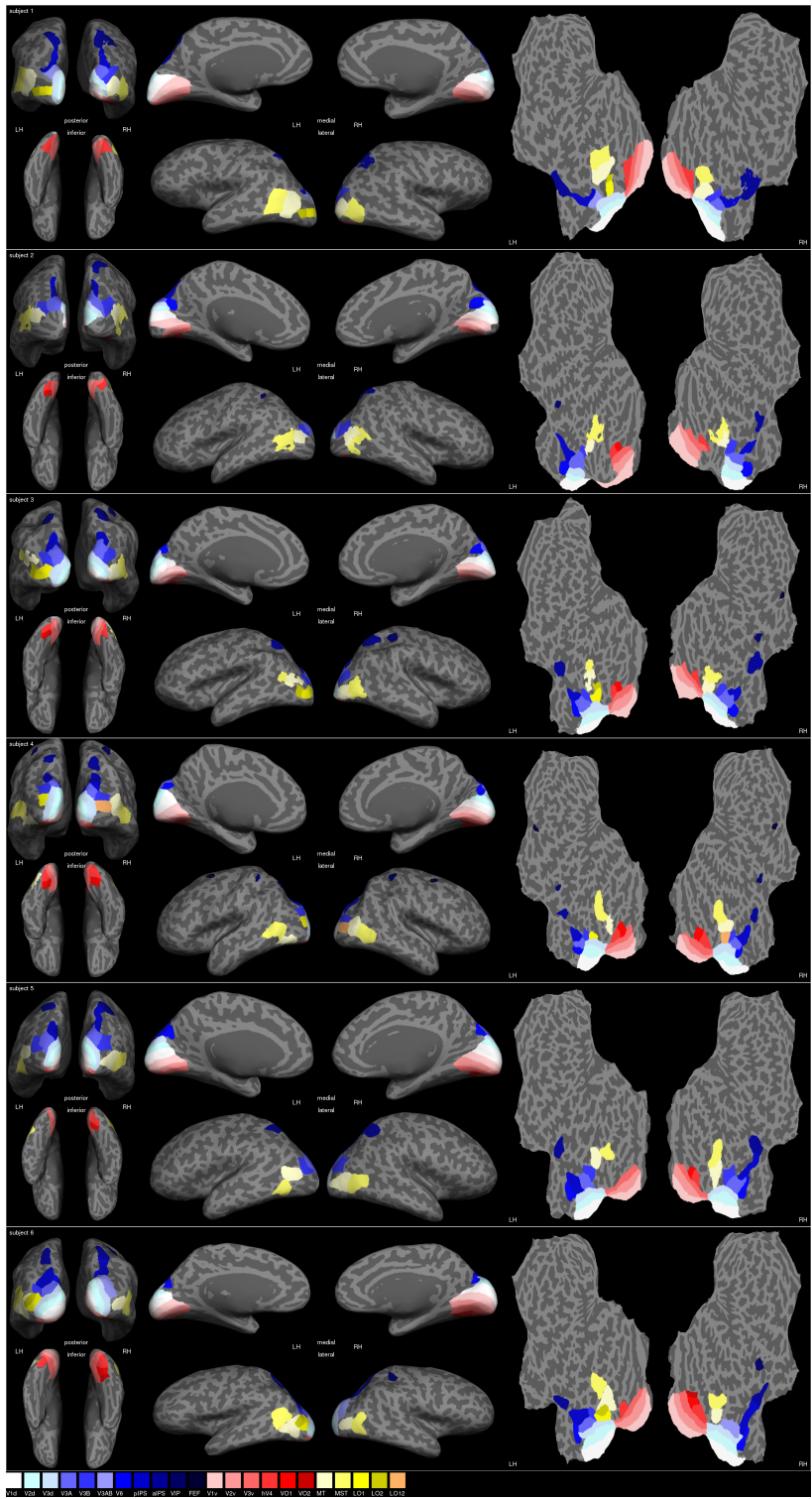


Figure 4.1

Shows the visual areas of subjects 1-6, including composite visual areas V3AB and LO12. On the left side inflated brain surfaces can be seen in posterior, inferior, lateral and medial views. On the right side flattened brain surfaces (flat maps) are displayed. Visual areas have been drawn with three colour bases: blue for “dorsal stream” areas, red for “ventral stream” areas and yellow for motion-sensitive areas.

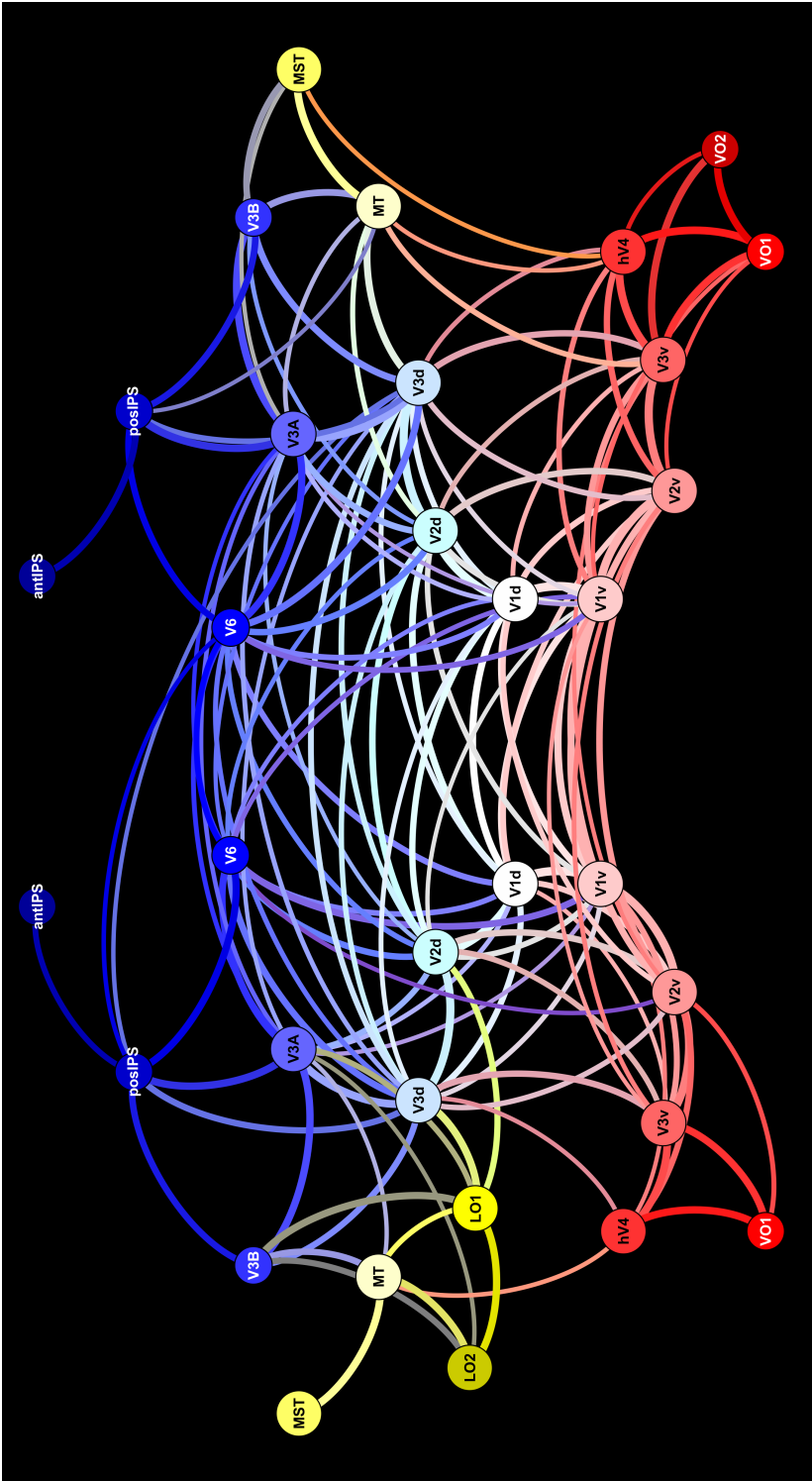


Figure 4.2

Shows the network description of the structural network of analysed visual areas. For consistency within this text the nodes of visual areas have been coloured according to the same scheme as Figure 4.1. Edges have been coloured by “averaging”/mixing the colours of the nodes they are connecting. The thickness of an edge reflects the logarithmised number of streamlines between visual areas. The size of a node shows the number of times a visual area has been measured across the test subjects.

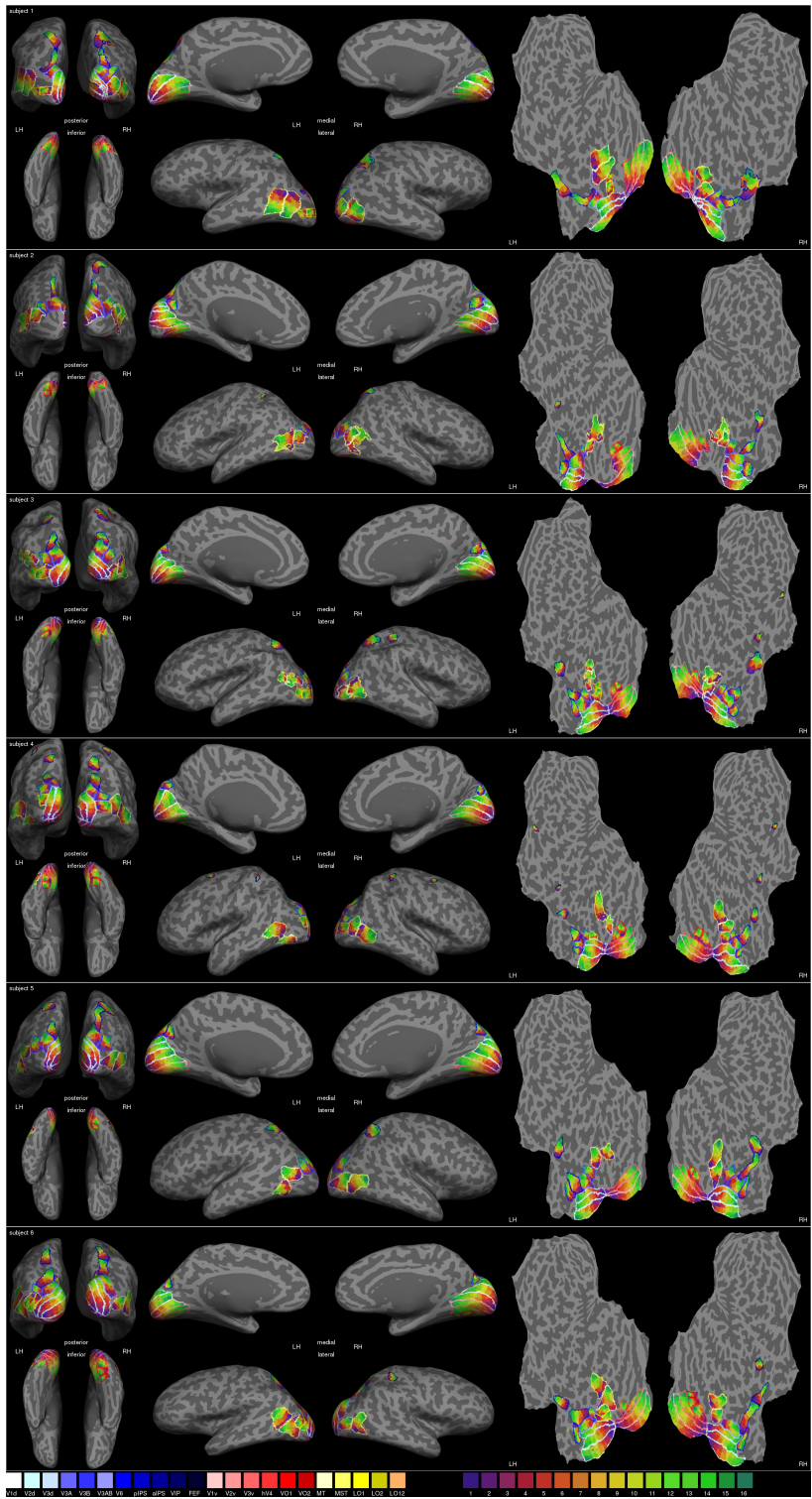


Figure 4.3

Shows the algorithmically defined regions of the visual areas of all subjects, including composite visual areas V3AB and LO12. On the left side inflated brain surfaces can be seen in posterior, inferior, lateral and medial views. On the right side flattened brain surfaces (flat maps) are displayed. The contours of the visual areas have been drawn with three colour bases: blue for “dorsal stream” areas, red for “ventral stream” areas and yellow for motion-sensitive areas. The visual regions have been drawn with sixteen colours for which their indices have been giving on the adjacent colour scale.

The connectivity patterns between visual areas

For all subjects every visual area was subdivided into 16 regions (the results of the visual area division procedure are displayed in Figure 4.3). To see how a visual area projects onto the rest of the brain we have created connectivity maps for all visual areas and every subject.

A sample map for V1v in the left hemisphere for subject 4 and 6 can be seen in Figure 4.4 (for all other connectivity maps see Supplementary figures A.1-A.37). From Figure 4.4 it can be seen that within the same hemisphere the colouring pattern from central to peripheral parts of left V1v is retained also within the visual areas V1d, V2 and V3. However the peripheral regions of left V1v project less intensively onto the visual regions of left V2, V3 as projections from central regions of left V1v are projecting more predominantly onto left V2 and specifically V3d. The colouring pattern of the contralateral visual regions V1, V2d and V3d look similar to ipsilateral V1v. However in contrast to ipsilateral visual regions peripheral regions from left hemispheric V1v project more intensively on the contralateral visual regions compared to central regions. In summary this suggests that central projections from left hemispheric V1v are predominantly projecting to higher level visual areas V2 and V3, while peripheral projections are predominant in right hemispheric visual areas V1, V2 and V3.

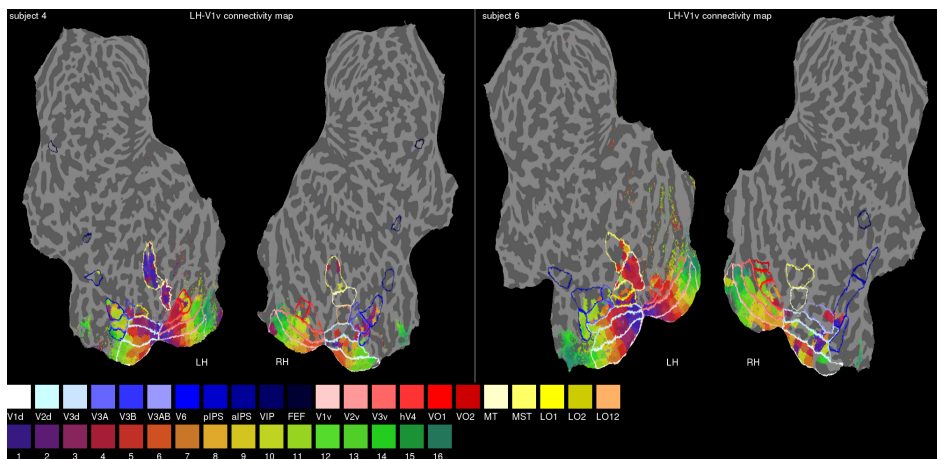


Figure 4.4

Shows the connectivity maps for the left hemispheric visual area V1v of subject 4 and 6 on their brain flat maps. The coloured contours indicate the borders of the subjects' visual areas. Within visual area V1v in the left hemisphere each of the 16 regions received a unique colour corresponding to the index of the region (see legend). The colours in the rest of the brain display which of the sixteen V1v regions project most to that particular vertex or region. In case no streamlines were found between V1v and a vertex or region no colours were assigned. The holes within visual areas in the flat maps are the result of projection errors from labelled voxels to surface vertices.

As the connectivity maps only visualise the maximum projections between one visual area and the rest of the brain, we have also created coloured coded connectivity matrices to give a more complete visualisation of how visual regions are interconnected with one another. The connectivity matrices of all visual areas pairs have been assembled in a larger connectivity matrix in Figure 4.5 (for the individual connectivity matrices of subject 1-6 see Supplementary figures A.38, A.39, A.40, A.41, A.42 and A.43 respectively). Figure 4.6 shows an example connectivity pattern between the visual regions of V1d and V2d in the left hemisphere. It can be noticed that higher entries within the matrix can be mostly found above the main diagonal, which was typical for all connectivity patterns between visual areas V1, V2 and V3. The off-diagonal patterns suggest that projections from posterior ranked regions of earlier visual areas are fanning out towards more anterior ranked regions of higher visual areas. These observations from the connectivity matrices are consistent with those made from the connectivity maps in Figure 4.4 and suggest that representations from posterior (central) regions of V1 become more predominant with increasing hierarchy.

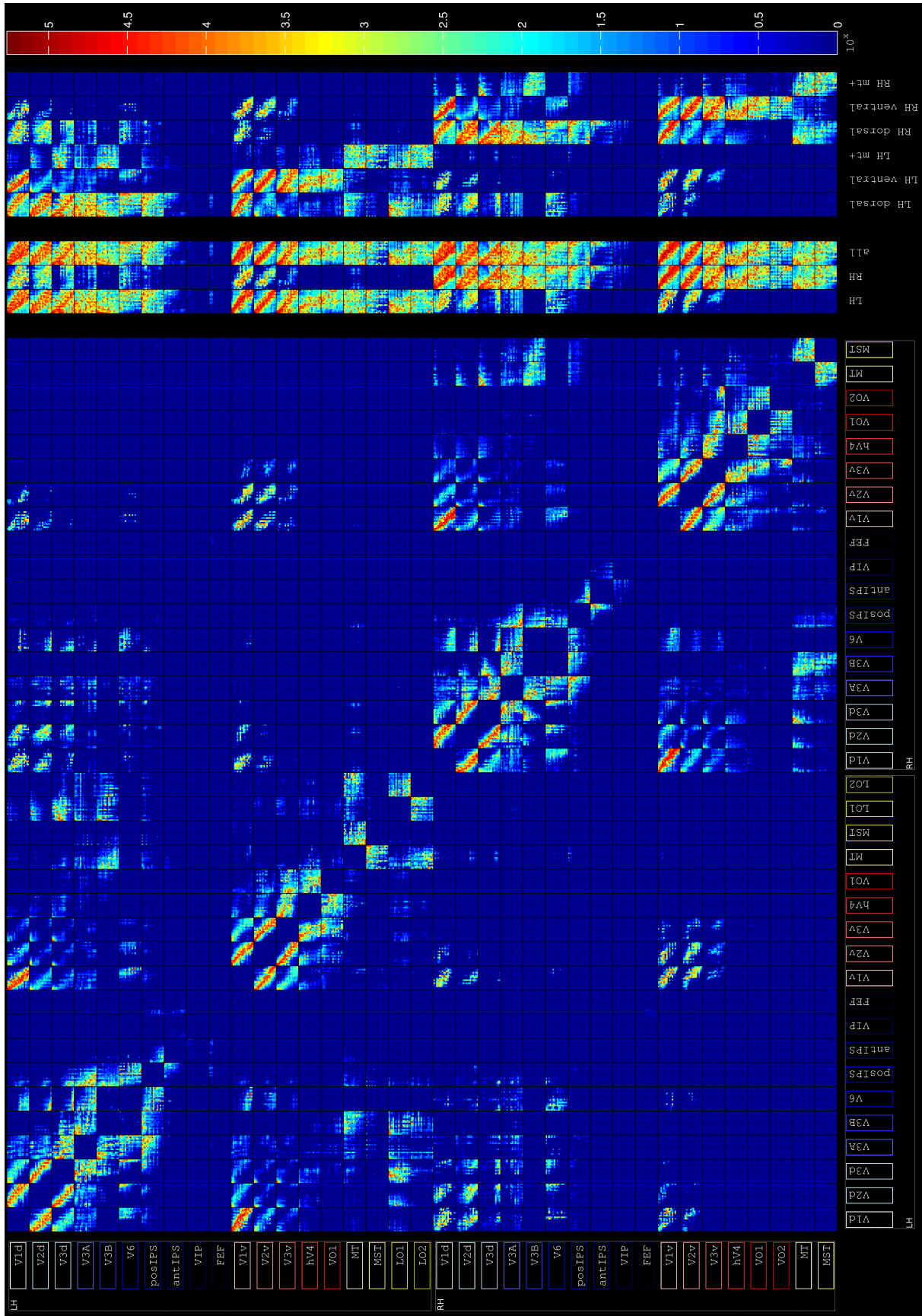
A Mann-Whitney U-test showed that left and right V3A, V6, posIPS and left V3B had statistically significantly more streamlines from anterior visual regions compared to posterior ones ($p_{2tailed-FDR}(q=.001)<.01$ for right posIPS otherwise $p_{2tailed-FDR}(q=.001)<.001$, see Table 4.2). In right V3B this pattern was reversed ($p_{2tailed-FDR}(q=.001)<.001$). To plot this difference in values the 16×16 matrices were reduced to 1×16 row vectors through column summation, such that the first 8 values reflect the connections to V3A or V3B from posterior areas of V1, V2 and V3. In Figure 4.7 a visualisation of the distribution using the row vectors has been given. With the same analysis for visual area hV4, VO1 and VO2 in Table 4.2 and Figure 4.7 it can be seen that in contrast to V3A, hV4 has significantly more streamlines from posterior visual regions of V1, V2 and V3 compared to anterior ones ($p_{2tailed-FDR}(q=.001)<.001$). However visual areas VO1 and VO2 have significantly more streamlines from anterior regions than from posterior regions of V1, V2 and V3 ($p_{2tailed-FDR}(q=.001)<.001$).

Voxel based spectral clustering of visual areas

Splitting visual areas with a spectral clustering algorithm into two clusters mostly resulted in a scattered division pattern of voxels. A typical connectivity map for such a scattered pattern is given in Figure 4.8. Unlike the central/peripheral organisation of V1v it can be noticed that no similar separation of anterior and posterior regions has been accomplished by clustering based on whole brain connectivity patterns.

Figure 4.5 (facing page)

Shows a 592×592 matrix which consists of a 37×37 grid of 16×16 matrices. Each of the 16×16 matrices describes the connectivity pattern between different visual regions, like the one shown in Figure 4.6. The 16×16 connectivity patterns of a visual area have also been grouped by matrix summation on the right side of the matrix for the left hemisphere ('LH'), the right hemisphere ('RH'), the whole brain ('all'), blue labelled visual areas ('LH/RH dorsal'), red labelled visual areas ('LH/RH ventral') and yellow labelled visual areas ('LH/RH MT+').



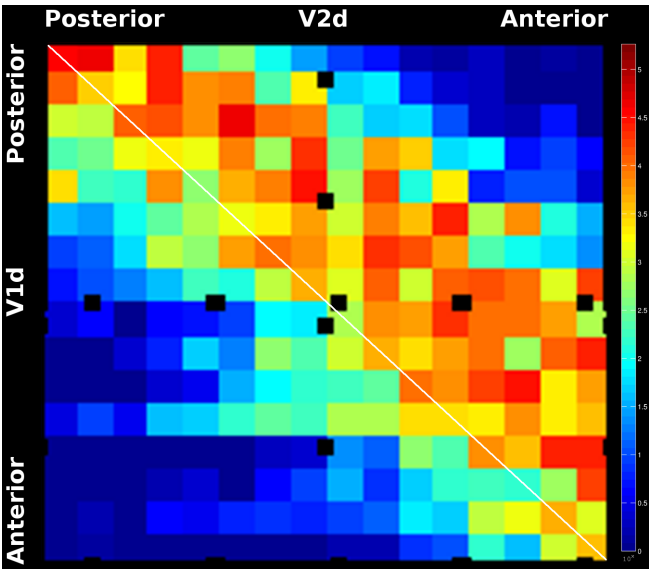


Figure 4.6
Shows how the 16 visual regions of V1d and the 16 visual regions V1v in the left hemisphere are interconnected with one another. The colour reflect the logarithmised numbers of streamlines between different visual regions. The top left entry of the matrix is the connectivity strength between the most posterior visual regions of V2v and V1d and the bottom right entry shows the strength between the most anterior visual regions of both visual areas. The matrix has superimposed black dots which render the boundaries of the matrices quadrants and a white line has been drawn to mark the main diagonal.

Visual Area	<i>U</i> ₂₅₄	<i>Z</i>	<i>p</i> _{2tailed-FDR(<i>q</i>=.001)}
LH-V3A	2811.0	−9.08	< .001
LH-V3B	6264.0	−3.35	< .001
LH-V6	1646.5	−11.17	< .001
LH-posIPS	4398.5	−6.58	< .001
LH-hV4	4512.0	6.21	< .001
LH-VO1	5370.5	−4.77	< .001
RH-V3A	4074.0	−6.95	< .001
RH-V3B	5981.0	3.92	< .001
RH-V6	756.0	−12.59	< .001
RH-posIPS	6703.0	−2.77	< .01
RH-hV4	2319.5	9.92	< .001
RH-VO1	2334.5	−9.90	< .001
RH-VO2	2206.5	−10.60	< .001

Table 4.2
Mann-Whitney U test results for differences in connectivity for visual areas to anterior and posterior regions of V1, V2 and V3.

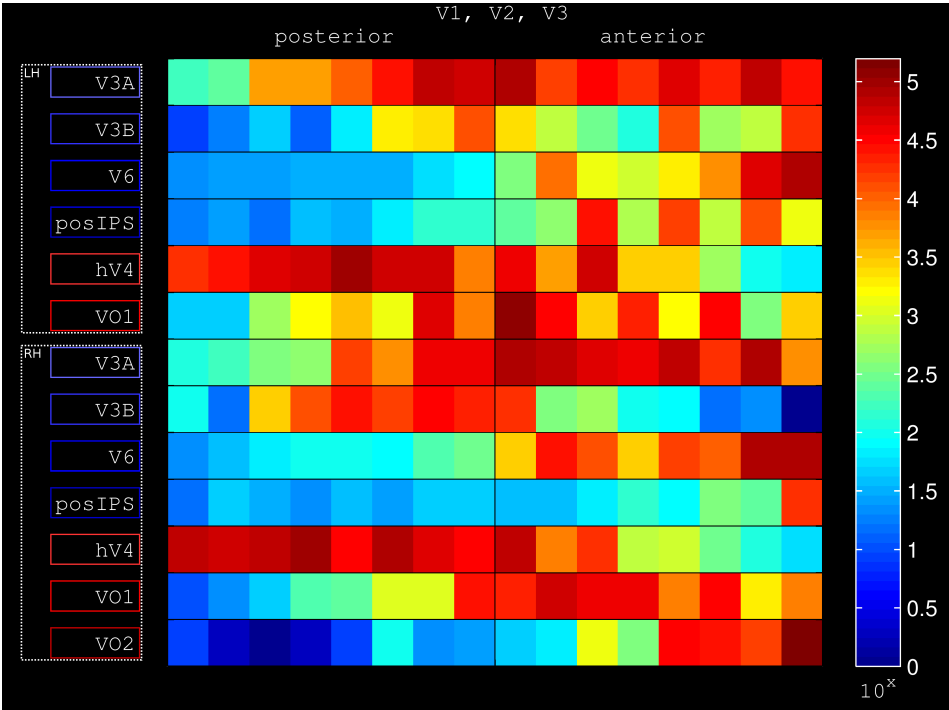


Figure 4.7
Shows the distribution of streamlines from anterior and posterior regions of V1, V2 and V3 map onto left and right V3A, V3B, posIPS, hV4, VO1 and right VO2.

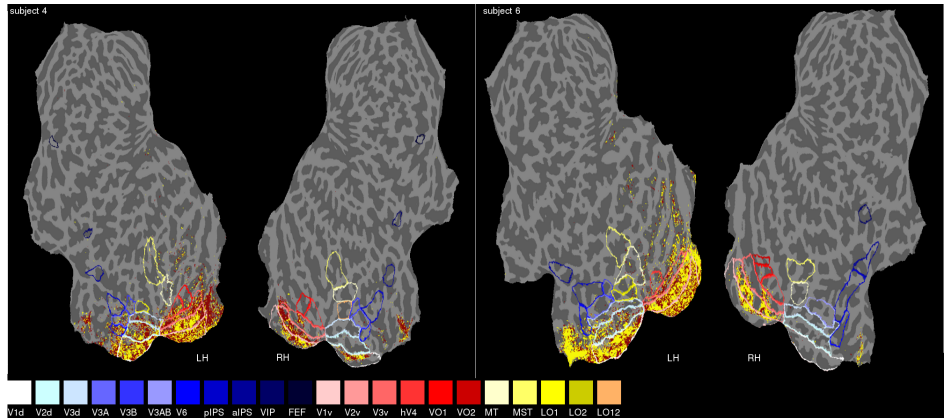


Figure 4.8
Shows the spectral clustering result of V1v for subject 4 and 6. Within visual area V1v the yellow and red vertices represent the two groups vertices computed by the clustering algorithm. Outside the visual area V1v the red and yellow dots reflect which of the two groups has the most streamlines connected to that particular vertex.

Discussion

This study has produced a description of the visual system's projectome: the network of streamlines between visual areas and their connectivity patterns. With it we aim to show whether known properties of the visual system are reflected in their connectivity patterns. The results therefore add to literature on the visual system by providing various perspectives on the complex white matter connectivity patterns between visual areas. Many of the connections found are consistent with invasive tracer studies in macaques (Felleman and Van Essen, 1991; Reid et al., 2009). While for other connections, like a connection between MST and V6 in macaques (Galletti et al., 2001), we did not find evidence exceeding the threshold limit of a thousand streamlines. In the following paragraphs the results are discussed in order of the previously stated four hypotheses and we conclude with an outlook on future work.

The modular organisation of visual areas

The constructed network between visual areas has a modular organisation which corresponds with the 'what' and 'where' streams of the visual system (Baizer et al., 1991; Ungerleider and Haxby, 1994). The dorsal and ventral parts of primary visual cortex V1 were not members of two different modules, because of their strong inter-connectivity. V1 showed more affinity with the dorsal module instead of the ventral module. From the results however it does not follow that V1 is a 'dorsal' stream area. Instead, the participation of V1 in the dorsal module may be due to the fact that the constructed network has a larger quantity of visual areas belonging to the 'where' stream than those belonging to the 'what' stream. The force-based informed layout of the graph in Figure 4.2 affirms these properties, as dorsal and ventral visual areas were grouped together and positioned according to their presumed hierarchy (Reid et al., 2009).

While the results show that visual areas can be grouped into two modules, they also display their inter modular connectivity patterns. A node connectivity analysis revealed that visual areas V1, V3A and V3d were the most central areas within the network, which may imply their role as gateways between the two different modules. The results therefore reconcile the view that visual processing mainly follows two pathways, while there is observed cross-talk between the two pathways (Schenk and McIntosh, 2010; de Haan and Cowey, 2011).

The projections between V1, V2 and V3

From the connectivity maps of ventral V1v in Figure 4.4 it can be seen that the maximum projections between regions of visual areas follow a pattern that is similar to the pattern of eccentricity maps (Larsson and Heeger, 2006; Wandell et al., 2007). Furthermore the 16x16 matrices between visual areas V1, V2 and V3 typically showed an off-diagonal connectivity pattern. The pattern suggests that the more central visual field projections from V1 are fanning out with increasing hierarchy within the visual system, while the more peripheral regions of V1 are less dominantly projecting onto the regions of V2

and V3. Research on population receptive fields has shown that population receptive field sizes increase with increasing eccentricity and across visual areas V1, V2 and V3 with increasing hierarchy (Dumoulin and Wandell, 2008; Amano et al., 2009; Harvey and Dumoulin, 2011). From their research follows that regions from earlier visual areas project to a larger array of regions of higher level visual areas. The off-diagonal connectivity pattern between visual areas V1, V2 and V3 observed in this study may be related to the observed difference of population receptive field sizes, as the pattern indicates that more anterior ranked regions of V2 and V3 receive input from a larger array of earlier visual regions than more posterior ranked regions.

The projections of V1, V2 and V3 to higher level visual regions

By comparing the distribution of posterior and anterior streamlines from visual areas V1, V2 and V3 onto dorsal areas V3A, V3B, V6 and antIPS and ventral areas hV4, VO1 and VO2 we detected statistically significant differences. The results for the tested dorsal areas, with the exception of right V3B, show that they have more connections with anterior regions than with posterior regions of V1, V2, V3. This outcome has correspondence with the theory that dorsal areas receive preferentially input from peripheral field representations (Baizer et al., 1991; Gattas et al., 1997). The exception for right V3B with this theory may be explained with observations which show that right V3B primarily activates to stimuli presented in the central visual field (Larsson and Heeger, 2006). The results for the tested ventral areas showed hV4 had more streamlines from posterior regions of V1, V2 and V3, while areas VO1 and VO2 were more connected to anterior regions. Since the visual areas VO1 and VO2 have only been recently discovered (Brewer et al., 2005) and posterior regions of V3v (with larger population receptive fields) primarily project onto VO1 and VO2 it is unclear whether the observed connectivity patterns for VO1 and VO2 diverge from the theory that ventral stream areas preferentially process central field representations (Baizer et al., 1991; Gattas et al., 1997).

Automatic clustering of visual areas

Research on diffusion-based clustering of brain regions (Johansen-Berg et al., 2004; Solano-Castiella et al., 2010; Mars et al., 2011) has shown that parts of the brain can be subdivided into contiguous areas based on their connectivity patterns. The automatic clustering approach of visual areas however showed that the peripheral and central visual field regions cannot be trivially distinguished with their connectivity pattern to the rest of the brain. More remarkably the used clustering approach did not result in contiguous areas but resulted in two groups of multiple unconnected areas.

Future work

The present work has shown the benefits of constructing the visual system's projectome, however the field of diffusion-based MRI techniques is continuously progressing. Recent applications are able to distinguish layer-specific differences in in-vitro human primary

cortex (Kleinnijenhuis et al., 2012). Developments of MR multiplexing techniques like blipped CAIPIRINHA (Setsompop et al., 2012) and PINS (Norris et al., 2011) foretell that the frontier for diffusion-based techniques is shifting as imaging data can be acquired quicker and with higher resolution (McNab et al., 2013). With this in mind it is important to continue revisiting the visual systems projectome and obtain connectivity maps with increased detail. Future work should also consider the use of high-resolution layer specific functional MRI techniques at 7 Tesla (Polimeni et al., 2010) to add a description of the functional projectome in resting-state conditions (Gusnard and Raichle, 2001). Further functional neuroimaging research is likely to reveal new retinotopic defined visual areas and including these in the projectome may aid in the discovery of new maps (Wandell and Winawer, 2011). Finally there is an opportunity to investigate the plasticity and morphometry of the visual system's projectome under disease or training, genetic and developmental conditions.

5

**Neocortical network damage assessment
by homotopic lesion mapping
on healthy subjects**

Abstract

This study introduces a region of interest (ROI) based analysis method to estimate the effect of a lesion on the neocortical structural network. The approach simulates the impact of lesions within specific ROIs on the neocortical structural networks of a population of healthy controls (n=52) imaged with high angular resolution diffusion weighted imaging (HARDI) protocol. The lesion effect was estimated by determining three network measures: node efficiency, node degree and betweenness centrality in the neocortical network with and without the lesion. Ten stroke lesions from subjects with visual field defects and two simulated lesions were examined with the goal of creating topographic damage maps which reveal the local and global effects of a lesion to the neocortical network in both hemispheres. A correlation analysis showed that the observed reduction in node efficiency in the occipital lobe and the visual field defect of the subjects had statistically significant correlation coefficients. The method proposed here can therefore be seen as complementary to voxel-based lesion-symptom mapping methods by providing a graph theoretical perspective on the effect of a lesion on the neocortical network.

*“Measure what is measurable,
and make measurable what is not so.”*

-Galileo Galilei-

Introduction

As the human brain circumscribes a complex network structure, damage to the brain is often not only confined to its local surroundings but has also global ramifications (Andrews, 1991; Seitz et al., 1999; Stam et al., 2009). Some examples are the effects of a tumour or stroke on cognition (Bates et al., 2003; Bosma et al., 2009). Cognitive impairment is common after stroke, and its frequency is likely to increase with improving stroke survival. To prevent further cognitive decline after stroke, we need to better understand its aetiology (Van Dijk and De Leeuw, 2012). Studying the macroscopic structural network of the brain provides an opportunity to determine the aetiology of cognitive impairments after stroke (Honey and Sporns, 2008; Alstott et al., 2009; Johansen-Berg et al., 2010; Johansen-Berg, 2010). By determining how specific lesions affect the network of the brain and its underlying cognitive functions one could then use this information to provide tailored rehabilitation programs which optimise and stimulate recovery (Jang et al., 2008; Johansen-Berg, 2010).

While determining the location and scope of a lesion has advanced with modern MRI techniques (Le Bihan, 2003; Johansen-Berg et al., 2010; Crofts et al., 2011), it remains a difficult task to predict or assess the impact on the neocortical network of a lesion such as a cerebral vascular attack. Previous work by Bates et al., 2003; Rorden et al., 2007; Smith et al., 2013? has shown that the severity of a lesion is related to where it is located. While theoretical work (Honey and Sporns, 2008; Alstott et al., 2009) has indicated that the impact of cortical lesions may be driven by the neocortical network centrality of the missing cortical structure. More recently, network changes in the contra-lateral hemisphere of real lesions were shown by comparing the network structure of patients with that of healthy control subjects (Crofts et al., 2011).

In this study we propose a region of interest (ROI) based simulation method, which estimates the effect of a lesion on the rest of the network. Structural networks were generated with high angular resolution diffusion weighted magnetic resonance imaging data for a healthy control population and network measures were estimated with and without a specific ROI. The impact of a lesion on the connectivity of the neocortical network was then simulated by homotopically mapping ten lesions of stroke patients with visual field defects on the networks of the control population. In addition two simulated lesions in the prefrontal and motor cortex, which would not cause visual field defects, were added in the analyses as test conditions. The approach was used to examine changes in the network measures: node efficiency, node degree and betweenness centrality, which measure the global and local connectedness of a particular

node to the rest of the network. The reduction of these measures, in essence the loss in network connectivity, caused by a lesion was interpreted as the effect of a lesion. We hypothesised that the ten stroke lesions would cause a visible reduction in occipital lobe regions whereas the simulated lesions in prefrontal and motor cortex would only mildly affect the occipital lobe. Our analyses show that the measured simulated damage is related to the visual field defect of the patients and provide a topographic estimate of the most affected brain areas.

Material and methods

Ethics statement

The study was conducted at the Donders Institute for Brain, Cognition and Behaviour, Radboud University Nijmegen the Netherlands. Approval was obtained from the local ethics committee (Commissie Mensgebonden Onderzoek region Arnhem-Nijmegen, The Netherlands). All participants provided written informed consent in accordance with the declaration of Helsinki.

Participants

To simulate actual lesions we scanned thirteen patients with visual field defects and used ten subjects for data analysis (1 female, 9 males, mean age, 61.37 ± 5.96 (SD) yr, right handed). For this study we included only subjects who had a visible stroke related lesion in the white matter or neocortex. Three subjects were excluded because their symptoms were related to a lesion in the thalamus, a small and difficult to detect lesion in the neocortex and a countercoup contusion.

For the reference dataset in the simulation we used 52 healthy subjects under the age of 35 [37 females, 15 males, mean age, 22.59 ± 2.89 (SD) yr] from the Donders Institute Connectivity Data Set 1 (DICOD1, Nijhuis et al., 2013). Exclusion criteria for the used dataset were: left-handedness, incomplete DWI data, and neurological or psychiatric disorders and processing errors.

MRI acquisition

All subjects were scanned on a Siemens 3T TIM Trio system with a 32 channel head coil at the Donders Institute for Brain, Cognition and Behaviour, Radboud University Nijmegen.

Anatomical scan

High resolution anatomical scans were acquired using a T1-weighted 3D MPRAGE sequence with TE=3.03ms, TR=2300ms, TI=1100ms, a flip angle of 8°, FOV=256mm, 192 slices with 1mm thickness and a 256×256 imaging matrix resulting in 1mm isotropic voxels.

Diffusion weighted imaging (only for reference dataset)

Diffusion weighted imaging volumes were acquired using a single-shot echo-planar imaging (EPI) sequence with phase encoding in the anterior to posterior direction, with TE=101 ms, TR=13.0s, FOV=220mm, 70 slices with 2mm thickness and an 110×110 imaging matrix resulting in 2mm isotropic voxels. Measurements were taken in 256 non-collinear directions at a b-value of 1500 s/mm². In addition, 28 volumes were acquired with b=0 s/mm².

Data analysis

The goal of the analysis is to simulate the effect of a lesion in the brains of healthy subjects. Three network parameters: betweenness centrality, node degree (Barthelemy, 2004) and node efficiency were estimated for the neocortical structural network with or without lesion. Node degree is the number of connections of a node to other nodes. Betweenness centrality describes the fraction of shortest paths between arbitrary nodes through a specific node. We define node efficiency as the average efficiency in communication (Latora and Marchiori, 2001) of a particular node with all other nodes in the network. The results of the network analysis were displayed and evaluated on the Freesurfer average brain surface (Fischl et al., 1999). Subsequent paragraphs will describe the simulation procedure.

Non-linear mapping of lesions from patients to healthy subject dataset

The anatomical scans of all subjects were non-linearly co-registered using FNIRT (Smith et al., 2004) to the MNI152 1mm standard space (Grabner et al., 2006). The patients' lesions were manually segmented using MRICron (Rorden and Brett, 2000) and non-linearly mapped via the MNI template brain onto the healthy subjects of the reference dataset. Brain lesions were marked with the *-inmask* option of FNIRT such that the lesions did not contribute towards the estimation of the non-linear transformation parameters. In addition to the ten lesions from our participants we also created two fictitious lesions in the right prefrontal and motor cortex of the MNI template using MRICron's 3D sphere drawing tool.

Simulating effect of lesion on healthy subject dataset

For each of the 52 healthy subjects we created connectomes (Sporns et al., 2005; Hagmann et al., 2008; Rubinov and Sporns, 2010) with a template free approach which considers twenty different brain parcellations as network configurations (Nijhuis et al., 2011). For each brain in the reference dataset the betweenness centrality, the node degree and the node efficiency were determined for each of the twenty different network configurations. The value of a network measure for a voxel was then given by the average value of a network measure over the twenty nodes which a voxel fell within. The connectivity parameters were then projected from voxelspace to Freesurfer (Fischl et al., 1999) surface overlays. All surface overlays were then mapped onto the Freesurfer

average surface where they were smoothed and averaged to account for anatomical variability between healthy subjects. The procedure yielded damage maps which estimate for each lesion the locations of the most affected brain regions within the neocortical network. To give a large-scale assessment per lesion of which brain areas are most affected, we then tested for hemispheric differences in average reduction of the network measures between the pre-frontal, parietal, occipital and temporal lobes using independent two-sample t-tests.

Estimation of visual field damage and correction with cortical magnification factors

The visual field damage was estimated with manual Goldmann perimetry. With this method, a circular shaped light stimulus is presented against a white background. The stimulus has a diameter of 1° and a luminance of 320 cd/m^2 . The background has a luminance of 10 cd/m^2 . The subject is required to fixate his/her gaze on a central fixation point. During fixation, the stimulus is moved from the periphery of the visual field towards the central visual field along several visual angles until the subject detects the stimulus. In this way, absolute visual field defects are mapped. The eccentricity of a certain visual angle at which the stimulus is detected is recorded as the visual field border at that angle. Measurements are repeated twice at all angles that were probed during perimetry and the average of these measurements is used for establishing the visual field border. A more elaborate description can be found in Bergsma and Van der Wildt, 2010. With the results from the perimetry we then estimated the percentage of visual field damage for 5, 10, 20,... and 90 degrees of eccentricity. A neocortical damage percentage factor was then estimated by adjusting the solid angle of the visual field damage in square degrees with the cortical magnification factors for visual area V1 in Wu et al., 2012: $Ma = 405.3 / (E + 1.717)^2$. For the fictitious lesions 11 and 12 we assumed no visual field damage.

Evaluation of the simulated effect of a lesion

To evaluate the simulated effect of a lesion we compared the average reduction and reduction fraction in node efficiency, node degree and betweenness centrality in the occipital lobe as defined in the PALS-12 atlas (Van Essen, 2005) with the estimated neocortical damage factor, the visual field damage percentage and lesion volume using a correlation analysis.

Results

For each lesion we have simulated its effect on a sample population of healthy subjects. See Figure 5.1 for the twelve lesions displayed in MNI space and Table 5.1 for their corresponding visual field defects as measured with Goldmann perimetry. The impact of all lesions were simulated by determining network measures with and without lesions yielding in surface maps which display the reduction and reduction ratios in node efficiency, node degree and betweenness centrality.

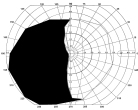
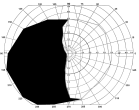
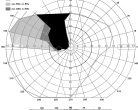
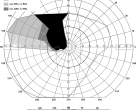
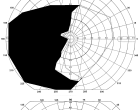
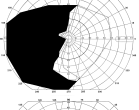

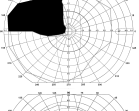

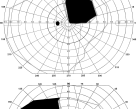
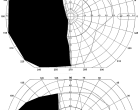
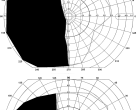


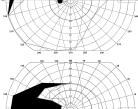
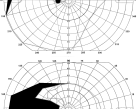
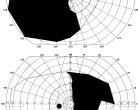
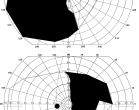
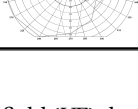
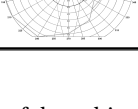
subject	measured visual field		percentage of VF damage	
	left eye	right eye	unadjusted	adjusted
1			49.2%	40.7%
2			19.9%	24.0%
3			48.1%	32.2%
4			22.6%	20.8%
5			8.6%	16.9%
6			48.9%	33.8%
7			15.6%	6.4%
8			17.8%	14.7%
9			44.6%	30.4%
10			20.9%	26.4%

Table 5.1
Lists the visual field (VF) damage of the subjects as measured in the left and right eye. The red and green boundaries indicate the boundaries of the subjects visual field and the grey or black filled areas mark their (partial) visual field defects. The adjusted areal visual field damage scores are corrected with a cortical magnification factor which considers that the central visual field occupies a larger portion from the neocortex than the peripheral visual field (Wu et al., 2012).

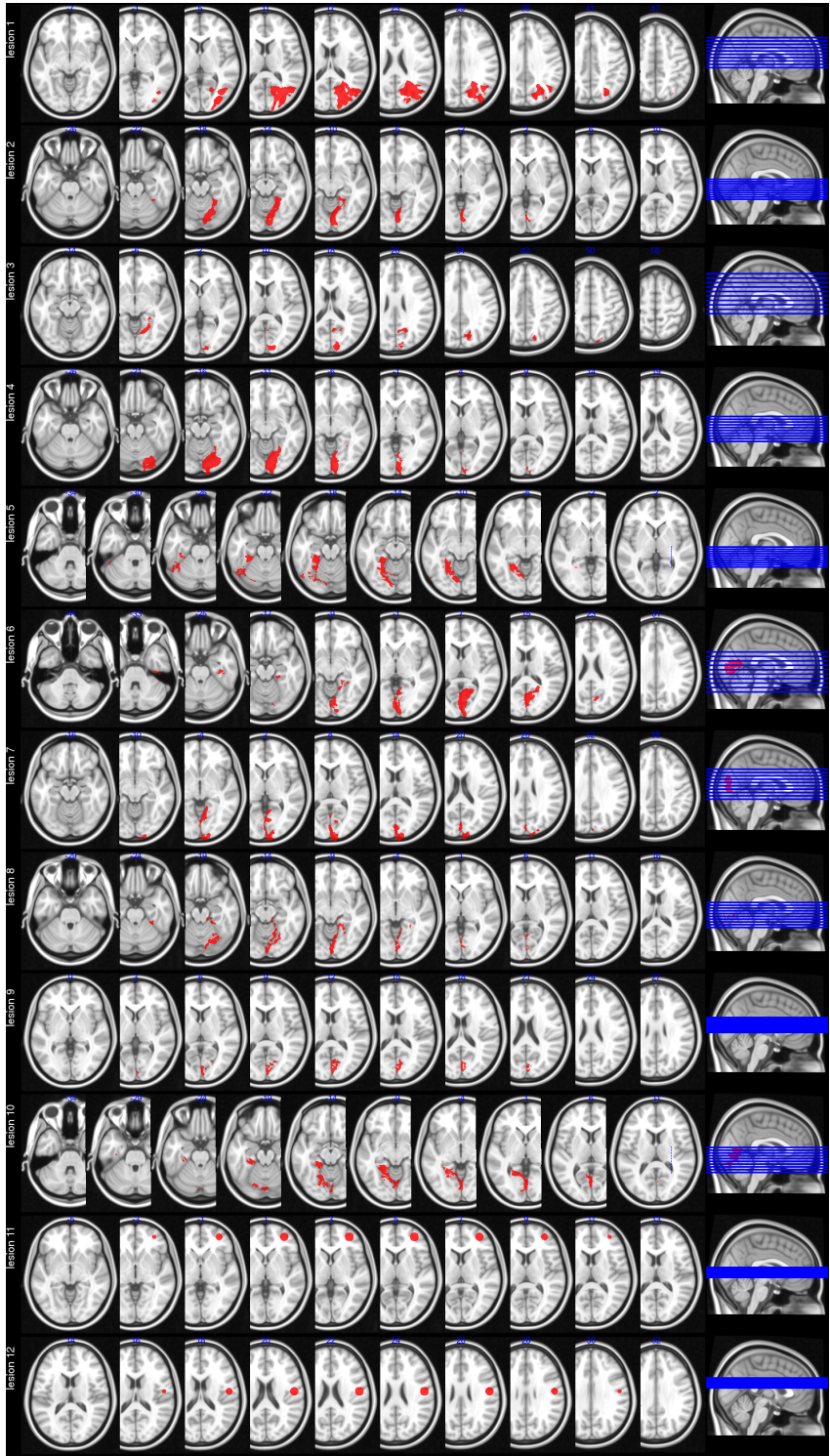


Figure 5.1

Shows the 12 lesions used in this study in MN152 1mm space. Lesion 1-10 are from the stroke subjects and lesion 11 and 12 have been fictitiously created. Each row shows 9 equidistant axial slices including their z-positions and a sagittal view which shows the position of the axial slices.

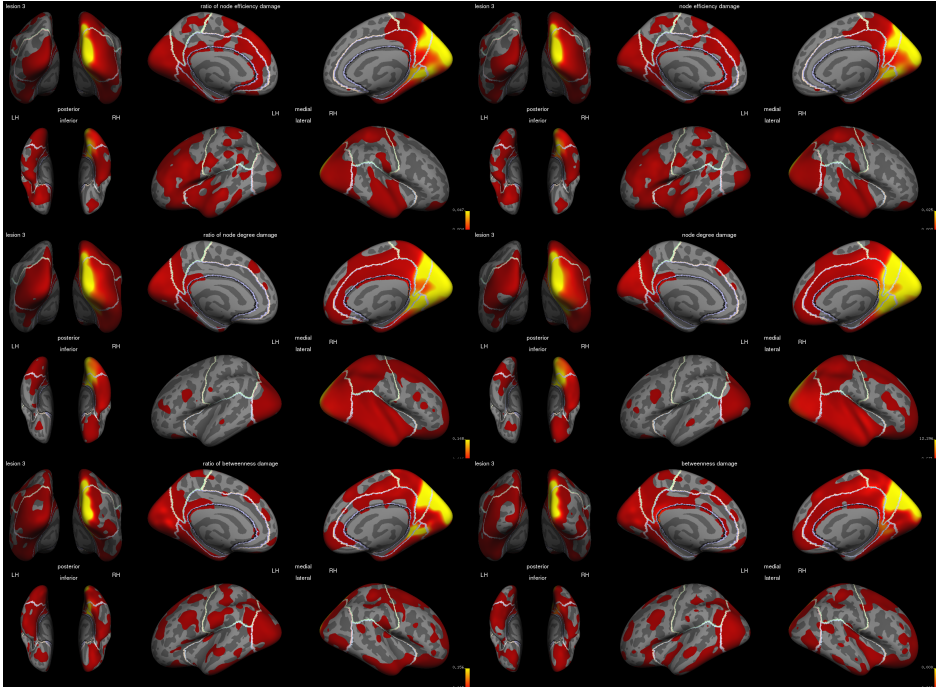


Figure 5.2

shows the upper 50% of affected neocortical regions for lesion 3 on the inflated average Freesurfer surface as estimated by the reduction and reduction fraction of the network measures: betweenness centrality, node degree, node efficiency. Overlaid with colour are the borders of the occipital, parietal, limbic, temporal and frontal lobes as defined with the PALS-12 atlas.

We found that the damage maps using different network measures overlapped substantially and that the vertex-wise distribution of the network measures' reduction fraction were also similar (see Figure 5.2 for the damage maps of lesion 3, displaying the 50th percentile of the most affected areas and Figure 5.3 for the vertex-wise distributions of network measures). In the following paragraphs we will report the observed locations of affected brain areas, their hemispheric differences and evaluate the results of the simulation with a correlation analysis.

The affected brain regions for the simulated lesions

The node efficiency damage maps for all lesions are given in Figure 5.4. Each map was thresholded with a node efficiency factor of 0.003 to highlight the most affected areas and to compare the estimated impact of different lesions. The damage maps display that the impact of a lesion is strongest in neocortical areas adjacent to the lesions. The maps show also that reduction in node efficiency is spread across both hemispheres in homotopic and heterotopic neocortical areas. For lesion number 1 all neocortical areas were above the threshold, as the lesion was comparatively larger than other lesions in this study.

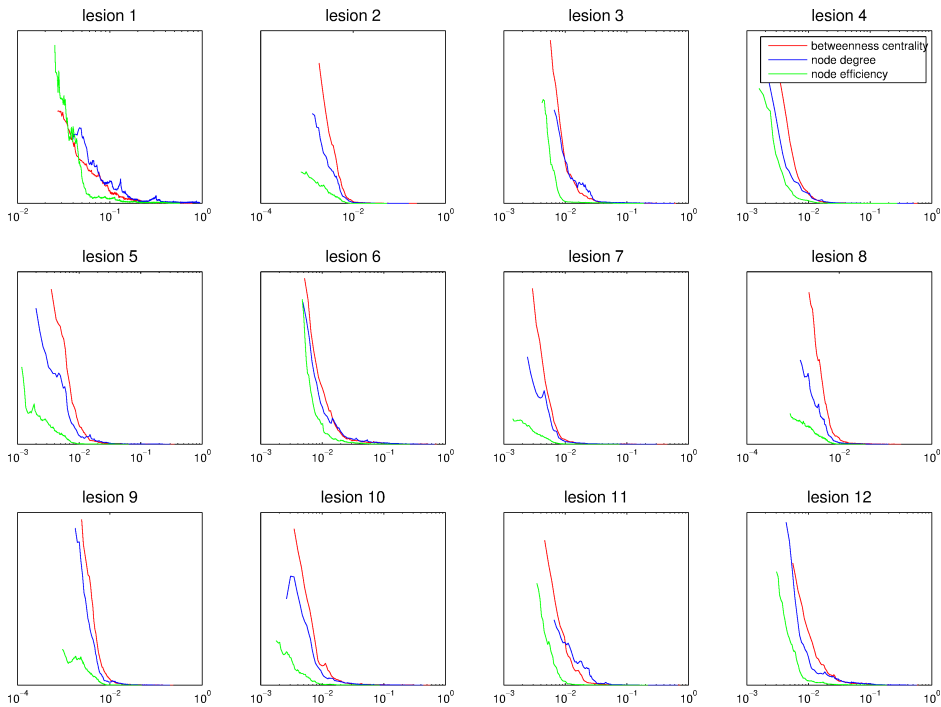


Figure 5.3
Shows the value distributions of the 50% most affected neocortical regions for all lesions using the network measures: betweenness centrality, node degree, node efficiency.

Hemispheric differences in simulated lesion effect

Table 5.2-4 compare the average reduction in network measures per lobe in the left and right hemisphere. We observed that consistent with the location of the lesion the occipital lobe of the ipsilateral hemisphere was always most affected. For the other lobes the location of the lesion did not predict which hemisphere would be most affected. Despite ten out of twelve lesions being located in the right hemispheres, there were proportionally more affected lobes in the left hemisphere than in the right hemisphere. For the two left hemispheric lesions the simulations indicated that for all except one pair of lobes the lobes of the left side of the brain were more affected than the lobes of the right hemisphere.

Evaluation of the simulated effect of a lesion

A correlation analysis (see Figure 5.5) between the average of different network measures of the occipital lobe and the estimated visual field related neocortical damage factor yielded statistically significant Pearson correlation coefficients between $r_{10}=.61$ and $r_{10}=.67$ with $p<.05$ (Spearman rank correlation coefficients between $rs_{10}=.62$, $p<.05$ and $rs_{10}=.77$, $p<.005$). Correlating the average network measures for the occipital lobe with the visual field damage percentage let to weaker Pearson correlation coefficients be-

lesion	hemisphere	occipital	parietal	limbic	temporal	frontal
1	right	RH	RH	RH	RH	RH
2	right	RH	LH	LH	LH	LH
3	right	RH	RH	RH	RH	LH
4	right	RH	LH	LH	LH	LH
5	left	LH	LH	LH	LH	LH
6	right	RH	RH	RH	RH	LH
7	right	RH	LH	LH	LH	LH
8	right	RH	LH	LH	LH	LH
9	right	RH	LH	LH	LH	LH
10	left	LH	LH	LH	LH	LH
11	right	RH	RH	LH	RH	RH
12	right	RH	RH	LH	RH	RH

Table 5.2

Lists for each subject which hemisphere has a higher average node efficiency reduction in the occipital, parietal, limbic, temporal and frontal lobes as defined with the PALS-12 atlas. All hemispheric differences were statistically significant with Bonferroni correction ($n=60$) with $p_{FWER} < .001$, $t_{>25564} > 3.292$. For 56.7% of the lobes the effect of the lesions is higher on the left hemisphere.

tween $r_{10}=.53$, n.s. and $r_{10}=.64$, $p<.05$ (Spearman rank correlation coefficients between $rs_{10}=.57$, n.s. and $rs_{10}=.70$, $p<.05$). Correlating the size of a lesion with the estimated neocortical damage factor yielded a Pearson correlation coefficient of $r_{10}=.64$, $p<.05$ and a Spearman correlation of $rs_{10}=.59$ with $p<.05$.

lesion	hemisphere	occipital	parietal	limbic	temporal	frontal
1	right	RH	RH	RH	RH	RH
2	right	RH	LH	RH	RH	LH
3	right	RH	RH	RH	RH	RH
4	right	RH	LH	RH	RH	LH
5	left	LH	LH	LH	LH	LH
6	right	RH	RH	LH	RH	RH
7	right	RH	RH	RH	RH	LH
8	right	RH	LH	RH	RH	LH
9	right	RH	RH	RH	RH	LH
10	left	LH	LH	LH	LH	LH
11	right	RH	RH	RH	RH	RH
12	right	RH	RH	RH	RH	RH

Table 5.3

Lists for each subject which hemisphere has a higher average node degree reduction in the occipital, parietal, limbic, temporal and frontal lobes as defined with the PALS-12 atlas. All hemispheric differences were statistically significant with Bonferroni correction (n=60) with $p_{FWER} < .001$, $t_{>25564} > 3.292$. For 31.7% of the lobes the effect of the lesions is higher on the left hemisphere.

lesion	hemisphere	occipital	parietal	limbic	temporal	frontal
1	right	RH	RH	RH	RH	RH
2	right	RH	LH	RH	RH	LH
3	right	RH	RH	RH†	RH	RH
4	right	RH	RH	LH	RH	LH
5	left	LH	RH	LH	LH	LH
6	right	RH	RH	RH	RH	RH
7	right	RH	LH	LH	LH	LH
8	right	RH	RH	RH	RH	LH
9	right	RH	RH	RH	LH	LH
10	left	LH	LH	LH	LH	LH
11	right	RH	RH	LH	RH	RH
12	right	RH	RH	LH	RH	RH

† marks statistically significance with Bonferroni correction (n=60) with $p_{FWER} < .005$, $t_{>25564} > 3.090$

Table 5.4

Lists for each subject which hemisphere has a higher average betweenness centrality reduction in the occipital, parietal, limbic, temporal and frontal lobes as defined with the PALS-12 atlas. All except one hemispheric differences were statistically significant with Bonferroni correction (n=60) with $p_{FWER} < .001$, $t_{>25564} > 3.292$. For 36.7% of the lobes the effect of the lesions is higher on the left hemisphere.

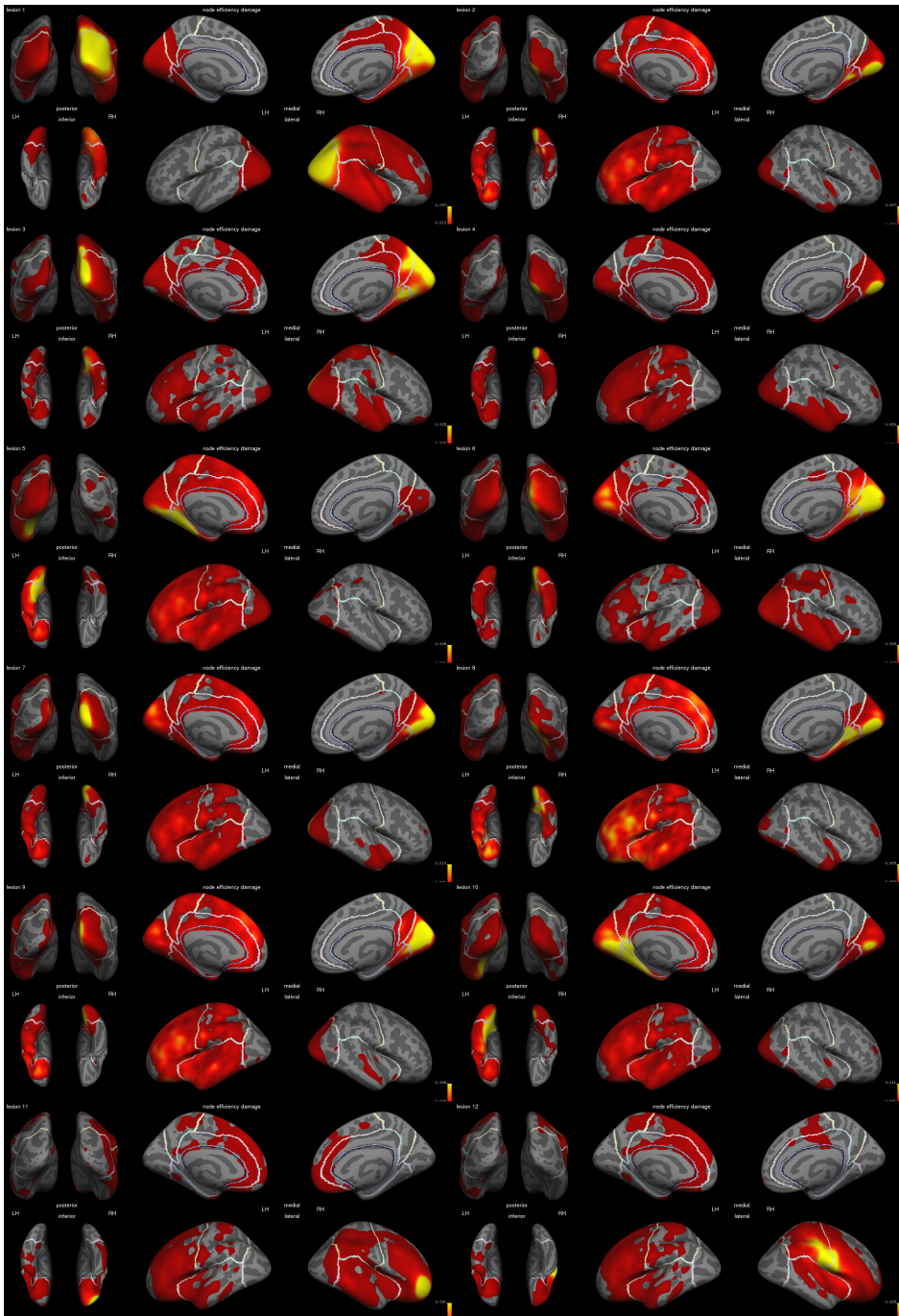


Figure 5.4

Shows for all simulated lesions the neocortical regions on the inflated average Freesurfer surface with a reduction of more than 0.003 in node efficiency. Overlaid with colour are the borders of the occipital, parietal, limbic, temporal and frontal lobes as defined with the PALS-12 atlas.

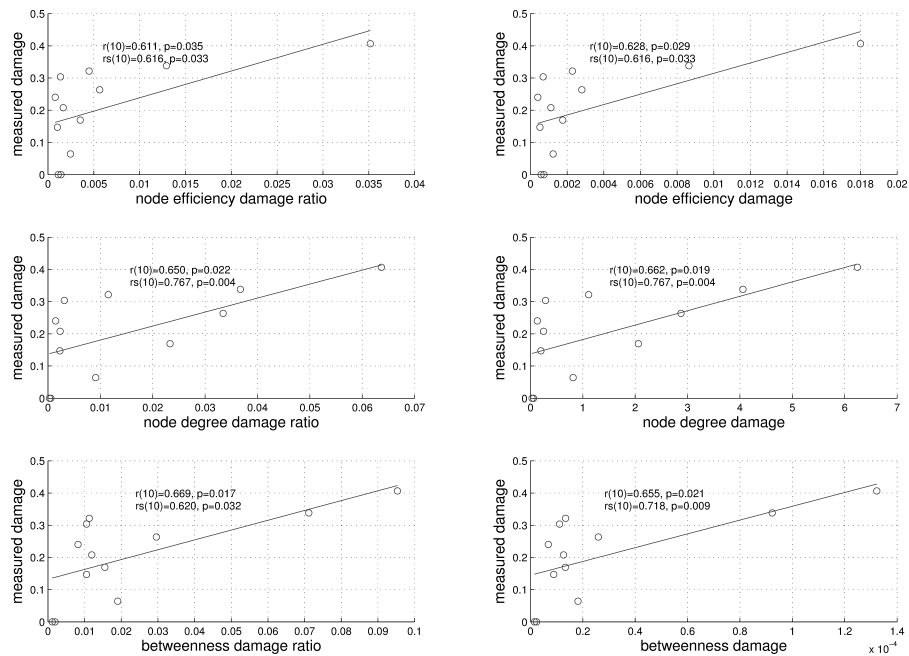


Figure 5.5
Shows the scatter plots of the subjects average occipital lobe node efficiency, node degree and betweenness centrality damage and damage reduction versus their adjusted visual field damage scores. For the fictitious lesions we assumed that their visual field damage is 0. The lines are the best linear fits for the datapoints. Each panel includes the Pearson and Spearman coefficients $r(10)$ and $rs(10)$ and their p-values for the correlation between the datapoints.

Discussion

This study has developed an approach for analysing the impact of a brain lesion to the neocortical network. The results provide for each simulated lesion topographic neocortical network impact maps on the average cortical surface, which estimate affected areas in the ipsilateral and contralateral hemisphere. The approach can be seen as complimentary to voxel-based lesion mapping methods (Bates et al., 2003; Rorden et al., 2007; Smith et al., 2013) by providing a graph theoretical perspective on the effect of a lesion to the neocortical network. Evaluating the effect of a lesion showed similar regions for the three different network measures: node efficiency, node degree, betweenness centrality. Node efficiency would appear to be the most natural of the three measures used, because it is a global connectivity measure which considers the connectivity of node to the whole network, and because damage to the network will evoke a reduction in node efficiency unlike betweenness centrality. However differences in the network measures may be valuable to distinguish in a neocortical region different types of lesion effects. Using several network measures in unison with a multivariate approach should therefore be considered when the goal of the analysis is to identify a certain type of effect in an affected region.

The affected brain regions for the simulated lesions

As anticipated we found that the effect of a lesion was strongest in the neocortical areas adjacent to the simulated lesion, as these areas are more likely to be disconnected from the rest of the neocortical network. Furthermore the damage maps also displayed the global effect of a lesion to the rest of the network. These observed non-local lesion effects are possibly linked with Monakow's concept of diaschisis. It considers that remote areas from a focal lesion have depressed metabolism and cerebral blood flow which may be brought about by acute neurotransmitter changes and degeneration of fiber tracts (Seitz et al., 1999; Brodtmann et al., 2007).

Hemispheric differences in simulated lesion effect

Consistent with previous findings by Crofts et al., 2011 we found that the contra-lateral hemisphere of a lesion showed a reduction in node efficiency. To our surprise however we found that the simulated effect was stronger in many lobes of the left hemispheres than in the lobes of the right hemisphere, despite the fact that most of the lesions were located in the right hemisphere. This was especially true for the left frontal lobe and the measured reduction in node efficiency across hemispheres. The results suggest that regions in the left hemisphere are more at risk of being affected by a lesion causing visual field defects than lobes in the right hemisphere. It is well established that neurocognitive function, anatomy and the structural networks of the hemispheres are asymmetrical organized (Toga and Thompson, 2003; Nijhuis et al., 2013). The stronger effect on the left hemisphere by visual field defects may be related the language dominance and higher small-worldness indices in the left hemisphere.

Evaluation of the simulated effect of a lesion

The correlation analysis showed that simulated effect of the lesions in the occipital lobe was statistically significantly correlated with visual field related neocortical damage factor, indicating a measurable relationship between the estimated damage and impairment. The results suggest that simulating a lesion on a healthy control population may be beneficial to identifying lesion effects.

However in order to use the simulated network damage of the occipital lobe as a predictor for visual field defects, additional properties about the visual system within the simulation should be considered. At the moment the simulation only includes neocortical connections and therefore does not consider damage to incoming fibres of the optic radiation from the lateral geniculate nucleus.

Conclusions & Future work

The impact of a lesion is difficult to assess without knowing the network conditions before the damage occurred. The proposed method circumvents this problem by simulating homotopic lesions in a population of healthy controls, such that a damage map can be derived which visualizes the strongest and most likely affected areas. With the approach we were able to show how a neocortex can be locally and globally affected by a lesion. Effectively we created a methodology based on a connectivity database, which can also be extended to other research questions which are concerned with the underlying structural connectivity patterns for certain regions of interest. Using a larger population database one could furthermore extend the approach by aiming to match individual subjects with a subset of subjects with similar brains in the database to derive more representative network measures.

6

Summary and discussion

“The future influences the present just as much as the past.”
-Friedrich Nietzsche-

The goal of this thesis was to map connectivity in the human brain with macroscopic networks in order to better understand how neocortical areas are functionally and structurally connected with one another. The studies presented in this thesis examined connectivity patterns in the human as measured with magnetic resonance imaging (MRI) methods combined with graph theoretical techniques. The results provide new insights as to how the neocortex is wired together through white matter axonal connections and show that structural connectivity patterns in the brain can be related to observed brain function. This chapter will briefly summarise the main findings of the chapters 2-5, discuss their implication and complete this thesis with an outlook on future research.

Summary of the findings

The aim of **chapter 2** was to provide an alternative to atlas-based nodal configurations which have well known deficits for functional network analysis (Smith et al., 2010). Three different methods to automatically parcel the neocortex into functional distinct brain areas were investigated. The results showed that the neocortical brain parcellations based on structural information, such as folding patterns or axonal connectivity patterns, overlap with functionally defined areas. In the following chapters preference was therefore given to model neocortical networks with automatically or functionally defined parcellation schemes over the use of atlas-based nodal configurations.

In **chapter 3** the question of: “where are the hubs within the neocortical network?” was addressed. To overcome unwanted fragmentation of hubs by a particular node configuration individual brains were modelled with multiple parcellations. The approach showed that network parameters such as node degree and betweenness centrality are topographically distributed on the neocortex, analogous to how urban hubness is distribution on the surface of the earth (see Figure 6.1). For an average population of young adults a topographic hub map of the human neocortical network was then created which showed that neocortical hubs correspond with key areas from known cognitive networks. Analysing the map showed that several hubs are asymmetrically organised across hemispheres and that hubs differed across gender. The results further showed that females have more hubs with higher betweenness centrality than males and that males have multiple hubs with a higher node degree. Female networks had higher small-world indices in both hemispheres compared to males.

The goal of **chapter 4** was to investigate the connectivity patterns between neocortical areas of the visual system. The neocortical visual system was chosen because it is a subnetwork of the neocortex for which numerous functionally defined nodes are known from the literature. In this study, visual areas were defined on the basis of their response

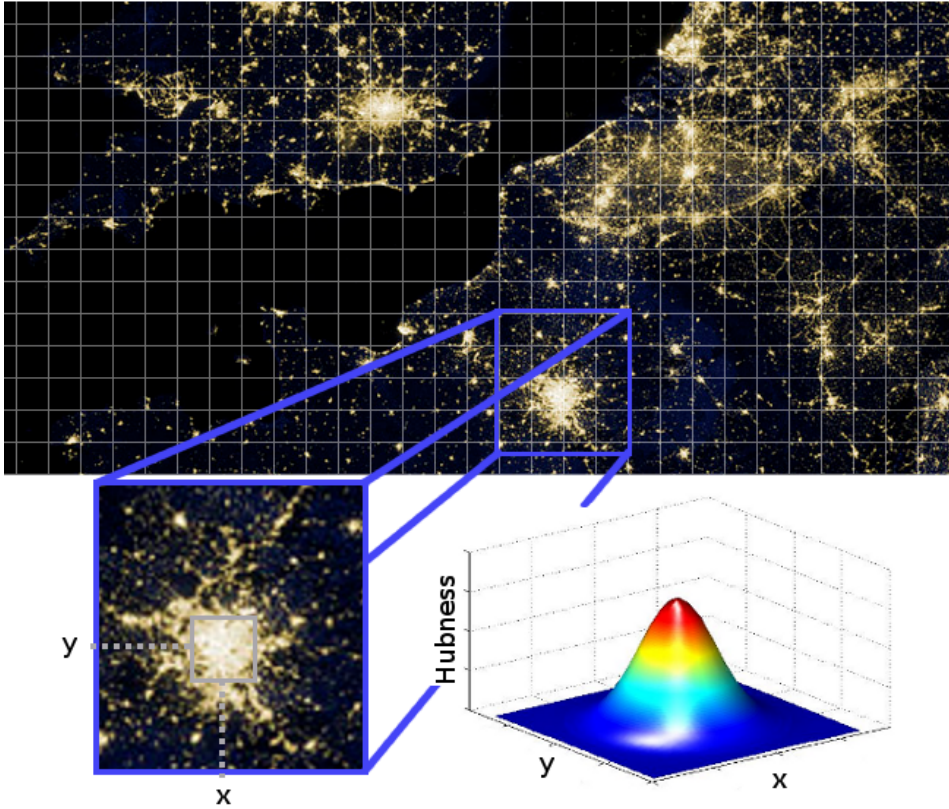


Figure 6.1

Shows a satellite image of Western Europe by night as photographed by (NASA's Earth Observatory/NOAA/DOD, 2012) overlaid with a 2D grid parcelling scheme. Urban hubness can be measured by the light intensity within a square. Depending on the location of the square the hubness score will differ, following a topographic pattern as illustrated in the lower part of the figure with (x, y) dependent square positions in Paris, France.

to visual stimulation as measured with functional MRI combined with retinotopic mapping. The connectivity patterns between visual areas were then estimated with probabilistic tractography at the voxel level. The results give a plausible description of the complex white matter connectivity patterns between visual areas. Analysis showed that the structural network of the visual system is grouped into a dorsal and ventral module, which are commonly referred to as the 'what' and 'where' streams of the visual system (Ungerleider and Haxby, 1994). Furthermore, the inter-areal structural connectivity patterns correspond with the retinotopic organisation of the visual system, e.g. the activation patterns to visual ring stimuli as seen in eccentricity maps (Wandell and Winawer, 2011).

The final research in **chapter 5** explored the possibilities for assessing neocortical network damage by simulating lesions in the neocortical networks within a population of healthy controls. This was accomplished by homotopically mapping lesions from

subjects with visual field defects to a healthy control population. For the healthy controls, neocortical networks were then constructed with and without the inclusion of the lesion. The effect of the lesion on the network was then approximated by differences in network measures. The results of the lesion simulation were calculated and displayed with the topographic mapping approach used in **chapter 3**. The maps revealed that brain regions adjacent to a lesion are affected most in their network connectivity while regions distant from the lesion are also affected, consistent with Monakow's concept of diaschisis that remote areas from a focal lesion may have depressed metabolic function. The results also showed that the left frontal lobe had larger reduction in connectedness than the right frontal lobe for most lesions, which may be related to the asymmetry of the macroscopic networks. Further analysis showed that the observed network damage in the occipital lobe is statistically significantly correlated with the visual field defect of the subjects.

Discussion

Euler's original approach to solve the Königsberg bridge problem illustrates the importance of adequate node and edge selection. When creating a macroscopic network model of the human brain, there are two fundamental questions a researcher should ask: "what are the nodes?" and "what are the connections?". Different macroscopic models have distinctive qualities to capture specific aspects of the human brain and hence there are no universal answers. To answer these questions a researcher should therefore lead with yet another question: "what is the purpose of the macroscopic network model?" and then make a conscious choice by weighing which representation best serves their investigation. The better a macroscopic brain network model is tailored towards the needs of a research question the easier it will be to find answers.

Regarding the connections for a macroscopic network model, current literature distinguishes mainly between two concepts: functional connectivity and structural connectivity. Functional connectivity has been defined as the "*correlation between spatially remote neurophysiological events*" (Friston, 1994). On a macroscopic network scale one could therefore argue that all brain regions are functionally connected with one another and form a complete graph as the neurophysiological events between brain regions are always correlated with one another. In recent literature, the interpretation of what constitutes a functional connection between brain regions has broadened and is approached with different methods (Horwitz, 2003; Lee et al., 2003).

Structural connectivity, in contrast to functional connectivity is narrowly defined and can only be inferred by the presence or the possibility of a physical connection. For research concerned with macroscopic network models of the brain, the answer to "what are the connections between the nodes?" is therefore straightforward: the axons between the neurons of the nodes, which can be predominantly found in the cerebral white matter. How structural connections between nodes can be measured non-invasively in living beings is currently extensively studied with diffusion weighted imaging techniques. Although the current techniques are not able to infer with certainty

whether a connection exists or does not exist, they are able to detect actual axonal connections on a macroscopic scale as studies with brain phantoms have shown (Fillard et al., 2011). In the studies of this thesis, structural connectivity has been approached with recent high angular resolution diffusion weighted imaging (HARDI) techniques in combination with probabilistic and deterministic tractography. Deterministic tractography methods in this thesis were chosen for modelling of the full neocortical network in **chapters 3 and 5**, because they are known to have a low false positive rate for long distance connections (Guevara et al., 2010). Probabilistic tractography was chosen in **chapters 2 and 4** because the connectivity patterns on a voxel level were of interest.

The selection of nodes for modelling brain networks at the macroscopic level forms the greatest challenge to create an adequate connectome. Much recent research in connectomics has avoided tackling this challenge by using anatomical brain templates as network models. These studies have benefited from having an anatomically uniform network model across subjects, which enables the determination of group differences at the node level. The ROI approach for the topographic hub maps presented in **chapter 3** provides a plausible alternative for group analysis with high resolution connectomes. An underlying argument for such an approach would be that group differences should be most visible in structural hubs as they have the most influence on the functioning of the neocortical network. However, whenever possible, it is logically most coherent to model macroscopic brain networks with functionally defined areas as in **chapter 4**. Such an approach makes it possible to define functionally homotopic areas across subjects and therefore also creates networks that can be compared on a node level. Unfortunately, mapping functionally defined brain areas is still subject to elaborate experimentation and automatic approaches such as the ones presented in **chapter 2** should be further explored.

Future research and conclusion

Like so much other research, this thesis was driven by the prospects emerging from its results. While diffusion-based tractography methods are not perfected yet, the results throughout this thesis could be consistently linked with observations from neuroscientific and clinical research. The results are therefore contributing to current research by providing different perspectives on the macroscopic neocortical network architecture of the human brain. Consequently the results should also encourage and stimulate future research to image and analyse the brain at greater detail and to investigate further the correspondence between brain function and architecture.

The investigation in **chapter 2** showed that there is an opportunity to generate automatic parcellation schemes for modelling an individual connectome. An intermediate solution lies in hybrid semi-automatic nodal configuration schemes which integrate known functional specialised neocortical areas with automatic parcellation for the remaining unassigned cortical areas. Hybrid parcelling approaches could additionally consider to demarcate nodes based on the topographic hubness scores, as in **chapter 3**. The automatic parcellation methods enable a researcher to compare global network pa-

rameters across subjects. However, the drawback of the methods presented in **chapter 2** is that the nodes across subjects cannot be trivially matched with one another and further experimentation with graph matching would be required to enable effective comparisons of the local network structures.

The results from **chapter 4** showed that with a macroscopic network model the connectivity patterns between visual areas can be mapped. It could therefore be interesting to map these connectivity patterns at greater detail with a more elaborate approach or by targeting only a subset of the visual areas.

In **chapter 5** a connectivity database-based methodology was created which effectively can also be extended to other research questions that are concerned with the underlying structural connectivity patterns for certain regions of interest. Using a larger population database, one could furthermore extend the lesion simulation approach proposed in **chapter 5** by aiming to match individual subjects with a subset of similar subjects in the database to derive more representative network measures. The measured lesion impact from the simulation approach in **chapter 5** showed a correspondence with the measured visual defect of subjects. However in order to have better measures for predicting visual field defects, knowledge from the visual network as presented in **chapter 4** needs to be considered and integrated in the simulation model.

At the time of writing this thesis the Human Connectome Project funded by the National Institutes of Health (NIH) in the United States is in the process of collecting a publicly available dataset of over a 1000 subjects imaged at a greater detail than the subjects used in this thesis. Therefore in the near future there will be ample opportunity to extend the research presented in this thesis. With the larger quantity and improved quality in imaging data, research can aspire to further map developmental, training and disease-related differences in the neocortical structural network. Beyond the research presented in this thesis, there is also an opportunity to integrate knowledge from the macroscopic model to a higher level model on the mesoscopic or microscopic scale. Recently the European Union has given an unprecedented Flagship research grant of approximately 1 billion euro to the Human Brain Project, which aims to simulate the actual working of the brain at the microscopic scale.

Research on the human connectome at the moment is at an exciting frontier and what we will ultimately discover remains unknown. Some scientists, like Sebastian Seung, go as far as by saying that: “*we are our connectome*”. Similar expressions have been made about the genome — that we are defined by our DNA. During the course of my investigations I saw seemingly converging evidence unfold relating brain function and brain structure. Hence I became also inclined to say that we are indeed defined by our physical structures such the connectome or even the genome for that matter. However, as Richard Dawkins pointed out, some entities which he called memes, e.g. ideas and certain patterns of behaviour, are not transmitted by genes but have a life of their own. Therefore to see how the structure of the brain corresponds with how we function as a human being, we would need a structured approach to map our psyche as a collection of traits or memes. All humans form a complex interconnected network of relations which

influence one another forming, as I would like call it: a distributed network of evolving menomes. Therefore, I end this thesis by hypothesising that mapping menomes may play an important role in understanding our connectome and vice versa.

“I think that ideas exist outside of ourselves. I think somewhere, we’re all connected off in some very abstract land. But somewhere between there and here ideas exist.”

-David Lynch-

A

ppendix

References

- Achard, S., Bullmore, E., 2007. Efficiency and cost of economical brain functional networks. *PLoS computational biology* 3, e17.
- Achard, S., Salvador, R., Whitcher, B., Suckling, J., Bullmore, E., 2006. A resilient, low-frequency, small-world human brain functional network with highly connected association cortical hubs. *Journal of Neuroscience* 26, 63-72.
- Alexander, D.C., 2005. Multiple-fiber reconstruction algorithms for diffusion MRI. *Annals of the New York Academy of Sciences* 1064, 113-33.
- Alluri, V., Toivaiainen, P., Jääskeläinen, I.P., Glerean, E., Sams, M., Brattico, E., 2012. Large-scale brain networks emerge from dynamic processing of musical timbre, key and rhythm. *NeuroImage* 59, 3677-89.
- Alstott, J., Breakspear, M., Hagmann, P., Cammoun, L., Sporns, O., 2009. Modeling the impact of lesions in the human brain. *PLoS computational biology* 5, e1000408.
- Amano, K., Wandell, B., Dumoulin, S.O., 2009. Visual field maps, population receptive field sizes, and visual field coverage in the human MT+ complex. *Journal of neurophysiology* 2704 -2718.
- Amaral, L.A.N., Scala, A., Barthelemy, M., Stanley, H.E., 2000. Classes of small-world networks. *Proceedings of the National Academy of Sciences of the United States of America* 97, 11149-52.
- Amunts, K., Schleicher, a, Bürgel, U., Mohlberg, H., Uylings, H.B., Zilles, K., 1999. Broca's region revisited: cytoarchitecture and intersubject variability. *The Journal of comparative neurology* 412, 319-41.
- Andersen, B.B., Gundersen, H.J.G., Pakkenberg, B., 2003. Aging of the human cerebellum: a stereological study. *The Journal of comparative neurology* 466, 356-65.
- Andersson, J.L.R., Skare, S., 2002. A model-based method for retrospective correction of geometric distortions in diffusion-weighted EPI. *NeuroImage* 16, 177-99.
- Andrews, R.J., 1991. Transhemispheric diaschisis. A review and comment. *Stroke; a journal of cerebral circulation* 22, 943-949.
- Arnoldussen, D.M., Goossens, J., Van den Berg, A. V., 2011. Adjacent visual representations of self-motion in different reference frames. *Proceedings of the National Academy of Sciences of the United States of America* 108, 11668-73.
- Aron, A.R., Robbins, T.W., Poldrack, R.A., 2004. Inhibition and the right inferior frontal cortex. *Trends in cognitive sciences* 8, 170-7.
- Ayala, C., Croft, J.B., Greenlund, K.J., Keenan, N.L., Donehoo, R.S., Malarcher, A.M., Mensah, G.A., 2002. Sex differences in US mortality rates for stroke and stroke subtypes by race/ethnicity and age, 1995-1998. *Stroke; a journal of cerebral circulation* 33, 1197-201.
- Baizer, J.S., Ungerleider, L.G., Desimone, R., 1991. Organization of visual inputs to the inferior temporal and posterior parietal cortex in macaques. *The Journal of neuroscience: the official journal of the Society for Neuroscience* 11, 168-90.
- Barthelemy, M., 2004. Betweenness centrality in large complex networks. *The European Physical Journal B-Condensed Matter and Complex Systems* 38, 163-168.
- Basser, P., Mattiello, J., Le Bihan, D., 1994a. Estimation of the effective self-diffusion tensor from the NMR spin echo. *Journal of Magnetic Resonance. Series B* 247-254.
- Basser, P., Mattiello, J., Le Bihan, D., 1994b. MR diffusion tensor spectroscopy and imaging. *Biophysical journal* 66, 259-67.
- Bassett, D.S., Bullmore, E., Verchinski, B. A., Mattay, V.S., Weinberger, D.R., Meyer-Lindenberg, A., 2008. Hierarchical organization of human cortical networks in health and schizophrenia. *The Journal of neuroscience: the official journal of the Society for Neuroscience* 28, 9239-48.
- Bassett, D.S., Bullmore, E.T., 2009. Human brain networks in health and disease. *Current opinion in neurology* 22, 340-7.
- Bassett, D.S., Bullmore, E.T., Meyer-Lindenberg, A., Apud, J.A., Weinberger, D.R., Coppola, R., 2009. Cognitive fitness of cost-efficient brain functional networks. *Proceedings of the National Academy of Sciences of the United States of America* 106, 11747-11752.
- Bastian, M., Heymann, S., Jacomy, M., 2009. *Gephi: An open source software for exploring and manipulating networks*.
- Bates, E., Wilson, S.M., Saygin, A.P., Dick, F., Sereno, M.I., Knight, R.T., Dronkers, N.F., 2003. Voxel-based lesion-symptom mapping. *Nature neuroscience* 6, 448-50.
- Beckmann, C.F., DeLuca, M., Devlin, J.T., Smith, S.M., 2005. Investigations into resting-state connectivity using independent component analysis. *Philosophical transactions of the Royal Society*

- of London. *Series B, Biological sciences* 360, 1001-1013.
- Behrens, T.E.J., Johansen-Berg, H., Woolrich, M.W., Smith, S.M., Wheeler-Kingshott, C.A., Boulby, P.A., Barker, G.J., Sillery, E.L., Sheehan, K., Ciccarelli, O., Thompson, A.J., Brady, J.M., Matthews, P.M., 2003. Non-invasive mapping of connections between human thalamus and cortex using diffusion imaging. *Nature neuroscience* 6, 750-757.
- Behrens, T.E.J., Woolrich, M.W., Jenkinson, M., Johansen-Berg, H., Nunes, R.G., Clare, S., Matthews, P.M., Brady, J.M., Smith, S.M., 2003. Characterization and propagation of uncertainty in diffusion-weighted MR imaging. *Magnetic resonance in medicine: official journal of the Society of Magnetic Resonance in Medicine / Society of Magnetic Resonance in Medicine* 50, 1077-88.
- Belin, P., Zatorre, R.J., Lafaille, P., Ahad, P., Pike, B., 2000. Voice-selective areas in human auditory cortex. *Nature* 403, 309-312.
- Benjamini, Y., Hochberg, Y., 1995. Controlling the false discovery rate: a practical and powerful approach to multiple testing. *Journal of the Royal Statistical Society. Series B* 57, 289-300.
- Bergsma, D.P., Van der Wildt, G., 2010. Visual training of cerebral blindness patients gradually enlarges the visual field. *The British journal of ophthalmology* 94, 88-96.
- Berntsen, E.M., Rasmussen, I.-A., Samuelsen, P., Xu, J., Haraldseth, O., Lagopoulos, J., Malhi, G.S., 2006. Putting the brain in Jeopardy: a novel comprehensive and expressive language task? *Acta Neuropsychiatrica* 18, 115-119.
- Binder, J.R., Desai, R.H., Graves, W.W., Conant, L.L., 2009. Where is the semantic system? A critical review and meta-analysis of 120 functional neuroimaging studies. *Cerebral cortex (New York, N.Y.: 1991)* 19, 2767-96.
- Biswal, B.B., Mennes, M., Zuo, X.-N., Gohel, S., Kelly, C., et al., 2010. Toward discovery science of human brain function. *Proceedings of the National Academy of Sciences of the United States of America* 107, 4734-9.
- Blondel, V.D., Guillaume, J., Lambiotte, R., Lefebvre, E., 2008. Fast unfolding of communities in large networks. *Journal of Statistical Mechanics: Theory and Experiment* 2008, 6.
- Bosma, I., Reijneveld, J.C., Klein, M., Douw, L., Van Dijk, B.W., Heimans, J.J., Stam, C.J., 2009. Disturbed functional brain networks and neurocognitive function in low-grade glioma patients: a graph theoretical analysis of resting-state MEG. *Nonlinear biomedical physics* 3, 9.
- Brandes, U., 2001. A faster algorithm for betweenness centrality*. *Journal of Mathematical Sociology* 25, 163-177.
- Brewer, A. a, Liu, J., Wade, A.R., Wandell, B. a, 2005. Visual field maps and stimulus selectivity in human ventral occipital cortex. *Nature neuroscience* 8, 1102-9.
- Brin, S., Page, L., 1998. The anatomy of a large-scale hypertextual Web search engine. *Computer networks and ISDN systems* 30.
- Brodmann, K., 1909. *Vergleichende Lokalisationslehre der Grosshirnrinde in ihren Prinzipien dargestellt auf Grund des Zellenbaues*. Barth.
- Brodtmann, A., Puce, A., Darby, D., Donnan, G., 2007. fMRI demonstrates diaschisis in the extrastriate visual cortex. *Stroke; a journal of cerebral circulation* 38, 2360-3.
- Buckner, R.L., Andrews-Hanna, J.R., Schacter, D.L., 2008. The brain's default network: anatomy, function, and relevance to disease. *Annals of the New York Academy of Sciences* 1124, 1-38.
- Bullmore, E., Sporns, O., 2009. Complex brain networks: graph theoretical analysis of structural and functional systems. *Nature reviews. Neuroscience* 10, 186-98.
- Catani, M., Allin, M.P.G., Husain, M., Pugliese, L., Mesulam, M.M., Murray, R.M., Jones, D.K., 2007. Symmetries in human brain language pathways correlate with verbal recall. *Proceedings of the National Academy of Sciences of the United States of America* 104, 17163-8.
- Catani, M., Ffytche, D.H., 2005. The rises and falls of disconnection syndromes. *Brain: a journal of neurology* 128, 2224-39.
- Catani, M., Jones, D.K., Ffytche, D.H., 2005. Perisylvian language networks of the human brain. *Annals of neurology* 57, 8-16.
- Chelazzi, L., Miller, E.K., Duncan, J., Desimone, R., 1993. A neural basis for visual search in inferior temporal cortex. *Nature* 363, 345-7.
- Christopoulos, G.I., Tobler, P.N., Bossaerts, P., Dolan, R.J., Schultz, W., 2009. Neural correlates of value, risk, and risk aversion contributing to decision making under risk. *The Journal of neuroscience: the official journal of the Society for Neuroscience* 29, 12574-83.
- Cohen, L., Lehericy, S., Chochon, F., Lemer, C., Rivaud, S., Dehaene, S., 2002. Language-specific tuning of visual cortex? Functional properties of the Visual Word Form Area. *Brain: a journal of neurology* 125, 1054-69.
- Cole, M.W., Pathak, S., Schneider, W., 2010. Identify-

- ing the brain's most globally connected regions. *NeuroImage* 49, 3132-48.
- Cole, M.W., Schneider, W., 2007. The cognitive control network: Integrated cortical regions with dissociable functions. *NeuroImage* 37, 343-60.
- Cook, P.A., Bai, Y., Hall, M.J., Nedjati-Gilani, S., Seunarine, K.K., Alexander, D., 2006. Camino: Open-Source Diffusion-MRI Reconstruction and Process. *Proc. 14th Ann. Mtg. of ISMRM*, p. 2759.
- Corbetta, M., Akbudak, E., Conturo, T.E., Snyder, A.Z., Ollinger, J.M., Drury, H.A., Linenweber, M.R., Petersen, S.E., Raichle, M.E., Van Essen, D.C., Shulman, G.L., 1998. A common network of functional areas for attention and eye movements. *Neuron* 21, 761-73.
- Crofts, J.J., Higham, D.J., Bosnell, R., Jbabdi, S., Matthews, P.M., Behrens, T.E.J., Johansen-Berg, H., 2011. Network analysis detects changes in the contralesional hemisphere following stroke. *NeuroImage* 54, 161-9.
- Dale, A.M., Fischl, B., Sereno, M.I., 1999. Cortical surface-based analysis: I. Segmentation and Surface Reconstruction. *NeuroImage* 9, 195-207.
- Damoiseaux, J.S., Rombouts, S.A.R.B., Barkhof, F., Scheltens, P., Stam, C.J., Smith, S.M., Beckmann, C.F., 2006. Consistent resting-state networks across healthy subjects. *Proceedings of the National Academy of Sciences of the United States of America* 103, 13848-13853.
- De Haan, E.H.F., Cowey, A., 2011. On the usefulness of "what" and "where" pathways in vision. *Trends in cognitive sciences* 15, 460-6.
- Dehaene, S., Cohen, L., 2011. The unique role of the visual word form area in reading. *Trends in cognitive sciences* 15, 254-62.
- Dosenbach, N.U.F., Nardos, B., Cohen, A.L., Fair, D.A., Power, J.D., Church, J.A., Nelson, S.M., Wig, G.S., Vogel, A.C., Lessov-Schlaggar, C.N., Barnes, K.A., Dubis, J.W., Feczko, E., Coalson, R.S., Pruett, J.R., Barch, D.M., Petersen, S.E., Schlaggar, B.L., 2010. Prediction of individual brain maturity using fMRI. *Science (New York, N.Y.)* 329, 1358-61.
- Dougherty, R.F., Koch, V.M., Brewer, A.A., Fischer, B., Modersitzki, J., Wandell, B.A., 2003. Visual field representations and locations of visual areas V1/2/3 in human visual cortex. *Journal of vision* 3, 586-98.
- Dukelow, S.P., DeSouza, J.F., Culham, J.C., Van den Berg, A. V., Menon, R.S., Vilis, T., 2001. Distinguishing subregions of the human MT+ complex using visual fields and pursuit eye movements. *Journal of neurophysiology* 86, 1991-2000.
- Dumoulin, S.O., Wandell, B. a, 2008. Population receptive field estimates in human visual cortex. *NeuroImage* 39, 647-60.
- Eickhoff, S., Walters, N.B., Schleicher, A., Kril, J., Egan, G.F., Zilles, K., Watson, J.D.G., Amunts, K., 2005. High-resolution MRI reflects myeloarchitecture and cytoarchitecture of human cerebral cortex. *Human brain mapping* 24, 206-15.
- Engel, S.A., Glover, G.H., Wandell, B.A., 1997. Retinotopic organization in human visual cortex and the spatial precision of functional MRI. *Cerebral cortex (New York, N.Y.: 1991)* 7, 181-92.
- Enright, A.J., Van Dongen, S., Ouzounis, C.A., 2002. An efficient algorithm for large-scale detection of protein families. *Nucleic acids research* 30, 1575-84.
- Essen, D.C. Van, 1997. A tension-based theory of morphogenesis and compact wiring in the central nervous system. *Nature* 385, 313-318.
- Felleman, D.J., Van Essen, D.C., 1991. Distributed hierarchical processing in the primate cerebral cortex. *Cerebral cortex (New York, N.Y.: 1991)* 1, 1-47.
- Ferrier, D., 1876. *The functions of the brain*. GP Putnam's Sons.
- Fillard, P., Descoteaux, M., Goh, A., Gouttard, S., Jeurissen, B., Malcolm, J., Ramirez-manzanares, A., Reisert, M., Sakaie, K., Tensaouti, F., Yo, T., Mangin, J., Poupon, C., 2011. NeuroImage Quantitative evaluation of 10 tractography algorithms on a realistic diffusion MR phantom. *NeuroImage* 56, 220-234.
- Fischl, B., Van der Kouwe, A., Destrieux, C., Halgren, E., Segonne, F., Salat, D.H., Busa, E., Seidman, L.J., Goldstein, J., Kennedy, D., Caviness, V., Makris, N., Rosen, B., Dale, A.M., 2004. Automatically parcellating the human cerebral cortex. *Cerebral cortex (New York, N.Y.: 1991)* 14, 11-22.
- Friston, K.J., 1994. Functional and effective connectivity in neuroimaging: A synthesis. *Human brain mapping* 2, 56-78.
- Fruchterman, T.M.J., Reingold, E.M., 1991. Graph drawing by force-directed placement. *Software: Practice and Experience* 21, 1129-1164.
- Galletti, C., Gamberini, M., Kutz, D.F., Fattori, P., Lupino, G., Matelli, M., 2001. The cortical connections of area V6: an occipito-parietal network processing visual information. *The European journal of neuroscience* 13, 1572-88.
- Gattas, R., Sousa, a P., Mishkin, M., Ungerleider, L.G., 1997. Cortical projections of area V2 in the macaque. *Cerebral cortex (New York, N.Y.: 1991)* 7, 110-29.
- Gerlach, K.D., Spreng, R.N., Gilmore, A.W., Schac-

- ter, D.L., 2011. Solving future problems: default network and executive activity associated with goal-directed mental simulations. *NeuroImage* 55, 1816-24.
- Geschwind, N., 1965. Disconnexion syndromes in animals and man. I. *Brain: a journal of neurology* 88, 237-94.
- Gitelman, D.R., Nobre, a C., Parrish, T.B., LaBar, K.S., Kim, Y.H., Meyer, J.R., Mesulam, M., 1999. A large-scale distributed network for covert spatial attention: further anatomical delineation based on stringent behavioural and cognitive controls. *Brain: a journal of neurology* 122 (Pt 6), 1093-106.
- Goebel, R., Esposito, F., Formisano, E., 2006. Analysis of functional image analysis contest (FIAC) data with brainvoyager QX: From single-subject to cortically aligned group general linear model analysis and self-organizing group independent component analysis. *Human brain mapping* 27, 392-401.
- Gong, G., He, Y., Concha, L., Lebel, C., Gross, D.W., Evans, A.C., Beaulieu, C., 2009. Mapping anatomical connectivity patterns of human cerebral cortex using in vivo diffusion tensor imaging tractography. *Cerebral cortex (New York, N.Y.: 1991)* 19, 524-36.
- Gong, G., Jiang, T., Zhu, C., Zang, Y., Wang, F., Xie, S., Xiao, J., Guo, X., 2005. Asymmetry analysis of cingulum based on scale-invariant parameterization by diffusion tensor imaging. *Human brain mapping* 24, 92-8.
- Gong, G., Rosa-Neto, P., Carbonell, F., Chen, Z.J., He, Y., Evans, A.C., 2009. Age- and gender-related differences in the cortical anatomical network. *The Journal of neuroscience: the official journal of the Society for Neuroscience* 29, 15684-93.
- Goodale, M.A., Milner, A.D., 1992. Separate visual pathways for perception and action. *Trends in neurosciences* 15, 20-5.
- Grabner, G., Janke, A.L., Budge, M.M., Smith, D., Pruessner, J., Collins, D.L., 2006. Symmetric atlas and model based segmentation: an application to the hippocampus in older adults. *Medical image computing and computer-assisted intervention: MICCAI ...International Conference on Medical Image Computing and Computer-Assisted Intervention* 9, 58-66.
- Greve, D.N., Fischl, B., 2009. Accurate and robust brain image alignment using boundary-based registration. *NeuroImage* 48, 63-72.
- Griswold, M. a, Jakob, P.M., Heidemann, R.M., Nittka, M., Jellus, V., Wang, J., Kiefer, B., Haase, A., 2002. Generalized autocalibrating partially parallel acquisitions (GRAPPA). *Magnetic resonance in medicine: official journal of the Society of Magnetic Resonance in Medicine / Society of Magnetic Resonance in Medicine* 47, 1202-10.
- Guevara, P., Poupon, C., Rivière, D., Cointepas, Y., Descoteaux, M., Thirion, B., Mangin, J.-F., 2010. Robust clustering of massive tractography datasets. *NeuroImage* 54, 1975-1993.
- Guimerà, R., Amaral, L.A.N., 2005. Functional cartography of complex metabolic networks. *Nature* 433, 895-900.
- Guimerà, R., Mossa, S., Turtschi, A., Amaral, L.A.N., 2005. The worldwide air transportation network: Anomalous centrality, community structure, and cities' global roles. *Proceedings of the National Academy of Sciences of the United States of America* 102, 7794-9.
- Gusnard, D.A., Raichle, M.E., 2001. Searching for a baseline: functional imaging and the resting human brain. *Nature reviews. Neuroscience* 2, 685-694.
- Hagmann, P., Cammoun, L., Gigandet, X., Meuli, R., Honey, C.J., Wedeen, V.J., Sporns, O., 2008. Mapping the structural core of human cerebral cortex. *PLoS biology* 6, e159.
- Hagmann, P., Kurant, M., Gigandet, X., Thiran, P., Wedeen, V.J., Meuli, R., Thiran, J.-P., 2007. Mapping human whole-brain structural networks with diffusion MRI. *PLoS ONE* 2, e597.
- Hagmann, P., Sporns, O., Madan, N., Cammoun, L., Pienaar, R., Wedeen, V.J., Meuli, R., Thiran, J.-P., Grant, P.E., 2010. White matter maturation reshapes structural connectivity in the late developing human brain. *Proceedings of the National Academy of Sciences of the United States of America* 107, 19067-72.
- Hahn, E.L., 1950. Spin Echoes. *Physical Review* 80, 580-594.
- Harvey, B.M., Dumoulin, S.O., 2011. The relationship between cortical magnification factor and population receptive field size in human visual cortex: constancies in cortical architecture. *The Journal of neuroscience: the official journal of the Society for Neuroscience* 31, 13604-12.
- Henriksson, L., Karvonen, J., Salminen-Vaparanta, N., Railo, H., Vanni, S., 2012. Retinotopic maps, spatial tuning, and locations of human visual areas in surface coordinates characterized with multifocal and blocked fMRI designs. *PLoS ONE* 7, e36859.
- Honey, C.J., Sporns, O., 2008. Dynamical consequences of lesions in cortical networks. *Human brain mapping* 29, 802-9.

- Honey, C.J., Sporns, O., Cammoun, L., Gigandet, X., Thiran, J.P., Meuli, R., Hagmann, P., 2009. Predicting human resting-state functional connectivity from structural connectivity. *Proceedings of the National Academy of Sciences of the United States of America* 106, 2035-40.
- Honey, C.J., Thivierge, J.-P., Sporns, O., 2010. Can structure predict function in the human brain? *NeuroImage* 52, 766-76.
- Horwitz, B., 2003. The elusive concept of brain connectivity. *NeuroImage* 19, 466-470.
- Huk, A.C., Dougherty, R.F., Heeger, D.J., 2002. Retinotopy and functional subdivision of human areas MT and MST. *The Journal of neuroscience: the official journal of the Society for Neuroscience* 22, 7195-205.
- Humphries, M.D., Gurney, K., 2008. Network "small-world-ness": a quantitative method for determining canonical network equivalence. *PLoS ONE* 3, e0002051.
- Husain, M., Nachev, P., 2007. Space and the parietal cortex. *Trends in cognitive sciences* 11, 30-6.
- Iturria-Medina, Y., Sotero, R.C., Canales-Rodríguez, E.J., Alemán-Gómez, Y., Melie-García, L., 2008. Studying the human brain anatomical network via diffusion-weighted MRI and Graph Theory. *NeuroImage* 40, 1064-76.
- Jacomy, M., Heymann, S., Venturini, T., Bastian, M., 2011. *ForceAtlas2, a graph layout algorithm for handy network visualization*.
- Jang, S.H., Bai, D., Son, S.M., Lee, J., Kim, D.-S., Sakong, J., Kim, D.G., Yang, D.S., 2008. Motor outcome prediction using diffusion tensor tractography in pontine infarct. *Annals of neurology* 64, 460-5.
- Jarbo, K., Verstynen, T., Schneider, W., 2012. In vivo quantification of global connectivity in the human corpus callosum. *NeuroImage* 59, 1988-96.
- Jenkinson, M., Bannister, P., Brady, M., Smith, S., 2002. Improved Optimization for the Robust and Accurate Linear Registration and Motion Correction of Brain Images. *NeuroImage* 17, 825-841.
- Johansen-Berg, H., 2010. Behavioural relevance of variation in white matter microstructure. *Current opinion in neurology* 23, 351-8.
- Johansen-Berg, H., Behrens, T.E.J., Robson, M.D., Drobniak, I., Rushworth, M.F.S., Brady, J.M., Smith, S.M., Higham, D.J., Matthews, P.M., 2004. Changes in connectivity profiles define functionally distinct regions in human medial frontal cortex. *Proceedings of the National Academy of Sciences of the United States of America* 101, 13335-40.
- Johansen-Berg, H., Rushworth, M.F.S., 2009. Using diffusion imaging to study human connective anatomy. *Annual review of neuroscience* 32, 75-94.
- Johansen-Berg, H., Scholz, J., Stagg, C.J., 2010. Relevance of structural brain connectivity to learning and recovery from stroke. *Frontiers in systems neuroscience* 4, 146.
- Kaiser, M., 2011. A tutorial in connectome analysis: topological and spatial features of brain networks. *NeuroImage* 57, 892-907.
- Karnath, H.-O., Ferber, S., Himmelbach, M., 2001. Spatial awareness is a function of the temporal not the posterior parietal lobe. *Nature* 411, 950-3.
- Karnath, H.-O., Fruhmman Berger, M., Küker, W., Rorden, C., 2004. The anatomy of spatial neglect based on voxelwise statistical analysis: a study of 140 patients. *Cerebral cortex (New York, N.Y.: 1991)* 14, 1164-72.
- Kim, D.-S., Kim, M., 2005. Combining functional and diffusion tensor MRI. *Annals of the New York Academy of Sciences* 1064, 1-15.
- Kim, M., Ducros, M., Carlson, T., Ronen, I., He, S., Ugurbil, K., Kim, D.-S., 2006. Anatomical correlates of the functional organization in the human occipitotemporal cortex. *Magnetic resonance imaging* 24, 583-90.
- Kim, M., Ronen, I., Ugurbil, K., Kim, D.-S., 2006. Spatial resolution dependence of DTI tractography in human occipito-callosal region. *NeuroImage* 32, 1243-9.
- Klein, J.C., Rushworth, M.F.S., Behrens, T.E.J., Mackay, C.E., De Crespigny, A.J., D'Arceuil, H., Johansen-Berg, H., 2010. Topography of connections between human prefrontal cortex and mediodorsal thalamus studied with diffusion tractography. *NeuroImage* 51, 555-564.
- Kleinnijenhuis, M., Zerbi, V., Küsters, B., Slump, C.H., Barth, M., Van Cappellen van Walsum, A.-M., 2012. Layer-specific diffusion weighted imaging in human primary visual cortex in vitro. *Cortex; a journal devoted to the study of the nervous system and behavior* 1-14.
- Koch, M.A., Norris, D.G., Hund-Georgiadis, M., 2002. An investigation of functional and anatomical connectivity using magnetic resonance imaging. *NeuroImage* 16, 241-250.
- Kochunov, P., Glahn, D.C., Nichols, T.E., Winkler, A.M., Hong, E.L., Holcomb, H.H., Stein, J.L., Thompson, P.M., Curran, J.E., Carless, M.A., Olvera, R.L., Johnson, M.P., Cole, S.A., Kochunov, V., Kent, J., Blangero, J., 2011. Genetic Analysis of Cortical Thickness and Fractional Anisotropy of Water Dif-

- fusion in the Brain. *Frontiers in neuroscience* 5, 1-15.
- Konishi, S., Nakajima, K., Uchida, I., Sekihara, K., Miyashita, Y., 1998. No-go dominant brain activity in human inferior prefrontal cortex revealed by functional magnetic resonance imaging. *The European journal of neuroscience* 10, 1209-13.
- Laird, A.R., Fox, P.M., Eickhoff, S.B., Turner, J. a, Ray, K.L., McKay, D.R., Glahn, D.C., Beckmann, C.F., Smith, S.M., Fox, P.T., 2011. Behavioral interpretations of intrinsic connectivity networks. *Journal of cognitive neuroscience* 23, 4022-37.
- Lambiotte, R., Delvenne, J., Barahona, M., 2008. Laplacian dynamics and multiscale modular structure in networks. *arXiv preprint arXiv:0812.1770* 1-29.
- Larsen, C.C., Bonde Larsen, K., Bogdanovic, N., Laursen, H., Graem, N., Samuelsen, G.B., Pakkenberg, B., 2006. Total number of cells in the human newborn telencephalic wall. *Neuroscience* 139, 999-1003.
- Larsson, J., Heeger, D.J., 2006. Two retinotopic visual areas in human lateral occipital cortex. *The Journal of neuroscience: the official journal of the Society for Neuroscience* 26, 13128-42.
- Latora, V., Marchiori, M., 2001. Efficient Behavior of Small-World Networks. *Physical Review Letters* 87, 3-6.
- Le Bihan, D., 2003. Looking into the functional architecture of the brain with diffusion MRI. Nature reviews. *Neuroscience* 4, 469-80.
- Lee, L., Harrison, L.M., Mechelli, A., 2003. The Functional Brain Connectivity Workshop: report and commentary. *Network (Bristol, England)* 14, R1-15.
- Locke, S., Yakovlev, P.I., 1965. Transcallosal connections of the cingulum of man. *Archives of neurology* 13, 471-6.
- Luxburg, U. Von, 2007. A tutorial on spectral clustering. *Statistics and computing* 1-32.
- MacKay, D.J.C., 2002. *Information Theory, Inference & Learning Algorithms*, 1st ed. Cambridge University Press.
- Margulies, D.S., Vincent, J.L., Kelly, C., Lohmann, G., Uddin, L.Q., Biswal, B.B., Villringer, A., Castellanos, F.X., Milham, M.P., Petrides, M., 2009. Precuneus shares intrinsic functional architecture in humans and monkeys. *Proceedings of the National Academy of Sciences of the United States of America* 106, 20069-74.
- Mars, R.B., Jbabdi, S., Sallet, J., O'Reilly, J.X., Croxson, P.L., Olivier, E., Noonan, M.P., Bergmann, C., Mitchell, A.S., Baxter, M.G., Behrens, T.E.J., Johansen-Berg, H., Tomassini, V., Miller, K.L., Rushworth, M.F.S., 2011. Diffusion-weighted imaging tractography-based parcellation of the human parietal cortex and comparison with human and macaque resting-state functional connectivity. *The Journal of neuroscience: the official journal of the Society for Neuroscience* 31, 4087-100.
- McNab, J. a, Polimeni, J.R., Wang, R., Augustinack, J.C., Fujimoto, K., Stevens, A., Janssens, T., Fariar, R., Folkerth, R.D., Vanduffel, W., Wald, L.L., 2013. Surface based analysis of diffusion orientation for identifying architectonic domains in the in vivo human cortex. *NeuroImage* 69, 87-100.
- Mesulam, M.M., 1981. A cortical network for directed attention and unilateral neglect. *Annals of neurology* 10, 309-25.
- Mesulam, M.M., 1998. From sensation to cognition. *Brain: a journal of neurology* 121, 1013-52.
- Meynert, T., 1872. Der Bau der Gross-Hirnrinde und seine örtlichen Verschiedenheiten, nebst einem pathologisch-anatomischen Corollarium. Heuser.
- Miller, E.K., 1999. The prefrontal cortex: complex neural properties for complex behavior. *Neuron* 22, 15-7.
- Mori, S., Crain, B.J., Chacko, V.P., Van Zijl, P.C., 1999. Three-dimensional tracking of axonal projections in the brain by magnetic resonance imaging. *Annals of neurology* 45, 265-9.
- NASA's Earth Observatory/NOAA/DOD, 2012. Earth at Night [WWW Document]. URL <http://www.nasa.gov/multimedia/imagegallery/iodt.html>
- Newman, M., Girvan, M., 2004. Finding and evaluating community structure in networks. *Physical Review E* 69, 026113.
- Nieuwenhuys, R., Voogd, J., Van Huijzen, C., 2007. Ch. 15 Telencephalon: Neocortex, in: *The Human Central Nervous System*.
- Nijhuis, E.H.J., Van Cappellen van Walsum, A.-M., Norris, D.G., 2011. Mapping hubs in the neocortical structural network of the human brain shows lateralization, in: *Proc. 19th Ann. Mtg. of ISMRM*. p. 676.
- Nijhuis, E.H.J., Van Cappellen van Walsum, A.-M., Norris, D.G., 2013. Topographic hub maps of the human structural neocortical network. *PLoS ONE* 8, e65511.
- Norris, D.G., Koopmans, P.J., Boyacioglu, R., Barth, M., 2011. Power Independent of Number of Slices (PINS) radiofrequency pulses for low-power simultaneous multislice excitation. *Magnetic reso-*

- nance in medicine: official journal of the Society of Magnetic Resonance in Medicine / Society of Magnetic Resonance in Medicine 66, 1234-40.
- Ogawa, S., Lee, T.M., Kay, A.R., Tank, D.W., 1990. Brain magnetic resonance imaging with contrast dependent on blood oxygenation. *Proceedings of the National Academy of Sciences of the United States of America* 87, 9868-72.
- Pakkenberg, B., Gundersen, H.J., 1997. Neocortical neuron number in humans: effect of sex and age. *The Journal of comparative neurology* 384, 312-20.
- Pareto, V., 1971. *Manual of political economy*. Augustus M. Kelley, Publishers, New York, NJ, USA.
- Parker, G.J.M., Alexander, D.C., 2005. Probabilistic anatomical connectivity derived from the microscopic persistent angular structure of cerebral tissue. *Philosophical transactions of the Royal Society of London. Series B, Biological sciences* 360, 893-902.
- Parker, G.J.M., Haroon, H.A., Wheeler-Kingshott, C.A.M., 2003. A framework for a streamline-based probabilistic index of connectivity (PICO) using a structural interpretation of MRI diffusion measurements. *Journal of magnetic resonance imaging: JMRI* 18, 242-54.
- Patterson, K., Nestor, P.J., Rogers, T.T., 2007. Where do you know what you know? The representation of semantic knowledge in the human brain. *Nature reviews. Neuroscience* 8, 976-87.
- Pelvig, D.P., Pakkenberg, H., Stark, A.K., Pakkenberg, B., 2008. Neocortical glial cell numbers in human brains. *Neurobiology of Aging* 29, 1754-1762.
- Persky, R.W., Turtzo, L.C., McCullough, L.D., 2010. Stroke in women: disparities and outcomes. *Current cardiology reports* 12, 6-13.
- Petrea, R.E., Beiser, A.S., Seshadri, S., Kelly-Hayes, M., Kase, C.S., Wolf, P.A., 2009. Gender differences in stroke incidence and poststroke disability in the Framingham heart study. *Stroke; a journal of cerebral circulation* 40, 1032-7.
- Polimeni, J.R., Fischl, B., Greve, D.N., Wald, L.L., 2010. Laminar analysis of 7T BOLD using an imposed spatial activation pattern in human V1. *NeuroImage* 52, 1334-46.
- Pruessmann, K.P., Weiger, M., Scheidegger, M.B., Boesiger, P., 1999. SENSE: sensitivity encoding for fast MRI. *Magnetic resonance in medicine: official journal of the Society of Magnetic Resonance in Medicine / Society of Magnetic Resonance in Medicine* 42, 952-62.
- Raichle, M.E., Snyder, A.Z., 2007. A default mode of brain function: a brief history of an evolving idea. *NeuroImage* 37, 1083-1089.
- Reeves, M.J., Bushnell, C.D., Howard, G., Gargano, J.W., Duncan, P.W., Lynch, G., Khatiwoda, A., Lisa-beth, L., 2008. Sex differences in stroke: epidemiology, clinical presentation, medical care, and outcomes. *Lancet neurology* 7, 915-26.
- Reid, A.T., Krumnack, A., Wanke, E., Kötter, R., 2009. Optimization of cortical hierarchies with continuous scales and ranges. *NeuroImage* 47, 611-7.
- Roland, P.E., Larsen, B., Lassen, N.A., Skinhøj, E., 1980. Supplementary motor area and other cortical areas in organization of voluntary movements in man. *Journal of neurophysiology* 43, 118-36.
- Rorden, C., Brett, M., 2000. Stereotaxic display of brain lesions. *Behavioural neurology* 12, 191-200.
- Rorden, C., Karnath, H.-O., Bonilha, L., 2007. Improving lesion-symptom mapping. *Journal of cognitive neuroscience* 19, 1081-8.
- Rubinov, M., Knock, S. a, Stam, C.J., Micheloyannis, S., Harris, A.W.F., Williams, L.M., Breakspear, M., 2009. Small-world properties of nonlinear brain activity in schizophrenia. *Human brain mapping* 30, 403-16.
- Rubinov, M., Sporns, O., 2010. Complex network measures of brain connectivity: uses and interpretations. *NeuroImage* 52, 1059-69.
- Schall, J.D., 2004. On the role of frontal eye field in guiding attention and saccades. *Vision research* 44, 1453-67.
- Schenk, T., McIntosh, R.D., 2010. Do we have independent visual streams for perception and action? *Cognitive Neuroscience* 1, 52-62.
- Schirmer, A., Kotz, S.A., 2006. Beyond the right hemisphere: brain mechanisms mediating vocal emotional processing. *Trends in cognitive sciences* 10, 24-30.
- Schneider, W., 2009. Brain Connectivity competition.
- Scholz, J., Klein, M.C., Behrens, T.E.J., Johansen-Berg, H., 2009. Training induces changes in white-matter architecture. *Nature neuroscience* 12, 1370-1.
- Scoville, W.B., Milner, B., 1957. Loss of Recent Memory after Bilateral Hippocampal Lesions. *Journal of neurology, neurosurgery, and psychiatry* 20, 11-21.
- Seber, G.A.F., 2008. *Cluster Analysis, in: Multivariate Observations*. John Wiley & Sons, Inc., pp. 347-394.
- Seeley, W.W., Crawford, R.K., Zhou, J., Miller, B.L., Greicius, M.D., 2009. Neurodegenerative diseases target large-scale human brain networks. *Neuron* 62, 42-52.
- Seitz, R.J., Azari, N.P., Knorr, U., Binkofski, F., Herzog,

- H., Freund, H.-J., 1999. The Role of Diaschisis in Stroke Recovery. *Stroke; a journal of cerebral circulation* 30, 1844-1850.
- Sereno, M.I., Dale, a M., Reppas, J.B., Kwong, K.K., Belliveau, J.W., Brady, T.J., Rosen, B.R., Tootell, R.B., 1995. Borders of multiple visual areas in humans revealed by functional magnetic resonance imaging. *Science (New York, N.Y.)* 268, 889-93.
- Setsompop, K., Gagoski, B. a, Polimeni, J.R., Witzel, T., Wedeen, V.J., Wald, L.L., 2012. Blipped-controlled aliasing in parallel imaging for simultaneous multislice echo planar imaging with reduced g-factor penalty. *Magnetic resonance in medicine: official journal of the Society of Magnetic Resonance in Medicine / Society of Magnetic Resonance in Medicine* 67, 1210-24.
- Seunarine, K., Cook, P., Embleton, K., Parker, G., Alexander, D., 2006. A general framework for multiple-fibre PICO tractography. *Proc Medical Image Understanding and Analysis*.
- Shi, J., Malik, J., 2000. Normalized Cuts and Image Segmentation. *IEEE transactions on pattern analysis and machine intelligence* 22, 888-905.
- Silva, G.S., Lima, F.O., Camargo, E.C.S., Smith, W.S., Lev, M.H., Harris, G.J., Halpern, E.F., Koroshetz, W., Furie, K.L., 2010. Gender differences in outcomes after ischemic stroke: role of ischemic lesion volume and intracranial large-artery occlusion. *Cerebrovascular diseases (Basel, Switzerland)* 30, 470-5.
- Smith, S.M., Fox, P.T., Miller, K.L., Glahn, D.C., Fox, P.M., Mackay, C.E., Filippini, N., Watkins, K.E., Toro, R., Laird, A.R., Beckmann, C.F., 2009. Correspondence of the brain's functional architecture during activation and rest. *Proceedings of the National Academy of Sciences of the United States of America* 106, 13040-5.
- Smith, S.M., Jenkinson, M., Woolrich, M.W., Beckmann, C.F., Behrens, T.E.J., Johansen-Berg, H., Bannister, P.R., De Luca, M., Drobnjak, I., Flitney, D.E., Niazy, R.K., Saunders, J., Vickers, J., Zhang, Y., De Stefano, N., Brady, J.M., Matthews, P.M., 2004. Advances in functional and structural MR image analysis and implementation as FSL. *NeuroImage* 23 Suppl 1, S208-19.
- Smith, S.M., Miller, K.L., Salimi-Khorshidi, G., Webster, M., Beckmann, C.F., Nichols, T.E., Ramsey, J.D., Woolrich, M.W., 2010. Network Modelling Methods for fMRI. *NeuroImage* 54, 875-891.
- Smith, D. V, Clithero, J. a, Rorden, C., Karnath, H.-O., 2013. Decoding the anatomical network of spatial attention. *Proceedings of the National Academy of Sciences of the United States of America* 110, 1518-23.
- Solano-Castiella, E., Anwender, A., Lohmann, G., Weiss, M., Docherty, C., Geyer, S., Reimer, E., Friederici, A.D., Turner, R., 2010. Diffusion tensor imaging segments the human amygdala in vivo. *NeuroImage* 49, 2958-65.
- Sporns, O., Honey, C.J., Kötter, R., 2007. Identification and classification of hubs in brain networks. *PLoS ONE* 2, e1049.
- Sporns, O., Tononi, G., Kötter, R., 2005. The human connectome: A structural description of the human brain. *PLoS computational biology* 1, e42.
- Stam, C.J., De Haan, W., Daffertshofer, A., Jones, B.F., Manshanden, I., Van Cappellen van Walsum, a M., Montez, T., Verbunt, J.P. a, De Munck, J.C., Van Dijk, B.W., Berendse, H.W., Scheltens, P., 2009. Graph theoretical analysis of magnetoencephalographic functional connectivity in Alzheimer's disease. *Brain: a journal of neurology* 132, 213-24.
- Steinberg, L., 2008. A Social Neuroscience Perspective on Adolescent Risk-Taking. *Developmental review: DR* 28, 78-106.
- Stejskal, E.O., Tanner, J.E., 1965. Spin Diffusion Measurements: Spin Echoes in the Presence of a Time-Dependent Field Gradient. *The Journal of Chemical Physics* 42, 288.
- Stensaas, S.S., Eddington, D.K., Dobelle, W.H., 1974. The topography and variability of the primary visual cortex in man. *Journal of neurosurgery* 40, 747-55.
- Studholme, C., Constable, R.T., Duncan, J.S., 2000. Accurate alignment of functional EPI data to anatomical MRI using a physics-based distortion model. *IEEE transactions on medical imaging* 19, 1115-27.
- Swisher, J.D., Sexton, J. a, Gatenby, J.C., Gore, J.C., Tong, F., 2012. Multishot versus single-shot pulse sequences in very high field fMRI: a comparison using retinotopic mapping. *PLoS ONE* 7, e34626.
- Talbot, S.A., Marshall, W.H., 1941. Physiological studies on neural mechanisms of visual localization and discrimination. *American Journal of Ophthalmology* 24, 1255-1264.
- Thiebaut de Schotten, M., Ffytche, D.H., Bizzi, A., Dell'Acqua, F., Allin, M., Walshe, M., Murray, R., Williams, S.C., Murphy, D.G.M., Catani, M., 2011. Atlasing location, asymmetry and inter-subject variability of white matter tracts in the human brain with MR diffusion tractography. *NeuroImage* 54, 49-59.
- Thorvaldsen, P., Asplund, K., Kuulasmaa, K., Rajakanigas, A.M., Schroll, M., 1995. Stroke incidence,

- case fatality, and mortality in the WHO MONICA project. World Health Organization Monitoring Trends and Determinants in Cardiovascular Disease. *Stroke; a journal of cerebral circulation* 26, 361-7.
- Toga, A.W., Thompson, P.M., 2003. Mapping brain asymmetry. *Nature reviews. Neuroscience* 4, 37-48.
- Tomasi, D., Volkow, N.D., 2011. Functional connectivity hubs in the human brain. *NeuroImage*.
- Tuch, D.S., Weisskoff, R.M., Belliveau, J.W., Wedeen, V., 1999. High angular resolution diffusion imaging of the human brain, in: *Proc. 7th Ann. Mtg. of ISMRM*. p. 321.
- Tuladhar, A.M., Ter Huurne, N., Schoffelen, J.-M., Maris, E., Oostenveld, R., Jensen, O., 2007. Parieto-occipital sources account for the increase in alpha activity with working memory load. *Human brain mapping* 28, 785-92.
- Turken, A.U., Dronkers, N.F., 2011. The neural architecture of the language comprehension network: converging evidence from lesion and connectivity analyses. *Frontiers in systems neuroscience* 5, 1.
- Ungerleider, L.G., Haxby, J. V., 1994. "What" and "where" in the human brain. *Current opinion in neurobiology* 4, 157-65.
- Van den Heuvel, M.P., Sporns, O., 2011. Rich-Club Organization of the Human Connectome. *Journal of Neuroscience* 31, 15775-15786.
- Van Dijk, E.J., De Leeuw, F.-E., 2012. Recovery after stroke: more than just walking and talking again If you don't look for it, you won't find it. *European journal of neurology: the official journal of the European Federation of Neurological Societies* 19, 189-90.
- Van Dongen, S., 2000. *Graph clustering by flow simulation*.
- Van Essen, D.C., 2005. A Population-Average, Landmark- and Surface-based (PALS) atlas of human cerebral cortex. *NeuroImage* 28, 635-62.
- Vincent, D.J., Bloomer, C.J., Hinson, V.K., Bergmann, K.J., 2006. The range of motor activation in the normal human cortex using bold FMRI. *Brain topography* 18, 273-80.
- Virsu, V., Rovamo, J., 1979. Visual resolution, contrast sensitivity, and the cortical magnification factor. *Experimental brain research. Experimentelle Hirnforschung. Expérimentation cérébrale* 37, 475-94.
- Visser, E., Qin, S., Zwiers, M., 2010. EPI distortion correction by constrained nonlinear coregistration improves group fMRI, in: *Proc. 18th Ann. Mtg. of ISMRM*. p. 3459.
- Vos, S.B., Jones, D.K., Viergever, M.A., Leemans, A., 2011. Partial volume effect as a hidden covariate in DTI analyses. *NeuroImage* 55, 1566-76.
- Wandell, B.A., Dumoulin, S.O., Brewer, A.A., 2007. Visual field maps in human cortex. *Neuron* 56, 366-83.
- Wandell, B.A., Winawer, J., 2011. Imaging retinotopic maps in the human brain. *Vision research* 51, 718-37.
- Wang, R., Benner, T., Sorensen, A.G., Wedeen, V.J., 2007. Diffusion Toolkit: A Software Package for Diffusion Imaging Data Processing and Tractography, in: *Proc. 15th Ann. Mtg. of ISMRM*. p. 3720.
- Wedeen, V.J., Wang, R.P., Schmahmann, J.D., Benner, T., Tseng, W.Y.I., Dai, G., Pandya, D.N., Hagmann, P., D'Arceuil, H., De Crespigny, a J., 2008. Diffusion spectrum magnetic resonance imaging (DSI) tractography of crossing fibers. *NeuroImage* 41, 1267-77.
- Wilms, M., Eickhoff, S.B., Specht, K., Amunts, K., Shah, N.J., Malikovic, A., Fink, G.R., 2005. Human V5/MT+: comparison of functional and cytoarchitectonic data. *Anatomy and embryology* 210, 485-95.
- Wu, J., Yan, T., Zhang, Z., Jin, F., Guo, Q., 2012. Retinotopic mapping of the peripheral visual field to human visual cortex by functional magnetic resonance imaging. *Human brain mapping* 33, 1727-40.
- Wyller, T.B., Sørdring, K.M., Sveen, U., Ljunggren, A.E., Bautz-Holter, E., 1997. Are there gender differences in functional outcome after stroke? *Clinical rehabilitation* 11, 171-9.
- Xiang, H.-D., Fonteijn, H.M., Norris, D.G., Hagoort, P., 2010. Topographical functional connectivity pattern in the perisylvian language networks. *Cerebral cortex (New York, N.Y.: 1991)* 20, 549-60.
- Xue, R., Van Zijl, P.C.M., Crain, B.J., Solaiyappan, M., Mori, S., 1999. In vivo three-dimensional reconstruction of rat brain axonal projections by diffusion tensor imaging. *Magnetic resonance in medicine: official journal of the Society of Magnetic Resonance in Medicine / Society of Magnetic Resonance in Medicine* 42, 1123-1127.
- y Cajal, S., Azoulay, L., 1894. *Les nouvelles idées sur la structure du système nerveux: chez l'homme et chez les vertébrés*. Paris:C. Reinwald & Cie.
- Zalesky, A., Fornito, A., Harding, I.H., Cocchi, L., Yücel, M., Pantelis, C., Bullmore, E.T., 2010. Whole-brain anatomical networks: does the choice of nodes matter? *NeuroImage* 50, 970-83.

Zhang, S., Li, C.R., 2012. Functional connectivity mapping of the human precuneus by resting state fMRI. *NeuroImage* 59, 3548-62.

Zwiers, M.P., 2010. Patching cardiac and head motion artefacts in diffusion-weighted images. *NeuroImage* 53, 565-75.

Nederlandse samenvatting

Dit proefschrift handelt over het modelleren van menselijke hersenen met macroscopische netwerken. De doelstelling was beter in de kaart te brengen, hoe gebieden op de hersenschors functioneel en structureel met elkaar verbonden zijn. In de studies van dit proefschrift werden daarbij de verbindings-patronen onderzocht door middel van grafentheoretische analyses, gemeten met magnetische resonantie beeldvormingstechnieken (MRI). De resultaten geven er nieuw inzicht in hoe gebieden in de hersenschors via banen in de witte stof met elkaar verbonden zijn en hoe deze gerelateerd kunnen worden aan gemeten hersenfunctie. In de volgende paragrafen worden de belangrijkste bevindingen van de hoofdstukken 2-5 kort samengevat.

De bevindingen

Het doel van de studie beschreven in **hoofdstuk 2** is het vinden van geautomatiseerde alternatieven voor anatomisch-gebaseerde indelingen van de hersenen. Deze anatomisch-gebaseerde indelingen staan er namelijk bekend om hun tekortkomingen wanneer deze gebruikt worden bij een functionele netwerkanalyse van de hersenen (Smith et al., 2010). Drie verschillende methoden om de hersenschors geautomatiseerd in te delen in functioneel gespecialiseerde hersengebieden werden onderzocht. De resultaten tonen aan dat de hersenindelingen die gebaseerd waren op structurele eigenschappen, zoals de vouwpatronen van de hersenen of de verbindings-patronen van de witte stofbanen, overlappen met functioneel gespecialiseerde hersengebieden. In de vervolg studies werd daarom de voorkeur gegeven aan het modelleren van de netwerken van de hersenen via automatische of functioneel gedefinieerde indelings-methoden in plaats van de gebruikelijke anatomische hersenindelingen.

Hoofdstuk 3 richt zich op de vraag waar de knooppunten zich binnen het structurele netwerk van de hersenen bevinden. Knooppunten in een netwerk, ook wel hubs genoemd, werden bepaald met twee grafentheoretische maten: de *graad van een punt* en *“betweenness centrality”*. De *graad van een punt*, omschrijft het aantal verbindingen dat een punt heeft met de rest van het netwerk en de *“betweenness centrality”* van een punt omschrijft de fractie van de kortste paden binnen het netwerk dat door een punt gaat. Om versnippering van hersenknooppunten tijdens het modelleren te voorkomen werden de netwerken van hersenen met verschillende indelingen geanalyseerd. Met deze aanpak bleek dat de *graad* en *“betweenness centrality”* topografisch verdeeld zijn over de hersenschors, analoog aan de verdeling van bevolkings-knooppunten over het oppervlak van de aarde (zie figuur 6.1). De studie levert twee topografische knooppunten-kaarten op van het netwerk van de menselijke hersenschors voor een gemiddelde bevolking van jongvolwassenen. Uit deze kaarten blijkt dat de knooppunten van de hersenschors overeenkomen met belangrijke gebieden van bekende cognitieve netwerken. Een analyse van de kaart laat zien dat er meerdere hubs asymmetrisch verdeeld zijn over de beide hersenhelften en dat de kwaliteiten van de knooppunten verschillen bij man en vrouw. De resultaten laten zien aan dat vrouwen meer hubs met hogere *“betweenness centrality”* hebben dan mannen en dat mannen meer hubs met

een hogere *graad* hebben. Verder werd ook de topologie van de netwerken bestudeerd waaruit volgde dat netwerken van vrouwen in vergelijking tot die van mannen hogere *small-world* indices in de beide hersenhelften hebben.

De studie beschreven in **hoofdstuk 4** richt zich op het onderzoek naar de structurele verbindings-patronen tussen hersenschors gebieden van het visuele systeem. Het visuele systeem werd gekozen omdat het een goed onderzocht subnetwerk van de hersenschors is, waarin talrijke functioneel gedefinieerde gebieden uit de literatuur bekend zijn. In deze studie werden visuele gebieden gedefinieerd op basis van hun activatiepatronen op visuele stimulatie, gemeten met functionele MRI. Deze techniek wordt in de literatuur met “*retinopic mapping*” omschreven. Vervolgens werden de verbindingspatronen tussen visuele gebieden bepaald met probabilistische tractografie op het voxel niveau. De resultaten geven een plausibele beschrijving van de complexe verbindingspatronen tussen de visuele gebieden. De analyse van het structurele netwerk van het visuele systeem heeft aangetoond dat het gegroepeerd is in een dorsale en ventrale module. De gevonden modules staan ook bekend als de ‘wat’ en ‘waar’ stromen van het visuele systeem (Ungerleider en Haxby, 1994). Verder werden ook de structurele verbindings-patronen tussen visuele gebieden bestudeerd. Uit de analyse volgt dat deze patronen overeenstemmingen vertonen met bekende activatie-patronen in visuele gebieden bij visuele stimulaties (Wandell en Winawer, 2011).

De laatste studie in **hoofdstuk 5** onderzoekt de mogelijkheden voor het beoordelen van schade aan het netwerk van de hersenschors, door middel van het simuleren van laesies in de netwerken van de hersenschors bij een populatie van gezonde controles. Dit werd bewerkstelligd door laesies van patiënten met gezichtsvelddefecten naar een gezonde controlepopulatie homotoop te verplaatsen. Binnen de gezonde controles werden hersennetwerken aangemaakt met en zonder een laesie. Het effect van de laesie op het netwerk werd gemeten met verschillende graaftheoretische maten. De resultaten van de laesie simulatie werden berekend en weergegeven door middel van de topografische methode uit **hoofdstuk 3**. Uit de verkregen topografische kaarten blijkt dat hersenregio's die grenzen aan een laesie binnen het netwerk het meest getroffen zijn, terwijl regio's die verder van de laesie afstaan in mindere mate eveneens getroffen zijn. Deze bevindingen sluiten aan bij Monakow's diaschisis concept, dat veronderstelt dat perifere gebieden van een focale laesie een gereduceerd metabolisme kunnen krijgen. De resultaten tonen aan dat bij de meeste laesies de linker frontaal kwab ten opzichte van de rechter frontaal kwab meer afname in verbondenheid ondervond. Verondersteld wordt dat deze bevindingen gerelateerd zouden moeten zijn aan asymmetrisch georganiseerde hersenschors netwerken. Met behulp van verdere analyses werd aangetoond dat de waargenomen netwerk schade in de occipitale kwab significant gecorreleerd is aan de gezichtsveldafwijking van de patiënten.

List of publications

Nijhuis, E.H.J., Van Cappellen van Walsum, A.-M., Norris, D.G., 2013. Topographic Hub Maps of the Human Structural Neocortical Network. *PLoS ONE* 8, e65511.

Nijhuis, E.H.J., Swisher, J.D., Arnoldussen, D.M., Jehee, J.F.M., van den Berg, A.V., Van Cappellen van Walsum, A.-M., Norris, D.G., (*in review*). Exploring the Connectivity Patterns of Human Neocortical Visual Areas.

Nijhuis, E.H.J., Bergsma, D., van den Berg, A.V., Van Cappellen van Walsum, A.-M., Norris, D.G., (*submitted*). Neocortical network damage assessment by homotopic lesion mapping on healthy subjects.

Nijhuis, E.H.J., Visser E., Swisher, J.D., Arnoldussen, D.M., van den Berg, A.V., Van Cappellen van Walsum, A.-M., Norris, D.G., (*in preparation*). Automatic whole-brain parcellation for macroscopic network modeling.

Visser, E., Nijhuis, E.H.J., Buitelaar, J.K., Zwiers, M.P., 2011. Partition-based mass clustering of tractography streamlines. *NeuroImage* 54, 303-312.

Nijhuis, E.H.J., Xiang, H.D., Hagoort P., Norris, D.G., (*in preparation*). Genetic modulation of Broca's and Wernicke's area as structural hubs in the large-scale brain network.

Curriculum vitae

Emil H.J. Nijhuis was born 22nd May, 1980 in Kiel, Germany as the youngest child in a Dutch immigrant family with two brothers and one sister. Classic music, puzzles and board games were key activities within his family and he developed a fondness for the board-game *Go* as a young teenager. Playing the game for less than a year he accomplished to win the German Junior Go Championships. Shortly after that he went on to study the game in Japan for a year as a protégé of Chizu Kobayashi. There he competed as an Insei (apprentice) at the boarding school of the Japanese Go Association, the Nihon Ki-in. Returning home he completed his Abitur at the Gymnasium and followed his siblings to the University of Amsterdam to study computer science and mathematics. Throughout his studies he continued to play Go actively and went on to become a two times Dutch national champion (2003 and 2004) while also performing at the international top-level by becoming 4th at the European Go Congress (2001) and 3rd at the World Amateur Go Championships (2004). For his master thesis entitled “Learning Patterns in Game of Go” (2006) he tackled his favorite game with his supervisor Nikos Vlassis by developing supervised learning methods for graphs which were aimed to teach complex and high-level expert knowledge to computer software. While planning to expand his Go research to interactive learning methods he worked for Apollon as a consultant in the gaming industry. Developing a late fascination for the human brain he switched discipline in 2009 when he received an opportunity to start a PhD project on functional and structural brain networks at the Donders Institute for the University of Twente under the supervision of David Norris and Anne-Marie van Cappellen van Walsum. In the first year he led a team effort for the winning entry on automatic brain parcellation methods of the Pittsburgh Brain Competition. His PhD project focused on analyzing structural connectivity patterns and their relation to cognitive function in healthy and damaged brains. Currently he continues his research on brain networks as a post-doctoral researcher at Donders Institute and aspires to continue his career in academia.

Donders graduate school for cognitive neuroscience series

1. van Aalderen-Smeets, S.I. (2007). *Neural dynamics of visual selection*. Maastricht University, Maastricht, the Netherlands.
2. Schoffelen, J.M. (2007). *Neuronal communication through coherence in the human motor system*. Radboud University Nijmegen, Nijmegen, the Netherlands.
3. de Lange, F.P. (2008). *Neural mechanisms of motor imagery*. Radboud University Nijmegen, Nijmegen, the Netherlands.
4. Grol, M.J. (2008). *Parieto-frontal circuitry in visuomotor control*. Utrecht University, Utrecht, the Netherlands.
5. Bauer, M. (2008). *Functional roles of rhythmic neuronal activity in the human visual and somatosensory system*. Radboud University Nijmegen, Nijmegen, the Netherlands.
6. Mazaheri, A. (2008). *The Influence of Ongoing Oscillatory Brain Activity on Evoked Responses and Behaviour*. Radboud University Nijmegen, Nijmegen, the Netherlands.
7. Hooijmans, C.R. (2008). *Impact of nutritional lipids and vascular factors in Alzheimer's Disease*. Radboud University Nijmegen, Nijmegen, the Netherlands.
8. Gaszner, B. (2008). *Plastic responses to stress by the rodent urocortinergic Edinger-Westphal nucleus*. Radboud University Nijmegen, Nijmegen, the Netherlands.
9. Willems, R.M. (2009). *Neural reflections of meaning in gesture, language and action*. Radboud University Nijmegen, Nijmegen, the Netherlands.
10. van Pelt, S. (2009). *Dynamic neural representations of human visuomotor space*. Radboud University Nijmegen, Nijmegen, the Netherlands.
11. Lommertzen, J. (2009). *Visuomotor coupling at different levels of complexity*. Radboud University Nijmegen, Nijmegen, the Netherlands.
12. Poljac, E. (2009). *Dynamics of cognitive control in task switching: Looking beyond the switch cost*. Radboud University Nijmegen, Nijmegen, the Netherlands.
13. Poser, B.A. (2009). *Techniques for BOLD and blood volume weighted fMRI*. Radboud University Nijmegen, Nijmegen, the Netherlands.
14. Baggio, G. (2009). *Semantics and the electrophysiology of meaning. Tense, aspect, event structure*. Radboud University Nijmegen, Nijmegen, the Netherlands.
15. van Wingen, G.A. (2009). *Biological determinants of amygdala functioning*. Radboud University Nijmegen Medical Centre, Nijmegen, the Netherlands.
16. Bakker, M. (2009). *Supraspinal control of walking: lessons from motor imagery*. Radboud University Nijmegen Medical Centre, Nijmegen, the Netherlands.
17. Aarts, E. (2009). *Resisting temptation: the role of the anterior cingulate cortex in adjusting cognitive control*. Radboud University Nijmegen, Nijmegen, the Netherlands.
18. Prinz, S. (2009). *Waterbath stunning of chickens - Effects of electrical parameters on the electroencephalogram and physical reflexes of broilers*. Radboud University Nijmegen, Nijmegen, the Netherlands.
19. Knippenberg, J.M.J. (2009). *The N150 of the Auditory Evoked Potential from the rat amygdala: In search for its functional significance*. Radboud University Nijmegen, Nijmegen, the Netherlands.
20. Dumont, G.J.H. (2009). *Cognitive and physiological effects of 3,4-methylenedioxymethamphetamine (MDMA or 'ecstasy') in combination with alcohol or cannabis in humans*. Radboud University Nijmegen, Nijmegen, the Netherlands.
21. Pijnacker, J. (2010). *Defeasible inference in autism: a behavioral and electrophysiological approach*. Radboud University Nijmegen, Nijmegen, the Netherlands.
22. de Vrijer, M. (2010). *Multisensory integration in spatial orientation*. Radboud University Nijmegen, Nijmegen, the Netherlands.
23. Vergeer, M. (2010). *Perceptual visibility and appearance: Effects of color and form*. Radboud University Nijmegen, Nijmegen, the Netherlands.
24. Levy, J. (2010). *In Cerebro Unveiling Unconscious Mechanisms during Reading*. Radboud University Nijmegen, Nijmegen, the Netherlands.
25. Treder, M. S. (2010). *Symmetry in (inter)action*. Radboud University Nijmegen, Nijmegen, the Netherlands.
26. Horlings C.G.C. (2010). *A Weak balance; balance and falls in patients with neuromuscular disorders*. Radboud University Nijmegen, Nijmegen, the Netherlands.
27. Snaphaan, L.J.A.E. (2010). *Epidemiology of post-stroke behavioural consequences*. Radboud Uni-

- versity Nijmegen Medical Centre, Nijmegen, the Netherlands.
28. Dado - Van Beek, H.E.A. (2010). *The regulation of cerebral perfusion in patients with Alzheimer's disease*. Radboud University Nijmegen Medical Centre, Nijmegen, the Netherlands.
 29. Derks, N.M. (2010). *The role of the non-preganglionic Edinger-Westphal nucleus in sex-dependent stress adaptation in rodents*. Radboud University Nijmegen, Nijmegen, the Netherlands.
 30. Wyczesany, M. (2010). *Covariation of mood and brain activity. Integration of subjective self-report data with quantitative EEG measures*. Radboud University Nijmegen, Nijmegen, the Netherlands.
 31. Beurze S.M. (2010). *Cortical mechanisms for reach planning*. Radboud University Nijmegen, Nijmegen, the Netherlands.
 32. van Dijk, J.P. (2010). *On the Number of Motor Units*. Radboud University Nijmegen, Nijmegen, the Netherlands.
 33. Lapatki, B.G. (2010). *The Facial Musculature - Characterization at a Motor Unit Level*. Radboud University Nijmegen, Nijmegen, the Netherlands.
 34. Kok, P. (2010). *Word Order and Verb Inflection in Agrammatic Sentence Production*. Radboud University Nijmegen, Nijmegen, the Netherlands.
 35. van Elk, M. (2010). *Action semantics: Functional and neural dynamics*. Radboud University Nijmegen, Nijmegen, the Netherlands.
 36. Majdandzic, J. (2010). *Cerebral mechanisms of processing action goals in self and others*. Radboud University Nijmegen, Nijmegen, the Netherlands.
 37. Snijders, T.M. (2010). *More than words - neural and genetic dynamics of syntactic unification*. Radboud University Nijmegen, Nijmegen, the Netherlands.
 38. Grootens, K.P. (2010). *Cognitive dysfunction and effects of antipsychotics in schizophrenia and borderline personality disorder*. Radboud University Nijmegen Medical Centre, Nijmegen, the Netherlands.
 39. Nieuwenhuis, I.L.C. (2010). *Memory consolidation: A process of integration - Converging evidence from MEG, fMRI and behavior*. Radboud University Nijmegen Medical Centre, Nijmegen, the Netherlands.
 40. Menenti, L.M.E. (2010). *The right language: differential hemispheric contributions to language production and comprehension in context*. Radboud University Nijmegen, Nijmegen, the Netherlands.
 41. van Dijk, H.P. (2010). *The state of the brain, how alpha oscillations shape behaviour and event related responses*. Radboud University Nijmegen, Nijmegen, the Netherlands.
 42. Meulenbroek, O.V. (2010). *Neural correlates of episodic memory in healthy aging and Alzheimer's disease*. Radboud University Nijmegen, Nijmegen, the Netherlands.
 43. Oude Nijhuis, L.B. (2010). *Modulation of human balance reactions*. Radboud University Nijmegen, Nijmegen, the Netherlands.
 44. Qin, S. (2010). *Adaptive memory: imaging medial temporal and prefrontal memory systems*. Radboud University Nijmegen, Nijmegen, the Netherlands.
 45. Timmer, N.M. (2011). *The interaction of heparan sulfate proteoglycans with the amyloid β protein*. Radboud University Nijmegen, Nijmegen, the Netherlands.
 46. Crajé, C. (2011). *(A)typical motor planning and motor imagery*. Radboud University Nijmegen, Nijmegen, the Netherlands.
 47. van Grootel, T.J. (2011). *On the role of eye and head position in spatial localisation behaviour*. Radboud University Nijmegen, Nijmegen, the Netherlands.
 48. Lamers, M.J.M. (2011). *Levels of selective attention in action planning*. Radboud University Nijmegen, Nijmegen, the Netherlands.
 49. Van der Werf, J. (2011). *Cortical oscillatory activity in human visuomotor integration*. Radboud University Nijmegen, Nijmegen, the Netherlands.
 50. Scheeringa, R. (2011). *On the relation between oscillatory EEG activity and the BOLD signal*. Radboud University Nijmegen, Nijmegen, the Netherlands.
 51. Bögels, S. (2011). *The role of prosody in language comprehension: when prosodic breaks and pitch accents come into play*. Radboud University Nijmegen, Nijmegen, the Netherlands.
 52. Ossewaarde, L. (2011). *The mood cycle: hormonal influences on the female brain*. Radboud University Nijmegen, Nijmegen, the Netherlands.
 53. Kuribara, M. (2011). *Environment-induced activation and growth of pituitary melanotrope cells of *Xenopus laevis**. Radboud University Nijmegen, Nijmegen, the Netherlands.
 54. Helmich, R.C.G. (2011). *Cerebral reorganization in Parkinson's disease*. Radboud University Nij-

- megen, Nijmegen, the Netherlands.
55. Boelen, D. (2011). *Order out of chaos? Assessment and treatment of executive disorders in brain-injured patients*. Radboud University Nijmegen, Nijmegen, the Netherlands.
 56. Koopmans, P.J. (2011). *fMRI of cortical layers*. Radboud University Nijmegen, Nijmegen, the Netherlands.
 57. van der Linden, M.H. (2011). *Experience-based cortical plasticity in object category representation*. Radboud University Nijmegen, Nijmegen, the Netherlands.
 58. Kleine, B.U. (2011). *Motor unit discharges - Physiological and diagnostic studies in ALS*. Radboud University Nijmegen Medical Centre, Nijmegen, the Netherlands.
 59. Paulus, M. (2011). *Development of action perception: Neurocognitive mechanisms underlying children's processing of others' actions*. Radboud University Nijmegen, Nijmegen, the Netherlands.
 60. Tieleman, A.A. (2011). *Myotonic dystrophy type 2. A newly diagnosed disease in the Netherlands*. Radboud University Nijmegen Medical Centre, Nijmegen, the Netherlands.
 61. van Leeuwen, T.M. (2011). *'How one can see what is not there': Neural mechanisms of grapheme-colour synaesthesia*. Radboud University Nijmegen, Nijmegen, the Netherlands.
 62. van Tilborg, I.A.D.A. (2011). *Procedural learning in cognitively impaired patients and its application in clinical practice*. Radboud University Nijmegen, Nijmegen, the Netherlands.
 63. Bruinsma, I.B. (2011). *Amyloidogenic proteins in Alzheimer's disease and Parkinson's disease: interaction with chaperones and inflammation*. Radboud University Nijmegen, Nijmegen, the Netherlands.
 64. Voermans, N. (2011). *Neuromuscular features of Ehlers-Danlos syndrome and Marfan syndrome; expanding the phenotype of inherited connective tissue disorders and investigating the role of the extracellular matrix in muscle*. Radboud University Nijmegen Medical Centre, Nijmegen, the Netherlands.
 65. Reelick, M. (2011). *One step at a time. Disentangling the complexity of preventing falls in frail older persons*. Radboud University Nijmegen Medical Centre, Nijmegen, the Netherlands.
 66. Buur, P.F. (2011). *Imaging in motion. Applications of multi-echo fMRI*. Radboud University Nijmegen, Nijmegen, the Netherlands.
 67. Schaefer, R.S. (2011). *Measuring the mind's ear: EEG of music imagery*. Radboud University Nijmegen, Nijmegen, the Netherlands.
 68. Xu, L. (2011). *The non-preganglionic Edinger-Westphal nucleus: an integration center for energy balance and stress adaptation*. Radboud University Nijmegen, Nijmegen, the Netherlands.
 69. Schellekens, A.F.A. (2011). *Gene-environment interaction and intermediate phenotypes in alcohol dependence*. Radboud University Nijmegen, Nijmegen, the Netherlands.
 70. van Marle, H.J.F. (2011). *The amygdala on alert: A neuroimaging investigation into amygdala function during acute stress and its aftermath*. Radboud University Nijmegen, Nijmegen, the Netherlands.
 71. De Laat, K.F. (2011). *Motor performance in individuals with cerebral small vessel disease: an MRI study*. Radboud University Nijmegen Medical Centre, Nijmegen, the Netherlands.
 72. Mädebach, A. (2011). *Lexical access in speaking: Studies on lexical selection and cascading activation*. Radboud University Nijmegen, Nijmegen, the Netherlands.
 73. Poelmans, G.J.V. (2011). *Genes and protein networks for neurodevelopmental disorders*. Radboud University Nijmegen, Nijmegen, the Netherlands.
 74. van Norden, A.G.W. (2011). *Cognitive function in elderly individuals with cerebral small vessel disease. An MRI study*. Radboud University Nijmegen Medical Centre, Nijmegen, the Netherlands.
 75. Jansen, E.J.R. (2011). *New insights into V-ATPase functioning: the role of its accessory subunit Ac45 and a novel brain-specific Ac45 paralog*. Radboud University Nijmegen, Nijmegen, the Netherlands.
 76. Haaxma, C.A. (2011). *New perspectives on pre-clinical and early stage Parkinson's disease*. Radboud University Nijmegen Medical Centre, Nijmegen, the Netherlands.
 77. Haegens, S. (2012). *On the functional role of oscillatory neuronal activity in the somatosensory system*. Radboud University Nijmegen, Nijmegen, the Netherlands.
 78. van Barneveld, D.C.P.B.M. (2012). *Integration of exteroceptive and interoceptive cues in spatial localization*. Radboud University Nijmegen, Nijmegen, the Netherlands.
 79. Spies, P.E. (2012). *The reflection of Alzheimer disease in CSF*. Radboud University Nijmegen Medical Centre, Nijmegen, the Netherlands.
 80. Helle, M. (2012). *Artery-specific perfusion measurements in the cerebral vasculature by magnetic*

- resonance imaging. Radboud University Nijmegen, Nijmegen, the Netherlands.
81. Egetemeir, J. (2012). *Neural correlates of real-life joint action*. Radboud University Nijmegen, Nijmegen, the Netherlands.
 82. Janssen, L. (2012). *Planning and execution of (bi)manual grasping*. Radboud University Nijmegen, Nijmegen, the Netherlands.
 83. Vermeer, S. (2012). *Clinical and genetic characterisation of Autosomal Recessive Cerebellar Ataxias*. Radboud University Nijmegen Medical Centre, Nijmegen, the Netherlands.
 84. Vrins, S. (2012). *Shaping object boundaries: contextual effects in infants and adults*. Radboud University Nijmegen, Nijmegen, the Netherlands.
 85. Weber, K.M. (2012). *The language learning brain: Evidence from second language and bilingual studies of syntactic processing*. Radboud University Nijmegen, Nijmegen, the Netherlands.
 86. Verhagen, L. (2012). *How to grasp a ripe tomato*. Utrecht University, Utrecht, the Netherlands.
 87. Nonkes, L.J.P. (2012). *Serotonin transporter gene variance causes individual differences in rat behaviour: for better and for worse*. Radboud University Nijmegen Medical Centre, Nijmegen, the Netherlands.
 88. Joosten-Weyn Banningh, L.W.A. (2012). *Learning to live with Mild Cognitive Impairment: development and evaluation of a psychological intervention for patients with Mild Cognitive Impairment and their significant others*. Radboud University Nijmegen Medical Centre, Nijmegen, the Netherlands.
 89. Xiang, H.D. (2012). *The language networks of the brain*. Radboud University Nijmegen, Nijmegen, the Netherlands.
 90. Snijders, A.H. (2012). *Tackling freezing of gait in Parkinson's disease*. Radboud University Nijmegen Medical Centre, Nijmegen, the Netherlands.
 91. Rouwette, T.P.H. (2012). *Neuropathic Pain and the Brain - Differential involvement of corticotropin-releasing factor and urocortin 1 in acute and chronic pain processing*. Radboud University Nijmegen Medical Centre, Nijmegen, the Netherlands.
 92. van de Meerendonk, N. (2012). *States of indecision in the brain: Electrophysiological and hemodynamic reflections of monitoring in visual language perception*. Radboud University Nijmegen, Nijmegen, the Netherlands.
 93. Sterrenburg, A. (2012). *The stress response of forebrain and midbrain regions: neuropeptides, sex-specificity and epigenetics*. Radboud University Nijmegen, Nijmegen, The Netherlands.
 94. Uithol, S. (2012). *Representing Action and Intention*. Radboud University Nijmegen, Nijmegen, The Netherlands.
 95. van Dam, W.O. (2012). *On the specificity and flexibility of embodied lexical-semantic representations*. Radboud University Nijmegen, Nijmegen, The Netherlands.
 96. Slats, D. (2012). *CSF biomarkers of Alzheimer's disease; serial sampling analysis and the study of circadian rhythmicity*. Radboud University Nijmegen Medical Centre, Nijmegen, the Netherlands.
 97. Van Nuenen, B.F.L. (2012). *Cerebral reorganization in premotor parkinsonism*. Radboud University Nijmegen Medical Centre, Nijmegen, the Netherlands.
 98. van Schouwenburg, M.R. (2012). *Fronto-striatal mechanisms of attentional control*. Radboud University Nijmegen, Nijmegen, The Netherlands.
 99. Azar, M.G. (2012). *On the theory of reinforcement learning: methods, convergence analysis and sample complexity*. Radboud University Nijmegen, Nijmegen, The Netherlands.
 100. Meeuwissen, E.B. (2012). *Cortical oscillatory activity during memory formation*. Radboud University Nijmegen, Nijmegen, The Netherlands.
 101. Arnold, J.F. (2012). *When mood meets memory: neural and behavioral perspectives on emotional memory in health and depression*. Radboud University Nijmegen, Nijmegen, The Netherlands.
 102. Gons, R.A.R. (2012). *Vascular risk factors in cerebral small vessel disease: a diffusion tensor imaging study*. Radboud University Nijmegen Medical Centre, Nijmegen, the Netherlands.
 103. Wingbermühle, E. (2012). *Cognition and emotion in adults with Noonan syndrome: A neuropsychological perspective*. Radboud University Nijmegen, Nijmegen, The Netherlands.
 104. Walentowska, W. (2012). *Facing emotional faces. The nature of automaticity of facial emotion processing studied with ERPs*. Radboud University Nijmegen, Nijmegen, The Netherlands.
 105. Hoogman, M. (2012). *Imaging the effects of ADHD risk genes*. Radboud University Nijmegen, Nijmegen, The Netherlands.
 106. Tramper, J. J. (2012). *Feedforward and feedback mechanisms in sensory motor control*. Radboud University Nijmegen, Nijmegen, The Netherlands.
 107. Van Eijndhoven, P. (2012). *State and trait char-*

- acteristics of early course major depressive disorder. Radboud University Nijmegen Medical Centre, Nijmegen, the Netherlands.
108. Visser, E. (2012). *Leaves and forests: Low level sound processing and methods for the large-scale analysis of white matter structure in autism*. Radboud University Nijmegen, Nijmegen, The Netherlands.
 109. van Tooren-Hoogenboom, N. (2012). *Neuronal Communication in the Synchronized Brain. Investigating the functional role of visually-induced gamma band activity: lessons from MEG*. Radboud University Nijmegen, Nijmegen, The Netherlands.
 110. Henckens, M.J.A.G. (2012). *Imaging the stressed brain. Elucidating the time- and region-specific effects of stress hormones on brain function; a translational approach*. Radboud University Nijmegen, Nijmegen, The Netherlands.
 111. van Kesteren, M.T.R. (2012). *Schemas in the brain: Influences of prior knowledge on learning, memory, and education*. Radboud University Nijmegen, Nijmegen, The Netherlands.
 112. Brenders, P. (2012). *Cross-Language Interactions in Beginning Second Language Learners*. Radboud University Nijmegen, Nijmegen, The Netherlands.
 113. Ter Horst, A.C. (2012). *Modulating motor imagery. Contextual, spatial and kinaesthetic influences*. Radboud University Nijmegen, Nijmegen, The Netherlands.
 114. Tesink, C.M.J.Y. (2013). *Neurobiological insights into language comprehension in autism: context matters*. Radboud University Nijmegen, Nijmegen, The Netherlands.
 115. Böckler, A. (2013). *Looking at the world together. How others' attentional relations to jointly attended scenes shape cognitive processing*. Radboud University Nijmegen, Nijmegen, The Netherlands.
 116. van Dongen, E.V. (2013). *Sleeping to Remember. On the neural and behavioral mechanisms of sleep-dependent memory consolidation*. Radboud University Nijmegen, Nijmegen, The Netherlands.
 117. Volman, I. (2013). *The neural and endocrine regulation of emotional actions*. Radboud University Nijmegen, Nijmegen, The Netherlands.
 118. Buchholz, V. (2013). *Oscillatory activity in tactile remapping*. Radboud University Nijmegen, Nijmegen, The Netherlands.
 119. Van Deurzen, P.A.M. (2013). *Information processing and depressive symptoms in healthy adolescents*. Radboud University Nijmegen, Nijmegen, The Netherlands.
 120. Whitmarsh, S. (2013). *Nonreactivity and Metacognition in Mindfulness*. Radboud University Nijmegen, Nijmegen, The Netherlands.
 121. Vesper, C. (2013). *Acting Together: Mechanisms of Intentional Coordination*. Radboud University Nijmegen, Nijmegen, The Netherlands.
 122. Lagro, J. (2013). *Cardiovascular and cerebrovascular physiological measurements in clinical practice and prognostics in geriatric patients*. Radboud University Nijmegen Medical Centre, Nijmegen, the Netherlands.
 123. Eskenazi, T.T. (2013). *You, Us & Them: From motor simulation to ascribed shared intentionality in social perception*. Radboud University Nijmegen, Nijmegen, The Netherlands.
 124. Ondobaka, S. (2013). *On the conceptual and perceptual processing of own and others' behavior*. Radboud University Nijmegen, Nijmegen, The Netherlands.
 125. Overvelde, J.A.A.M. (2013). *Which practice makes perfect? Experimental studies on the acquisition of movement sequences to identify the best learning condition in good and poor writers*. Radboud University Nijmegen, Nijmegen, The Netherlands.
 126. Kalisvaart, J.P. (2013). *Visual ambiguity in perception and action*. Radboud University Nijmegen Medical Centre, Nijmegen, The Netherlands.
 127. Kroes, M. (2013). *Altering memories for emotional experiences*. Radboud University Nijmegen, Nijmegen, The Netherlands.
 128. Duijnhouwer, J. (2013). *Studies on the rotation problem in self-motion perception*. Radboud University Nijmegen, Nijmegen, The Netherlands.
 129. Nijhuis, E.H.J. (2013). *Macroscopic Networks in the Human Brain: Mapping connectivity in healthy and damaged brains*. University of Twente, Enschede, The Netherlands.

Supplementary material (available in digital version)

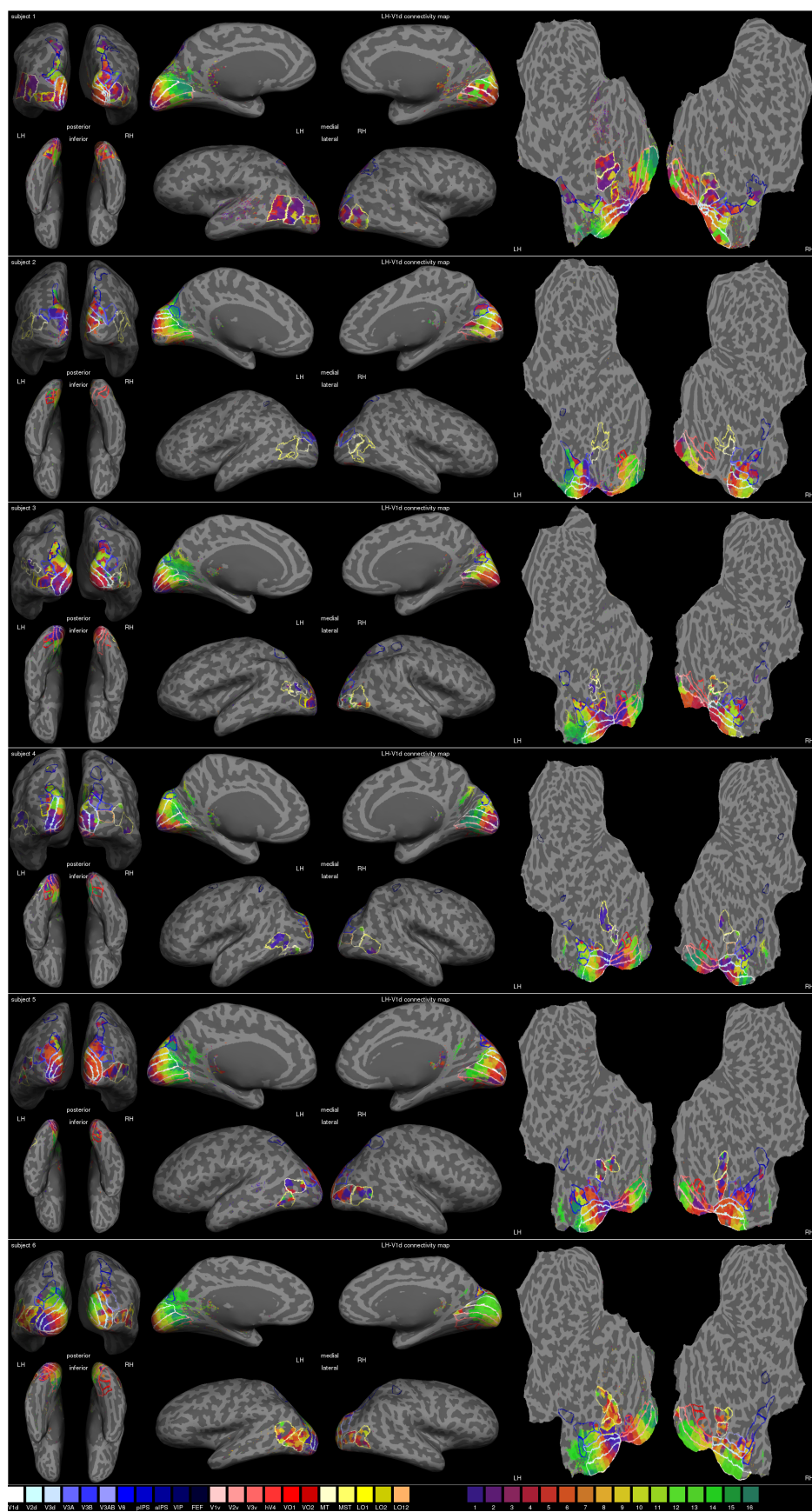
Supplementary figures A.1-37 show the connectivity maps for all visual areas on their brain flat maps and inflated surfaces. The coloured contours indicate the borders of the subjects' visual areas. Within a specific analysed visual area each of the 16 regions received a unique colour corresponding to the index of the region (see legends). The colours in the rest of the brain display which of the sixteen regions of a specific visual area project most to that particular vertex or region. In case no streamlines were found between the considered visual area and a vertex or region no colours were assigned. The holes within visual areas in the flat maps are the result of projection errors from labelled voxels to surface vertices. Table A.1 gives the list of available connectivity maps.

Supplementary figures A.38-43 show the individual connectivity matrices of each subject's mapped visual network. The 592×592 matrices consist of 37×37 grids of 16×16 matrices. Each of the 16×16 matrices describes the connectivity pattern between different visual regions, like the one shown in Figure 4.6.

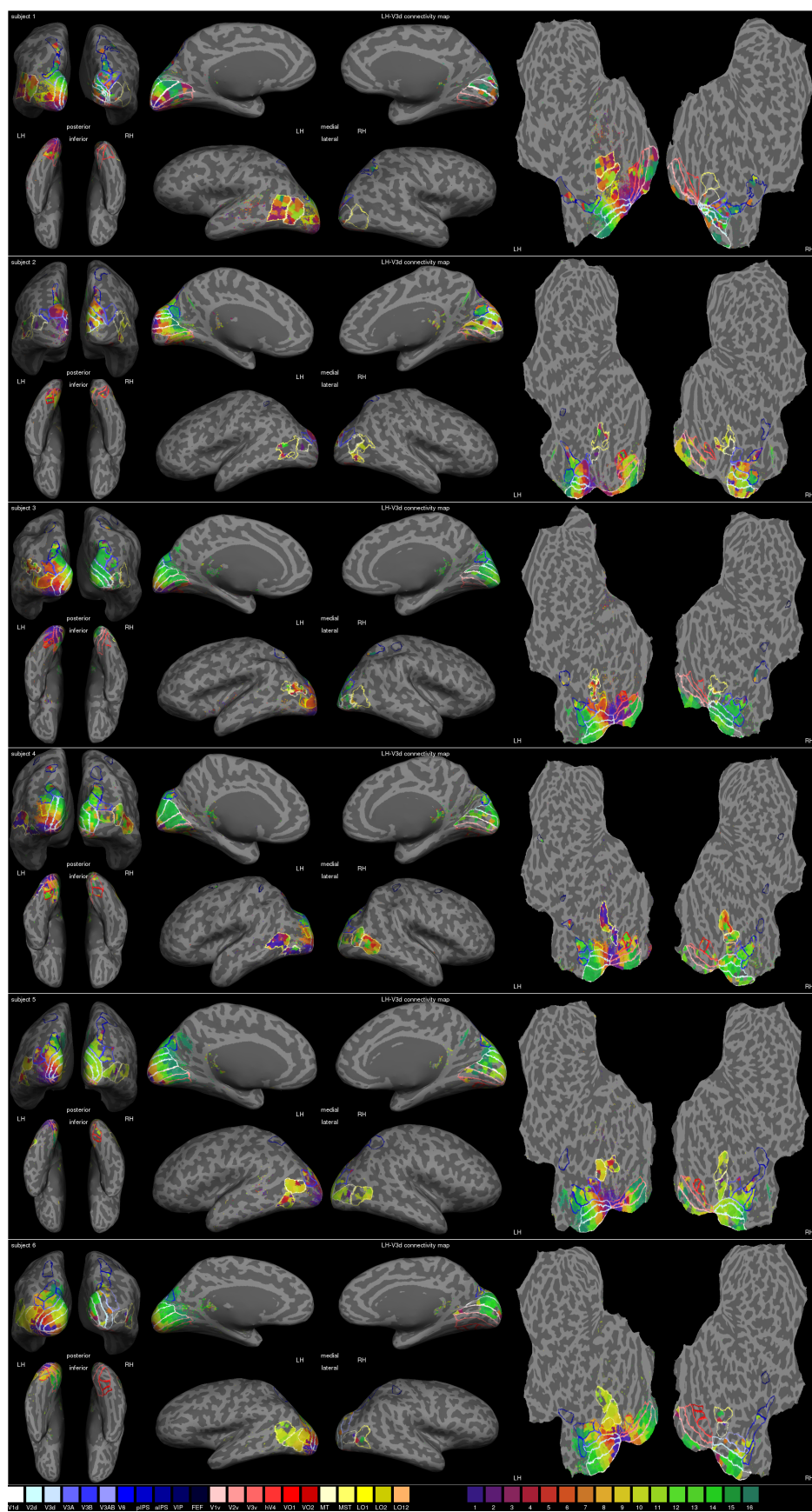
Visual area		Figure ids		# subjects	
		LH	RH	LH	RH
V1d	dorsal primary visual cortex	A.1	A.20	6	6
V2d	dorsal visual area 2	A.2	A.21	6	6
V3d	dorsal visual area 3	A.3	A.22	6	6
V3A	visual complex V3 part A	A.4	A.23	5	5
V3B	visual complex V3 part B	A.5	A.24	5	5
V6	visual area 6	A.6	A.25	5	5
posIPS	posterior intraparietal sulcus	A.7	A.26	6	6
antIPS	anterior intraparietal sulcus	A.8	A.27	5	6
VIP	ventral intraparietal area	A.9	A.28	2	3
FEF	frontal eye field	A.10	A.29	1	2
V1v	ventral primary visual cortex	A.11	A.30	6	6
V2v	ventral visual area 2	A.12	A.31	6	6
V3v	ventral visual area 3	A.13	A.32	6	6
hV4	human visual area 4	A.14	A.33	5	6
VO1	ventral occipital cortex area 1	A.15	A.34	3	3
VO2	ventral occipital cortex area 2	n.a.	A.35	0	1
MT	medial temporal area	A.16	A.36	6	6
MST	medial superior temporal area	A.17	A.37	6	6
LO1	lateral occipital cortex area 1	A.18	n.a.	4	0
LO2	lateral occipital cortex area 2	A.19	n.a.	3	0

Table A.1

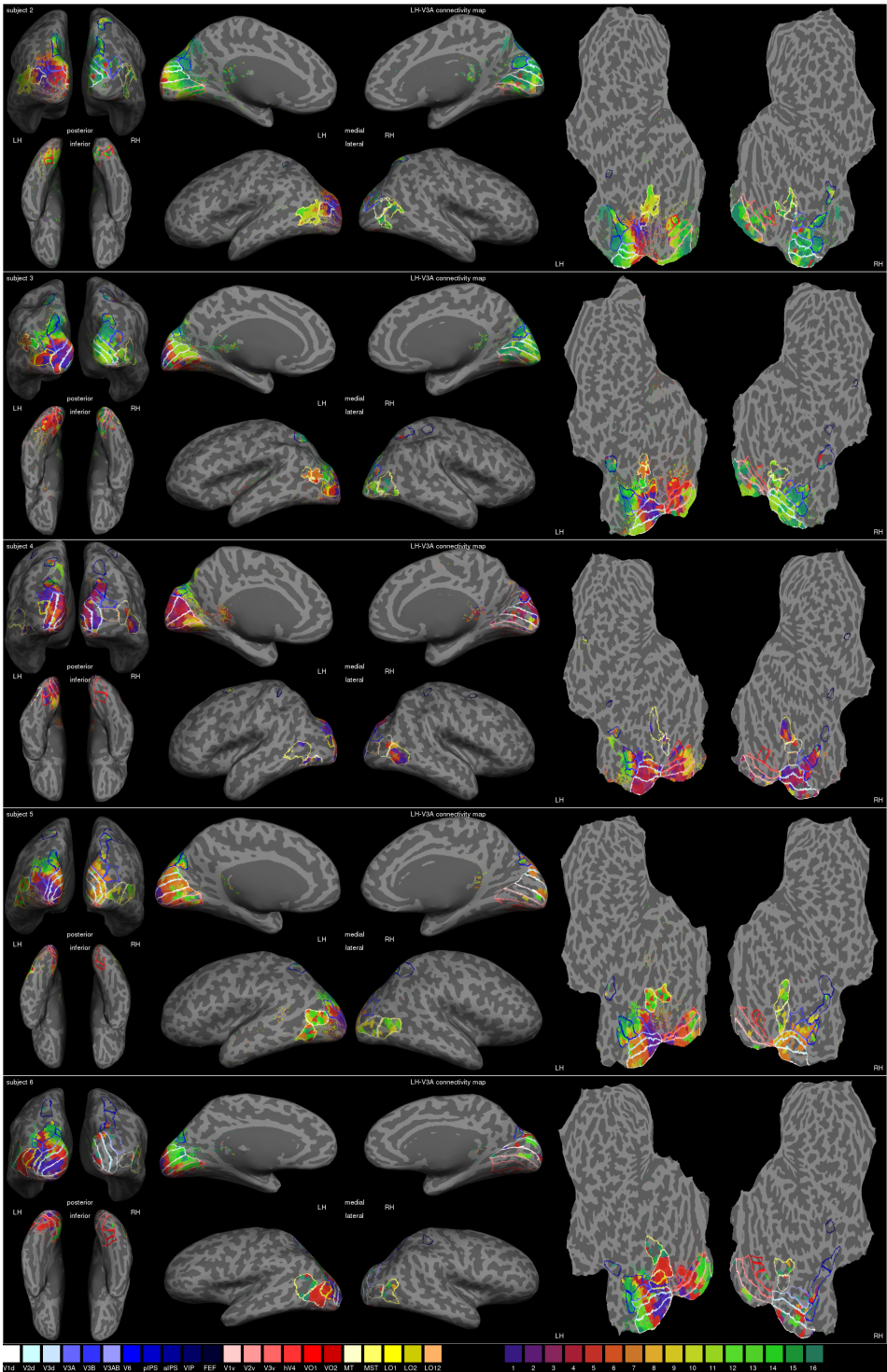
Shows how many subjects have been mapped for a particular visual map and what the Supplementary figure id for the connectivity maps are ('LH'= left and 'RH'=right hemisphere.)



Supplementary figure A.1 Shows the connectivity maps of V1 dorsal in the left hemisphere for subjects 1-6.

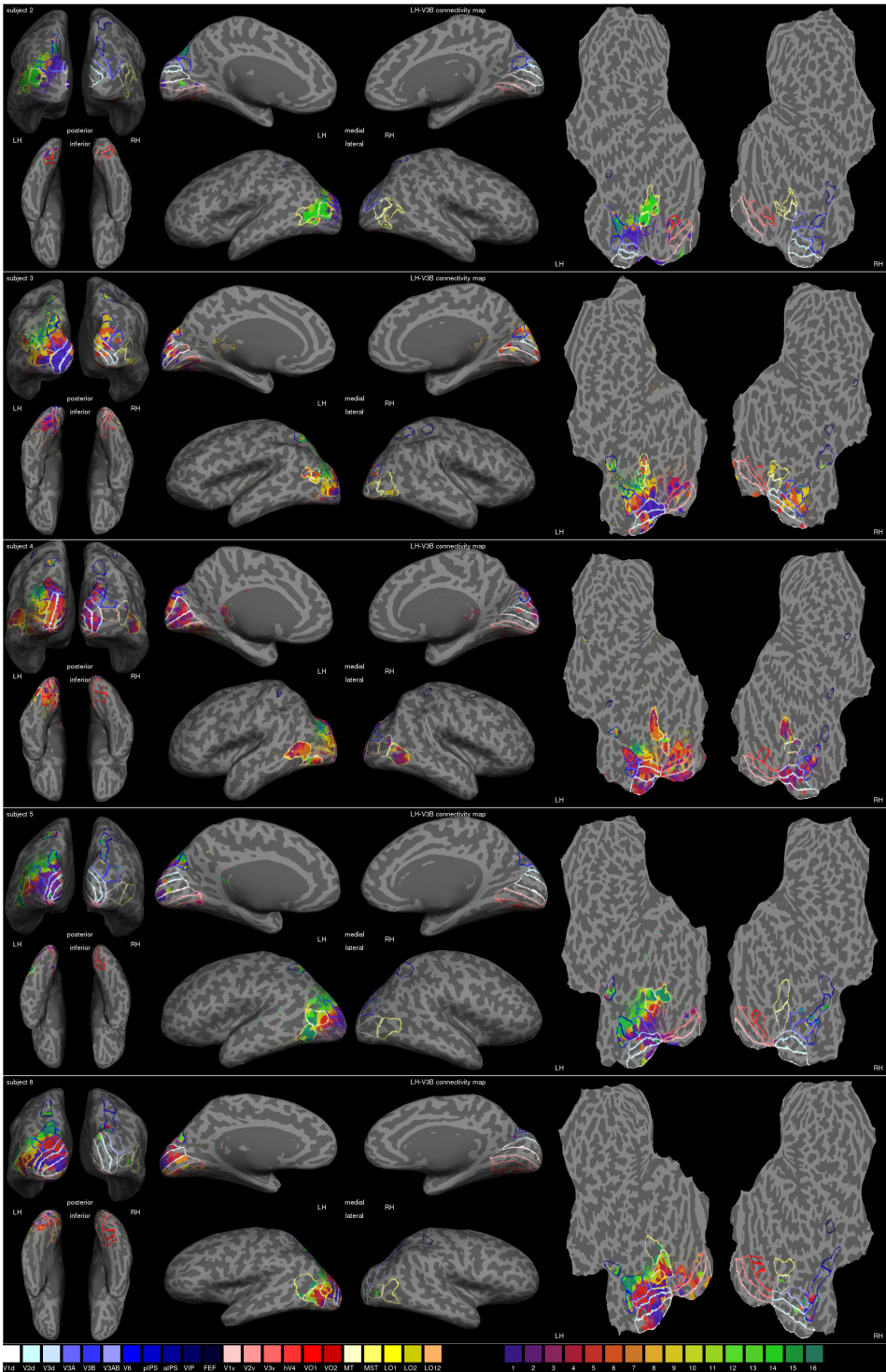


Supplementary figure A.3 Shows the connectivity maps of V3 dorsal in the left hemisphere for subjects 1-6.



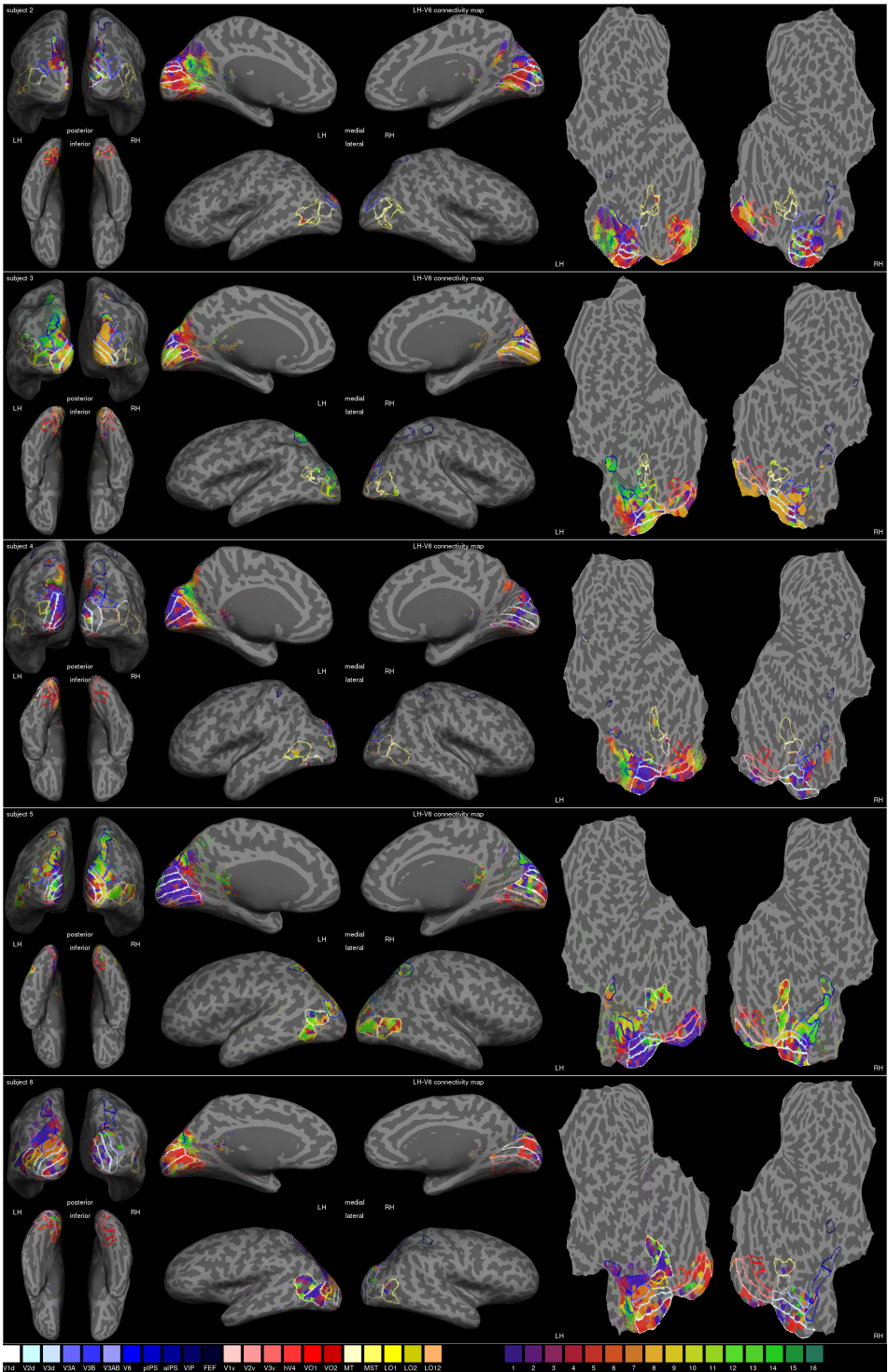
Supplementary figure A.4

Shows the connectivity maps of V3A in the left hemisphere for subjects 2-6.



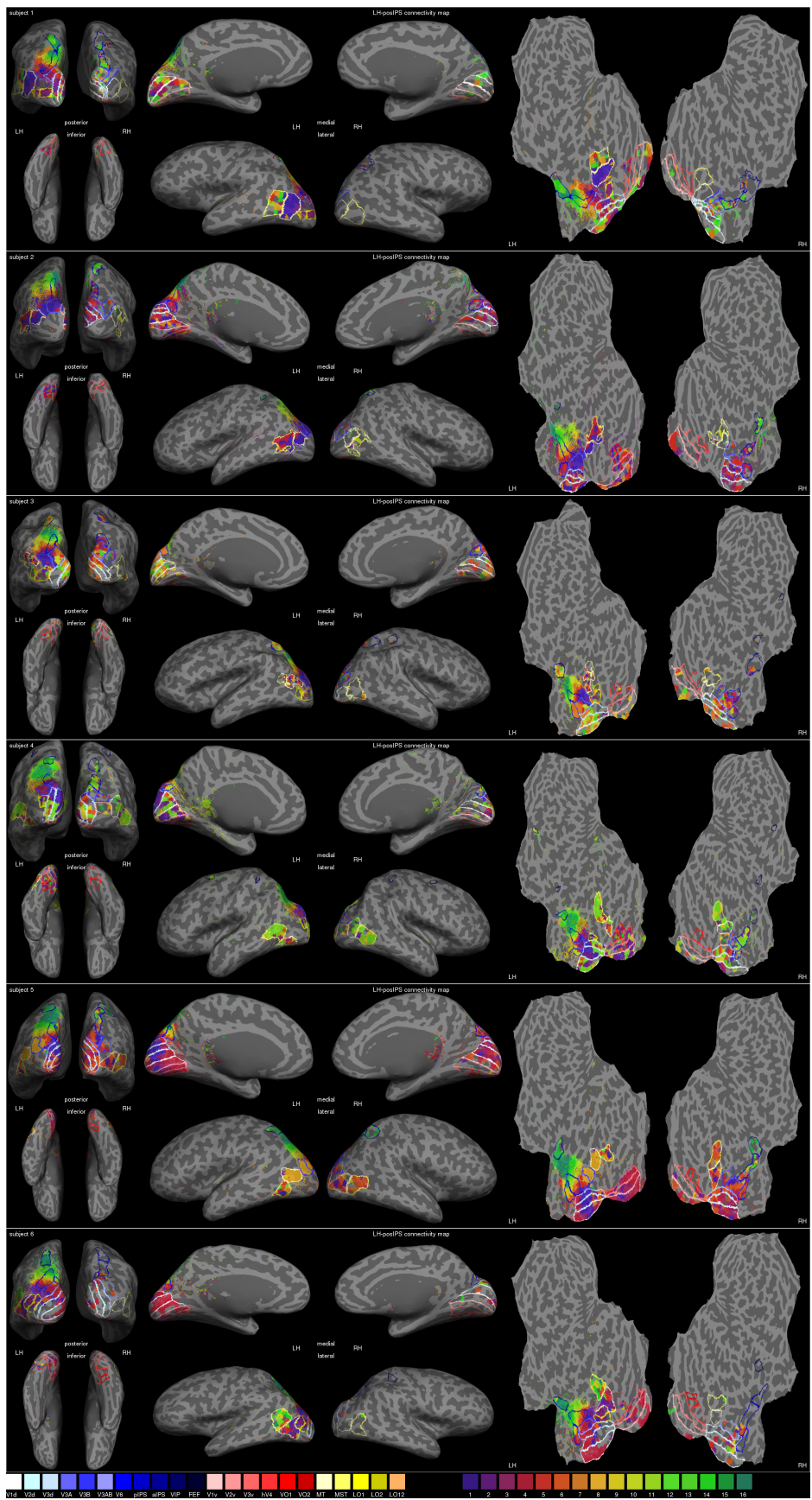
Supplementary figure A.5

Shows the connectivity maps of V3B in the left hemisphere for subjects 2-6.

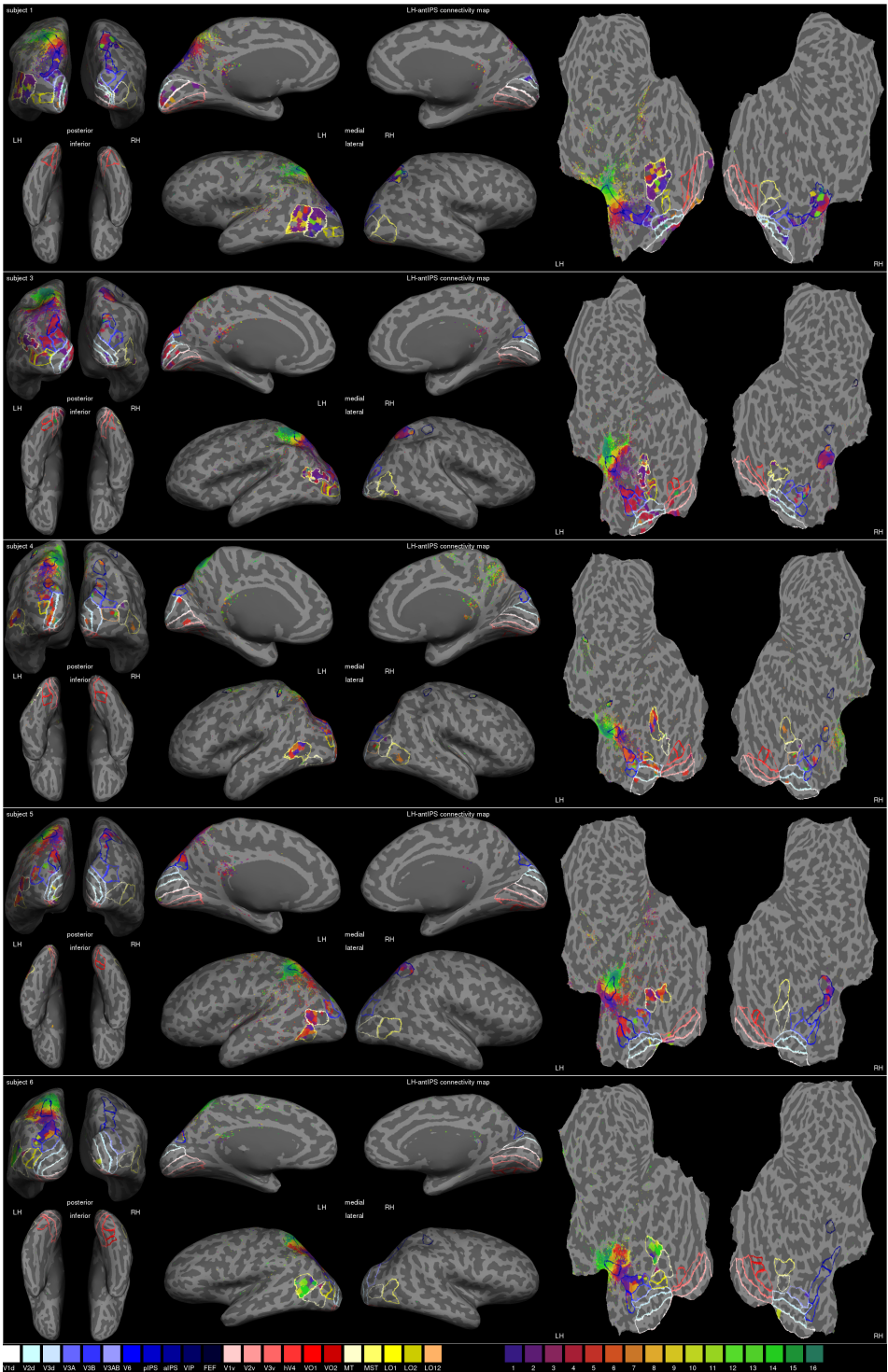


Supplementary figure A.6

Shows the connectivity maps of V6 in the left hemisphere for subjects 2-6.

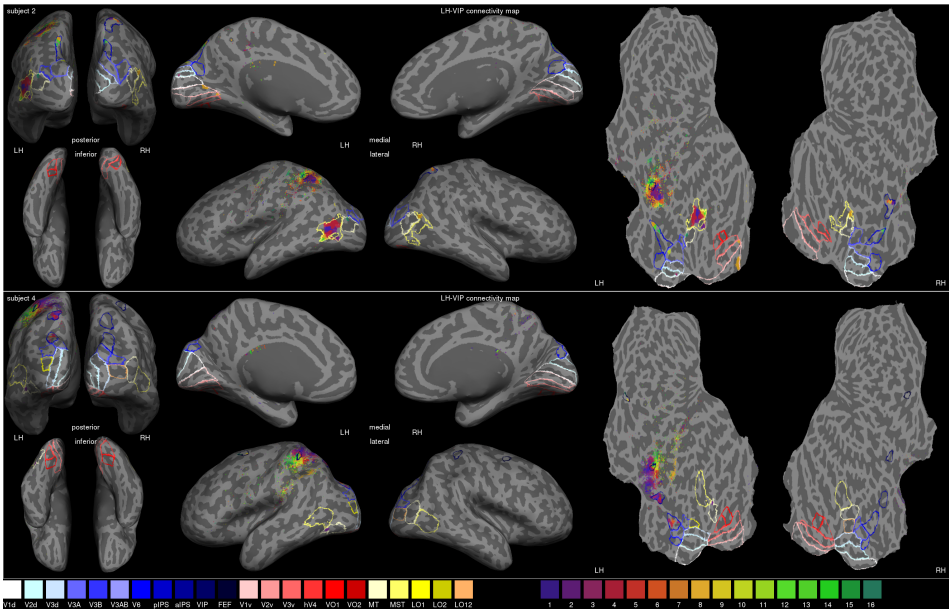


Supplementary figure A.7 Shows the connectivity maps of posterior IPS in the left hemisphere for subjects 1-6.



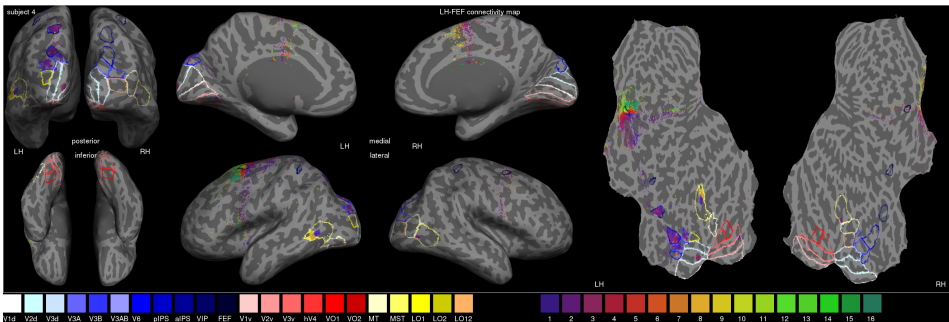
Supplementary figure A.8

Shows the connectivity maps of anterior IPS in the left hemisphere for subjects 1, 3-6.



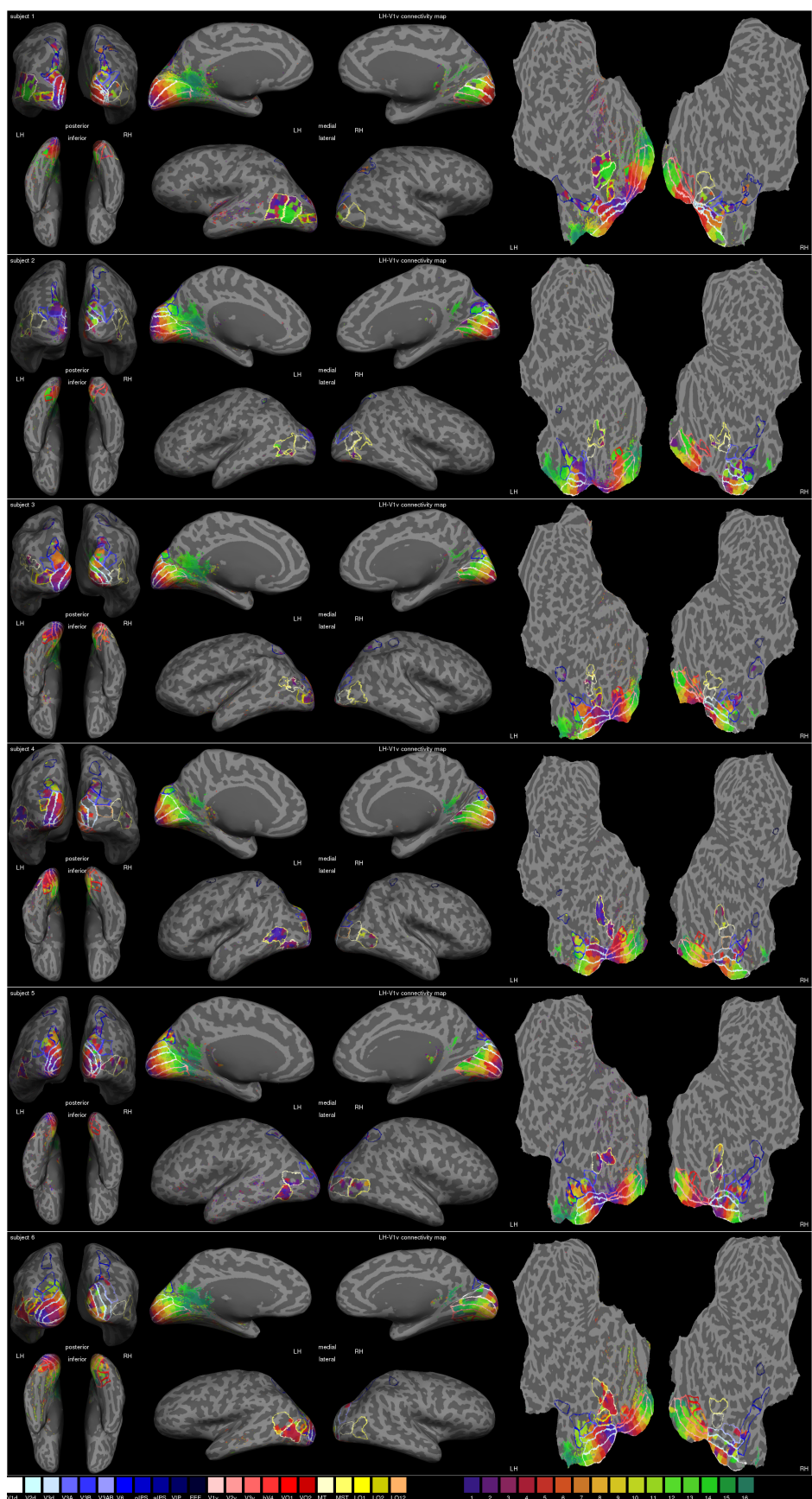
Supplementary figure A.9

Shows the connectivity maps of VIP in the left hemisphere for subjects 2 and 4.



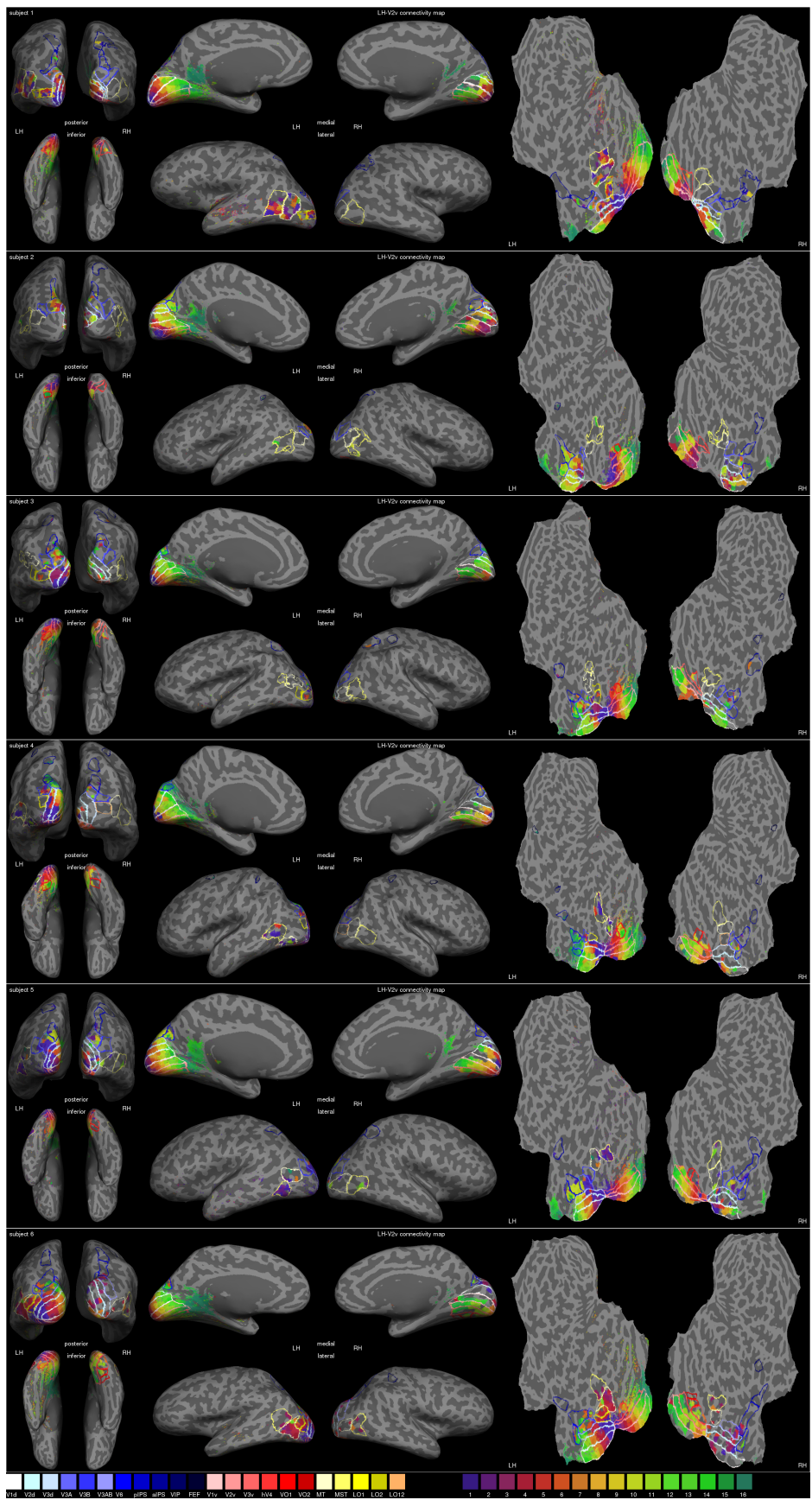
Supplementary figure A.10

Shows the connectivity map of FEF in the left hemisphere for subject 4.

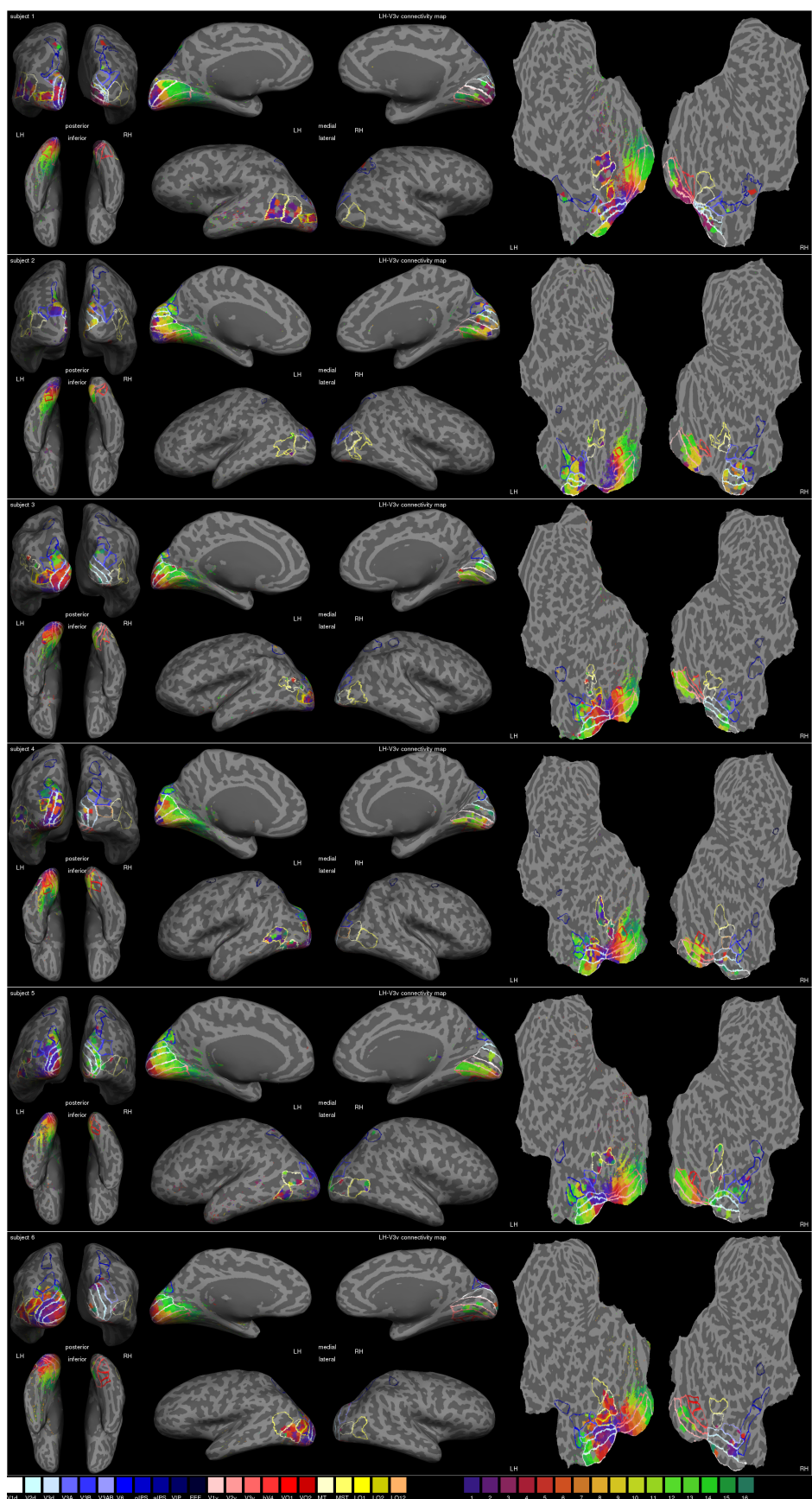


Shows the connectivity maps of V1 ventral in the left hemisphere for subjects 1-6.

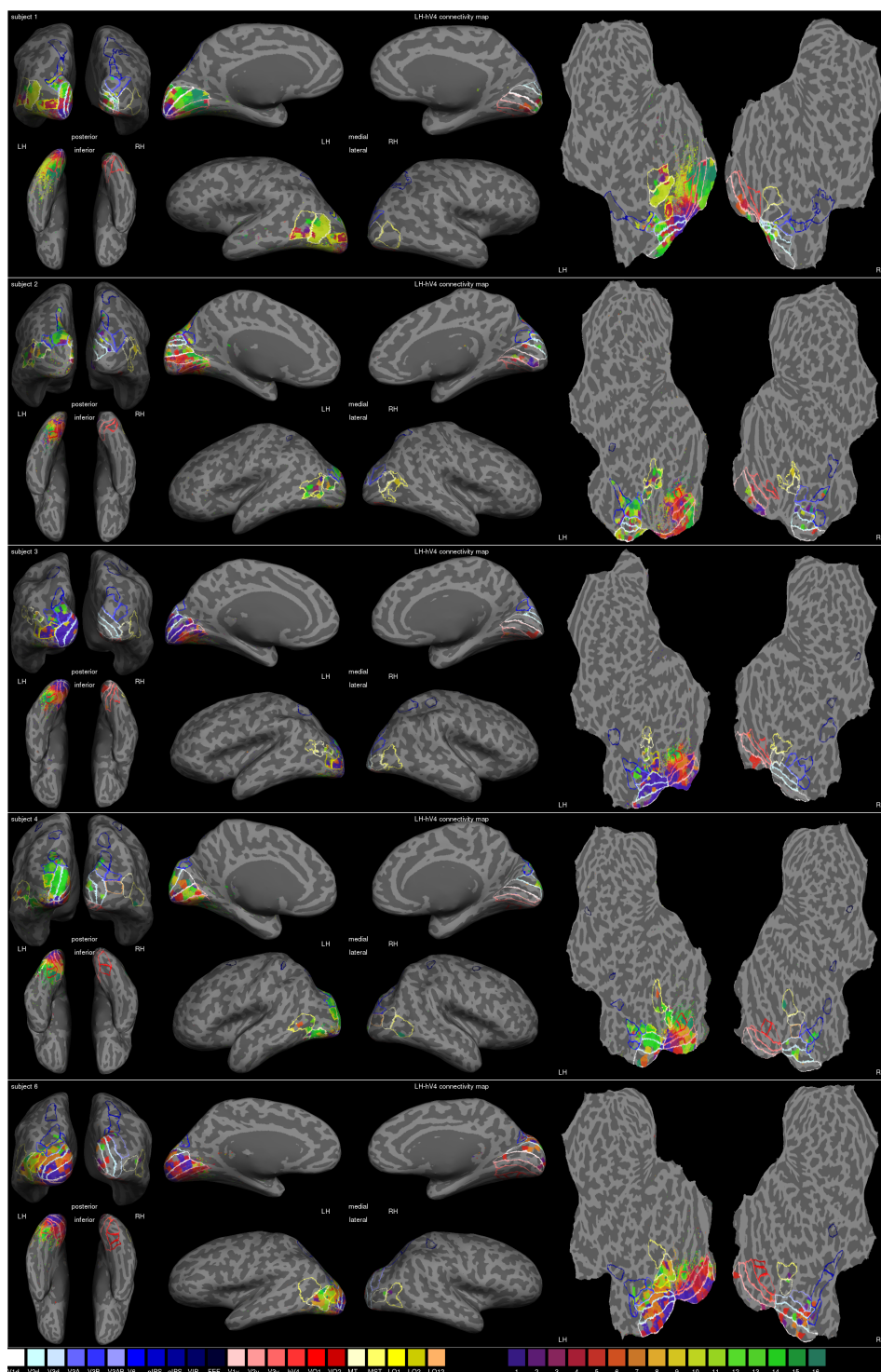
Supplementary figure A.1.1



Supplementary figure A.12 Shows the connectivity maps of V2 ventral in the left hemisphere for subjects 1-6.

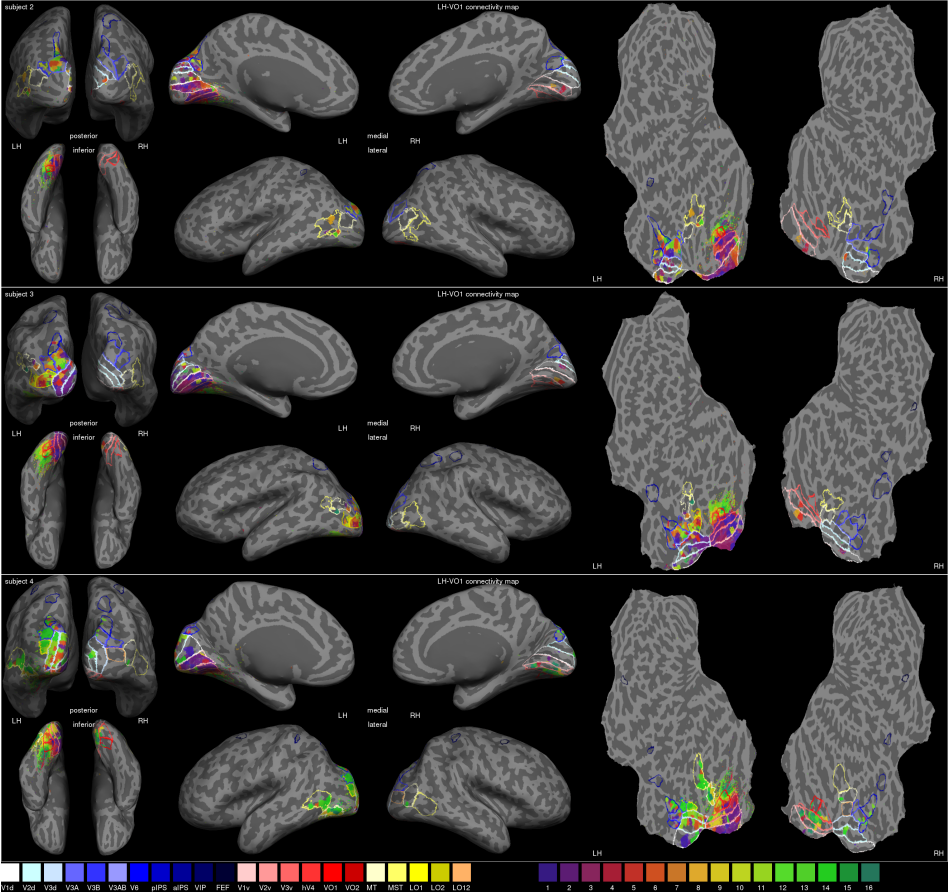


Supplementary figure A.13 Shows the connectivity maps of V3 ventral in the left hemisphere for subjects 1-6.

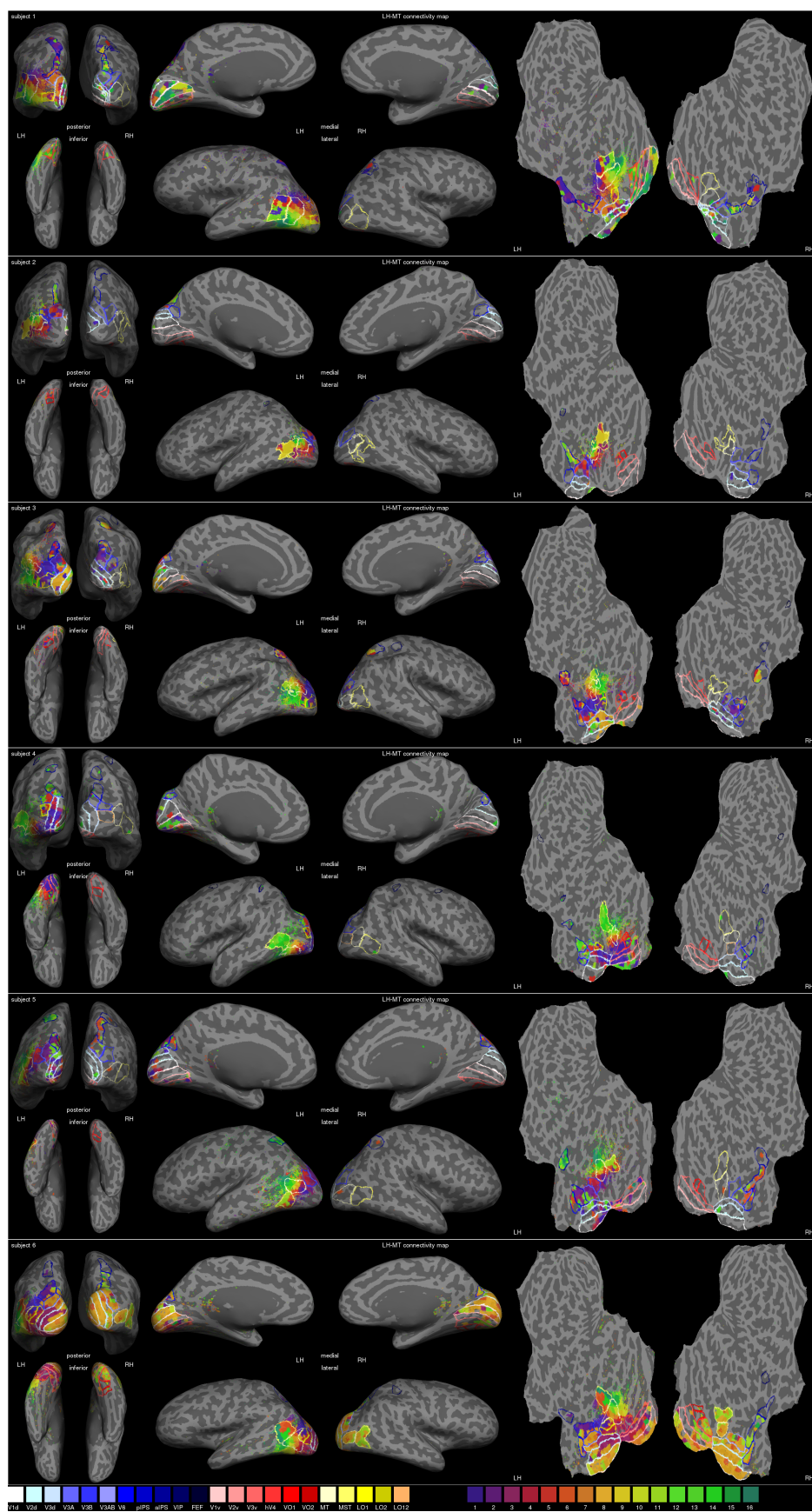


Supplementary figure A.14

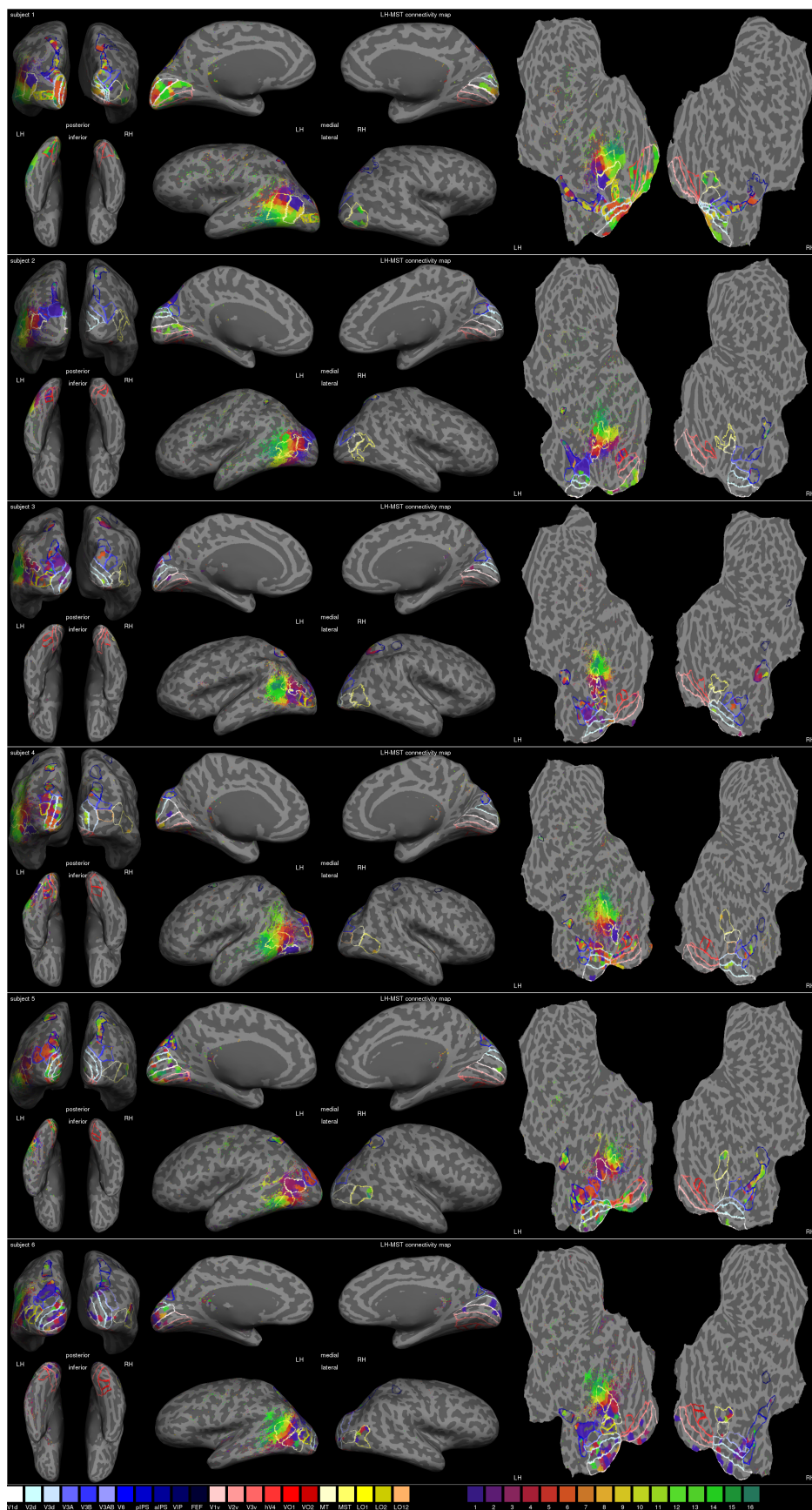
Shows the connectivity maps of hV4 in the left hemisphere for subjects 1-4, 6.



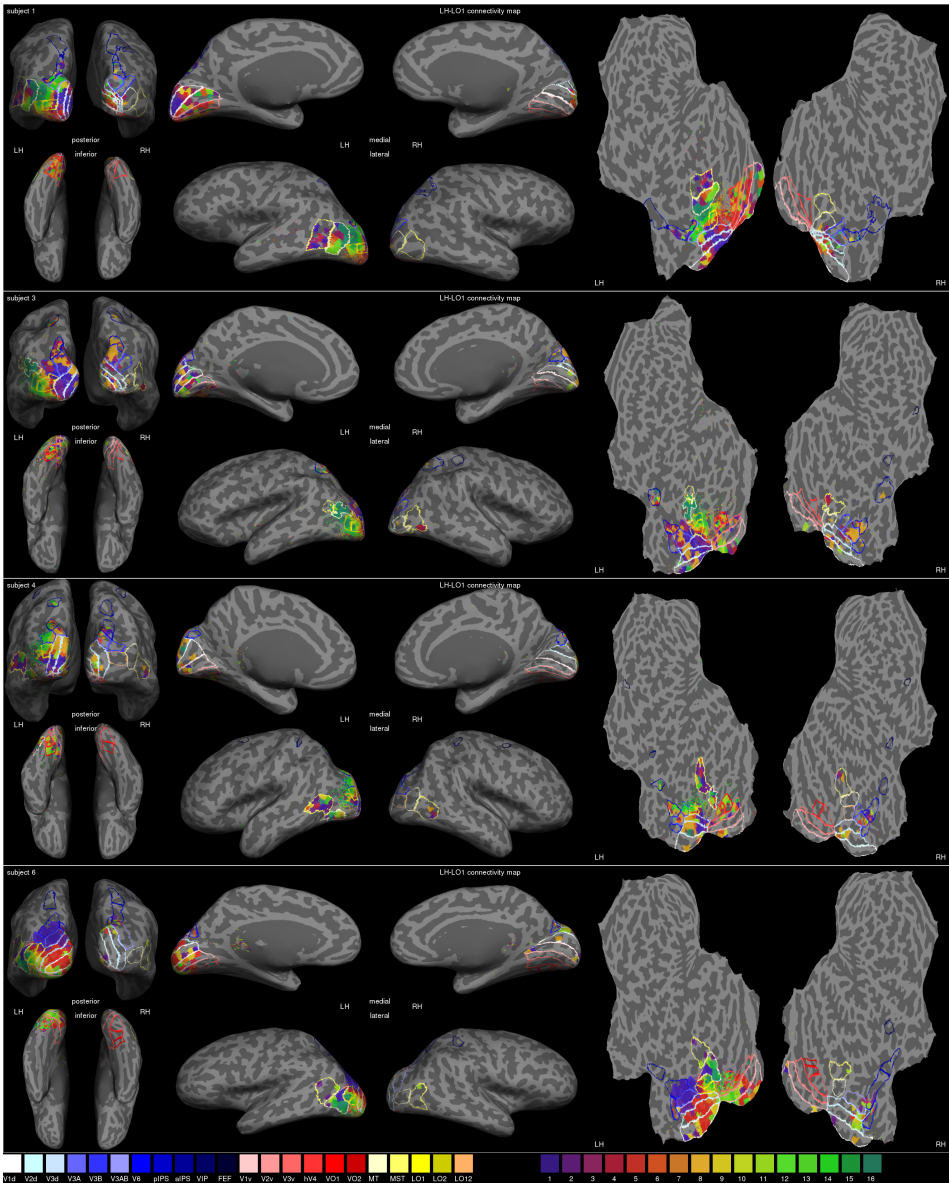
Supplementary figure A.15
Shows the connectivity maps of VO1 in the left hemisphere for subjects 2-4



Supplementary figure A.16 Shows the connectivity maps of MT in the left hemisphere for subjects 1-6.

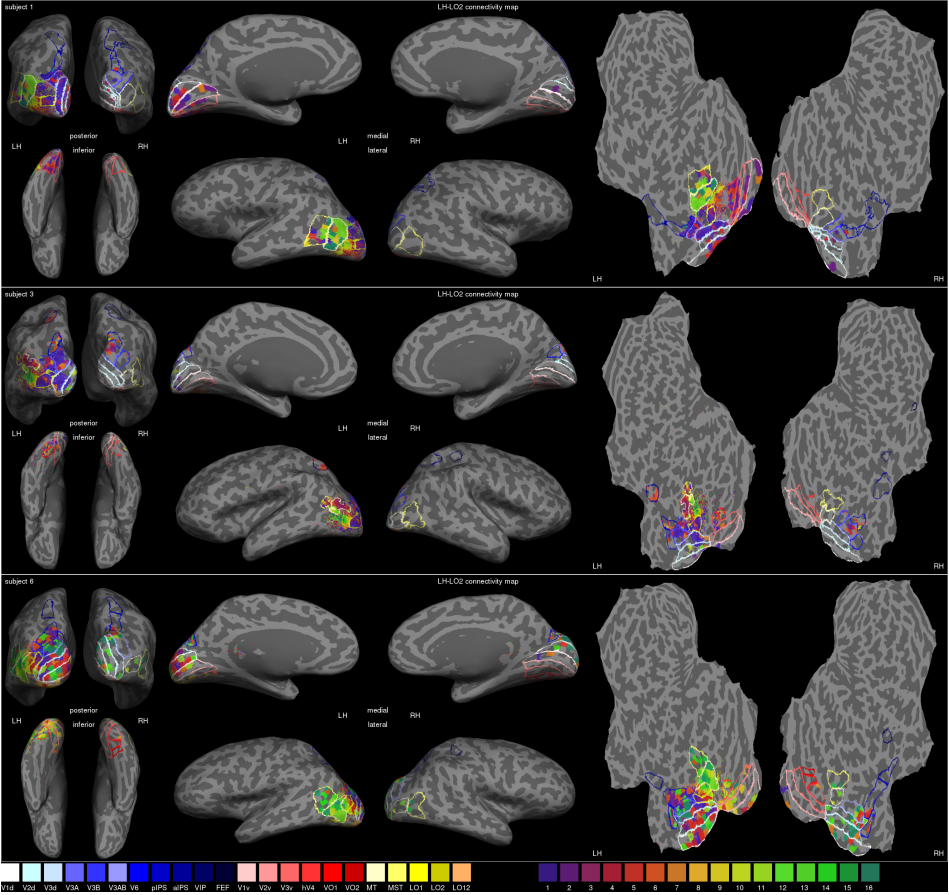


Supplementary figure A.17 Shows the connectivity maps of MST in the left hemisphere for subjects 1-6.



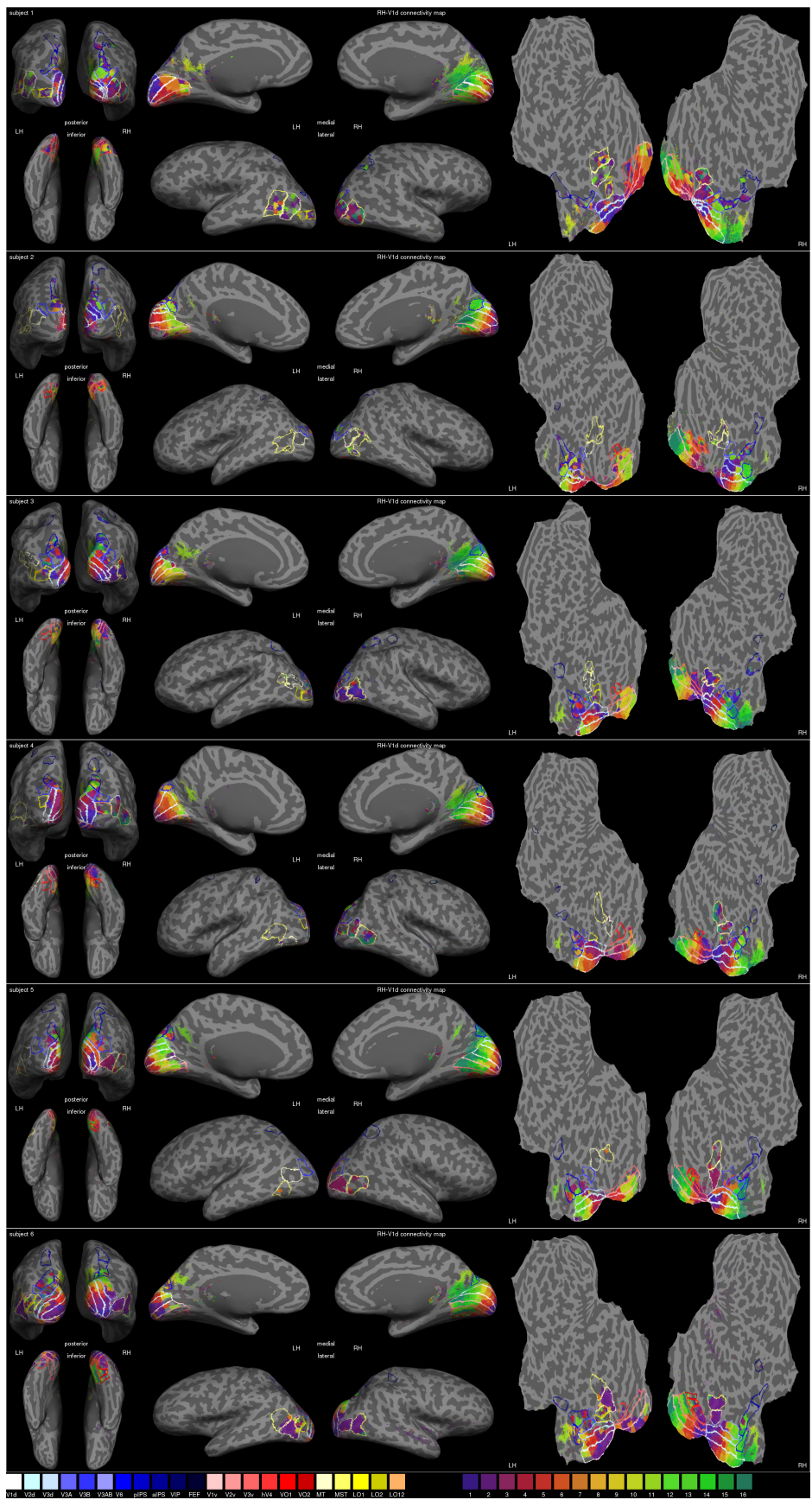
Supplementary figure A.18

Shows the connectivity maps of LO1 in the left hemisphere for subjects 1, 3, 4 and 6



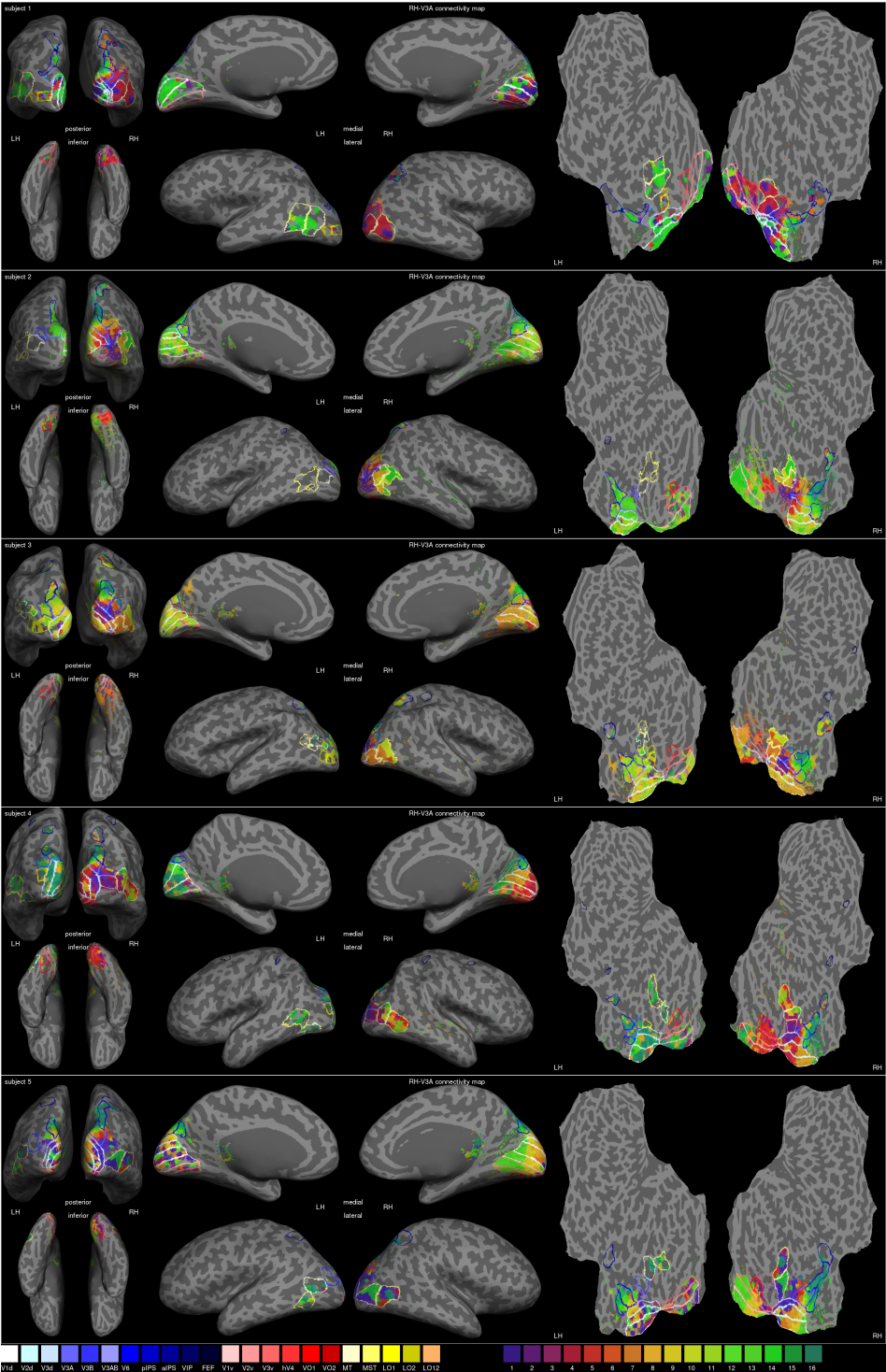
Supplementary figure A.19

Shows the connectivity maps of LO2 in the left hemisphere for subjects 1, 3 and 6



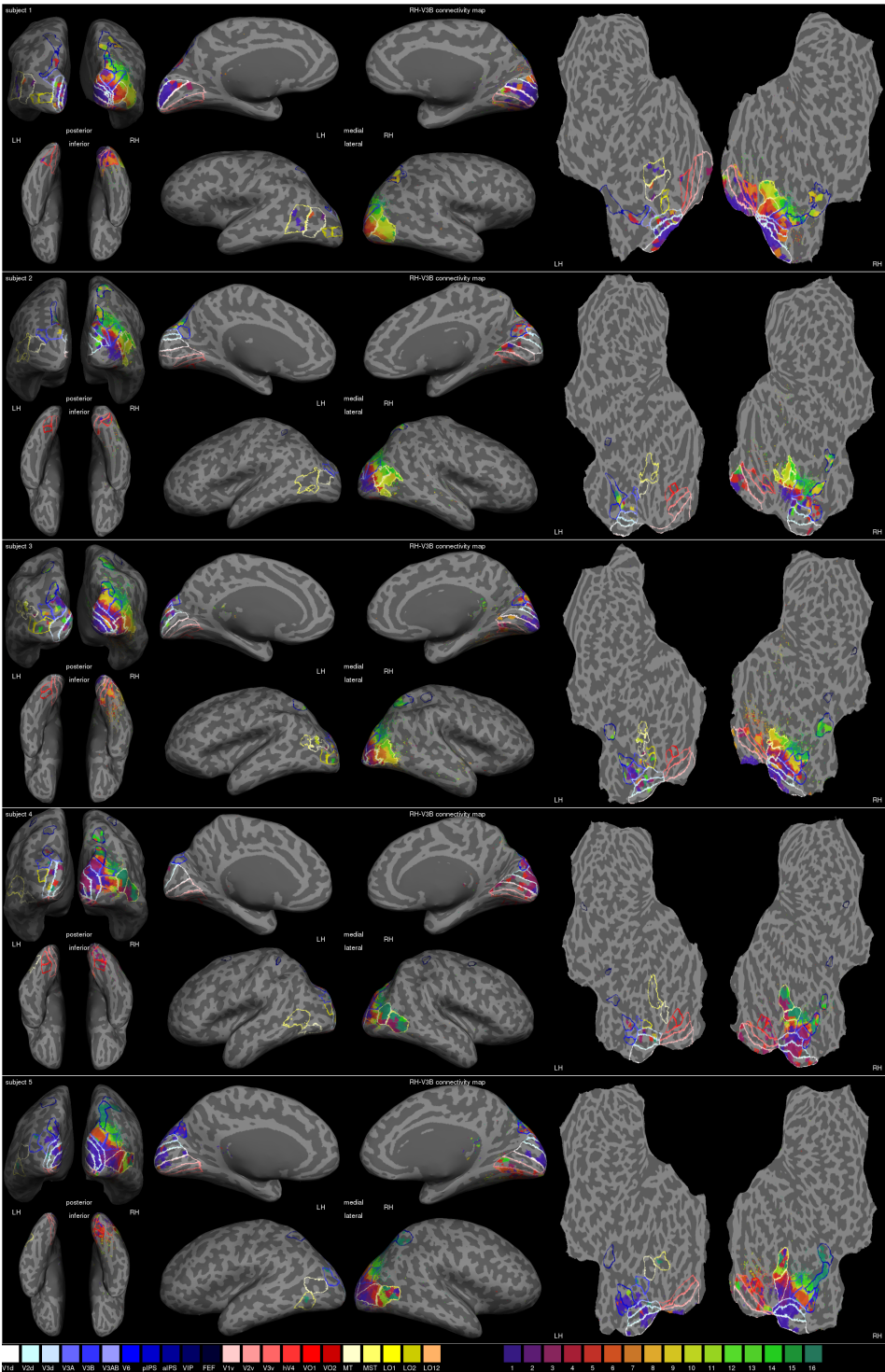
Shows the connectivity maps of V1 dorsal in the right hemisphere for subjects 1-6.

Supplementary figure A.20



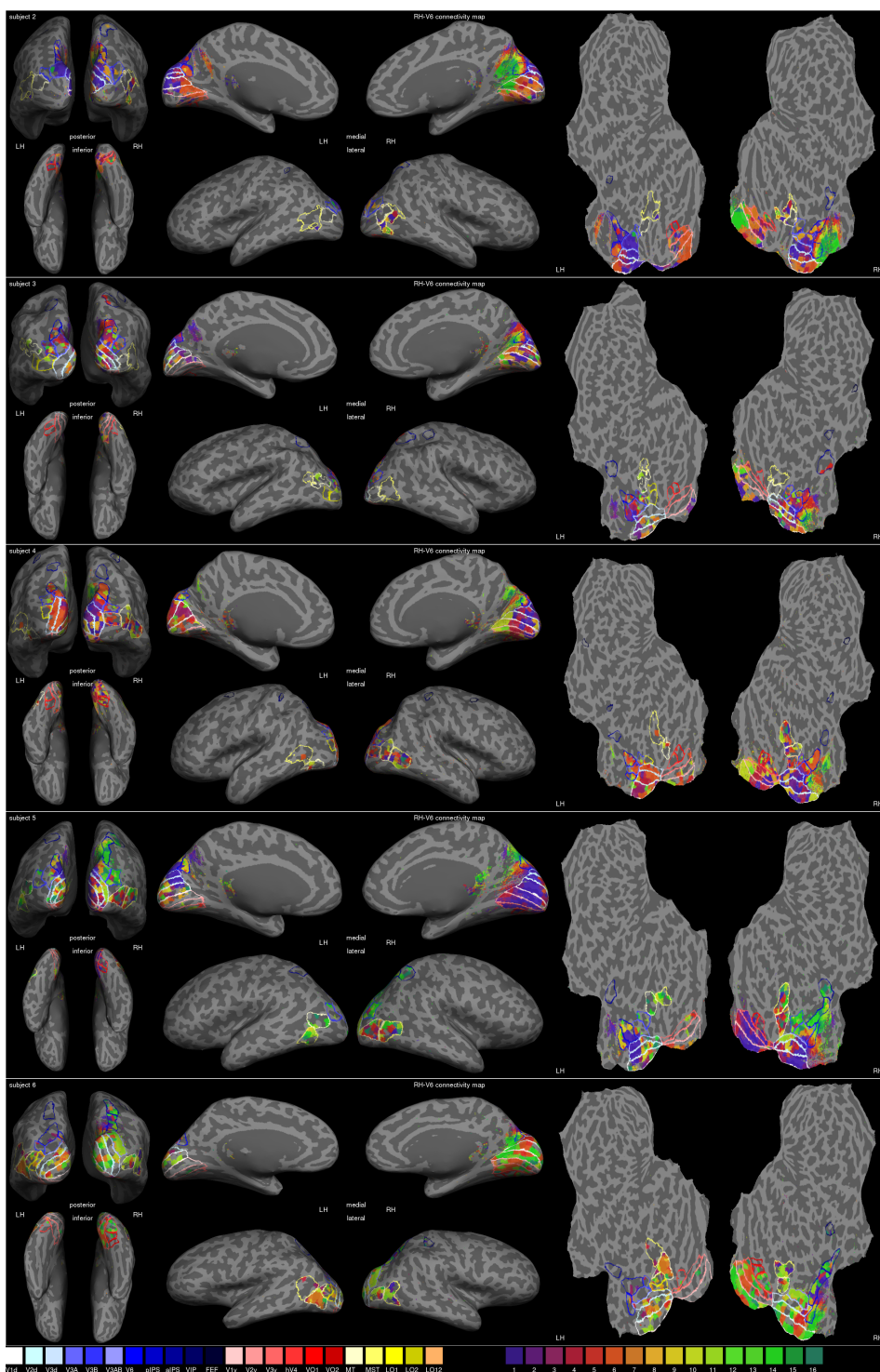
Supplementary figure A.23

Shows the connectivity maps of V3A in the right hemisphere for subjects 1-5.



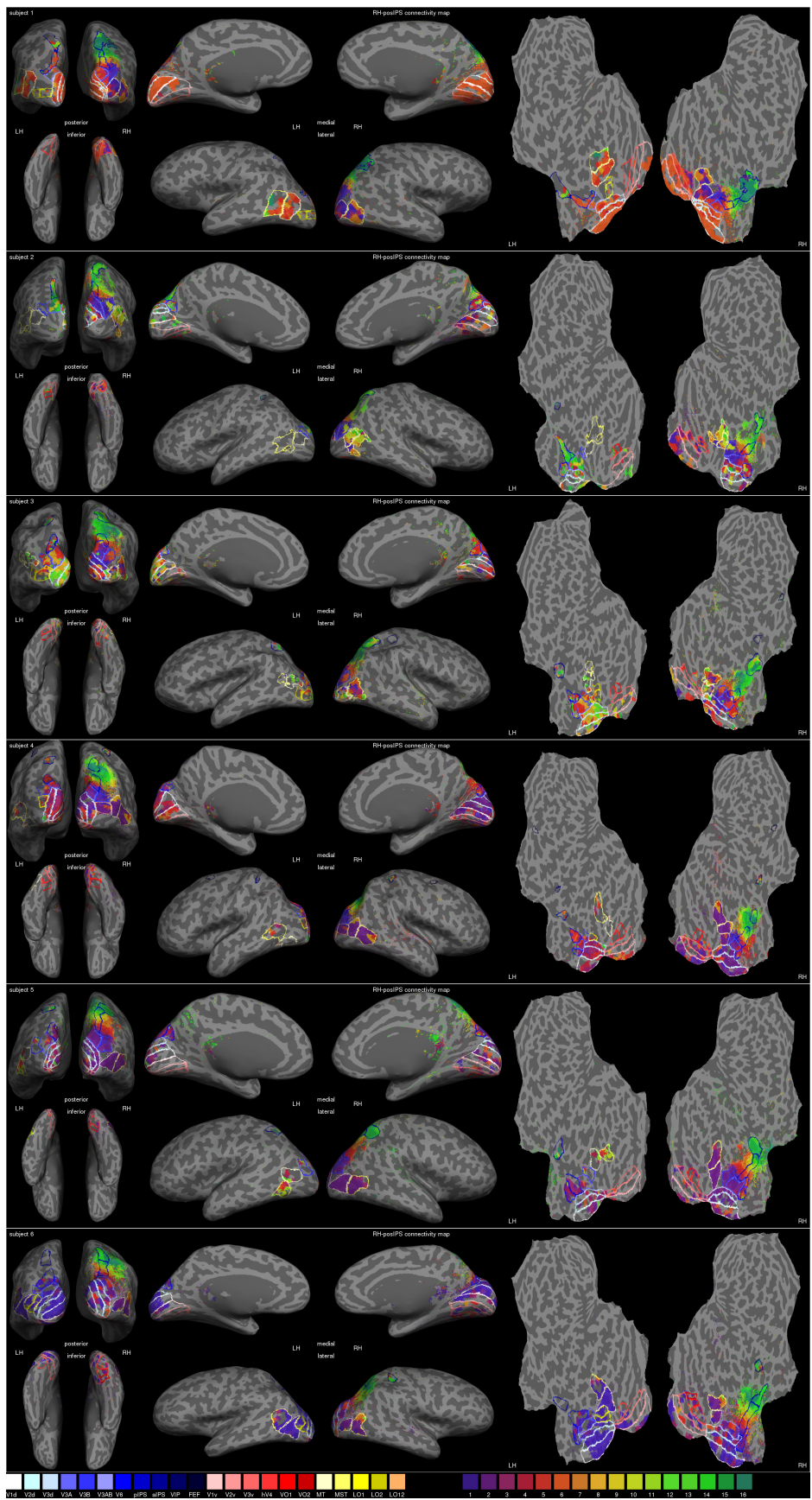
Supplementary figure A.24

Shows the connectivity maps of V3B in the right hemisphere for subjects 1-5.

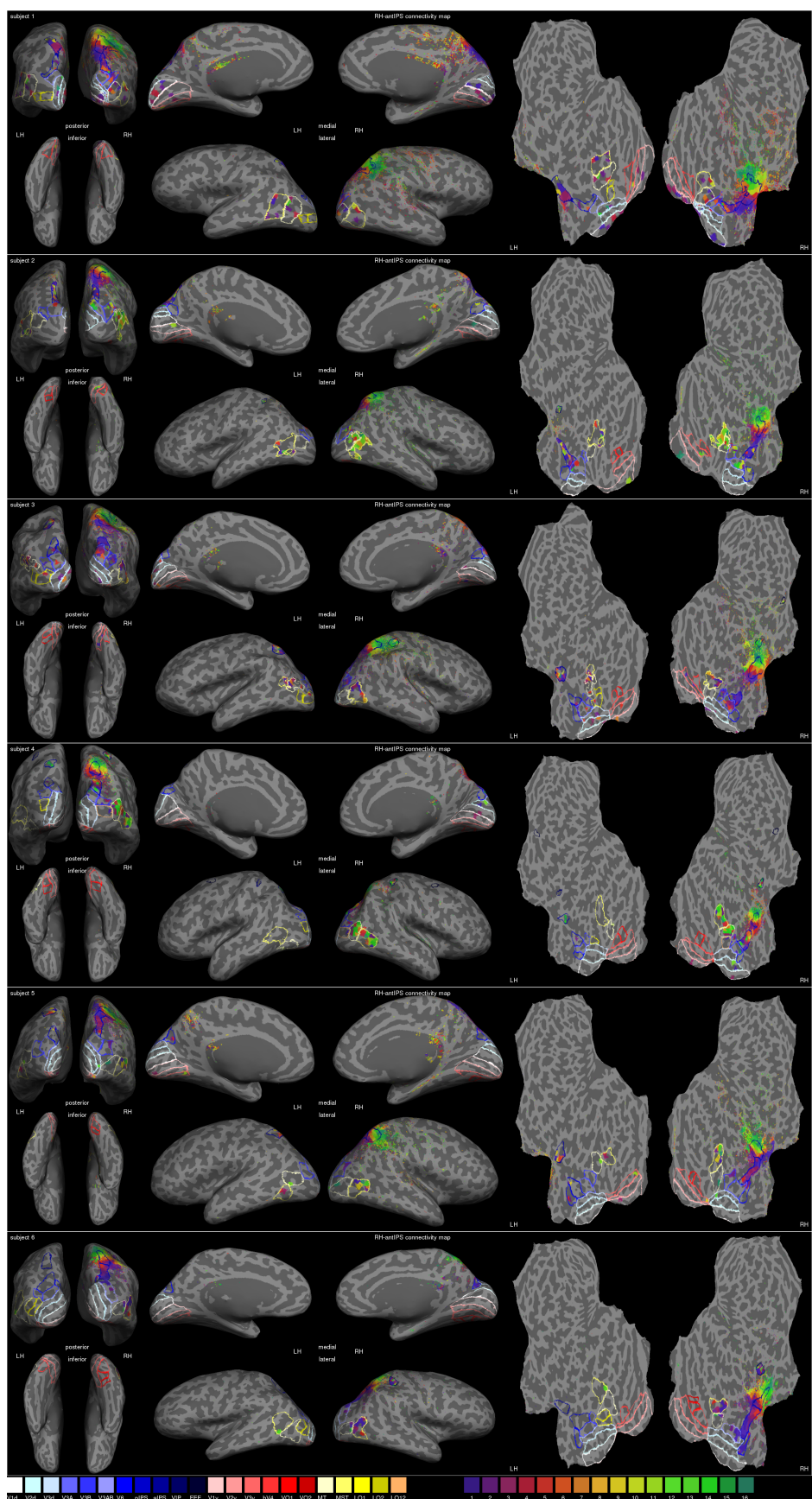


Supplementary figure A.25

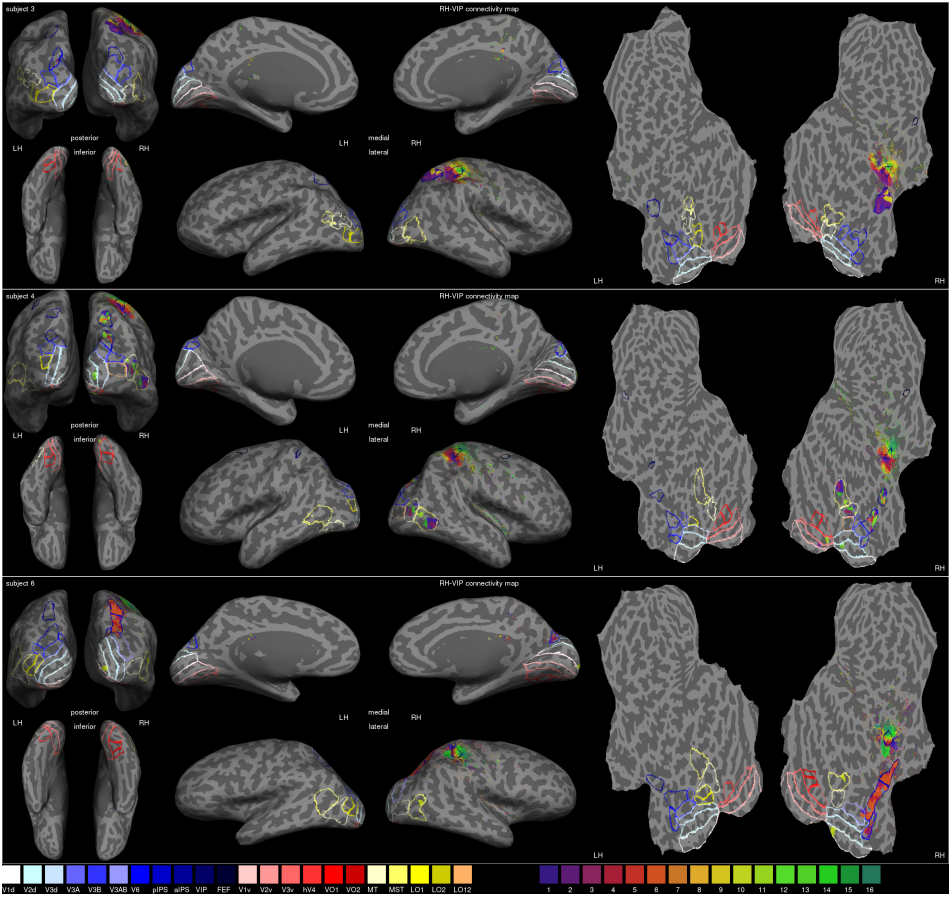
Shows the connectivity maps of V6 in the right hemisphere for subjects 2-6.



Supplementary figure A.26 Shows the connectivity maps of posterior IPS in the right hemisphere for subjects 1-6.

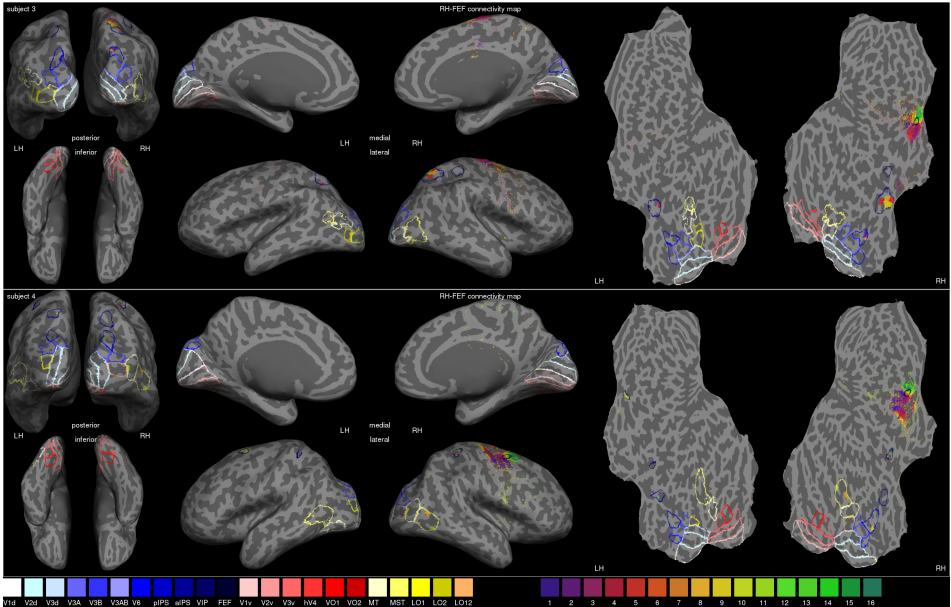


Supplementary figure A.27 Shows the connectivity maps of anterior IPS in the right hemisphere for subjects 1-6.

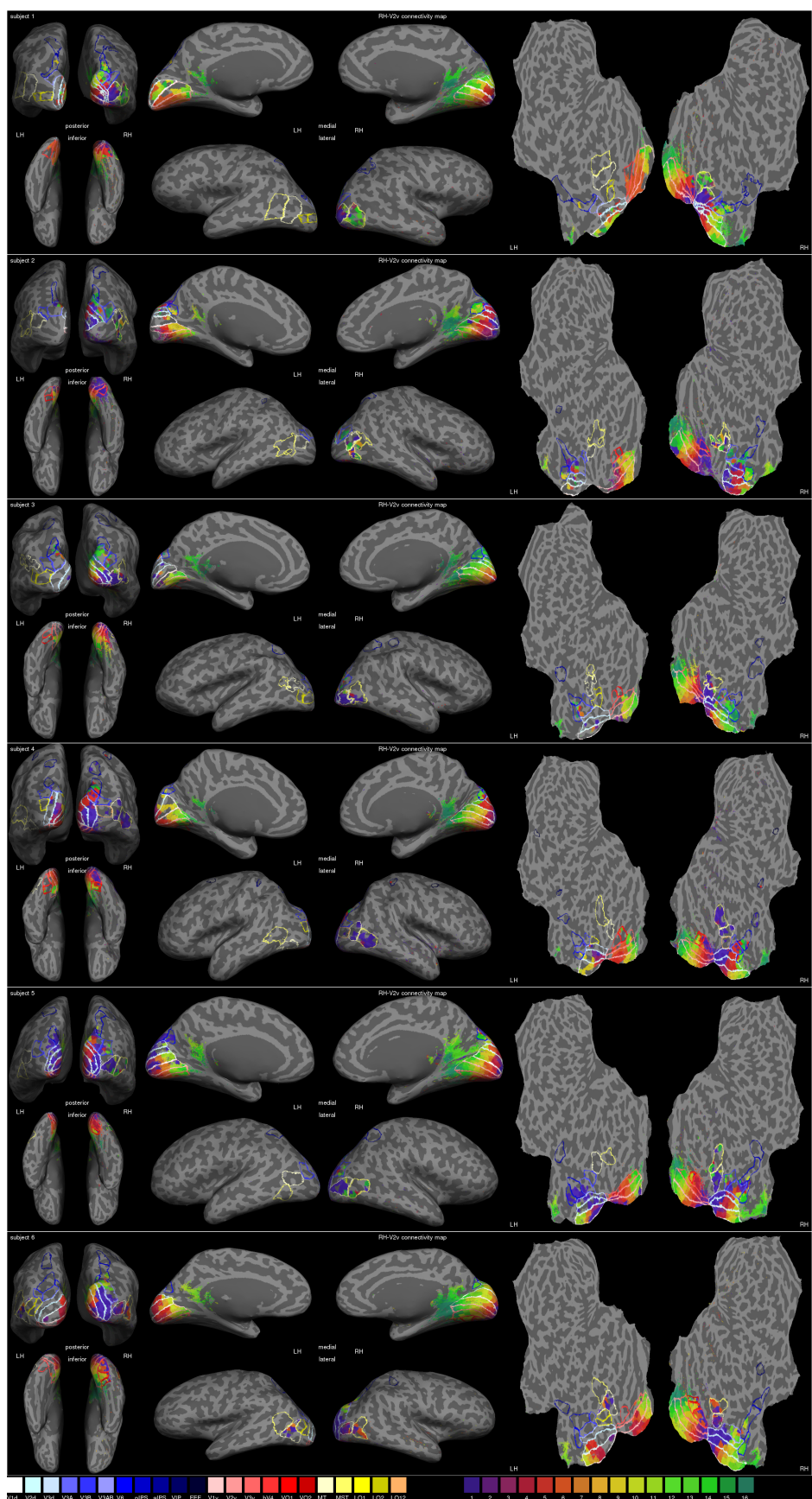


Supplementary figure A.28

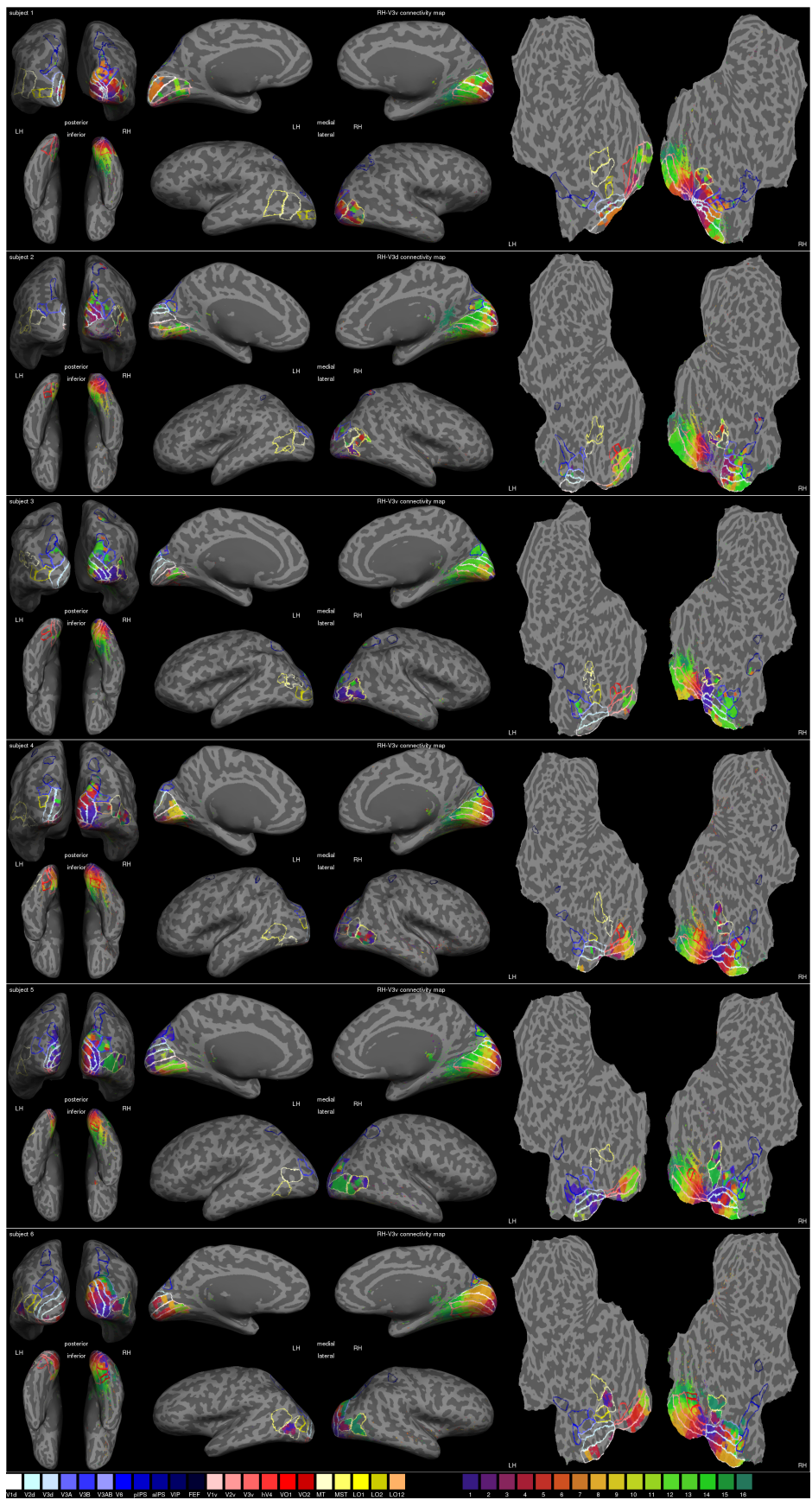
Shows the connectivity maps of VIP in the right hemisphere for subjects 3, 4 and 6.



Supplementary figure A.29
Shows the connectivity maps of FEF in the right hemisphere for subjects 3 and 4.

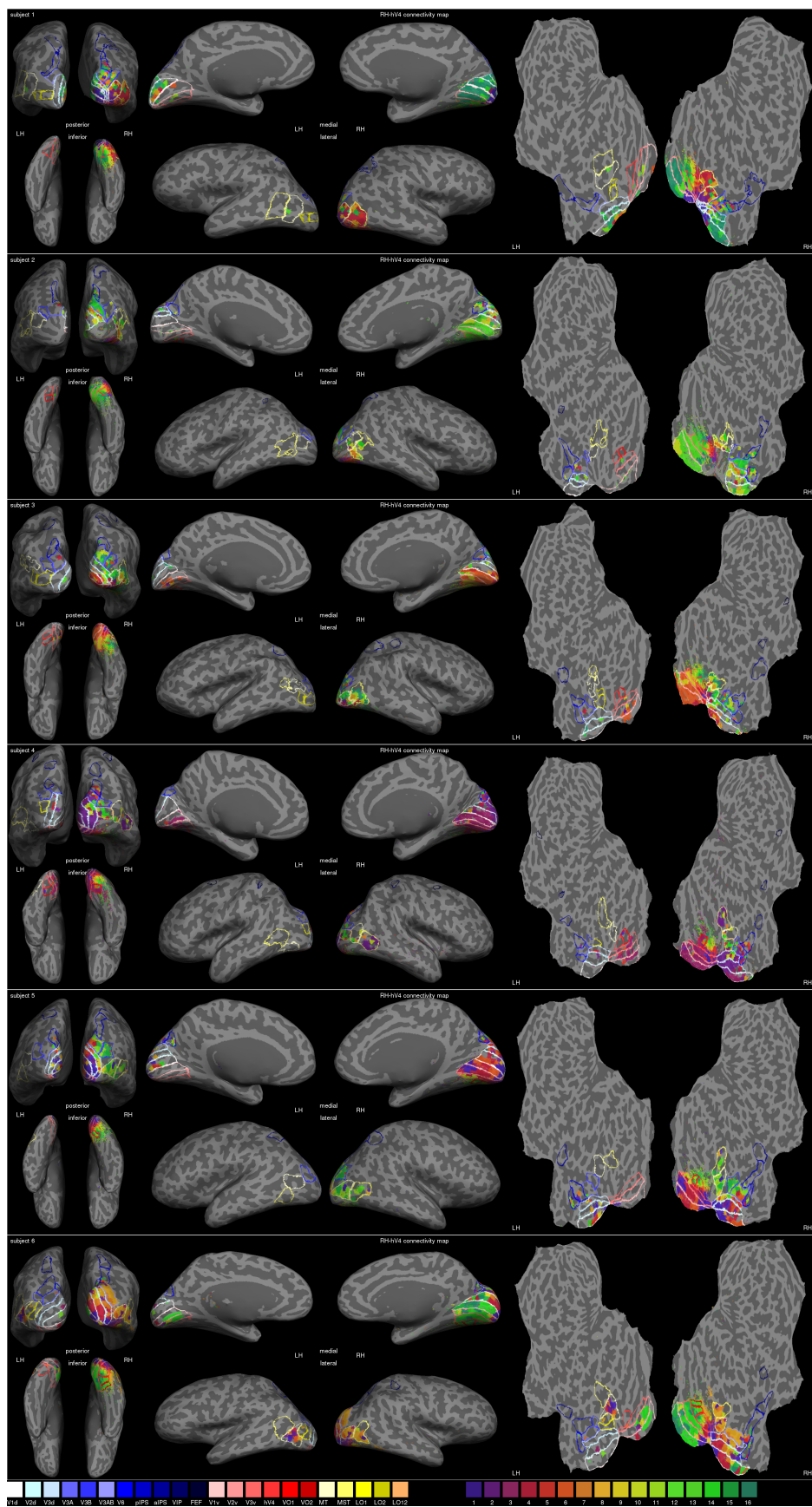


Supplementary figure A.31 Shows the connectivity maps of V2 ventral in the right hemisphere for subjects 1-6.

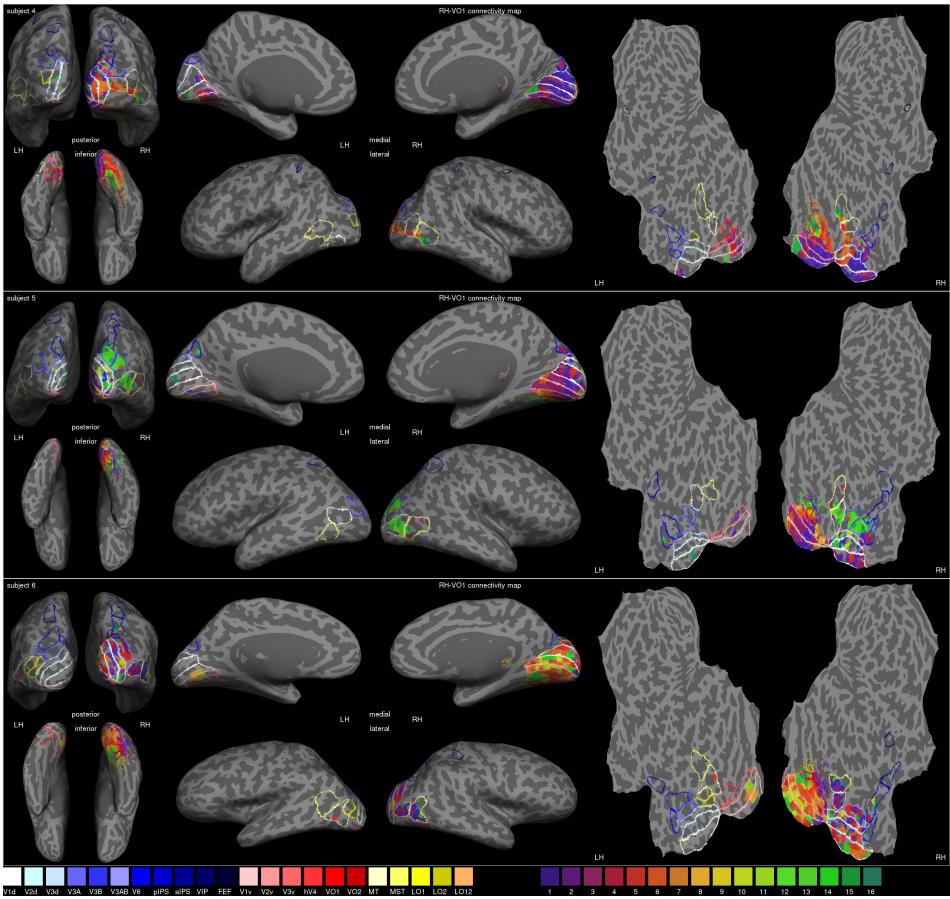


Shows the connectivity maps of V3 ventral in the right hemisphere for subjects 1-6.

Supplementary figure A.32

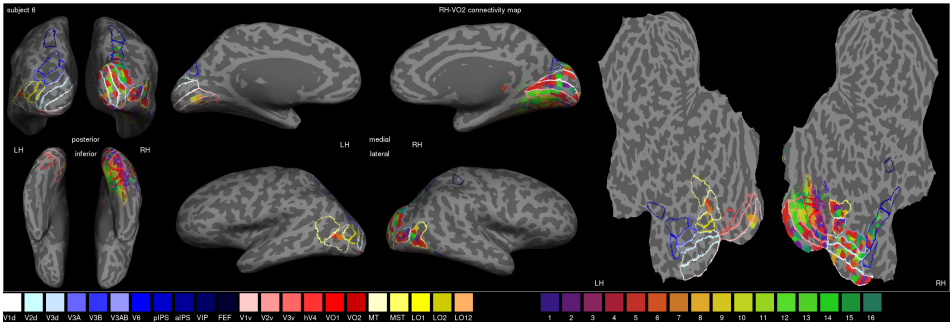


Supplementary figure A.33 Shows the connectivity maps of hV4 in the right hemisphere for subjects 1-6.



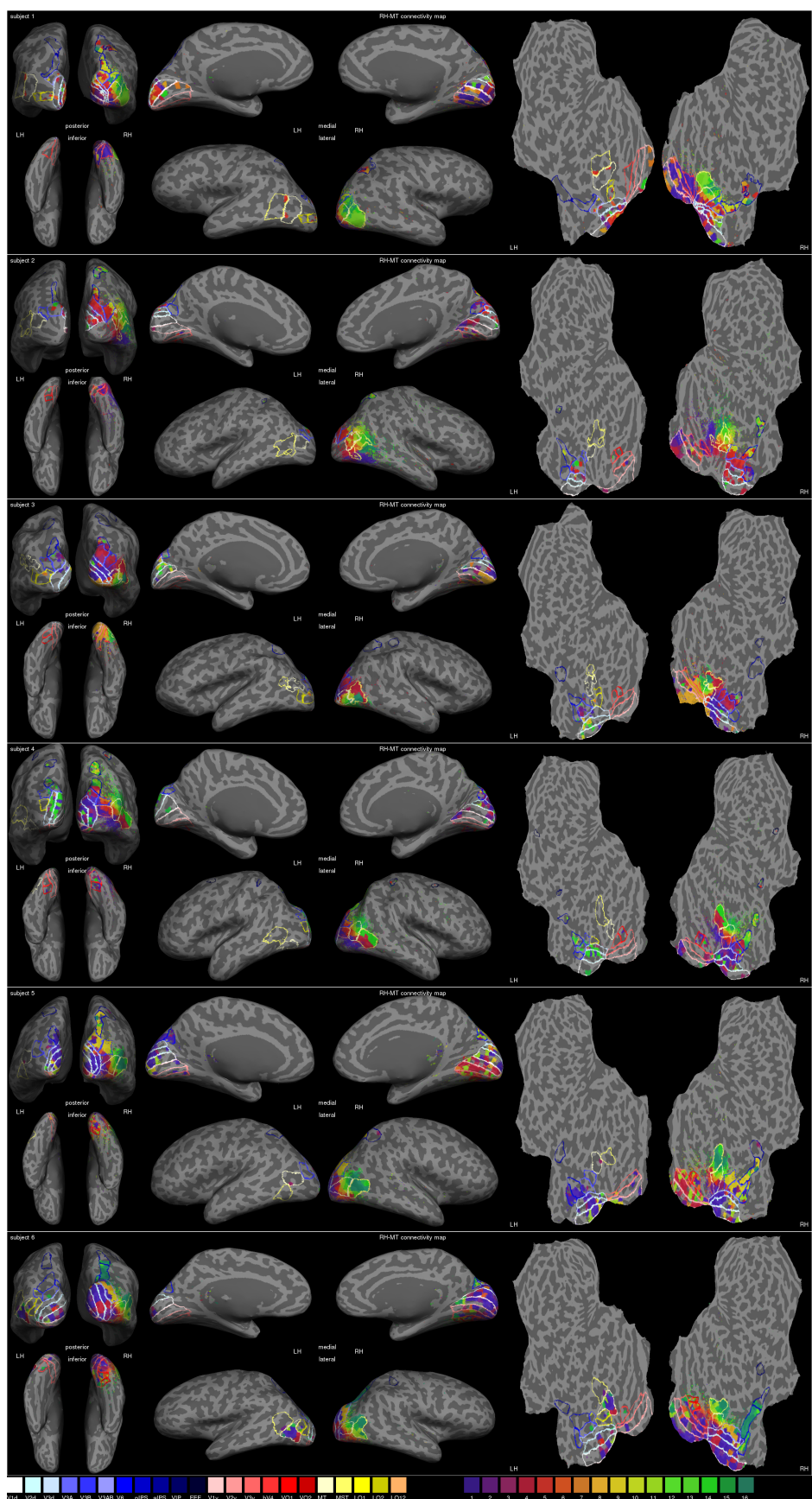
Supplementary figure A.34

Shows the connectivity maps of VO1 in the right hemisphere for subjects 4-6

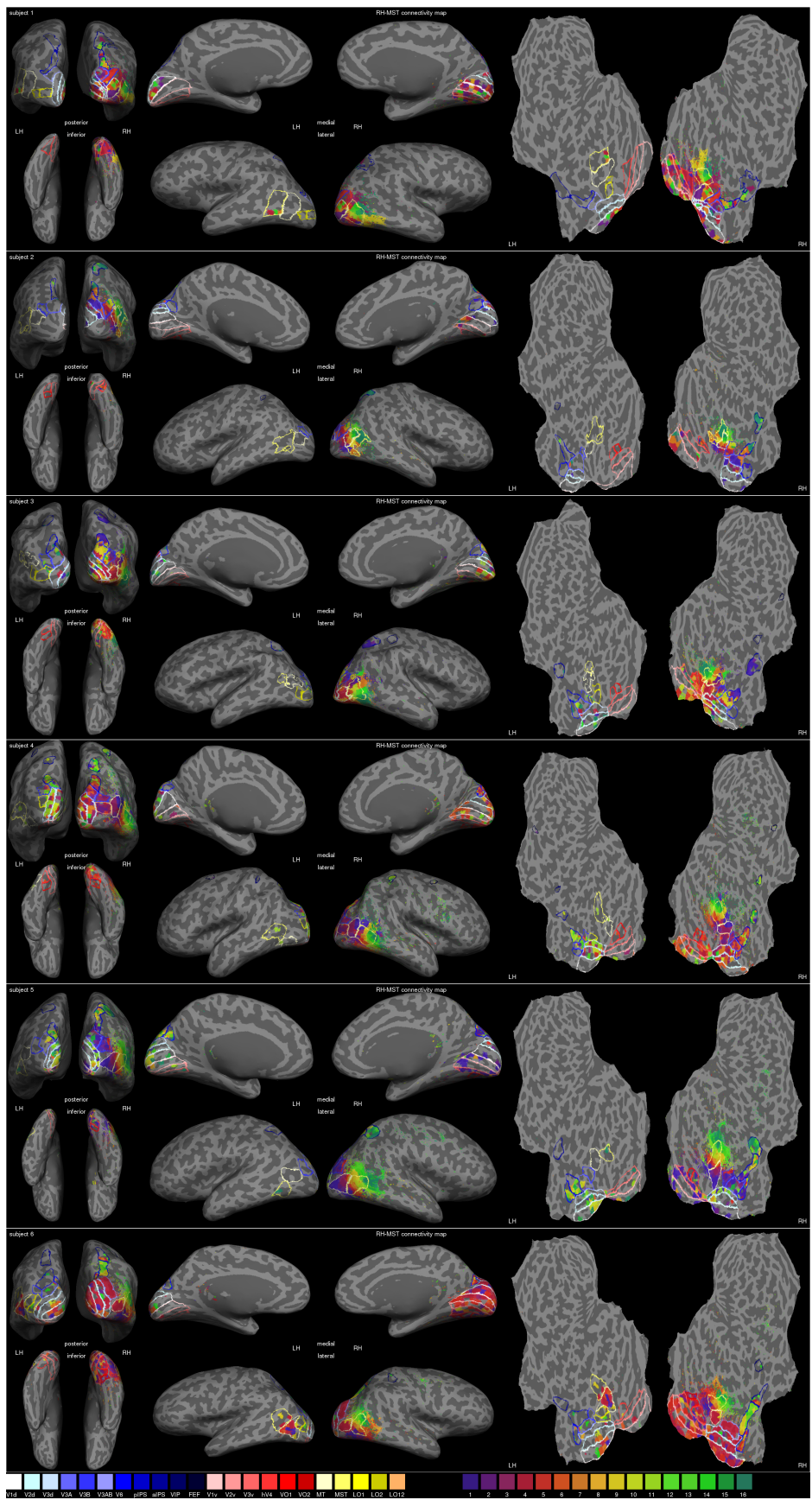


Supplementary figure A.35

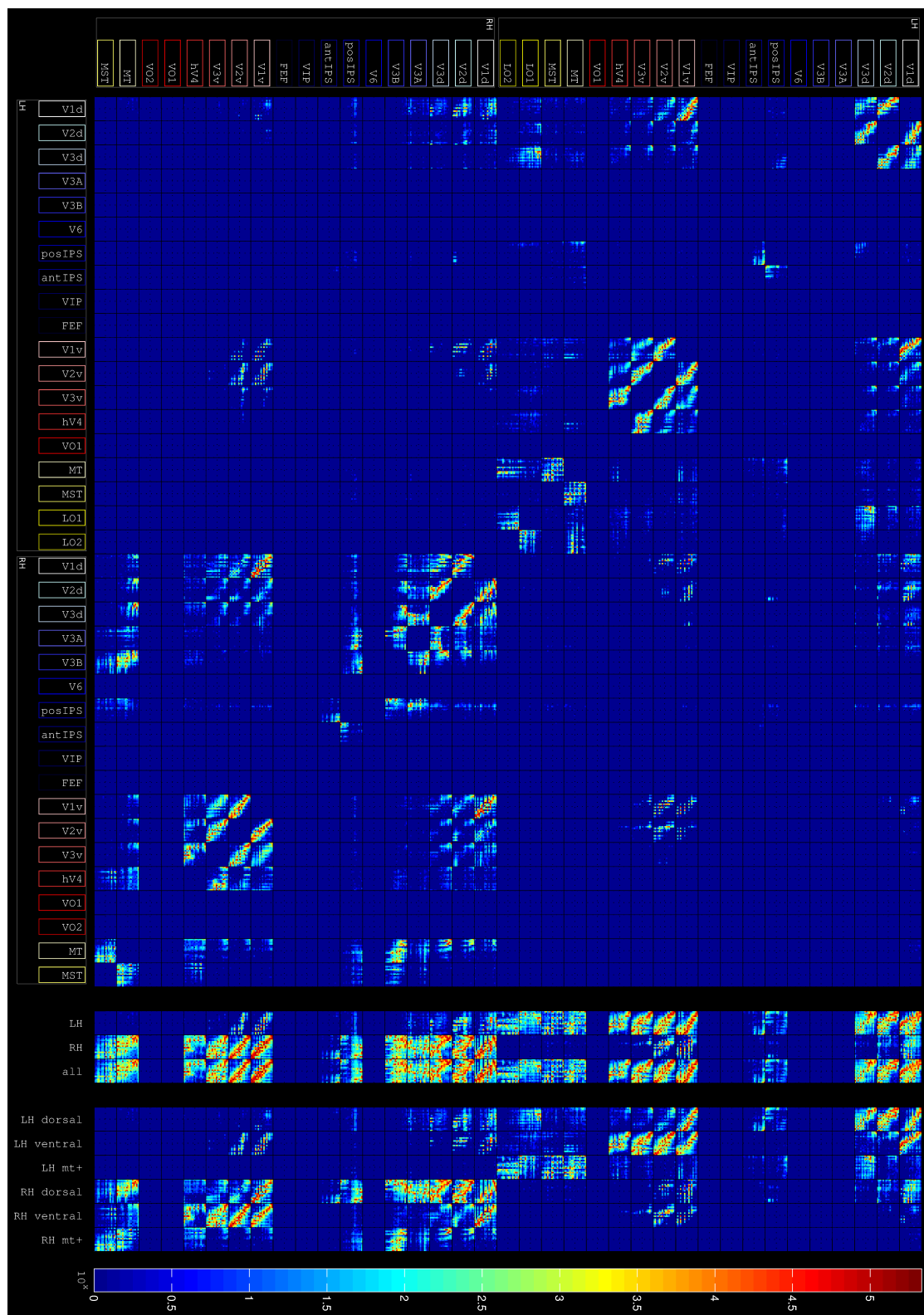
Shows the connectivity map of VO1 in the right hemisphere for subject 6



Supplementary figure A.36 Shows the connectivity maps of MT in the right hemisphere for subjects 1-6.

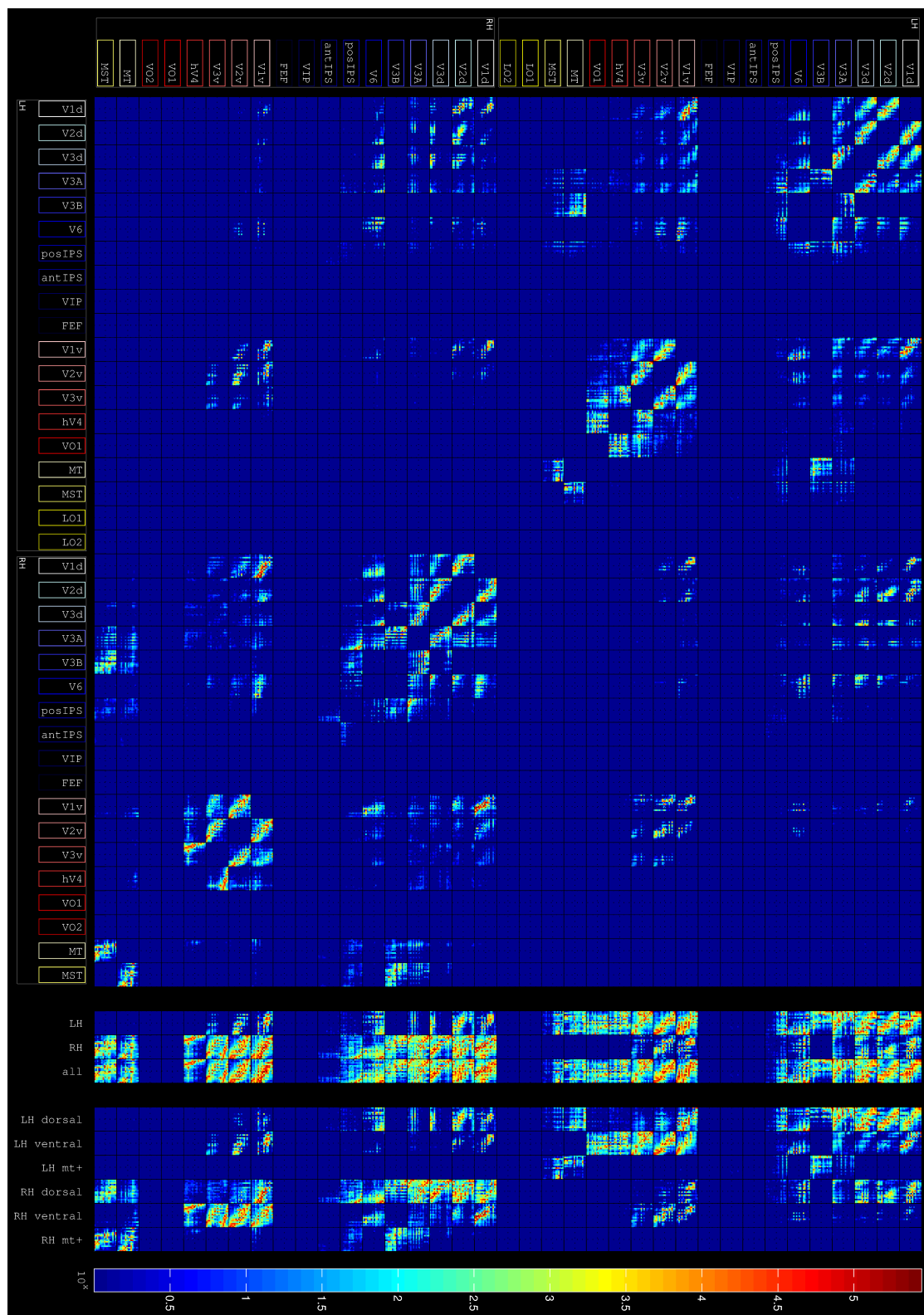


Supplementary figure A.37 Shows the connectivity maps of MST in the right hemisphere for subjects 1-6.



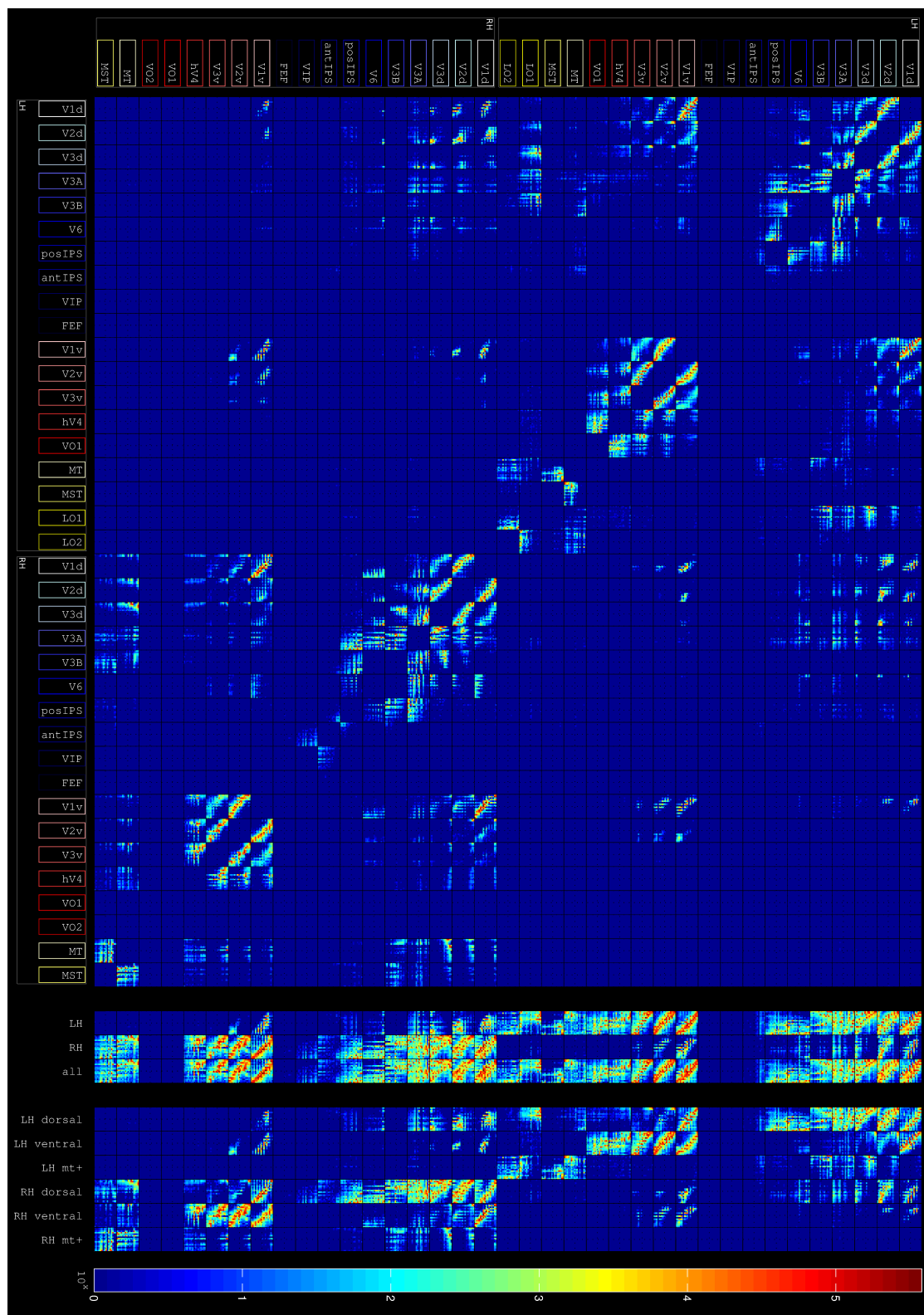
Supplementary figure A.38

Shows the individual connectivity matrices of the visual network of subject 1. The 16×16 connectivity patterns of a visual area have also been grouped by matrix summation on the right side of the matrix for the left hemisphere ('LH'), the right hemisphere ('RH'), the whole brain ('all'), blue labelled visual areas ('LH/RH dorsal'), red labelled visual areas ('LH/RH ventral') and yellow labelled visual areas ('LH/RH MT+').



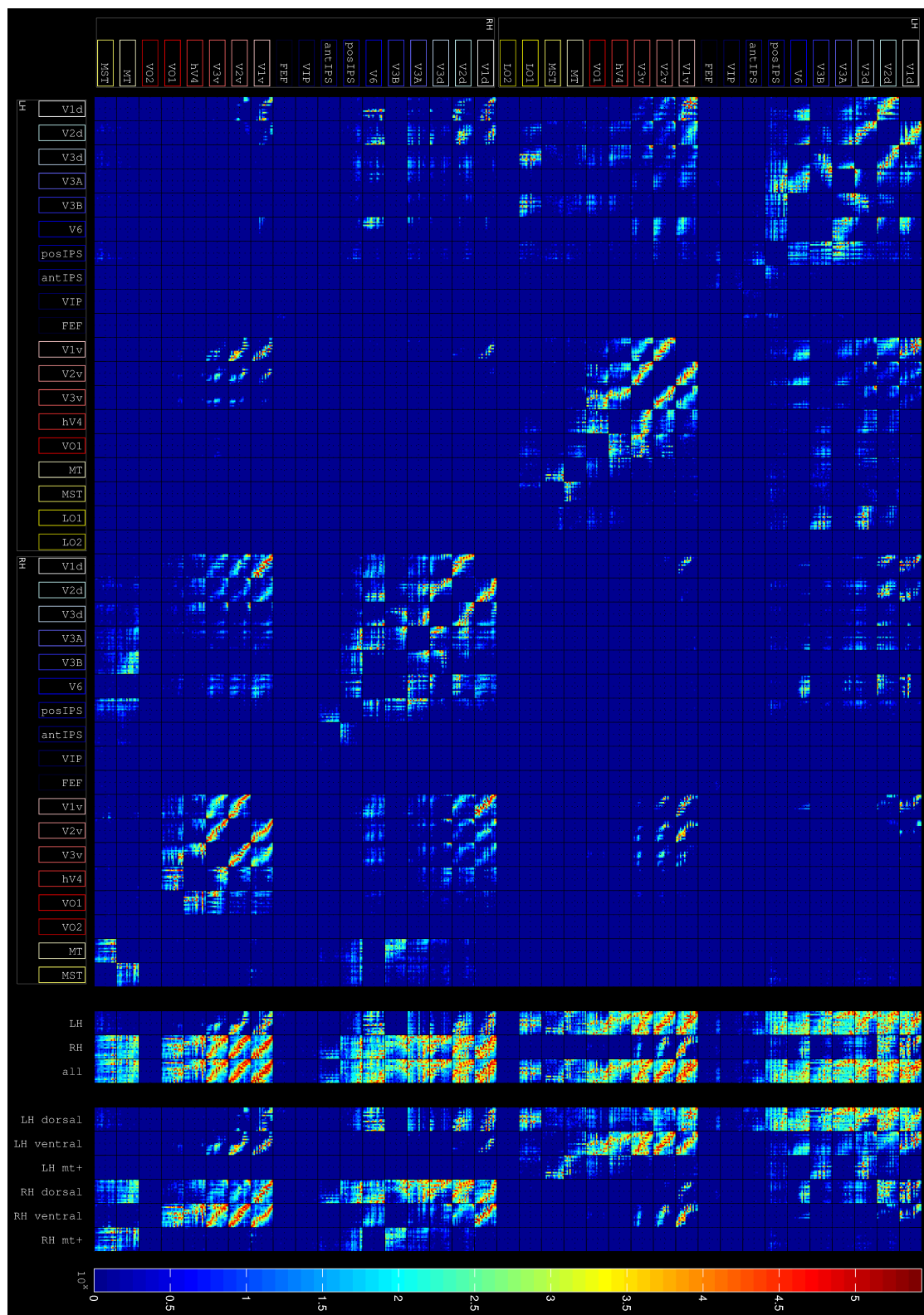
Supplementary figure A.39

Shows the individual connectivity matrices of the visual network of subject 2. The 16x16 connectivity patterns of a visual area have also been grouped by matrix summation on the right side of the matrix for the left hemisphere ('LH'), the right hemisphere ('RH'), the whole brain ('all'), blue labelled visual areas ('LH/RH dorsal'), red labelled visual areas ('LH/RH ventral') and yellow labelled visual areas ('LH/RH MT+').



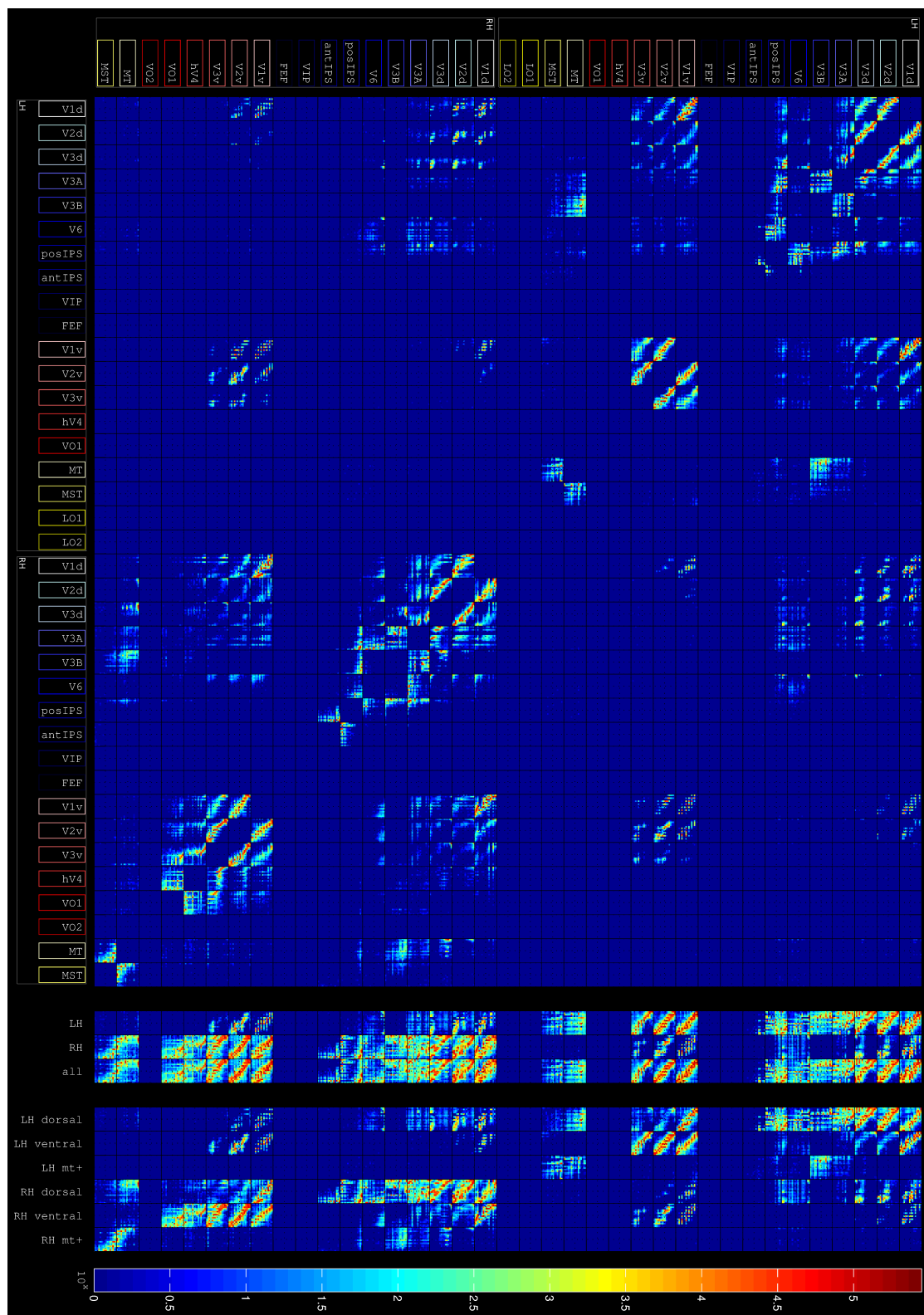
Supplementary figure A.40

Shows the individual connectivity matrices of the visual network of subject 3. The 16×16 connectivity patterns of a visual area have also been grouped by matrix summation on the right side of the matrix for the left hemisphere ('LH'), the right hemisphere ('RH'), the whole brain ('all'), blue labelled visual areas ('LH/RH dorsal'), red labelled visual areas ('LH/RH ventral') and yellow labelled visual areas ('LH/RH MT+').



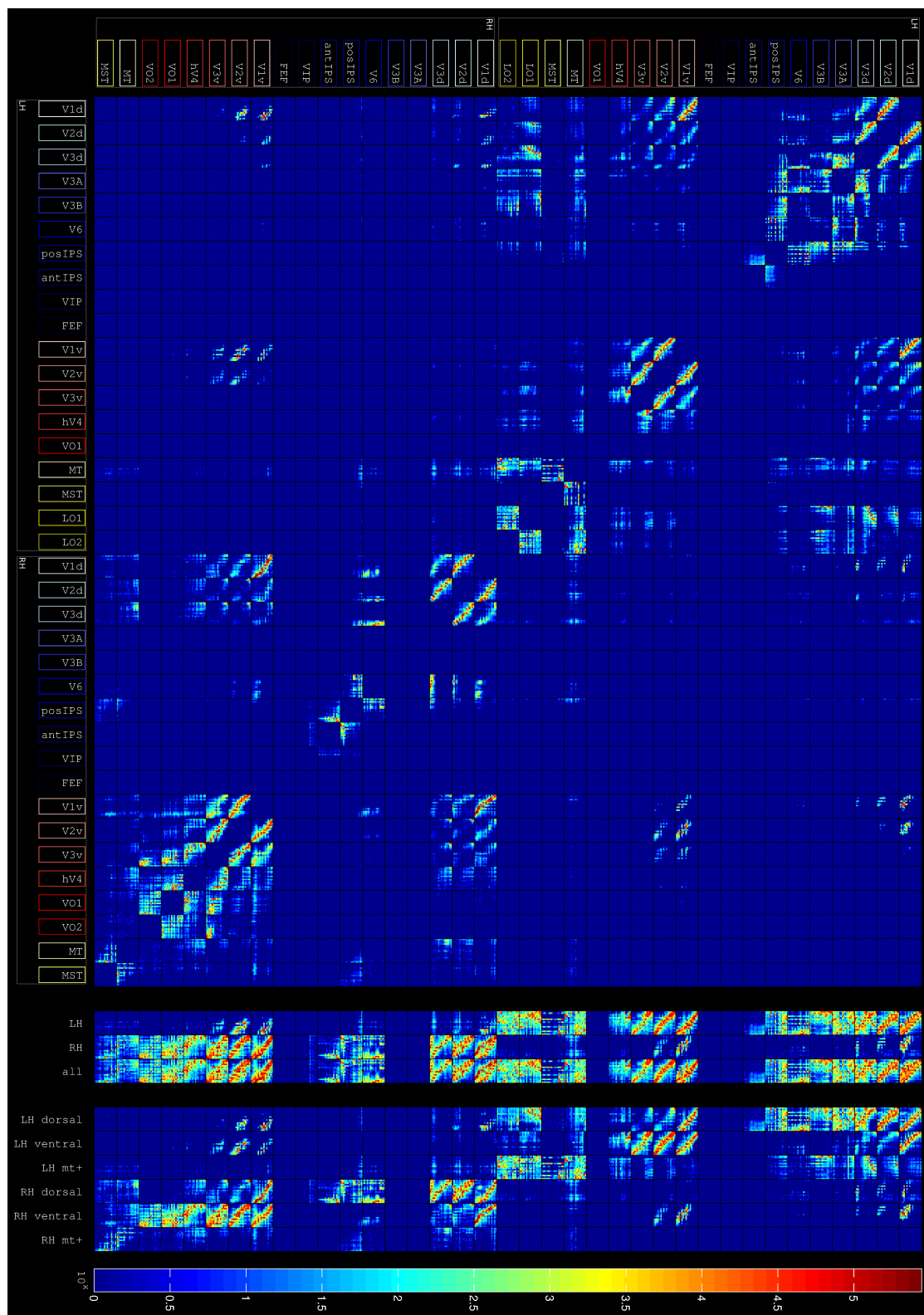
Supplementary figure A.41

Shows the individual connectivity matrices of the visual network of subject 4. The 16×16 connectivity patterns of a visual area have also been grouped by matrix summation on the right side of the matrix for the left hemisphere ('LH'), the right hemisphere ('RH'), the whole brain ('all'), blue labelled visual areas ('LH/RH dorsal'), red labelled visual areas ('LH/RH ventral') and yellow labelled visual areas ('LH/RH MT+').



Supplementary figure A.42

Shows the individual connectivity matrices of the visual network of subject 5. The 16×16 connectivity patterns of a visual area have also been grouped by matrix summation on the right side of the matrix for the left hemisphere ('LH'), the right hemisphere ('RH'), the whole brain ('all'), blue labelled visual areas ('LH/RH dorsal'), red labelled visual areas ('LH/RH ventral') and yellow labelled visual areas ('LH/RH MT+').



Supplementary figure A.43

Shows the individual connectivity matrices of the visual network of subject 6. The 16×16 connectivity patterns of a visual area have also been grouped by matrix summation on the right side of the matrix for the left hemisphere ('LH'), the right hemisphere ('RH'), the whole brain ('all'), blue labelled visual areas ('LH/RH dorsal'), red labelled visual areas ('LH/RH ventral') and yellow labelled visual areas ('LH/RH MT+').

Propositions

accompanying the PhD thesis:

Macroscopic Networks in the Human Brain

Mapping connectivity in healthy and damaged brains

by Emil H.J. Nijhuis

1. Structural connectivity patterns in the human brain may be an important identifier of brain function.
2. The hubs of the human neocortex are topographically distributed.
3. The visual system has two main process streams: a dorsal stream and a ventral stream. This can be seen also in the connectivity patterns of the visual system.
4. Diffusion weighted imaging techniques are beneficial for understanding brain damage.
5. “If our brains were simple enough for us to understand them, we'd be so simple that we couldn't.” - Ian Stewart
6. (corollary to proposition 5) Trying to understand and describe the whole brain on your own is in opposition to economical principles and will lead to higher labour costs and scientific production inefficiency.
7. (corollary to proposition 6) Neuroscience is best practised in large diverse teams with experts in multiple topics from different disciplines.
8. Science not executed in a humaneness spirit will lose its most important source of virility.
9. As a scientist or engineer your probability to have published in the journal Nature in 2006 is less than $p < .00344$.
10. “Imagination is more important than knowledge.” - Albert Einstein